FEBRUARY, 1952

Journal of METALS

February JOURNAL OF METALS Highlights:

"A Survey of Zebra Roof Practice" - p. 132
"Research In Progress" - p. 148
"Low Melting Gallium Alloys" - p. 153

Freyn-Design

provides the steel industry with integrated... specialized... comprehensive engineering services. Consultation, design and construction. Raw materials to finished products.

1914 - - - 1952

KOPPERS

METALLURGICAL PLANT DESIGN AND CONSTRUCTION

Freyn Engineering

DEPARTMENT OF KOPPERS COMPANY, INC.

Journal of METALS

VOL. 4, NO. 2 FEBRUARY, 1952

Published to provide a continuing, authoritative, and up-to-date record of technological, engineering, and economic progress in all branches of the metals industry by the Metals Branch American Institute of Mining and Metallurgical Engineers, Inc. 29 West 39th Street, New York 18

THOMAS E. LLOYD
Manager of Publications
Editor, Journal of Metals

A. S. COHAN Associate Editor
D. G. GARRETT MARGARET BAGG
Assistant Editors
GRACE PUGSLEY Production Manager
W. J. SEWING Asst. Prod. Mgr.

METALS BRANCH COUNCIL
C. C. Long Chairman
E. O. Kirkendall Secretary
R. M. Brick IMD Chairman
T. L. Joseph ISD Chairman
O. C. Ralston EMD Chairman
M. Gensamer D. S. Eppelsheimer
H. K. Work Evan Just

TECHNICAL PUBLICATIONS COMMITTEE
J. T. Laudermilk Chairman
E. J. Kennedy, Jr. Secretary

AUXILIARY PUBLICATIONS COMMITTEE CHAIRMEN
M. Gensamer Institute of Metals Div.
A. G. Forrest Iron & Steel Div.
J. Glosser Extract. Metal Div.

JAMES A. STANGARONE
Advertising Manager
B. C. SNELL
Regional Manager, Pittsburgh
1110 McDonald Place, Sewickley, Pa.

The AIME Publishes
Journal of Metals
Mining Engineering
Journal of Petroleum Technology

COVER

The photograph shows the charging floor for one of the electric furnaces at the $100 million ferroalloy plant of Electro Metallurgical Co., a division of Union Carbide & Carbon Corp. When completed in 1953, the plant at Marietta, Ohio, will be the largest in the world. The covered furnaces are of the submerged-arc type and operate 24 hr a day. Molten ferroalloy at the bottom of the furnace is tapped periodically.

NEWS

Journal of Metals Reporter	131	New Products	121
Annual Meeting Program	143	AIME News	217
Employment Service	115	Coming Events	220
Meet the Authors	115	Personals	219
"Drift of Things"	129	Books for Engineers	124

TECHNICAL FEATURES

A Survey of Zebra Roof Practice — C. E. Cagley — 132
Rapid Analysis of Boron in Alloys — H. Blumenthal — 140
Progress Report: Low Shaft Blast Furnace — 142
Research In Progress — 144

TRANSACTIONS

Low Melting Gallium Alloys — R. M. Evans, R. T. Jaffee — 153
Cast Molybdenum of High Purity — D. W. P. Bergquist, R. B. Fischer — 157
Internal Friction Measurements on Iron Wires of Commercial Purity — Åke Josefsson, Eric Rudd — 161
Tensile Properties of Wrought Austenitic Manganese Steel in the Temperature Range from 100° to —196°C — H. C. Dodeken — 166
Silicon-Oxygen Equilibrium in Liquid Iron — N. A. Gokcen, J. Chipman — 171
Dislocation Collision and the Yield Point of Iron — A. N. Holden — 182
Kinetics and Orientation Relationships of Secondary Recrystallization in Silver — F. D. Fiss, P. H. Alexander, C. A. Dube — 189
Delay Time for the Initiation of Slip in Metal Single Crystals — T. E. Kramer, B. Maddin — 197
Diffraction Patterns and Crystal Structure of Si$_3$N$_4$ and Ge$_3$N$_4$ — W. C. Levin, K. G. Carroll, R. M. Fisher — 204
Effect of Temperature on the Lattice Parameters of Mg Alloys — R. S. Busk — 207
Crystal Structure of Ti$_2$Sn — Paul Pietrokowsky — 211
Mechanism of the Reduction of Oxides and Sulphides to Metals — C. Wagner — 214

TECHNICAL NOTES

Twinning in Silicon — E. J. Schmitz, F. W. von Batchelder — 165
Growth of Austenite in Cold-Rolled Tempered Martensite — A. E. Nehrenberg — 181
Effect of Cold Work and Annealing on the Thermoelectric Power of Molybdenum — J. H. Kittel — 196
Observations on the Occurrence of Ti$_2$X Phases — W. Rostoker — 209
Observations on the Lattice Parameters of the Alpha Solid Solution in the Ti-Al System — W. Rostoker — 212

Published the first day of each month by the American Institute of Mining and Metallurgical Engineers, Inc., 29 West 39th Street, New York 18, N. Y. Telephone: PEnnsylvania 6-9220. Subscription $8 per year for non-AIME members in United States and North, South and Central America; $9 foreign; $6 for AIME members; or $4 additional in connection with a subscription to "Mining Engineering" or "Journal of Petroleum Technology." Single copies, 75 cents; special issues, $1.50. The AIME is not responsible for any statement made or opinion expressed in its publications.
Copyright 1952 by the American Institute of Mining and Metallurgical Engineers, Inc. Reprints upon request.
Registered cable address, AIME New York. Indexed in Engineering Index, Industrial Arts Index and Chemical Abstracts. Entered as second-class matter Sept. 20, 1949, at the post office at New York, N. Y., under the Act of March 3, 1879. Additional entry established at Manchester, N. H.

MILLIONS of POUNDS

of Aluminum per year reclaimed with the help of

AJAX INDUCTION FURNACES

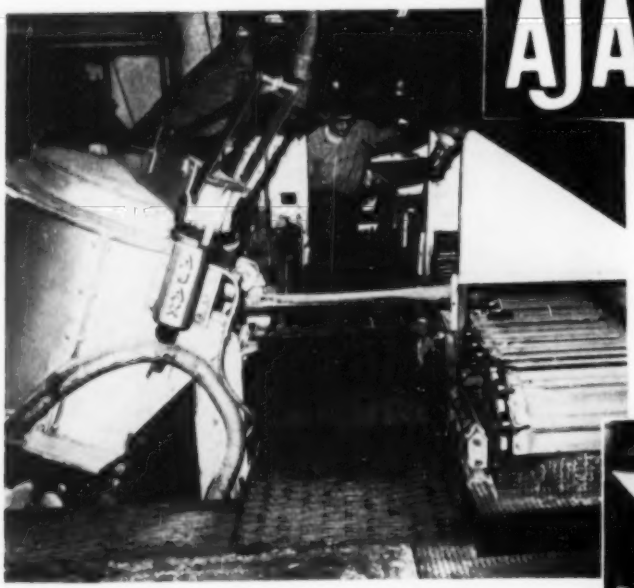

166 kW AJAX Induction Furnace in tilted position, pouring molten aluminum alloy through a coated trough into ingot molds on conveyor.

MAJOR AUTO MANUFACTURER RECOVERS SCRAP FROM MACHINING OPERATION BY MODERN MELTING PROCESS

Here is an interesting setup for reclaiming aluminum alloy chips, which is installed adjacent to the piston casting setup in one of the largest automobile manufacturing plants in the country. More than half of the aluminum needed for pistons in this plant comes from this scrap recovery program. A considerable net profit is realized, and aluminum purchases are lowered.

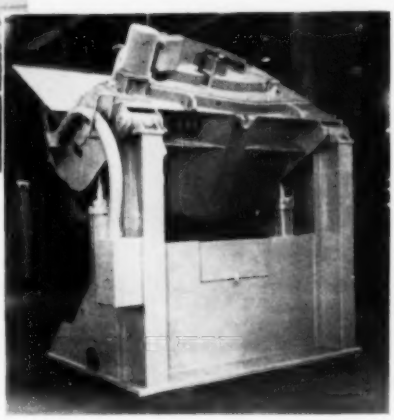

Above is a 330 kW furnace. AJAX Engineering Corporation manufactures low frequency electric induction furnaces in a great variety of sizes ranging from 20 to 1000 kW. This type of equipment has been adapted to the full range of non ferrous metals and alloys.

Send for Reprint of Article on Scrap Recovery by Induction Furnaces

AJAX TAMA-WYATT

AJAX ENGINEERING CORP., TRENTON 7, N. J.

INDUCTION MELTING FURNACE

AJAX ELECTRO METALLURGICAL CORP., and Associated Companies
AJAX ELECTROTHERMIC CORP., Ajax Northrup high frequency induction furnaces
AJAX ELECTRIC CO., INC., The Ajax Wyatt Electric Salt Bath Furnace
AJAX ELECTRIC FURNACE CORP., Ajax Hyatt Electric Furnaces for Melting

HIGHEST RESOLUTION for Every Magnification

Plus- WIDEST SELECTION of Resolving Powers

Photographic Mag	OBJECTIVES						EYEPIECES			Approx Bellows Draw In
	Achromatic		Fluorite		Apochromatic					
	Mag	N.A.	Mag	N.A.	Mag	N.A.	Mag	Hyper	Amp	

add **BORON** *this easy way!*

A cup to the ton
And the trick is done!

Cup and contents go into the ladle together, when you use the patented MCA Boron Cups (U. S. Patent 2,285,299) in making up a melt of Boron Steel.

For each ton of metal, you add one MCA cup, sealed and intact, precisely as you received it. Nothing could be simpler. Each cup contains the approved standard amount of MCA Ferro-Boron (U. S. Patents 2,285,299 and 2,509,281), which diffuses readily, incorporates Boron economically, and gives dependable, uniform results. On this or any metallurgical use of Molybdenum, Tungsten, or Boron, MCA technicians are always happy to be consulted.

AMERICAN Production, American Distribution, American Control, Completely Integrated

Offices: Pittsburgh, New York, Chicago, Cleveland, Detroit, Los Angeles, San Francisco

Sales Representatives: American Steel and Supply Co., Chicago; Edgar L. Fink, Detroit; Brumley-Donaldson Co., Los Angeles, San Francisco

Subsidiaries: Cleveland-Tungsten, Inc., Cleveland, O.; General Tungsten Manufacturing Co., Inc., Union City, N.J.

Works: Washington, Pa.; York, Pa.

MOLYBDENUM CORPORATION OF AMERICA
Grant Building Pittsburgh, Pa.

MCA

For a **high vacuum** furnace as you like it

Here's a ready-to-operate DPi high vacuum metallurgical furnace that's exactly what one manufacturer needed for his own special requirements—from the high vacuum pumping system that quickly draws vacuums on the order of 1 x 10^{-5} mm Hg, to the induction furnace itself complete with addition cup, bridge-breaking rod, and sight window.

In developing units of this kind, DPi draws on its own years of experience in solving high vacuum problems, and calls in expert manufacturing experience for solving the metal-heating problems involved. If your particular need is different, we can usually come up with the right answer.

Tilt-pouring, bottom-pouring, or interchangeable furnace assemblies—we can give you what you need and still hold high vacuum. And experience has taught us the right answers to such problems as furnace insulation under vacuum, handling of volatile components of the melt, designing for trouble-free operation and ease of maintenance.

If your interest runs to high vacuum furnaces, or to any other high vacuum applications, we will welcome an opportunity to talk with you. Just write or phone ***Distillation Products Industries,*** Vacuum Equipment Department, 607 Ridge Road West, Rochester 3, N. Y. (Division of Eastman Kodak Company)

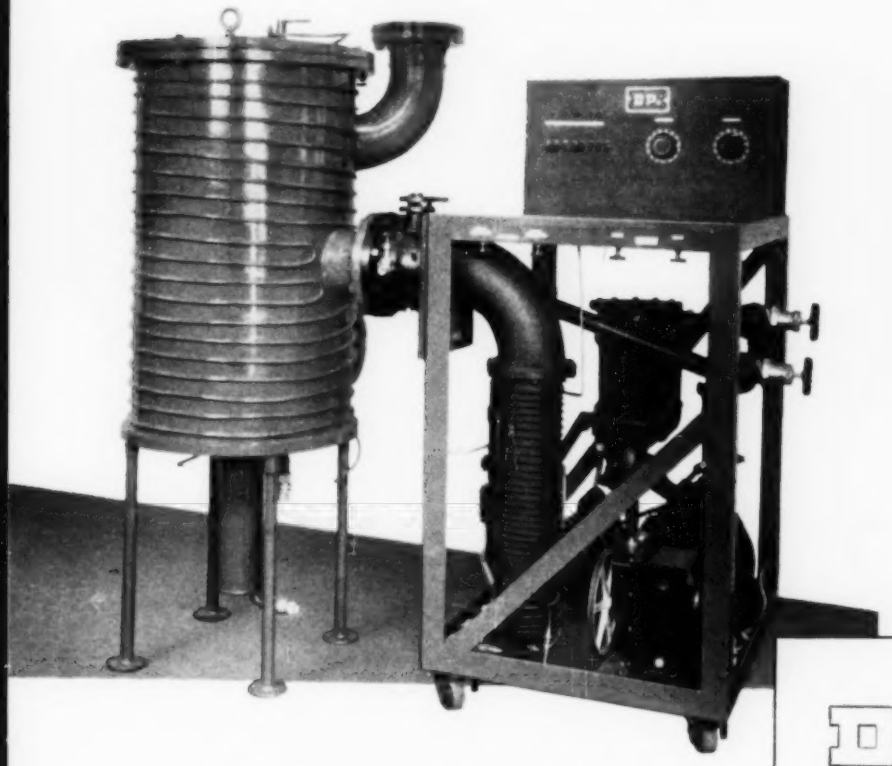

high vacuum research and engineering

DPi

Also . . . vitamins A and E . . . distilled monoglycerides . . . more than 3500 Eastman Organic Chemicals for science and industry

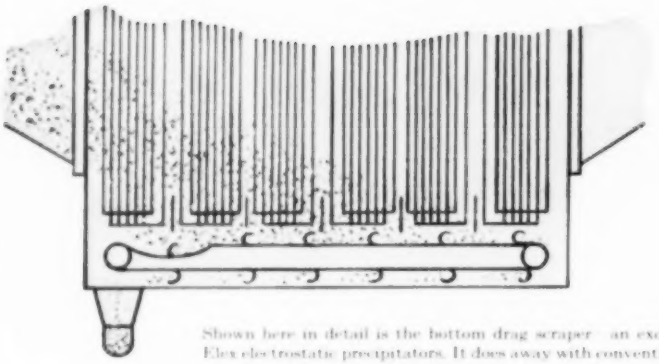

Let's be practical about precipitators

Shown here in detail is the bottom drag scraper—an exclusive feature of Koppers-Elex electrostatic precipitators. It does away with conventional hoppers and simplifies operation by removing dust continuously.

Continuous dust removal

is just one of the many advantages you get with

Koppers-Elex Electrostatic Precipitators

IN ADDITION to high recovery rates, Koppers-Elex electrostatic precipitators offer you *continuous dust removal*. The Koppers exclusive drag scraper operating on a flat bottom replaces the conventional type hopper—with its trouble of dust build-up and clogging. Dust is fed from the precipitator at a uniform rate which simplifies disposal or storage.

Other features of Koppers-Elex precipitators include separately energized multiple series fields which provide maximum collection of very fine particles. This same feature protects your investment in still another way since the outage of one field does not halt the gas-cleaning action of the precipitator.

To get maximum recovery and effective nuisance abatement, specify Koppers-Elex electrostatic precipitators. For the metallurgical field Koppers has two distinct designs: the dry dust precipitator for hearth, flash, fluidized roasters, etc. . . . and the acid mist precipitator for secondary cleaning.

IF YOU HAVE A GAS-CLEANING PROBLEM, write and outline the details for us to review. There is no obligation. Just address your letter to: KOPPERS COMPANY, INC., *Precipitator Dept.*, 262 Scott St., Baltimore 3, Maryland.

PERFORMANCE GUARANTEED!

Koppers engineers protect your investment in an electrostatic precipitator by guaranteeing both the recovery or gas-cleaning *efficiency* and the *residual content* left in the gas after cleaning. Koppers-Elex electrostatic precipitators are designed, engineered, fabricated, erected, and guaranteed *under one contract* by Koppers Company, Inc.

KOPPERS

Koppers-Elex ELECTROSTATIC PRECIPITATORS

MEET THE AUTHORS

A. E. NEHRENBERG

F. D. ROSI

J. H. KITTEL

I. R. KRAMER

R. S. BUSK

A. E. Nehrenberg (p. 181) graduated from South Dakota School of Mines, and is supervisor of research laboratory, Crucible Steel Co. of America, Harrison, N. J. He has served with Carnegie-Illinois Steel Corp., and Amertorp Corp. Bridge and bowling are enjoyed by this member of AIME, ASM, Institute of Metals, and British Iron & Steel Institute.

F. D. Rosi (p. 189), senior engineer in the metallurgical laboratory at Sylvania Electric Products, Inc., Bayside, L. I., graduated from Yale (B.E., M.E., Ph.D.). He has been metallurgist for International Silver Co., and held the rank of Lt. (jg) in the USNR. A member of AIME and Sigma Xi, his hobbies are tennis and sailing.

J. H. Kittel (p. 196), associate metallurgist, Argonne National Laboratory, Chicago, graduated from Washington State College. Formerly with NACA Lewis Flight Propulsion Laboratory, he likes camping, gardening, and photography.

I. R. Kramer (p. 197), a graduate of Johns Hopkins University (B.S., M.S., D.Eng.) is assistant to the president, Horizons Titanium Corp. After acquiring considerable industrial experience, he became head of the special alloys branch of ONR and then head of the metallurgy branch. Golf and photography are the hobbies of this member of AIME, ASM, and Sigma Xi.

R. S. Busk (p. 207) is a graduate of Colgate (B.A.) and Yale (D.Eng.) Universities, and director of the laboratory development div. of the magnesium laboratories of Dow Chemical Co., Midland, Mich. This member of AIME, ASM, and AAAS enjoys golf, chess, and bowling.

— Personnel Service —

The following employment items are made available to AIME members by a non-profit basis by the Engineering Societies Personnel Service, Inc., operating in cooperation with the Four Founder Societies. Local offices of the Personnel Service are at 2 W. 45th St., New York 18; 100 Farnsworth Ave., Detroit; 57 Post St., San Francisco; 84 E. Randolph St., Chicago 1. Applicants should address all replies to the proper box number, care of the New York office and include 6c in stamps for forwarding and returning application. The applicant agrees, if placed as a result of the Service, to pay the placement fee listed to the Service. AIME members may secure a weekly bulletin of services available for $2.50 a quarter, $1.0 a year.

POSITIONS OPEN

Control Metallurgist with some experience in induction melting of stainless and high temperature alloys, to be responsible for incoming and outgoing materials, inspection and pouring. Location, Ohio. Y6463.

Assistant Process Metallurgist, metallurgical degree, with background in nonferrous metallurgy, with some welding and brazing experience. Must be interested in solving the metallurgical problems which arise in casting, in drawing of rod and tube, and in rolling of nonferrous metals. Will advise production supervisors, and take charge of new processes, etc., from a metallurgical standpoint. Salary, $4316 to $5200 a year. Location, Connecticut. Y6460(a).

Junior Test Engineer, mechanical, to do physical testing of metals, materials, etc., for commercial laboratory. Salary, $3120 a year. Location, New York. Y6457.

Sales Engineer, preferably metallurgical graduate or some training in metallurgy, to sell metal testing equipment. Salary, $4500 to $5200 a year. Territory, New York and New England. Y6455.

Chief Engineer, over 40, mechanical or metallurgical graduate, with administrative, design, construction and plant engineering experience in metallurgical furnace field and mill construction. Salary, $15,000 a year. Location, western New York State. Y6446.

Assayer for routine smelter assaying mostly wet methods. Some opportunity for research or advancement in plant work. Moving expenses paid after three months. Salary, $3600 a year, or higher depending on experience. Location, Louisiana. Y6170.

Sales Engineer with commercial experience in nonferrous metallurgical fields, to sell aluminum, lead, zinc, bronzes, etc., for secondary smelter. Salary open. Location, New York Metropolitan Area. Y6149.

Metallurgist with at least three years' experience covering ferrous and nonferrous materials for test work, preparation of material specifications, heat treatment, welding, annealing at heavy industry manufacturing plant. Salary, $4800 to $5400 a year. Location, central Pennsylvania. Y6111.

Chemist-Metallurgist, 25 to 35, for work in nonferrous metal plant. Location, Brooklyn, N. Y. Y6535.

MATERIALS ENGINEER—Ph.D. in mechanical engineering or physical metallurgy capable of directing research and development on engineering materials problems of petroleum industry operations. Academic or industrial post-doctorate experience desirable. Location, California.

BOX B-3, JOURNAL OF METALS

METALLURGIST—Recent graduate, age 21-30, to be engaged in investigation of processing problems and maintenance of quality in Mid-Western plant producing copper and brass mill products. — Excellent opportunity to obtain knowledge of and experience in nonferrous metal processing. Please include details such as education, age, draft status, etc.

Reply to Box B-4
JOURNAL OF METALS

Physical Metallurgist
Solid State Physicist
Physical Chemist

Unusual opportunities for fundamental physico-metallurgical research in exceptionally well-equipped laboratory. Publication of work encouraged. Salary commensurate with training and experience. Attractive location, pleasant climate.

Box B-5
JOURNAL OF METALS

MEN AVAILABLE

Metallurgical Chemist, Assayer, Millman, experienced in ferrous and nonferrous analysis, assaying gold and silver, mill shift boss in cyanide mill; twenty-five years' miscellaneous experience. Age 63, single, health good, immediately available for responsible position. M-662.

NEW Streamlined AB SPEED PRESS

The most advanced design in press equipment for speed, convenience, and economy in the production of Bakelite and Transparent Molded Specimen Mounts ever presented to the metallurgist.

A revolutionary feature introduced in this new press is preheated Premolds. The preheat compartment reduces the curing time of thermosetting molds to one-third of the time usually required. It enables the operator to produce perfect Bakelite Mounts in 2½ to 3½ minutes. All necessary indicators and controls including pressure gauge, pyrometer, thermostats, timer and pilot lights are provided. No experience is required to produce perfect mounts. Automatic ram retraction saves time and effort.

The hinged press head is made with a semi-automatic lock and a hand wheel screw to close the mold securely. Heating blocks are arranged with a magnetic closure to snugly envelop the mold assembly. The interchange of thermostatically controlled heating units of 600 watt capacity is facilitated by convenient supports. Cooling blocks are located in a practical position in front of the press cabinet.

This new speed press is the result of long exacting experiment, with every effort devoted to designing the finest modern specimen press we are able to engineer.

No. 1330 AB Speed Press, complete for 1" mountings $420.00

No. 1330-2 AB Speed Press, complete for 1¼" mountings $440.00

No. 1330-3 AB Speed Press, complete for 1½" mountings $460.00

THE BUEHLER LINE OF SPECIMEN PREPARATION EQUIPMENT INCLUDES . . . CUT-OFF MACHINES • SPECIMEN MOUNT PRESSES • POWER GRINDERS • DISC GRINDERS • HAND GRINDERS • BELT SURFACERS • MECHANICAL AND ELECTRO POLISHERS • POLISHING CLOTHS • POLISHING ABRASIVES.

Buehler Ltd.

A PARTNERSHIP

165 WEST WACKER DRIVE CHICAGO 1, ILLINOIS

METALLURGICAL APPARATUS

Electro SINCE 1910

BULLETIN T-152

Electro TERCOD CRUCIBLES

MARKED SUPERIORITY CONTINUOUSLY DEMONSTRATED

Tercod — the original silicon carbide crucible, was the first major advance in crucible manufacture since the use of graphite in a clay crucible. This patented carbon bonded silicon carbide crucible, has effectively demonstrated through the years its marked superiority over other types of crucibles. It has been a major factor in the continued acceptance of crucible melting.

"Electro" is justly proud of its contribution to the foundry industries in the pioneering and development of the Tercod silicon carbide crucible. And, as foundry demands have increased for larger and better crucibles, Tercod has kept pace with improved patented glazes for protection, with a patented detachable lip for tilting furnace crucibles and currently on a new design for a crucible which offers faster melting, longer life and additional fuel economies.

Data presented in this bulletin is intended to provide the foundryman with accurate, up to date information on Electro Tercod crucibles to aid in his selection of the proper Tercod for his own conditions to achieve maximum utility at minimum cost.

Electro Refractories & Abrasives Corporation
PLANTS: BUFFALO, N. Y., U.S.A. and CAP-DE-LA-MADELEINE, P. Q., CANADA
344 DELAWARE AVENUE BUFFALO 2, NEW YORK

"S" TYPE Electro TERCOD CRUCIBLES

Recently the United States Patent Office assigned a patent to the Electro Refractories and Abrasives Corporation for a "Crucible for Metal Melting." This new invention in crucible design has been thoroughly field tested and has produced beneficial results far in excess of those anticipated.

Among the many advantages derived from this invention are:

1. *Fuel Economy.* In addition to the normal economy in fuel provided by Tercods, the new "S" type Tercod provides still further economies in fuel. The design of this crucible insures fuel combustion around the bottom and lower side wall of the crucible due to the greater combustion space in this area.
2. *Faster Melting.* Thorough, rapid combustion of the fuel at the bottom of the crucible promotes a faster melting rate because of more effective and efficient use of the fuel.
3. *Longer Crucible Life.* Many factors in the design of the "S" type crucible tend to promote long crucible life. The large combustion space means less wear on the crucible due to swirling action of the flame around the bottom and, also, helps to prevent flame impingement on the crucible. Thorough combustion near bottom of crucible helps to prevent a cyclone action at the top and so reduces slag cutting at the slag line. Premature cracking due to difference in expansion between the top and bottom of the crucible is largely eliminated.

Unfortunately, this design is not adapted to the smaller size crucibles. Advantages listed above would be just as effective but lack of stability encountered with smaller crucibles makes use of this design impractical for most small size crucibles.

BROAD BOTTOM TYPE

IMPROVED "S" TYPE

Electro TERCOD PEDESTAL BLOCKS

NO. 1 STANDARD SOLID BLOCK

NO. 2 GROOVED BLOCK

NO. 3 SECTIONAL BLOCK

NO. 4 SPECIAL BLOCK

A level, solid foundation under the crucible is necessary and the best is the most economical. The best support for a Tercod crucible is a Tercod pedestal block because the Tercod pedestal is similar in composition to the crucible. It has the same coefficient of expansion and the same ingredients so no strains are set up to cause cracking and no undesirable reactions take place. Tercod pedestal blocks have a very high crushing strength and very high refractoriness and will not soften, spall or slump at any normal furnace temperature.

Tercod pedestal blocks are furnished in four shapes as shown and can be produced in sizes from 5 inches to 20 inches in diameter and from 1 to 12 inches in height.

In ordering Tercod pedestal blocks the first dimension should refer to the diameter, the second to the height.

TERCOD CRUCIBLE LIDS

Crucible covers or lids are produced from the same refractory composition as the Tercod crucible and are used for covering the crucible to prevent oxidation and gassing of the metal in the crucible.

Lids can be furnished either with or without handles and are made in the following standard sizes: 6, 9, 12, 13, 15, and 17 inches in diameter.

TERCOD LINED CRUCIBLES

Since some alloys and the slags encountered with these alloys react with the silicon carbide in the Tercod crucible various linings have been developed to overcome this difficulty. These linings are formed integrally with the Tercod exterior of the crucible and provide a lining composition adapted to the metal being melted yet retaining most of the heat conducting and other beneficial properties of the Tercod.

The most common lining is fused alumina and it is particularly adapted to melting alloys high in nickel, chrome or iron. Even cast iron may be successfully melted in an alumina lined crucible although steel may not be melted in any Tercod since it reacts with the carbon bond.

Linings of fused magnesia, mullite, carbon and zircon are also produced for special applications.

CRUCIBLE SIZES AND CAPACITIES *for* BRASS MELTING

Crucible No.	Outside Height Inches	Top Outside Diameter Inches	Bilge Outside Diameter Inches	Bottom Outside Diameter Inches	Top Thickness Inches	Brass Water Capacity Pounds	Long Lip Type Pounds	Working Capacity Red Brass Pounds	Long Lip Type Pounds
**5	5 1/2	5 1/8	No Bilge	4 3/8	3/8	2		15.8	
*6	6 5/8	5 1/4	No Bilge	4	5/8	2.44		19.3	
*8	7 1/8	5 5/8	No Bilge	4 1/4	9/16	3.25		25.7	
10	8 1/4	6 1/4	6 3/4	5	3/4	4.5		36	
12	8 1/2	6 3/8	7	5	3/4	5.25		42	
14	8 5/8	6 1/4	7 1/4	5 1/8	5/8	6.25		50	
16	9 1/4	7	7 5/8	5 1/2	3/4	7.25		57	
18	9 1/4	7 1/2	8 1/8	5 3/4	11/16	8.5		67	
20	10 5/8	8	8 5/8	5 3/8	3/4	10		80	
25	10 7/8	8 1/4	9	6	7/8	12		95	
30	11 1/2	8 5/8	9 7/8	6 3/8	1	14		111	
35	12 1/2	9 1/4	9 7/8	6 7/8	7/8	16		127	
40	13	9 1/2	10 1/2	8 1/2	1 1/8	18		142	
45	14	9 5/8	11	8 1/8	1 1/16	21		166	
50	14 1/2	10 3/8	11 3/8	8 1/2	1 1/8	24		190	
60	15	11 1/8	12 1/8	9 1/2	1 3/16	28	23	221	182
70	15 3/4	11 3/8	12 1/2	9	1 3/16	32	27	254	215
80	16 3/8	12 1/8	13 1/8	10 1/4	1 3/16	36	31	285	246
90	17 1/2	12 5/8	13 5/8	9 1/2	1 1/4	40	35	317	277
100	17 1/4	13	14 1/4	11	1 3/8	44	38	348	301
125	17 5/8	13 1/8	14 7/8	10 5/8	1 1/8	50	44	396	348
150	19 3/8	13 7/8	15 1/4	11	1 1/4	60	53	475	420
150-S	19	14 1/2	15 1/8	8	1 5/16	60	53	475	420
175	19 3/4	14 3/8	15 3/4	11 1/2	1 5/16	70	61	553	483
200	20 7/8	15 1/2	17	12 7/8	1 1/2	80	67	633	531
225	21 3/8	15 5/8	17 3/8	13 3/8	1 1/4	90	75	712	594
225-S	21 1/4	15 1/4	17 1/2	9	1 3/8	90	75	712	594
250	21 3/4	16 1/4	17 7/8	13	1 3/8	100	85	792	673
275	23	16 5/8	18	12 3/8	1 1/2	110	95	872	752
275-S	22 1/2	16 1/2	18	9	1 3/8	110	95	871	752
300	23 1/2	16 7/8	18 1/2	13	1 1/2	120	105	950	832
300-S	23 1/2	16 5/8	18 1/4	9	1 3/8	120	105	950	832
400	25	18 3/8	20 1/8	14 1/2	1 5/16	160	148	1270	1172
400-S	24 3/4	19 1/2	20 1/4	10	1 1/4	160	145	1270	1150
*430	25 1/2	20 3/8	No Bilge	14 1/2	1 3/8	184	170	1460	1347
*430-S	25 1/2	20 3/8	No Bilge	10	1 3/8	178	164	1410	1300
*600	27 3/8	23 5/8	No Bilge	14 1/2	1 3/8	246	231	1950	1832
*600-S	27 3/8	23 5/8	No Bilge	12	1 1/2	251	236	1990	1870

**Shape A
*Shape C
All others Shape B

BOTTOM POUR CRUCIBLES (Shape E)

30	11 1/8	8 5/8	9 7/8	6 5/8	7/8	14		111	
150	19 1/2	14	15 1/8	10 1/2	1 1/2	60		475	
200	20 1/2	15	16 7/8	12 1/2	1 1/2	80		633	

DIMENSIONS AND CAPACITIES OF TERCOD CRUCIBLES *for* ALUMINUM

Crucible No.	Outside Height Inches	Top Outside Diameter Inches	Bottom Outside Diameter Inches	Top Thickness Inches	Gravity Water Capacity Pounds	Approximate Working Aluminum Capacity Pounds
1225-S	16	20 7/8	10	1 3/8	100	225
1245-S	17	20 7/8	10	1 3/8	109	245
1265-S	18	20 7/8	10	1 3/8	118	265
1290-S	19	20 7/8	10	1 3/8	129	290
1320-S	20 1/2	20 7/8	10	1 3/8	142	320
1345-S	22	20 7/8	10	1 3/8	153	345
1385-S	24	20 7/8	10	1 3/8	171	385
1400-S	25 1/2	20 7/8	10	1 3/8	178	400
1500-S	28	20 7/8	10	1 3/8	211	475
3200-S	15 1/2	20 7/8	10	1 3/8	89	200
3245-S	17	20 7/8	10	1 3/8	109	245
3260-S	17 1/2	20 7/8	10	1 3/8	116	260
3265-S	18	20 7/8	10	1 3/8	118	265
3290-S	19	20 7/8	10	1 3/8	129	290
3320-S	20 1/2	20 7/8	10	1 3/8	142	320
3345-S	22	20 7/8	10	1 3/8	153	345
3385-S	24	20 7/8	10	1 3/8	171	385
3400-S	25 1/2	20 7/8	10	1 3/8	178	400
3500-S	28	20 7/8	10	1 3/8	211	475
If above Crucibles are made with old style broad bottom, the bottom diameter is 14"; If above Crucibles are made with long lip for tilting furnaces, deduct 40 lbs. from working Aluminum Capacity. Crucibles above are all shape C.						
5255-S	14 1/2	23 3/8	12	1 1/2	100	225
5375-S	18 1/2	23 3/8	12	1 1/2	147	330
5435-S	20 1/2	23 3/8	12	1 1/2	167	375
5550-S	22 1/2	23 3/8	12	1 1/2	191	430
5600-S	27 3/8	23 3/8	12	1 1/2	251	565
7700-S	31 1/4	23 3/8	12	1 3/8	293	660
If above Crucibles are made with old style broad bottom, the bottom diameter is 14"; If above Crucibles are made with long lip, working capacity of aluminum is decreased by 30%. Crucibles above are Shape C.						
6335	17 1/2	25 3/4	20 1/2	1 1/2	169	380
6400	18	25 7/8	20 1/2	1 1/2	175	395
6425	18 3/8	26	20 1/2	1 1/2	189	425
6500	23	27	20 1/2	2 1/4	218	490
6590	25	27 5/8	20 1/2	2 1/4	244	550
6650	27 3/8	28 3/4	20 1/2	2 1/4	290	650
If above Crucibles are made with long lip, the working aluminum capacity is reduced by 90%. Crucibles in above series are Shape A and are not available in small bottom "S" type.						
10630-S	23 1/2	28 1/2	15	2 1/8	252	570
10720-S	26 1/8	27 3/4	15	2 1/8	290	650
10765-S	27 1/4	27 1/2	15	2 1/8	306	690
10810-S	28 3/4	27 1/4	15	2 1/8	328	740
10850-S	30 1/4	26 1/4	15	2 1/8	348	785
10900-S	31 1/2	26 1/4	15	2 1/8	356	800
10000-S	34 1/2	25 1/4	15	2 1/8	399	900
11100-S	37	25	15	2 1/8	444	1000
If above Crucibles are made with long lip, the working aluminum capacity is reduced by 130%. Crucibles in above series are shape B and are available only in small bottom type. Bilge Diameter is 28 1/8.						
20890-S	30	30 3/4	15	2	395	890
21000-S	33	30 3/4	15	2	444	1000
21115-S	35	30 3/4	15	2	495	1115
If above Crucibles are made with long lip, the working aluminum capacity is reduced by 150%. Crucibles above are shape C and are available only in small bottom type.						
200-B	15	22 1/4	12	1 1/2	89	200
250-B	17 1/2	22 1/2	12	1 1/2	110	250
300-B	18 1/2	22 1/2	12	1 1/2	133	300
350-B	16	27 1/8	12	1 3/4	156	350
400-B	17 1/2	27 3/8	12	1 3/4	179	400
450-B	19	27 5/8	12	1 3/4	200	450
500-B	20 1/2	28	12	1 3/4	222	500
550-B	21 1/4	28	12	1 3/4	244	550
600-B	22 3/4	28 1/2	12	1 3/4	267	600
700-B	22	34	15	2	311	700
800-B	23 3/4	34 1/4	15	2	356	800
900-B	25 1/2	34 1/2	15	2	399	900
1000-B	28	34 3/4	15	2	444	1000

Crucibles above are shape D and cannot be produced with long lip.

Electro TERCOD CRUCIBLES *for* ALUMINUM

Tercod Crucibles offer the following advantages for all melting and holding operations for aluminum and aluminum alloys.

1. *Cleanliness:* No component of the Tercod crucible is dissolved or will react with aluminum or any aluminum alloy; consequently, there is no undesirable pickup of iron or any other material.

2. *Economy:* Crucible melting is inherently economical. Low capital investment, low overhead charges and low maintenance costs result in cost-savings over other melting methods. Coupled with the long life of Tercods and fuel savings achieved through permanent high heat conductivity, the ultimate in low cost melting is obtained.

3. *Versatility:* Tercod crucibles are efficiently used for continuous or intermittent melting, holding or a combination of melting and holding with all the aluminum alloys and heated by oil, gas or electricity. Constant research in compositions, glazes and design has resulted in a product capable of satisfactorily meeting any condition.

The continuing acceptance of crucible melting has undoubtedly been promoted by the availability of the Tercod crucible. For clean, efficient, economical melting or holding of aluminum, there is a shape, size and composition to meet any condition.

TERCOD DETACHABLE LIP *for* TILTING FURNACE CRUCIBLES

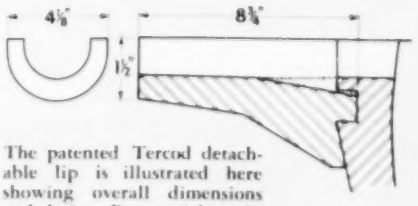

The patented Tercod detachable lip is illustrated here showing overall dimensions and design. For special applications certain other designs are available on special order.

OTHER *Electro* PRODUCTS for NON-FERROUS FOUNDRIES

CARE AND HANDLING OF YOUR *Electro* TERCOD CRUCIBLES

Handle your crucible carefully. Even a TERCOD crucible will crack or break if dropped or subjected to severe physical shock.

Store crucibles in a warm dry place — moisture will not damage TERCOD crucibles as much as clay graphite crucibles, but it is harmful.

Avoid wedging or dropping ingots during charging. Extra care will pay big dividends in crucible life. Also, cold ingots charged into hot metal may cause a "chill-back," which might cause the crucible to crack.

Avoid strongly basic fluxes which will attack the crucible and shorten its life.

Uniform and sufficient heat distribution around the crucible is essential. Uneven heat sets up strains which result in crucible failure.

Repair furnace linings and keep them in good shape. Uneven lining wear results in uneven heat distribution on the crucible.

The furnace atmosphere should be maintained from neutral to slightly oxidizing. Poor fuel economy and shortened crucible life will result from strongly oxidizing or strongly reducing atmospheric conditions.

Empty the crucible completely before allowing it to cool. With aluminum, scrape the crucible after each heat to prevent oxide build-up.

See that the crucible has good even support at all times — on the pedestal block, in the tongs and in the shanks.

When heating the crucible from room to operating temperature, the danger of cracking from localized thermal shock can be avoided by taking sufficient time to bring the crucible up to temperature slowly to avoid unnecessary strains.

It is essential with "sealed-in" units to allow for free expansion of the crucible. Therefore, do not clamp the cover too rigidly.

Tight squeezing is harmful and unnecessary.

Tongs should clear top of crucible and should cradle the crucible evenly below bilge. This is very important.

LININGS

Electro KELLOGG FURNACE LININGS

Inside Diameter Inches	Outside Diameter Inches	Outside Height Inches	Number In Crate	Inside Diameter Inches	Outside Diameter Inches	Outside Height Inches	Number In Crate
15	20	6 & 9	8	23	28	6 & 9	8
16	19 1/2	4 1/2	2	23	27	4 1/2	2
17	22	6 & 9	8	24	29	6 & 9	8
17	21	4 1/2	2	24	28	4 1/2	2
18	23	6 & 9	8	26	31	6 & 9	8
18	22	4 1/2	2	26	30	4 1/2	2
19	24	6 & 9	8	27	32	6 & 9	8
19	23	4 1/2	2	27	31	4 1/2	2
20	25	6 & 9	8	28	33	6 & 9	12
20	24	4 1/2	2	30	35	6 & 9	12
21	26	6 & 9	8	31	36	6 & 9	12
21	25	4 1/2	2	32	37	6 & 9	12
22	27	6 & 9	8	34	39	6 & 9	12
22	26	4 1/2	2	36	41	6 & 9	12

COVERS

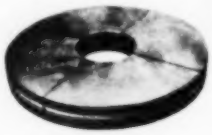

Electro KELLOGG CRUCIBLE FURNACE COVERS

Outside Diameter Inches	Hole Size Inches	No. of Sections
20	6 & 7	1 pc.
22	6	3 pc.
24	6 & 8	3 pc.
25	6 & 8	4 pc.
26	6 & 8	4 pc.
28	6 & 8	4 pc.
30	6 & 8	4 pc.
32	8	4 pc.
36	8	6 pc.
40	10	6 pc.

Others Available on Special Order

CEMENTS

Electro BUFFALO PATCH

Composed of silicon carbide grain, ceramic bonded for strength, hardness and refractoriness. No. 1 — High purity, fine grained, for any kind of patching. Will withstand 3250°F. No. 2 — General purpose, wide range of uses for temperatures up to 3250°F. No. 3 — Coarse grained for ramming only. Temperature range up to 3400°F. For complete information on Electro High Temperature Cements, write for Bulletin C-946.

Electro INSULATING CEMENT

This rugged cement with great mechanical strength minimizes radiation losses and prevents overheating of furnace shell. Forms hard, porous structure between shell and lining. Holds lining sections firmly together. Prevents flame leaks. Highly refractory. Superior to diatomaceous earth.

Electro Refractories & Abrasives Corporation

Manufacturers SPECIAL PURPOSE GRINDING WHEELS • SPECIAL REFRACTORIES and CEMENTS • STOPPER HEADS • ELECTRO-CARB SILICON CARBIDE BRIQUETS • ELECTRO-CARB Silicon Carbide

344 DELAWARE AVENUE BUFFALO 2, NEW YORK

REGIONAL WAREHOUSE LOS ANGELES 58, CALIF.

New Products

New Products | New Literature | New Services

For Further Information or Literature on any Product, Fill in the Coupon and Send to JOURNAL OF METALS
Students are Requested to Apply Directly to Manufacturers for Bulletins and Information

1—TINPLATE GAGE: Research and Control Instruments Div., *North American Philips Co.* has a new X-ray gage for measuring the thickness

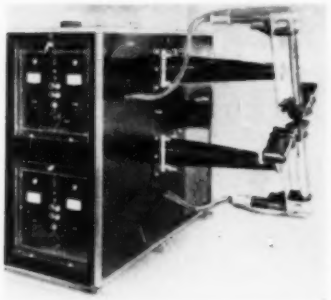

of tinplate coatings. It is designed to operate on 200-240 v, single phase, ac, 50 or 60 cycles, with full-wave rectification. It will handle tin coatings ranging in thickness from 0 to 150 micro-in. Readings are on a printing register, which indicates counts from top and bottom gages and gives the measurement totals simultaneously.

2—CHROME PURIFIER: A portable version of the Chrome Purifier, for recovering and purifying contaminated chrome plating baths, has been announced by *Illinois Water Treatment Co.* The ILLCO-WAY unit is available in four sizes for both portable and permanent installations. The unit operates on an ion exchange principle.

3—HOBBING DIE STEEL: Die casting diemakers and users now have a die steel that approaches hobbing ease of regular hobbing irons yet compares in strength to 5 pct chrome hot work die steel. Super Samson, the steel developed by *Carpenter Steel Co.*, is primarily for dies for diecasting aluminum and zinc.

4—INDUCTION HEATER: Multiple 2.5 kw units combined in a single cabinet are available for induction heating applications. Units can be removed and replaced, heating locations can be varied, and the unit fills a need between existing low power and medium high power machines. Input per section is 4 kva at 220 v, 60 cycles, single phase. Accessory equipment is supplied with the unit by *Induction Heating Corp.*

5—pH METER: For quick, accurate measurement of hydrogen-ion concentration, the Research and Control Instruments Div., *North American Philips Co.*, has introduced the Philips Universal pH Meter. It is designed for all pH and rH work, for potentiometric titrations, and for oxidation reduction-potential investigations. Measuring accuracy is 0.01 pH or 0.5 mv, it has a range of 0 to 14.15 pH and 0 to 1415 mv, and operates on 60 cycle ac.

6—BLAST CLEANING: A new wet blast machine, the Liquamatte, for work for which dry blasting is too severe, such as thin edges and sharp corners, has been developed by *American Wheelabrator & Equipment Corp.* Dies, rubber molds, plastic molds, and glass molds have been cleaned and finished by this equipment. Abrasive action can be controlled through the size of abrasives, ranging from 80 to 2500 mesh. The machine has a vertical pump for slurry recirculation, and it has many features for ease of operation, maintenance, and work accuracy.

7—TUBE BENDER: For making perfect offsets and bends up to 180° in $\frac{3}{8}$, $\frac{1}{2}$ and $\frac{5}{8}$ in. OD copper, brass, steel and other light gage tubing, *Tal Bender, Inc.*, has introduced a new tube bender. It is a hand tool, fast and simple to operate, and no vise or fixtures are needed. It weighs 5 lb.

8—FLOWMETER: Eliminating inaccurate bubble counting and watch timing, a line of precision flowmeters has been announced by *F. W. Dwyer Mfg. Co.* Changes in flow rates of gas or air in laboratory test work are readily observed with the unit. The standard unit includes a built-in control valve, and special scale ranges are available.

9—ELECTRODE HOLDER: Automatic electrode holders for electric

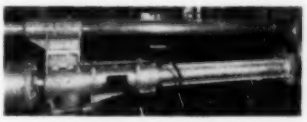

furnaces used in steel melting permits automatic slipping of the electrodes, reducing furnace down-time. *Whiting Corp.*

10—SWITCHGEAR: A new standard line of metal-clad switchgear, ranging in ratings from 2400 to 13,800 v, 150 to 500 mva, has been announced by *General Electric Co.* New design features include the magne-blast circuit breaker with interchangeable parts for different ratings, the electro-mechanical control device, improved insulating material, and a positive-acting mechanical interlock in the breaker elevating mechanism.

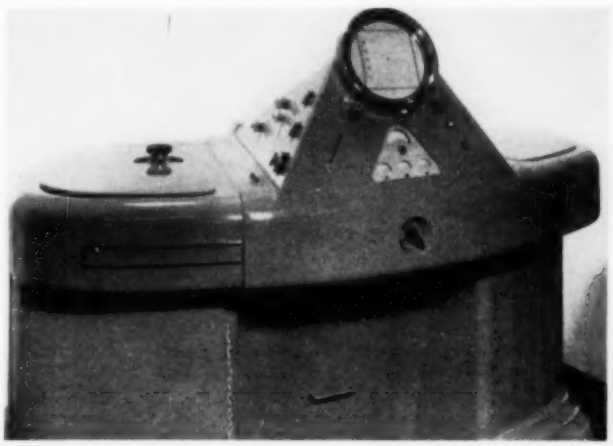

11—ELECTRON MICROSCOPE: A new electron microscope with continuous screen magnification from 1000 to 60,000 diam and capable of producing micrograms of 30 Angstroms resolution or better has been announced by Research and Control Instruments Div., *North American Philips Co.* Immediate changeover for electron diffraction patterns of pre-selected portions of a specimen is possible without change of pole pieces, specimen transfer, or re-evacuation. It has a large field and permits single photo exposures of areas that might require mosaics.

12—ALUMINUM TUBING: Utilitube, a general purpose aluminum coiled tube made of alloy B50S-O, is offered by *Aluminum Co. of America*. It combines low cost per foot, easy workability, and high fatigue strength. Air, vacuum, and hydraulics lines are recommended uses. It is sold in lengths up to 1000 ft or more, depending on size, and has good flaring and forming characteristics. It improves in mechanical properties at sub-zero temperatures, even as low as −320 F.

13—LIMIT SWITCH: A rotating type limit switch for applications where reversing operation is to be coordinated with the number of revolutions of a motor shaft or driven equipment has been announced by *General Electric Co.* The switch can be used to control motor-operated doors and windows, valves, baling operations, machine travel limits, etc. It can be adjusted to operate from 4 to 110 turns of the driving shaft with 5 turns over-travel in either direction.

14—DIESEL PLANT: A new 3000-w diesel electric plant powered by an air cooled full diesel Onan engine is announced by the *D. W. Onan & Sons, Inc.* Push-switch control for electric cranking, manual compression release, and an electrically heated glow-plug for cold weather starting are provided. Fuel consumption is about 0.155 gal per kw-hr at full rated load, and the unit generates 115-v, 60 cycle, single phase current. Other ac models in single phase produce 230 v and 115 to 230 v.

15—COIL CRADLES: Easy-Load is a new motor driven, automatic coil stock cradle of 3000 lb capacity that will take coiled sheet stock up to 48 in. OD and 15 in. wide. Built by *Rouse Machinery & Mfg. Co.*, the cradle has an actuating arm that operates on the inside or outside of the slack loop, and rolls are mounted in each of two individually controlled guide plates.

Free Literature

20—DRYERS: Steam tube, direct heat counterflow, direct heat parallel flow, and indirect heat hot air dryers manufactured by *Hardinge Co., Inc.*, are described and illustrated in a new brochure. A list of materials successfully processed in these Ruggles-Coles Rotary Dryers is included.

21—MOLD PLUGS: A revised catalog section covering National Carbon Mold Plugs has been issued by *National Carbon Co.*, listing advantages of carbon mold plugs, stock sizes, standard sizes supplied on order, and illustrating applications of these products. The information is listed as Catalog Section S-5600.

22—MOISTURE TELLER: Dessicators, moisture testers, speed ovens, and several laboratory items are described in a 12-p. illustrated booklet published by *Harry W. Dietert Co.*

23—OPEN HEARTH REFRACTORIES: Bulletin 751 of *Geo. P. Reintjes Co.* describes the company's universal nosing arch, designed for use in almost any heating furnace or the fantail nosing of open hearth furnaces. The arrangement of refractories around the arch shapes, along with the fastening arrangements are shown.

24—TABLETTING PRESS: A new multiple-screw extruder for compounding, extruding, coloring, and pelletizing in pharmaceutical, powder metal, and plastic preform industries is described in catalog No. 800, published by *F. J. Stokes Machine Co.* The presses are single punch and rotary, mechanical and hydraulic, and will produce pieces of ⅛ in. diam up to 6x10 in. in size at rates of 8 to 4000 per min.

25—HYDRAULIC FLUID: A 12-p. booklet describes properties and performance of Pydraul F-9, a nonflammable type hydraulic fluid. The fluid, developed for use in die casting machines, hydroelectric turbines, hydraulic presses, etc., is finding wide application in similar operations where a flammable pressure transfer fluid is hazardous. *Monsanto Chemical Co.*

26—FLUE GAS: An indicating and recording flue gas analyzer, developed by *Minneapolis Honeywell Co.*, Brown Instruments Div., is described in Instrumentation Data Sheet No. 1015-3a. The company's composite catalog No. 5000 consists of 28 pages of description of principal instruments, control devices, and related components.

27—REFRACTORY TABULATOR: Tabulations and formulae for calculating refractory requirements in building, repairing, or relining furnaces has been published by *Ironton Fire Brick Co.* Standard series fire brick, cupola blocks, wedge, key, arch and circle brick are listed, with unit dimensions and quantities needed to turn a circle. A table of temperature end points of pyrometric cones, and other data are included.

28—CRUCIBLES: Bulletin T-152, published by *Electro Refractories & Abrasives Corp.*, describes Tercod Crucibles, the original silicon carbide crucible. Sizes and capacities of crucibles for brass and aluminum, as well as other products for nonferrous foundries including furnace linings, crucible covers, patching cement and insulating cement, are described.

29—PRECISION TUBING: Fine seamless tubing to precision tolerances, available in sizes from 0.010 to ⅝ in. OD, in metal of almost any desired analysis is described in a catalog released by *Uniform Tubes*. Pointer tubing, some finer than hair, is described, as well as Metal-Shielded Wire.

30—SPECIMEN POLISHING: A 4-p. folder from *Buehler, Ltd.*, describes the advantages of diamond abrasives for polishing metallurgical specimens. Diamet-Hyprez is offered in three different particle sizes, all in 5 g and 18 g gun applicators.

31—ROOF TEMPERATURES: Temperature control of open hearth furnace roofs by means of *Minneapolis Honeywell Regulator Co.*, Brown Instrument Div.'s Radiamatic detecting unit coupled with the ElectroniK potentiometer controller, is described in bulletin 6.4-2a. The system is designed to protect against overheating or burning roofs of open hearths.

Journal of Metals
29 West 39th St
New York 18, N. Y.

February

Please send me: More information ☐ Free Literature ☐ Price Data ☐ on items indicated

1	2	3	4	5	6	7	8	9	10
11	12	13	14	15	16	17	18	19	20
21	22	23	24	25	26	27	28	29	30
31	32	33	34	35	36	37	38	39	40

Name Title
Company
Street
City and Zone State

Advertisement

ELECTROMET *Data Sheet*

A Digest of the Production, Properties, and Uses of Steels and Other Metals

Published by Electro Metallurgical Company, a Division of Union Carbide and Carbon Corporation, 30 East 42nd Street, New York 17, N. Y. • In Canada: Electro Metallurgical Company of Canada, Limited, Welland, Ontario

How VANADIUM improves engineering steels and helps conserve critical alloys

In these critical times when many alloying materials are scarce, you may be able to use vanadium to good advantage. Steels alloyed with vanadium meet most of the mechanical specifications for low-alloy engineering and structural steels. In fact, vanadium can often be used in engineering steels to replace at least part, if not all, of certain alloys now in critical supply.

The metallurgy of vanadium is well known. Small additions of vanadium—0.10 to 0.30 per cent—can be used effectively to give steel extra strength, toughness, and resistance to fatigue and wear. It improves engineering steels by increasing their yield strength without sacrificing ductility. The uniformly fine grain size of vanadium-bearing steels makes them tough and resistant to abrasion, fatigue, and impact.

Better Mechanical Properties

In the following table are typical analyses for carbon-vanadium and chromium-vanadium steels that are suitable for most applications where low-alloy, high-strength steels are required. The carbon-vanadium steel is compared with plain carbon steel, and the chromium-vanadium steel, with chromium-molybdenum steel. Note the excellent properties of the vanadium-bearing steels.

Fig. 1—Vanadium increases the strength, toughness, and wear resistance of engineering steels for many machine parts, such as this large crankshaft.

Improves Cast Iron

A small addition of vanadium, usually from 0.10 to 0.25 per cent, refines the grain of cast iron, and materially increases its strength and hardness. Moreover, vanadium may be used in cast iron to replace at least part, if not all, of certain alloys that are now in short supply.

Vanadium in Rimmed Steel

An addition of approximately 1 lb. of vanadium per ton of steel produces non-aging characteristics in a rimmed steel. These non-aging properties, together with improved deep-drawing characteristics and the good surface inherent in rimmed steels, make these steels of particular interest at the present time.

Grades of Ferrovanadium

ELECTROMET produces ferrovanadium containing 50 to 55 per cent vanadium for the production of vanadium-bearing steels and irons. The alloy is produced in three grades with maximum 0.25, 0.50, or 3.00 per cent carbon and maximum 1.50, 2.00, and 8.00 per cent silicon, respectively. Each grade is specially adapted to fill the different requirements of iron- and steel-making.

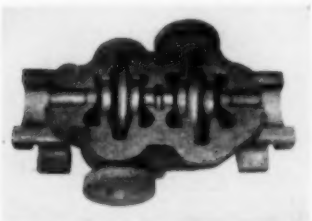

Fig. 2—Steel and iron castings treated with small additions of vanadium have high ductility and greater toughness and impact resistance.

Write for a copy of the booklet, "ELECTROMET Products and Service," which gives helpful information about the use of ferrovanadium and other alloying metals that ELECTROMET supplies. The booklet may be obtained from any ELECTROMET office in Birmingham, Chicago, Cleveland, Detroit, Los Angeles, New York, Pittsburgh, or San Francisco. In Canada: Welland, Ontario.

Properties of Vanadium Steels Compared With Other Engineering Steels

Typical Analysis, %	Carbon Steel	Carbon-Vanadium Steel	Chromium-Molybdenum Steel	Chromium-Vanadium Steel
Vanadium	—	0.16	—	0.16
Carbon	0.50	0.49	0.50	0.50
Manganese	0.71	0.77	0.80	0.79
Silicon	0.19	0.15	0.30	0.31
Chromium	—	—	0.95	0.98
Molybdenum	—	—	0.20	—
Annealed and Furnace-Cooled				
Tensile Strength, psi	90,600	100,000	100,000	99,500
Yield Point, psi	48,900	66,000	50,000	64,100
Elongation in 2 in., %	23.3	25.0	23.0	28.4
Reduction of Area, %	37.8	49.1	45.0	59.0
Izod Impact, ft.-lb.	13.5	26.0	17.0	44.0
Quenched and Tempered				
Tensile Strength, psi	134,900	134,500	232,000	232,800
Yield Point, psi	110,800	128,000	214,500	224,200
Elongation in 2 in., %	18.3	18.3	10.0	10.4
Reduction of Area, %	54.1	56.6	39.0	43.1
Izod Impact, ft.-lb.	54.0	65.0	12.0	12.0

The term "Electromet" is a registered trademark of Union Carbide and Carbon Corporation.

Books for Engineers

Chemistry of Uranium—The Element, Its Binary and Related Compounds, by J. J. Katz and E. Rabinovitch (National Nuclear Energy Series, Div. VIII, Vol. 5). *McGraw-Hill Book Co.* $7.25, 609 pp.—This first volume of a two volume treatise contains a detailed summary of the properties of the element uranium, its occurrence in nature, extraction from ores, and the physical and chemical properties of uranium metal. Binary compounds of uranium with H, O, N, and the halogens, among others, are discussed with methods of preparation and physical properties such as crystal structure, thermochemistry and volatility. A large proportion of the material is based on laboratory research of the Atomic Energy Project, into which has been integrated the results of a critical survey of the open literature.

Theory of Perfectly Plastic Solids, by W. Prager, P. G. Hodge, Jr. *John Wiley & Sons.* $5.50, 264 pp.—An introduction, on the intermediate level, to a branch of the general theory of plasticity. Although treating mathematical theory, the material has been chosen for its usefulness to the research engineer and the student of engineering. For example, the behavior of trusses, beams, slabs, etc., under various forces is considered as well as certain processes such as metal punching and extrusion.

Industrial Furnaces, Vol. I, by W. Trinks. *John Wiley & Sons.* $10.00, 526 pp.—This fourth edition of Vol. I has been thoroughly revised, and a large part completely rewritten. The work is a comprehensive exposition of the principles that underlie furnace operations and the design of furnaces for heating and annealing metals. The capacity, fuel economy, strength and durability of furnaces and the movement of gases in them are discussed theoretically and practically. Heat saving appliances are dealt with in detail.

Corrosion Guide, by E. Rabald. *Elsevier Publishing Co.* $12.50, 629 pp.—The major part of this practical reference work is composed of tables showing the interaction phenomena between more than 40 important construction materials (metallic and nonmetallic) and some 250 corrosive agents. Corrosion fundamentals are discussed in an introductory section, and a table of physical properties of materials involved is provided.

Manufacturing Equipment and Processes, by C. W. Lytle, A. F. Gould. *International Textbook Co.* $6.50, 759 pp.—Third edition of a useful survey of modern machine tools and fundamental manufacturing processes, intended for the engineer who needs to know production machinery with a view to selection or application for economic production. Essential operating principles are stressed, limitations in application are pointed out, and economic considerations are discussed. Photographs and explanatory drawings are used as needed.

Materials Buying Manual, by H. A. Knight. *Conover-Mast Publications.* $4.50, 340 pp.—Basic facts are given concerning a wide range of commodities used in industry covering general description, properties, production methods, commercial grades, uses, etc. Written primarily for industrial purchasing agents, the book is also useful as a general reference.

Gas Turbine Theory, by H. Cohen, G. F. C. Rogers. *Longmans, Green & Co.* $5.75, 291 pp.—The book contains chapters on adaptability of gas turbines, a study of the performance of various cycles, gas dynamics, methods of estimating the design-point performance of shaft power gas turbines and turbo-jet engines, theory of centrifugal and axial compressors, combustion systems and turbines, and closes with an estimation of gas turbine performance over the whole operating range.

Electro-Plating, by S. Field, A. D. Weill. *Pitman Publishing Corp.* $6.00, 346 pp.—The object of this book is to provide the practical plater with a review of the technical advances in his field. Chapters are devoted to fundamental principles, and practical information is given for the deposition of specific metals and alloys and for the testing of electrodeposits.

Aircraft Materials and Processes (Pitman Aeronautical Engineering Series), by G. F. Titterton. *Pitman Publishing Corp.* $5.00, 359 pp.—Essential information on materials and processes used in the construction of aircraft is described from a utilitarian point of view. The data are mainly from government sources and the SAE handbook.

Combustion, Flames and Explosions of Gases, by B. Lewis, G. von Elbe. *Academic Press, Inc.* $13.50, 795 pp. Part I of this treatise deals with the chemistry and kinetics of the reactions between oxygen and fuel gases. Part II provides an exhaustive treatment of flame propagation, covering combustion and detonation waves, ignition, fuel-jet combustion, and flame photography. Part III examines the state of the burned gas, and Part IV discusses the relation of the foregoing to a variety of technical combustion processes.

FBI Register of British Manufacturers, published for Federation of British Industries by Kelly's Directories Ltd. and *Iliffe & Sons Ltd.* $5.90, 882 pp.—This volume provides a substantial cross-section of the most important producers of British goods over a wide range of industry. Included are a classified buyers' guide, addresses, trade associations, trade marks and trade names.

ORDER YOUR BOOKS THROUGH AIME—Address Irene K. Sharp, Book Department. Ten per cent discount given whenever possible. Order Government publications direct from the agency concerned.

PROFESSIONAL SERVICES

Limited to AIME members, or to companies that have at least one AIME member on their staffs. Rates $40 per year per inch.

ST & CO.
ENGINEERS
CONSULTANTS
METALLURGISTS
Small Jobs Welcomed
SAM TOUR & CO., INC.
Laboratories and offices
44 Trinity Place, New York 6, N. Y.
Testing—Certifying
American Standards Testing Bureau, Inc.

LEWIS B. LINDEMUTH
Consulting Engineer
140 CEDAR STREET NEW YORK 6, N. Y.
STEEL PRODUCTION
DESIGN · OPERATION · CONSTRUCTION · METALLURGY

R. S. DEAN LABORATORIES, INC.
Consulting, Research, Development
Chemistry, Electrochemistry, & Metallurgy. Laboratory Research on a Contract Basis
5810—47TH AVENUE AP 2821
RIVERDALE, MD

MAX STERN
Consulting Engineer
150 Broadway New York 7, N. Y.

T. STARLING WINTERS
Consulting Engineer
100 East Palisade Ave. Englewood, N. J.

LEWIS

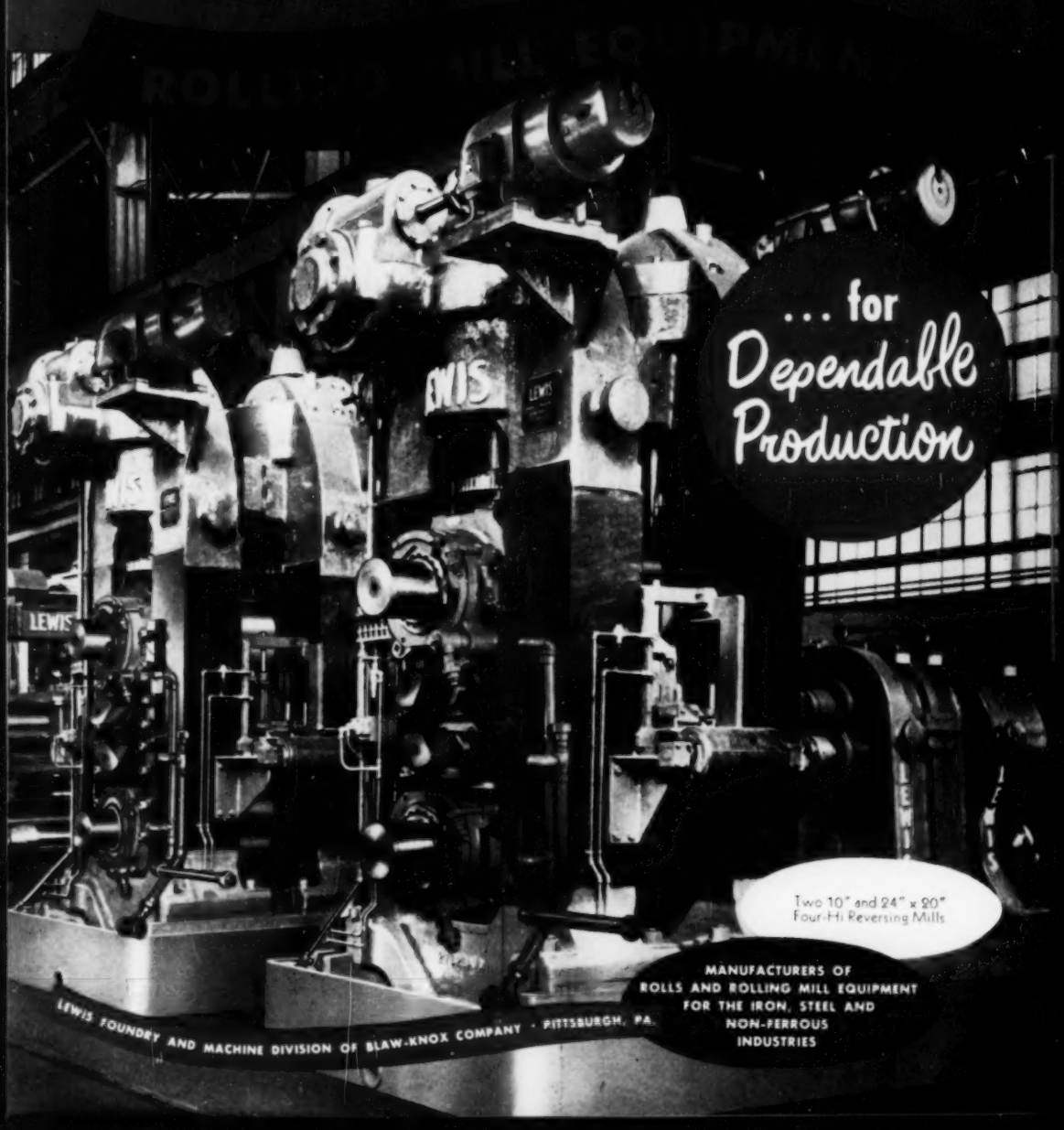

... for Dependable Production

Two 10" and 24" x 20" Four-Hi Reversing Mills

LEWIS FOUNDRY AND MACHINE DIVISION OF BLAW-KNOX COMPANY · PITTSBURGH, PA.

MANUFACTURERS OF ROLLS AND ROLLING MILL EQUIPMENT FOR THE IRON, STEEL AND NON-FERROUS INDUSTRIES

TEMPERATURES TO 2600° F.

with a HEVI DUTY
G-8156 HIGH TEMPERATURE
BOX FURNACE

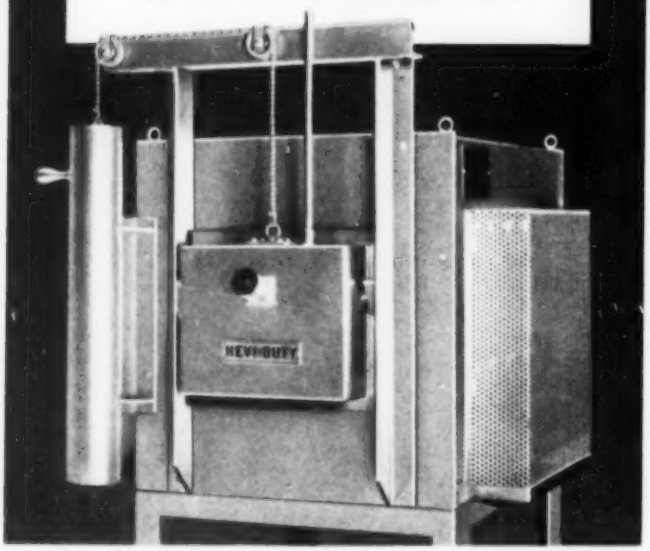

. . . for heat-treating operations requiring elevated temperatures for *RESEARCH* *CERAMICS* and *High Speed STEELS*

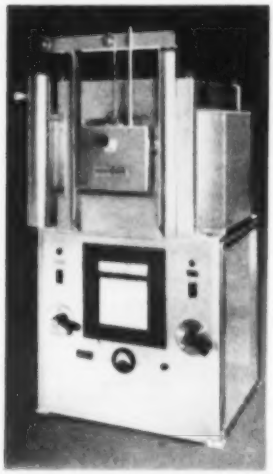

Silicon Carbide (* Globar) heating elements located above and below a sealed muffle assure even heat distribution throughout the work chamber. Connections for using a protective atmosphere are provided.

The furnace is available in several sizes with or without the control base as shown in the insert. Transformers, pyrometer and circuit breakers can be supplied as required.

Write for bulletin HD-741

* trademark, Carborundum Co.

HEVI DUTY ELECTRIC COMPANY

HEAT TREATING FURNACES **HEVI-DUTY** ELECTRIC EXCLUSIVELY

DRY TYPE TRANSFORMERS — CONSTANT CURRENT REGULATORS

MILWAUKEE 1, WISCONSIN

Industrial Notes . .

• General Electric Co. is spending $5 million to increase production of silicones at its Waterford, N. Y., plant.

• Palmoshield is a new lubricant that is expected to replace palm oil used in tinplate manufacture. It duplicates all chemical characteristics and looks, feels, acts, and handles like palm oil. Furthermore, it is made from freely available domestic materials. Tests have proved it equal to palm oil in every way.

• *Joseph T. Ryerson & Son, Inc., has acquired stocks and warehouse facilities formerly owned by the Seattle Steel Co., Seattle, and the Inland Empire Steel Co., Seattle, and Spokane. Carbon, alloy and stainless steel products, as well as brass, bronze, copper, aluminum and other products are carried in stock, as well as manufactured items such as drill rod, rock bits, drills, reamers and other equipment.*

• U. S. Steel reports progress at various new construction projects:

Fairless Works, Morrisville, Pa. —35 pct complete. One battery of coke ovens and one blast furnace in operation in early 1952, along with initial production of steel ingots. Full steelmaking capacity, 1,800,000 tons per year, will be reached by the third quarter of 1952.

Geneva Plant, Geneva, Utah—160,000 tons additional open hearth capacity in operation by first quarter, 1952. Facilities for hot rolled sheet production should be operating by second quarter, 1952.

Fairfield Works, Fairfield, Ala. —500,000 tons additional steel making capacity, in operation first quarter, 1953; and new sheet production facilities in operation by third quarter, 1953.

Orinoco Mining Co., Venezuela —First deliveries of Venezuelan iron ore, 1954.

• The Navy has completed test flights of a K-225 helicopter powered by a Boeing YT50 gas turbine. Jet gases turn the shaft of the rotor blades instead of being used for direct thrust. The engine uses low grade fuels, is half the weight of a piston engine, and is mechanically simpler.

• *Kaiser Aluminum & Chemical Corp. plans to double its proposed aluminum reduction plant and power facilities now under*

• • •

construction at Chalmette, near New Orleans. Originally, the plant was designed for 100,000 tons of aluminum per year, but the plant will be expanded before completion to 200,000 tons a year.

• Hooker Electrochemical Co., Niagara Falls, will build a new $10 million plant for producing chlorine and caustic soda at Montague, Mich. The new Hooker Type S-3A will be used to convert salt brine into chlorine, caustic soda, and hydrogen. Natural gas found during exploratory drilling indicates a possibility of sufficient gas to meet the plant's fuel requirements.

• Pennsylvania Salt Mfg. Co. is building an electrolytic chlorine-caustic soda unit at Calvert City, Ky., that will cost about $8 million. Also at Calvert City, Air Reduction Co. is building a calcium carbide and acetylene plant, and B. F. Goodrich Chemical Co. announced plans to build a vinyl chloride plant on the property adjacent to that of both Pennsalt and Air Reduction. Pennsalt will use the De Nora electrolytic mercury cell in Chlorine-Caustic soda production.

• Mallory-Sharon Titanium Corp., has established general offices in Niles, Ohio, effective Jan. 1, 1952. A titanium melting furnace, now located at Indianapolis, will be moved to Niles, and three new furnaces will be installed. Melting capacity is expected to reach 2 million lb per year in 1952.

• Two new continuous type, zone controlled, triple fired heating furnaces are being constructed for Pittsburgh Steel Co.'s new 66-in. hot strip mill at Allenport, Pa., by Rust Furnace Co. Heating capacity of each is more than 100 tons an hr.

• Westinghouse Electric Corp. is borrowing $250 million with an option for an additional $50 million from a group of institutional investors including insurance companies, pension funds, savings banks and universities. This will finance a $296 million expansion program, which includes 97 new projects including: A jet engine plant, five lamp plants, a plastics plant, expanded generator production plant, an aircraft armament plant, two electronic tube plants, and several other plant units for electronic equipment and small motors.

Microscope, camera and light source
in one convenient unit!

Leitz Panphot

Universal Metallograph

In the *Panphot*, Leitz offers the perfect combination of research microscope and reflex camera for the metallurgical research laboratory. Operating parts for observation and photomicrography are right at hand, and you can change from one to the other quickly and dependably . . . without moving from your chair. Light source, microscope and camera are permanently aligned in a single, easy-to-use instrument.

Designed to meet a wide range of needs, the *Panphot* permits the use of reflected light, darkfield illumination and polarized light. A full line of accessories is available to equip the instrument for all types of photomicrography, photomacrography and for drawing and projecting micro images. The *Panphot* takes 2¼" x 4¼" or 4" x 5" plates or cut film for both black and white and color work.

Another of the famous Leitz microscopes, recognized everywhere as the finest microscopes made anywhere.

For details, write Dept. JM

E. LEITZ, Inc., 304 Hudson Street, New York 13, N. Y.

LEITZ MICROSCOPES • LEITZ SCIENTIFIC INSTRUMENTS
BINOCULARS • LEICA CAMERAS AND ACCESSORIES

GROWTH OF A GOOD IDEA

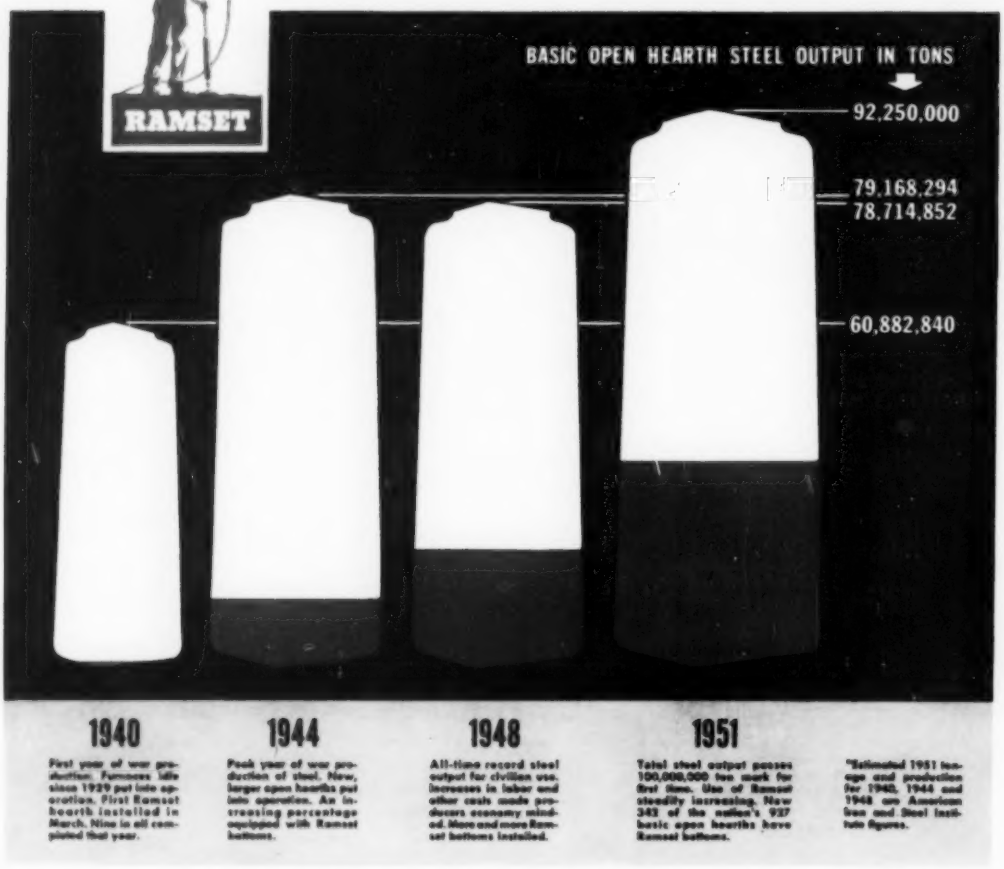
RAMSET
BASIC OPEN HEARTH STEEL OUTPUT IN TONS
92,250,000
79,168,294
78,714,852
60,882,840
1940
First year of war production. Furnaces idle since 1939 put into operation. First Ramset hearth installed in March. Nine in all completed that year.
1944
Peak year of war production of steel. Now, larger open hearths put into operation. An increasing percentage equipped with Ramset bottoms.
1948
All-time record steel output for civilian use. Increases in labor and other costs made producers economy minded. More and more Ramset bottoms installed.
1951
Total steel output passes 100,000,000 ton mark for first time. Use of Ramset steadily increasing. Now 343 of the nation's 927 basic open hearths have Ramset bottoms.
*Estimated 1951 tonnage and production for 1940, 1944 and 1948 are American Iron and Steel Institute figures.

STEEL production has nearly doubled since 1940, yet the number of open hearth furnaces has actually dropped. Larger capacities of the newer furnaces tell only part of the story. A major factor has been increased efficiency in the use of existing equipment.

Basic Refractories is proud to have contributed to this increased efficiency through the development of Ramset. Introduced in 1940 the use of this magnesia ramming mix has steadily increased until now over a third of all basic open hearths have Ramset bottoms.

There are three principal reasons why more and more rammed hearths are in use: (1) The refractory itself is right for the job—constantly improved through Basic research with the cooperation of practical steel makers; (2) Ramset rammed hearths save time, fuel, labor and brickwork compared with the traditional burned-in magnesite; (3) Correct installation procedure is supervised by skilled Basic engineers employing specially designed equipment.

We look forward to the continuing opportunity to serve the industry with more Ramset bottoms, thus to help produce more efficiently the increased tonnage of steel demanded for defense and civilian needs.

Basic Refractories Incorporated

845 HANNA BUILDING, CLEVELAND 15, OHIO

Exclusive Agents in Canada: REFRACTORIES ENGINEERING AND SUPPLIES, LTD., Hamilton and Montreal

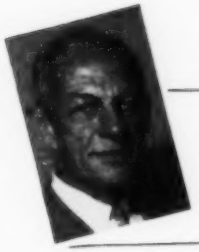

THE DRIFT OF THINGS

by Edward H. Robie

MANY engineers currently are working harder than usual, in part because of the demands being made upon them for increased production in the war effort, and in part because engineers are in short supply so that there is more to do for those who are available. In some instances the question has come up as to what additional payment, if any, should properly be made for overtime work, and to what extent is such payment legally permitted under the rules of the Salary Stabilization Board.

Most engineers employed in an executive, administrative, or outside salesman capacity are not paid for overtime. They are paid for doing a job instead of for the hours they put in, and are free to do all the unpaid home work they feel they should do after dinner, as well as to do a bit of thinking and worrying during wakeful hours in bed. But engineers employed in a strictly professional capacity normally have standard office hours. Some employers pay for overtime and some don't. Their practice as it existed on Jan. 25, 1951 may be continued. In the absence of such practice at that time, the Salary Stabilization Board says that the engineer may now receive additional compensation up to his straight-time rate for an extended work week. No formal approval of the Board is required. "A professional engineer," in the mind of the Board, "is a person employed in a professional capacity, who, by reason of his special knowledge of the mathematical and physical sciences and the principles and methods of engineering analysis and design, acquired by professional education and practical experience, is qualified to practice engineering."

Inducted Engineers

A letter from a young man just inducted into the service and fearful that his engineering training is not going to be utilized reached us last week from Fort Riley, Kan. The AIME, cooperating with the other Founder Societies, is doing what it can, through the Engineering Manpower Commission, to see that engineers are not being wasted in the military establishment. So we passed this young man's letter along to T. A. Marshall Jr., executive secretary of that Commission.

Mr. Marshall tells us that the normal procedure now being followed by the Army in handling Selective Service inductees is to have them first complete 16 weeks of basic training before assignment to specialized categories. During that time they are classified. If one has an engineering degree he should be classified as scientific and engineering personnel at the end of the basic training period. He should then be transferred to a technical detachment and assigned an MOS (Military Occupational Specialties) reflecting his education.

If a young man is looking for a commission, it might be added that the current policy in the Army is to transfer to OCS (Officer Candidate School) applicants for commissions in the infantry only. The local unit commander can give information on this point, based upon the aptitude shown in tests. In view of the current shortage of engineers, it is believed that a young man should seriously consider remaining in enlisted status unless he can obtain a commission in a branch of the service that can make full use of his technical skills. His work may thus be more to his liking even if his uniform is not.

New York or Atlantic City?

In which place is it preferable to hold the annual meeting of a professional society like the AIME—New York or Atlantic City? That is, a winter meeting. The American Society of Mechanical Engineers has held its recent meetings at Atlantic City, with increasing attendance and satisfaction. The American Institute of Chemical Engineers chose Atlantic City for its recent December annual meeting. Only twice has the AIME ever met in this famous seashore resort: in 1898 and 1904.

Chief advantages of going to Atlantic City over New York are that technical sessions are better attended, there being little else to do there in Winter; the cost to members is less, and hotel facilities are better adapted to a large meeting. As to cost, take a banquet, for instance. The Chalfonte—Haddon Hall, which caters especially to winter conventions, charges about $7 for a banquet dinner of standard quality. A similar dinner at the Statler in New York would cost about $8.50, and about $10.50 at the Waldorf-Astoria. (The charge for tickets is somewhat greater than this because of the cost of music, programs, flowers, and other incidentals.) Rooms, too, are somewhat less at Atlantic City, two in a room being accommodated for about $7 per day each, compared with $7 to $10 at a headquarters hotel in New York. On the other hand, AIME headquarters is put to some extra expense for staff travel, food and lodging, and members living in New York and environs are forced to pay a hotel bill. New York, of course, has more varied amusements to offer, plenty of big stores, and the glamour of a big city.

The choice may be discussed at the forthcoming meeting in New York. In the meantime if any reader cares to express an opinion one way or the other we shall be glad to hear it.

College Scholarships

Most parents of children in the later stages of high school find it necessary to give some consideration to the cost of a college education. Although salaries have increased substantially it seems that the cost of the necessities of life, such as food, housing, and maintaining the family automobile, have gone up even more, so the problem of financing the children's education is as acute as ever. Many overlook the possibility of scholarships, or feel that only a student at or near the top of his class has a chance to get one. As a matter of fact, close to 150,000 scholarships and more than 15,000 fellowships, worth some $42,000,000, are available in 1200 American colleges and universities.

Those who are interested should send 55c to the Superintendent of Documents, Government Printing Office, Washington 25, D. C. for a 248-page publication just issued by the U. S. Office of Education, entitled "Scholarships and Fellowships Available at Institutions of Higher Education."

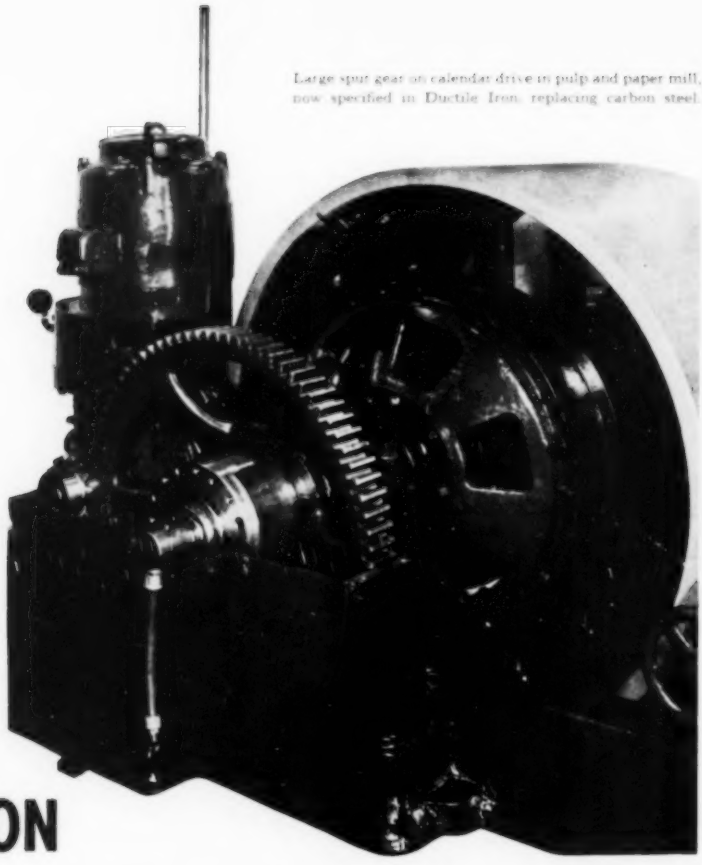

Large spur gear on calendar drive in pulp and paper mill, now specified in Ductile Iron, replacing carbon steel.

DUCTILE IRON

Proves Its Stamina in Machinery Gears

Black-Clawson Company of Hamilton, Ohio, reports several advantages obtained in their production of paper mill and allied equipment by replacing alloy gear castings and forgings with parts made from Ductile Iron.

The gear, illustrated, is typical of these Ductile Iron castings.

Not only has Black-Clawson saved critical materials by using Ductile Iron, but the ease of fabricating contributes to the maintenance of production schedules.

Black-Clawson foundries now produce Ductile Iron in five basic grades for castings that range from less than a pound to more than 7½ tons in weight. Tensile strengths up to 216,000 p.s.i. and hardness that exceeds 400 BHN, may be attained by heat treating Ductile Iron. This company also successfully welds Ductile Iron to steel, to stainless steel, and to itself.

Ductile Iron applications include as-cast and heat treated components for industrial, automotive and agricultural equipment. Also, for railway and other heavy industrial equipment, as well as that used in textile, electrical, marine and other fields too numerous to list.

Counsel and data on Ductile Iron are freely available to help promote intelligent utilization of critical materials. Send us details of your prospective uses, so that we may offer a list of sources from some 100 authorized foundries now producing Ductile Iron under patent licenses. A list of publications on Ductile Iron is available on request.

INCO

THE INTERNATIONAL NICKEL COMPANY, INC. 67 WALL STREET NEW YORK 5, N.Y.

Pioche Manganese Co., subsidiary of Combined Metals Reduction Co., Salt Lake City, will build a large rotary kiln near Pioche, Nev., to process manganese dioxide ore. The kiln, 175 ft long and 9 ft diam, has a cooler of the air quenching grate type. Standard Steel Corp., Los Angeles, is supplying the complete sintering unit.

The Army Signal Corps has developed a new dry battery that substitutes plentiful low-grade domestic manganese dioxide for the high-grade material found in quantity only in Africa. Doubled service life and reduction in storage and shipping costs will offset a slight increase in production costs.

1951 aluminum production totalled about 840,000 tons, 17 pct higher than in 1950. Production by the end of 1951 was at a rate of 5 million lb of primary metal per day. Alcoa has in operation reduction capacity totalling 897.5 million lb and is adding 410 million lb more capacity; Reynolds, 496 million lb in operation, 197 million lb under construction, and 120 million lb planned for 1953 operation; Kaiser, 350 million lb of capacity in operation, 240 million lb under construction, and 200 million lb planned for 1953 operation, and Anaconda Copper is planning reduction capacity of 108 million lb for 1953 operation. By the end of 1953, capacity should be 3018.5 million lb.

The Swedish state-owned Boliden Ore Co., by 1955, is expected to be producing 100,000 tons of iron ore a year and by 1957 will be producing at the proposed capacity of 200,000 tons a year. The project will cost about $3.5 million and costs will be amortized over five 12-month periods.

Production of nickel in the free world during 1951 approximated 259 million lb, 10 pct higher than in 1950. Canada produced 90 pct of this total, 275 million lb, as against 247 million lb in 1950.

Electrolytic cutting of metals has been announced by Columbia University, School of Engineering. Sectioning bars by electrolytic methods was developed to safeguard personnel against hazards of machine cutting metals exposed to high levels of atomic radiation. Russian technical literature has previously indicated machining metals by electrolytic methods, but this is believed the first successful electrolytic cutting of metal in this country.

A new basic metal reported to be stronger, lighter and cheaper than steel is announced by Ontario Research Foundation. Called Controlled Density Steel, the metal can be produced in finished and semifinished articles having any desired density and analysis within a wide range.

Tube Investments, Ltd., Birmingham, England, announced that its new rolling mills at South Wales Aluminium Co. are operating on a test basis, but it is not likely that enough aluminum will be available during 1952 for this plant to be economically operated.

The Research and Development Board of the Dept. of Defense has organized a committee of six representatives from university and industrial laboratories and six technical military officers to establish policies for development and military application of transistors.

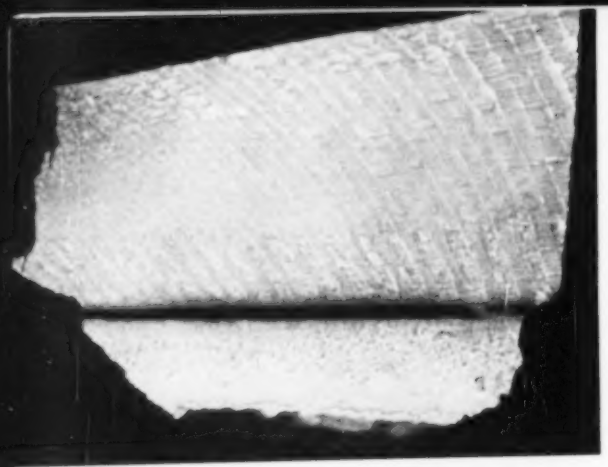

Zebra roof construction in a very large open hearth furnace showing no channeling and very little staggering

A Survey Of Zebra Roof Practice

THE Zebra roof for open hearth steel furnaces comprises rings of either regular or super-duty silica brick, alternated with rings of basic brick in areas of greatest wear—along back or front skews, or both, as shown in Fig. 1. Since mid-July 1950 this construction, which has been used since 1947 in some plants, has gained rapid popularity. This is because the Zebra roof is intermediate in cost and serviceability between an all-silica and an all-basic roof. The silica and basic brick supplement each other, each contributing toward results superior to those obtainable from all-silica roofs, regardless of whether they are built of regular or super-duty silica brick or combinations of the two. In Zebra roofs, the high hot-strength silica brick insures a mechanically stable roof, despite the relatively low hot-strength of the basic brick. The basic brick, superior in resistance to chemical attack by iron oxide and other basic fluxes, wear away more slowly than the adjacent silica brick. Thus, the basic brick protrude beyond the silica brick most of the time, thereby protecting them from the erosive effect of flame and furnace gases. The fact that some plants use super-duty silica brick between the basic rings indicates the superiority of Zebra construction over super-duty silica for the zones of greatest wear.

An industrywide survey made in March 1951 showed that about half of this country's ingot producing companies and plants were using Zebra roofs in nearly one third of the furnaces in the nation. An attempt to bring that survey up to date in November 1951 was not completed. Nevertheless, replies from 38 plants indicated that Zebra roofs are in use in at least 282 furnaces in these plants, and it is therefore believed that at least 300 furnaces in this country are now using this construction. Forty plants operating 355 furnaces (over and above those in which they are now using Zebra roofs) report that it is too early to determine the value of Zebra construction. At least 17 plants of 13 different companies are using Zebra roofs as standard construction in all of their 178 furnaces.

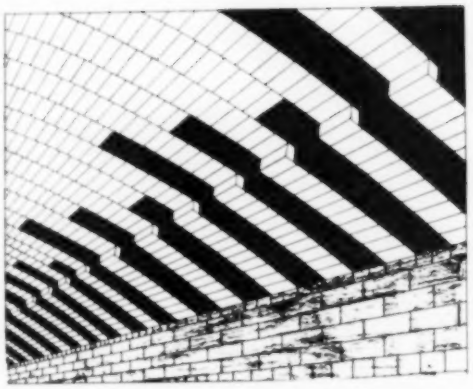

Fig. 1—Special basic roof brick with integral steel plates are alternated with silica brick in this typical open hearth Zebra roof construction. Alternate rings of basic and silica brick, which are most widely used, give best results.

Of 71 plants that answered the questionnaire, 37 use keys, 30 use wedges, and four have used both. One steel company that has used Zebra roofs in most of its plants for more than 4 years has found that keys are superior to wedges. Definite superiority for keys also was indicated in a split roof test in a cold metal shop, where keys were used in one-half of the furnaces and wedges in the other half, as shown in Fig. 2. Keys also have been found superior to wedges in one hot metal shop where Zebra roofs are standard in all furnaces.

Several plants have proved that Zebra roofs comprising two rings (12 in.) of silica to one 6-in. ring of basic brick give results inferior to those obtained from roofs composed of one 6-in. ring of silica to

C. E. GRIGSBY is Service Research Engineer for General Refractories Co., Philadelphia.

one 6-in. ring of basic. These two types of construction were compared in a split roof test in one plant, and as a result of the test the plant now uses a 1:1 ratio (6-in. basic : 6-in. silica) in all 21 furnaces. All but a few plants use a 1:1 ratio of basic to silica, the majority using 6-in. silica to 6-in. basic.

At least 80 plants operating 635 furnaces have tried Zebra roofs, and are now using them in almost half of these furnaces. It is not yet known whether this construction will be used in the remaining furnaces in these plants, but recent improvements in design of roof and arrangement of brick may expedite the acceptance of Zebra roofs in many of these furnaces.

There are now enough plants in which this construction has been standard practice in all furnaces from 1 to 4 years to indicate that the Zebra roof helps increase steel production. Thirteen plants operating 147 furnaces report increased production ranging from 2 to 10 pct, or more. Eight of these are plants in which Zebra roofs are standard in all furnaces. Seven plants report that these roofs reduce cost per ton of steel.

While in some plants Zebra construction may not be beneficial, it seems likely that there are many more where it would be helpful if the furnaces are operated with proper regard for the limitations of both basic and silica brick. Every type of roof including the all-basic roof has limitations, and Zebra roofs can be burned down if operated at excessively high temperatures or reducing atmospheres. More damage can be done to a silica or a Zebra roof in a few heats when conditions are reducing than occurs in many weeks of normal operation with an oxidizing atmosphere. In virtually all plants, the furnace atmosphere is oxidizing at least 95 pct of the time. As an added precaution against reducing conditions, two plants using Zebra roofs carry 10 pct excess air at all times.

Staggered Construction

There is a belief that using basic rings all of equal length in Zebra roofs will produce channeling and buckling near the end of the basic rings, where the basic brick are in contact with the silica brick. This apparently stems from experiences with solid basic shoulders. Channeling and buckling near the junction of basic and silica, which occurred with the solid basic shoulders, was probably because the basic brick did not extend out far enough from the skew to cover the zone of excessive wear.

Also, solid basic shoulders did not use the special chrome-magnesite roof brick used in virtually all Zebra roofs. A still further disadvantage of some of these shoulders was that they used either unplated basic brick or brick with only one plate in each joint. For best results with Zebra roofs, basic shoulders should have a double plate in every joint between basic brick to help hold spalls in place; and a single plate between basic and silica brick to minimize damaging reaction between the two kinds of brick. In view of these considerations, many successful users of Zebra roofs may reassess solid basic shoulders with a view to trying them either in conjunction with or to replace Zebra roofs.

Examinations of Zebra roofs after service and observations of many more while in service have failed to reveal any damaging action between silica and basic brick, either at the ends of the basic rings or along the sides of the basic rings where the steel plate on the basic brick is in contact with the silica brick. This is not surprising, because silica and

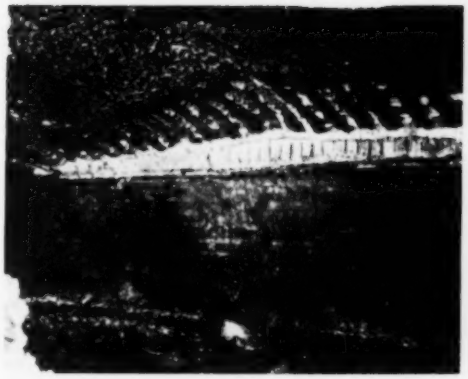

Fig. 2—Special basic roof brick keys, the six very dark rings at the right, are considerably thicker than the gouged out wedges of the same mix, the lighter colored rings at left. The junction of the two shapes is over the top hole.

chrome-magnesite brick used in virtually all Zebra roofs do not begin to react until 2910 F and react only slightly at 3000 F. The slight reaction that could occur at open hearth temperatures, if the basic brick were in direct contact with the silica brick, is eliminated because in all locations where they are adjacent the two types of brick are effectively separated by a 16 to 20 gage steel plate.

Channeling, sometimes occurring beyond the basic rings in both Zebra roofs and solid basic shoulders, may be because basic rings are too short. Since most furnaces are pushed harder when equipped with Zebra roofs or solid basic shoulders, it is not surprising that the zone of severe wear extends out farther from the skew than with an all-silica roof. Several operators who have returned to silica after using Zebra roofs tried to operate in the same way as with Zebra roofs. More extensive channeling occurred with all-silica construction. Thus, the increased area of the zone of greatest wear obviously was the result of increased severity of service conditions and was not caused by any reaction between basic and silica brick. The remedy is obvious. The basic rings must extend out far enough to include the new zone of increased wear resulting from more severe operating conditions.

Staggered Construction Not Essential

The original purpose of staggered construction was to guard against channeling near the junction of the basic and the silica, thus reducing the tendency of the roof to buckle when it gets thin. Naturally, any roof will buckle when it gets thin enough in a sufficiently large area. This is true with both ribbed ring roofs and bonded roofs, and especially with roofs that are poorly constructed or with roofs that do not have the proper rise per foot of span. Even in Zebra roofs, built with staggered construction, channeling and buckling will occur if the shortest ring of basic brick does not extend beyond the zone of greatest wear under the conditions to which the Zebra roof is subjected. Channeling will not occur with basic rings all of the same length if those rings extend beyond the zone of greatest wear. This is shown in Fig. 3b. If this zone extends out more than about 7 ft from the skews, the Super-Zebra roof, shown in Fig. 4, in which the Zebra construction

extends from skew to skew, should be considered. Several plants have found no difference in results with staggered construction, as compared to roofs built with basic rings all of equal length. This is to be expected, because staggered construction is fully effective only as far out from the skew as the length of the shortest basic ring.

Basic Brick Wasted

Basic brick located farther from the skew than the shortest basic ring are wasted, even in roofs constructed of one 6-in. basic ring to one 6-in. silica ring near the skews, and only two different lengths of basic rings. This is because the basic brick in the longest rings are too far apart to protect the silica brick properly, no matter how much the basic brick protrude beyond the silica. In such construction, Fig. 1, there are three rings, 18-in., of silica brick to one 6-in. basic brick ring in the section between the shortest and the longest ring of basic. When three different lengths of basic rings are employed in the pattern most commonly used, there are three rings of silica, 18-in., to one 6-in. basic ring in the sections of roof between the shortest and the medium length rings of basic brick; and five rings, 30-in., of silica brick between the basic rings in the sections of roof between the basic rings of medium and greatest length. Some plants use a medium length ring of basic brick on each side of each long ring of basic. This gives 18 in. of silica between the basic rings of shortest and medium length, and seven rings, 42-in., of silica brick between 6-in. wide basic rings in the zone between the longest and the medium length basic rings.

Zebra Roof Superior

Several plants that went back to silica roofs temporarily have resumed the use of Zebra roofs after finding that roof life with silica brick, operated under the conditions used for Zebra roofs, was much less than the minimum with Zebra roofs. In some cases there was a marked increase in roof life, as compared to silica, in the initial installation of Zebra roofs. Once the superiority of Zebra roofs was proved, the furnaces were pushed harder and harder for production with each succeeding campaign until finally the life with Zebra roofs was considered unsatisfactory. The decreased life of the silica roofs, used temporarily, proved that the service conditions with Zebra roofs had been more severe than could safely be used with either Zebra or all-silica construction.

There is a general reluctance to run split roof tests under present-day conditions, but this is usually the quickest and most economical way to evaluate any

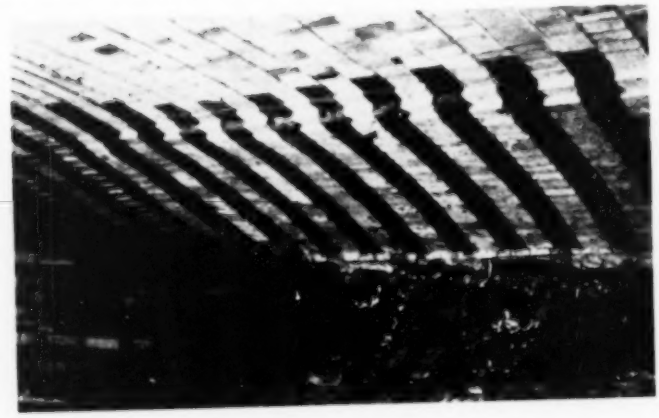

Fig. 3a—Special basic roof brick keys in rings 5½ ft long are used in 85 ton furnaces, giving outstanding results.

Fig. 3b — After 132 heats, the roof shown in Fig. 3a was still in perfect condition. Practice had been to patch most silica roofs at this time. This roof was still in excellent condition after 211 heats with no patches. It would have given 30 to 50 more heats but checker trouble caused a shutdown.

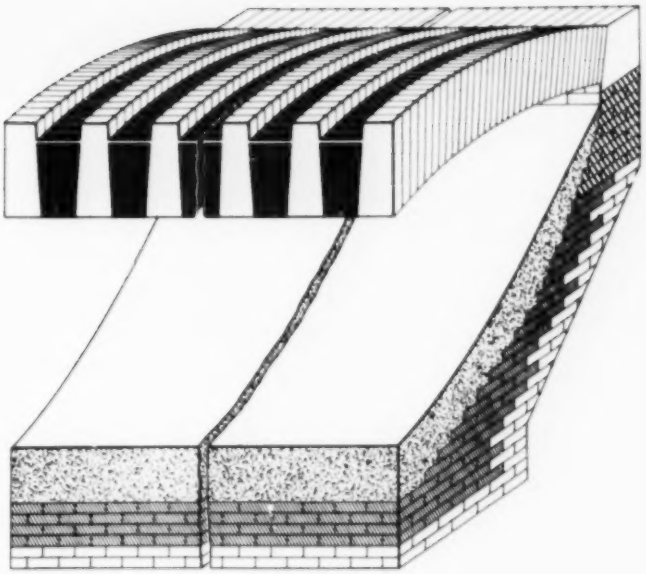

Fig. 4 — The Super Zebra roof, for use where rapid wear extends more than 7 ft from skews or where wear is uniform from skew to skew. Best results are expected with silica and basic brick, each 4½ in. wide at the fire face.

two different types of construction. It may prevent erroneous conclusions and, where doubt exists, too hasty rejection of a type of construction that can materially increase steel production. Since the properties of basic brick and silica brick are entirely different, it may be necessary to make some changes in practice to get best results with Zebra roofs.

Best results on any roof containing basic brick can be obtained only if the roof is operated with a minimum of variations in temperature. Silica brick, the most sensitive to thermal shock below 1200°F of all the ordinary refractories, are virtually spall-proof above 1200°F because they have negligible thermal expansion above that temperature. Since most open hearth roofs are never cooled below 1200°F, it is not necessary to limit the number or extent of temperature changes above this temperature when silica brick are used for the entire roof.

Basic refractories, particularly those high in magnesite, have the highest thermal expansion of all the commercial refractories. The result is that they expand and contract every time they are heated and cooled, the rate of change in volume being approximately the same in all temperature ranges. Each change in volume sets up stresses within the brick, which are not entirely relieved when the brick resumes its original size. The magnitude of the unrelieved stresses within the brick keeps increasing with each change in temperature, and the brick spalls when the stresses inside the brick exceed its strength. The relatively high thermal expansion of all basic brick makes it impossible for any basic brick to approach the resistance of silica brick to spalling above 1200°F. Since the thermal expansion of refractories cannot be changed, furnace operation should be adjusted to meet limitations of the roof brick being used.

Experience with the all-basic furnace has proved that best results are obtained when the basic roof is kept as hot as possible. In an all-basic furnace, each time there was a prolonged period when the roof was cooled below 2100°F, the resumption of operation was followed by a major peeling of the brick. In one plant it was found that where Zebra roofs gave less than average life, the furnace involved had invariably been plagued by excessive bottom trouble. Records probably would show similar results at other plants, a few of which have abandoned Zebra roofs because of such variable results.

Best results on any roof containing basic brick will be obtained by keeping the roof as hot as possible, preferably above 2500°F. It appears significant that in five plants using Zebra roofs in all furnaces, minimum roof temperature is 2400° to 2700°F.

The importance of keeping the roof hot has been proved at one plant where Zebra roofs are standard in all twelve 175-ton furnaces. Every effort is made to keep the roof hot, even to the extent of putting oil on the furnaces to maintain temperature. This shop has another advantage in that it uses relatively narrow, 4½-in., basic wedges, alternated with 4½-in. silica wedges, in the valley courses, and 6-in. silica ribs (since silica is the weak point in the roof, the narrower the rings of silica the better). The longest rings of basic brick extend 6 ft from the skew and the shortest extend out 5 ft. This construction, which is used along both front and back skews, has increased production more than 10 pct; increased roof life from 200 to 300 heats, or 50 pct; increased the heats to the first patch from 63 to 135, or 110 pct; and decreased the number of patches per campaign from 7 to 2, or 70 pct. A 12-in. temporary silica roof in this plant, operated in the same way as the Zebra roofs, was burned so badly that it had to be patched after 4 days.

The usual variations in operating conditions in an open hearth have opposite effects on silica brick and basic brick. Although these types of brick supplement each other chemically and physically, best results with Zebra roofs can be obtained only if the

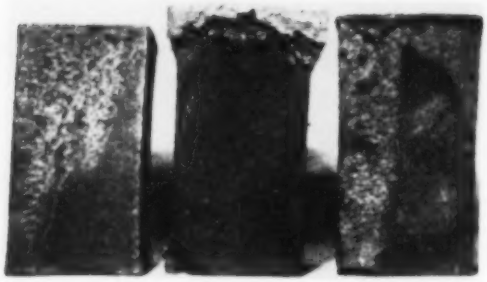

Fig. 5—Basic brick that have been subjected to iron oxide bursting action in an oxidizing atmosphere at 3000°F are shown here. Left: Magnesite-Chrome brick. Center: Chrome-Magnesite brick of low bursting resistance. Right: Special Chrome-Magnesite brick with good bursting resistance.

roof is operated with regard for the advantages and disadvantages of both types of brick. The temperature limitations of silica brick are well known. Even with the usual oxidizing conditions in an open hearth, silica roof brick always are near the temperature of rapid wear from sweats and burns. This is true even when the roof surface temperature is within the limits 3010° to 3040°F, which most authorities consider the maximum safe operating range for most silica brick. Reducing conditions, even for a few minutes, accelerate the rate of wear of silica brick by an almost unbelievable amount. Qualified observers report the loss of as much as 1 in. of silica roof in 5 min, or less, under strongly reducing conditions.

The best silica brick have an operating temperature limit not much above maximum bath temperature, and well below flame temperature. When this limiting temperature is exceeded, even for 5 or 10 min, the roof surface may be so roughened that it reflects heat less efficiently to the bath—thus slowing down production—and absorbs heat faster. The latter tends to cause further overheating. The effect of even so short a period of overheating may last for many days until slag corrosion causes the roof surface to become smooth again.

It is important, therefore, not only for maximum production but also for maximum roof life, to avoid even short periods of overheating of any roof containing silica brick. Silica brick comprise the weak part of the Zebra roof, and best results can be obtained only if the roof is operated without even short periods of reducing conditions, excessive temperatures, or both.

Limitations of Basic Brick

In addition to sensitivity to thermal shock, which requires keeping the roof hot for best results, basic brick have comparatively low hot strength. Extra care not to gouge the roof in the Zebra section during charging will pay dividends.

Basic brick containing substantial amounts of chrome ore behave the opposite of silica brick, in that they are benefited by strongly reducing atmospheres and by higher temperatures in the normal oxidizing atmospheres. In strongly reducing atmospheres, they show shrinkage instead of expansion when in contact with iron oxide at open hearth temperatures. Under strongly oxidizing conditions, such as those in most open hearths, these basic brick expand at temperatures between 2700° and 3200°F. Assuming sufficient time and iron oxide, the percent linear expansion increases rapidly from a fairly low amount at 2800°F to a high peak at 2900°F. The expansion at 3000°F is almost equal to that at 2900°F, but at 3100°F and 3200°F it is less than half as great as at 2900°F.

All open hearths are operated in such a way as to cause the maximum rate of bursting action from iron oxide vapors on brick containing chrome ore as a major constituent. Brick containing magnesite as the major constituent would give less bursting action than chrome-magnesite brick, as shown in Fig. 5, but, because of greater sensitivity to thermal shock and a tendency toward shrinkage spalling, they have been found definitely inferior to special chrome-magnesite roof brick in Zebra roofs.

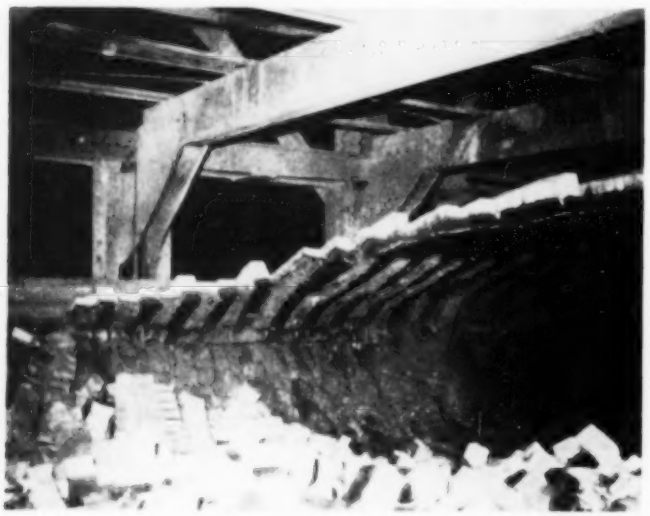

Fig. 6—In a plant that has used Zebra construction in all roofs for about 18 months, special basic roof brick wedges and super-duty silica brick are shown here at the end of a successful campaign. Basic rings are 3¾ ft and 4½ ft long. Channeling is near the skews.

A strongly reducing atmosphere or a temperature of 3100° to 3200° F would benefit chrome-magnesite brick, but neither condition is practical in a Zebra roof. The reducing atmosphere is undesirable for metallurgical reasons, since the open hearth process is an oxidizing process and cannot be operated otherwise. The disastrous effect of reducing atmospheres on silica brick has been previously noted, and roof life with silica brick operated at 3100° to 3200° F would be very short, even in an oxidizing atmosphere. Thus, the limitations imposed by metallurgical considerations and the use of silica brick make it necessary to operate a Zebra roof furnace with the limitations of silica brick in mind. The limitations of basic brick do not impose any insurmountable difficulties, so the limitations on Zebra roofs are essentially the limitations imposed by silica brick. The slight but important increase in temperature which the Zebra roof permits, is caused by the fact that the basic brick, protruding beyond the silica, make it necessary for the slag to become fluid enough to drop off by gravity.

Special Roof Brick Best

Best results in Zebra roofs, as in the all-basic furnace, are obtained from special chrome-magnesite brick, shown in Fig. 5, developed particularly for the all-basic furnace roof. The supremacy of these brick is the result of unique combination of desirable chemical and physical properties, which result from an entirely new concept in brick manufacture. The coarse particles of the brick comprise nonporous, volume-stable chrome ore, surrounded and protected from iron oxide by the magnesite fines portion of the brick. In addition to the better mix used in these brick, they are further improved by the exclusive use of steel plates that are firmly attached to and form an integral part of the four major faces of the brick. The brick cannot fall out of the plates during installation in the roof or in the heating-up period, prior to the formation of a monolithic structure in each ring. These special roof brick are used in nearly all Zebra roofs, and have replaced magnesite-chrome and ordinary chrome-magnesite brick in all plants where they have been compared in Zebra roofs. This is because they are more resistant to spalling, the prime destructive force in most Zebra roofs. This spalling seems to be the result of a combination of thermal shock and iron oxide bursting, the exact conditions which these special roof brick were designed to withstand.

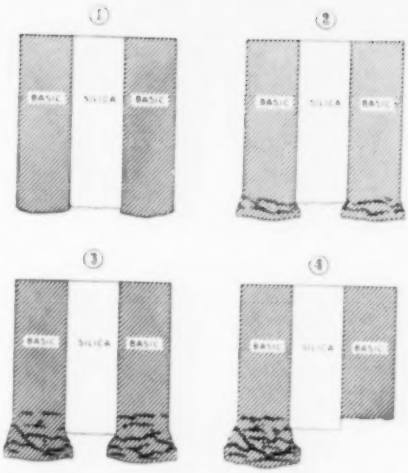

Fig. 8—This sketch shows the probable sequence of events in Zebra roof construction containing special chrome-magnesite roof brick. When the longest basic brick shown in part 4 of the sketch spalls off, the silica brick may extend beyond the basic brick temporarily. Then the cycle is repeated.

The superiority of these special roof brick over the other two types, in Zebra roofs and all-basic main roofs, is the result of a better balance of the required properties. The special brick have lower thermal expansion than magnesite-chrome brick and are, therefore, more resistant to spalling from thermal shock. As shown in Fig. 5, they are superior to ordinary chrome-magnesite brick in resistance in iron oxide bursting. They also have higher resistance to load and shrink less than any other brick at open hearth temperatures.

Results With No Staggering

The full extent of the fear of channeling and buckling without staggered construction is indicated by the fact that even plants that have proved that staggered construction is not necessary continue to use basic rings which differ in length from 6 to 9 in. This is apparently a sort of insurance against any kind of trouble. Figs. 6, 7a, and 7b show results at

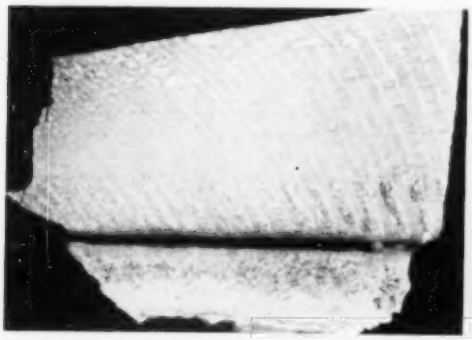

Fig. 7a—Special basic roof brick keys after 75 heats. Basic rings are 4 ft and 4½ ft long, and there is no sign of channeling.

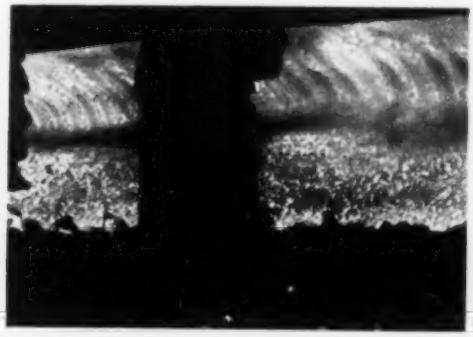

Fig. 7b—This is the same roof as that shown in Fig. 7a at the end of a successful campaign. Channeling is near the skews, but there is none near the end of the basic rings.

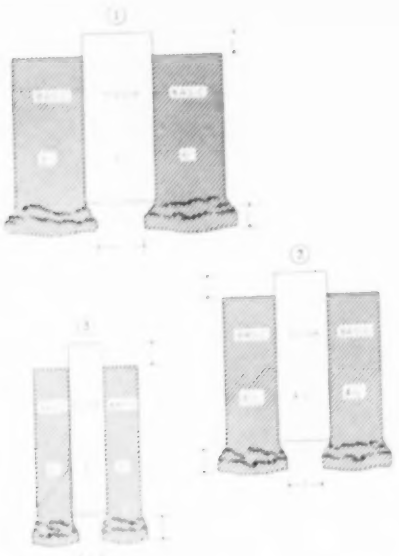

Fig. 9—Sketch shows the probable advantage of 3-in. silica keys over 6-in. and 4½-in. silica wedges in a Zebra roof built of special chrome magnesite roof brick. Since silica brick limit operating temperatures, 3-in. keys are recommended

two such plants, where the channeling is back near the skew and not near the junction of the basic and silica brick.

One plant using basic rings all of the same length is obtaining outstanding results. Fig. 3a shows that the rings of special steel-plated chrome-magnesite roof brick are not staggered. This is the first furnace in the history of the plant that did not have to be patched after 100 to 135 heats. The condition of the brick after 132 heats is shown in Fig. 3b. The basic brick are 1 to 3 in. longer than the silica brick and the roof is in excellent condition. There is no evidence of channeling near the junction of the two kinds of brick. The basic brick have expanded enough so that the rings of basic, which were originally the same width as the silica as shown in Fig. 3a, appear wider than the silica rings. This expansion obviously is beneficial no matter what width of silica rings are used, because it protects the silica much like the shelter of an overhanging cliff, as shown in Figs. 8 and 9.

The roof continued its superior performance, without repairs, until the furnace went down for a rebuild after the roof had given 211 heats. This rebuild was necessary because the north checkers became so plugged that the furnace was completely out of balance. During the time the furnace was operating on the north checkers, there was such excessive pressure in the furnace that the flame sting-out at the wicket hole in the charging doors was 3 to 4 ft long. This eroded the all-silica portion of the main roof, close to the knuckle.

Roof Life Nearly Doubled

Despite these severe operating conditions, the Zebra section of the roof was in such excellent condition (after 211 heats) that some 30 to 50 more heats could have been obtained on the roof had not the checker trouble caused the shutdown. Thus, the initial roof would have doubled the life of silica roofs, with no repairs, at this plant.

The second Zebra roof at this plant also was taken off after 161 heats because the checkers were plugged, giving excessive pressures, and because all walls above floor level failed. During the last week of the campaign, the silica portion of the roof on one end of the furnace wore away rapidly, indicating unbalanced operation and the need for longer rings of basic brick. The Zebra section of the roof was still in excellent condition despite this abuse. All nine furnaces at this plant now use this Zebra construction, with all basic rings of equal length, as shown in Fig. 3a.

At last reports, Jan. 15, 1952, a Zebra roof on a third furnace in this plant was in excellent condition after 186 heats, and that on a fourth looked the same after 176 heats. This construction will be continued in all furnaces. It is planned to extend the Zebra sections out farther from the back skews in some furnaces. Some Zebra panels along the front skews may be used on several furnaces where early failures have been encountered with all-silica construction.

Anything that increases the amount of iron oxide fumes in the furnace atmosphere (very light scrap or the use of oxygen for decarburization) will increase the amount of bursting action on the basic brick. This action will be increased by an increase in the amount by which the basic brick extends beyond the silica, because the brick will be exposed to iron oxide vapors on three faces instead of one. The basic brick are of no benefit until they extend beyond the silica far enough to protect them from the action of the furnace gases, and yet they must not extend so far as to give excessive bursting action. If the basic brick protrude too far (some plants report 5 in. max) they are more easily knocked off during charging and are most likely to spall from thermal shock. Only a brick such as the special chrome-magnesite roof brick which has a desirable combination of chemical and physical properties, can be expected to succeed in Zebra roofs.

How to Improve Roof Life

Since silica is the weak section of a Zebra roof, it is believed that, regardless of whether the basic brick expand in service or not, Figs. 8 and 9, all plants including those now using Zebra roofs as standard in all furnaces might benefit by a change to alternate rings of 3-in. basic and 3-in. silica keys. For a 15-in. roof, there would be no change in cost, as compared to regular Zebra construction but the use of 3-in. silica keys would reduce the width of exposed silica close to the practical minimum, as shown in Fig. 10. The next step toward better life would be to at least double the ratio of basic to silica in zones of greatest wear, thus changing the basic-silica ratio from 1:1 to 2:1 or more. Several plants are now making trials of the 3-in. basic keys, alternated with 3-in. silica keys, and results will be available in the near future. One plant uses a few rows of solid basic construction near the skews, then regular Zebra construction with 6-in. rings of basic alternated with 6-in. rings of silica. A variation of this idea would be all-basic construction for about

one third the length of the basic rings near the skews, then two basic to one silica for the next third, one basic to one silica for the last third, and finally 100 pct silica beyond the Zebra section.

Use in Bonded Roofs

At least five plants use regular ring construction successfully for the Zebra section of bonded roofs. In one of these plants, the roof life has been increased 33 pct; from 225 heats to 300 heats. This construction is standard in all 21 furnaces. This is the design recommended for bonded roofs, as it is believed better than the herringbone design or any of several others tried or being tried in bonded roofs—some of them in tilting furnaces.

The effect of the human element on Zebra roof life is indicated by the experience of one plant, where Zebra construction has been standard practice in all nine furnaces for more than a year. The roof life last winter averaged 175 heats, and during the past summer it dropped to about 130 heats. Realizing that this drop was caused by the hot weather, the vacation period, etc., use of Zebra roofs was continued. The decision was justified when the roof life began to increase steadily toward the winter average as the cooler weather returned. This should be of interest to plants which may have tried a Zebra roof in summer without success.

Super Zebra Roof Design

If the zone of greatest wear extends out more than about 7 ft from the skews, a special Super Zebra construction shown in Fig. 4 may be considered. In this design, the comparatively strong silica key wedges are used to support the basic brick, which have relatively low hot strength. In this way, the Zebra construction might safely extend all the way from skew to skew. As Fig. 4 shows, special straight-sided brick are used at the ends of this panel, thus making it possible to use this construction to any extent—from a few rings to the entire main roof.

One plant is making a trial of this construction in a band 6 ft wide over the tap hole. Another is considering a similar trial over the tap hole area, together with a trial of the 3-in. basic, 3-in. silica key construction in less severe sections on either side of the tap hole. A third plant probably will make a trial of the Super Zebra construction for the entire main roof, from knuckle to knuckle. Another promising use for the Super Zebra roof is in plants where Zebra roofs have not been used because roof wear is uniform from front to back. The use of Super Zebra roofs in such plants probably would extend roof life by an even greater percentage than it does in most plants, because channeling and buckling would be unlikely to occur.

Summary

Regular Zebra roof construction; the new 3-in. basic, 3-in. silica key Zebra roof; the Super Zebra roof; improved basic shoulders; or a combination of these, offer an excellent opportunity to increase steel production in most plants. Singly or in combination, these new types of roof make possible a greater increase in production than any other roof except the all-baste roof.

The 3-in. basic, 3-in. silica key arrangement is worth consideration by all satisfied users of Zebra roofs and should be of particular interest to those who have tried regular Zebra roofs without completely satisfactory results. The Super Zebra design is of interest primarily to plants whose roofs wear rapidly for a distance of more than 7 ft from the skews and those which wear uniformly from skew to skew.

For extra-severe service near the skews, a combination of two 3-in. basic keys to one 3-in. silica key, or improved solid basic shoulders may be of interest to some plants, in combination with regular Zebra or 3-in. basic, 3-in. silica key construction beyond the tough section.

Like all other roofs, Zebra roofs of all types have a definite temperature limit, but it is enough above that at which silica roofs can be safely operated to make an important increase in steel production.

Zebra roofs are being used as standard practice in both hot and cold metal shops and in both ring and bonded roofs. Greatest improvement over silica will be obtained by keeping the roof as hot as possible at all times to minimize spalling of the basic brick. Two plants where Zebra roofs have been standard in all furnaces for more than a year keep the roof temperature at 2700 F or above during charging, and 2000 F or above during major bottom repairs. They also carry up to 10 pct excess air at all times. These operators, along with many others, have proved that when Zebra roofs are operated with consideration for the limitations of both basic and silica brick, they will produce more steel, increase roof life, decrease patching, or all three. Since these roofs are giving such good results in so many plants, they can be made to do so in most others.

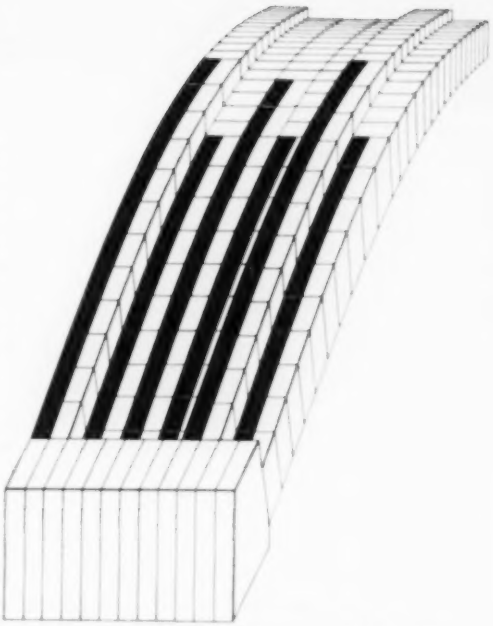

Fig. 10—This shows a suggested arrangement of 3 in. silica keys, alternated with 3 in. special basic roof brick keys in a ribbed roof using staggered construction. The staggered construction is optional, but the longer basic rings in this construction are close enough together to be of some benefit.

Rapid Analysis Determines

Boron in Alloys

by H. Blumenthal

In the chapter on Metals and Ferroalloys Used in the Manufacture of Steel the *Metals Handbook* describes the effect of the addition of boron to steels as follows: "Boron is used in steel for one purpose only—to increase the hardenability. . . . Only a few thousandths of 1 pct is ordinarily added." This small amount of boron added to steel is able to replace several hundred times its own weight of other elements which have the same hardening effect, such as manganese, chromium, molybdenum, and nickel. It has been shown, for instance, that in a normal 8645 steel 0.0012 pct boron has the same hardening effect as 1.33 pct nickel, 0.31 pct chromium, and 0.04 pct molybdenum combined. That means 0.0012 pct boron can save 1.68 pct of scarce and strategic metals. The tendency of boron to lower the austenitic grain coarsening temperature can be overcome by increase in the addition of aluminum, and the danger of boron being oxidized and thereby lost can be counteracted by the addition of complex alloys containing strong deoxidizers such as aluminum, calcium, titanium, or zirconium. In fact, addition of complex alloys instead of straight ferroboron or manganese boron can serve the triple purpose of adding boron, preventing its oxidation, and controlling the grain coarsening tendencies. While present knowledge of the behavior of boron in steel is far from complete, indications are that optimum effects are obtained with an addition of from 0.0008 to 0.003 pct of boron. When kept in this range the actual amount of boron present in a steel seems not to be critical. For this reason, the steel maker is not so much interested in a boron analysis of steel, as in the boron content of the addition agent. A list issued by the American Iron and Steel Institute giving the composition of "Boron and Alternate Steels" states only that "boron-treated steels . . . can be expected to have 0.0005 pct min boron content." If the boron content of the addition alloy is known, it is possible to stay in the range which gives the optimum effect.

The following investigation was undertaken to find a fast and accurate method to determine the boron content of simple and complex alloys used as addition agents in the production of boron steels. Table I gives the manufacturers' analyses of the investigated alloys.

H. BLUMENTHAL is Chief Chemist for American Electro Metal Corp., Yonkers, N. Y.

Previous Work

Boron generally has been determined in alloys by transforming the element into boric acid, separating this acid from the rest of the constituents, and titrating it with sodium hydroxide. All elements that would interfere in the titration by reacting with sodium hydroxide have been eliminated by three inherently different methods.[1] The oldest and still most common, originated by Chapin,[2] consists of distillation of boron in the form of methyl borate. The second,[3] separates the metals from the boron by plating them on a mercury cathode, and the third precipitates the metals with calcium 'carbonate,' barium hydroxide," or a mixture of sodium hydroxide and sodium carbonate.[4]

The first method, involving two distillations, is long and tedious. The second, which was not tested by the author, requires special apparatus and is believed not to function satisfactorily.[5] The method developed in the course of this investigation is based on the precipitation method, which was felt to require the least time, apparatus, and attention.

The sample was put in solution either by boiling slightly with aqua regia under a reflux condensor

Table I. Manufacturers' Analyses of Boron Agents, Pct

Element	1	Grainal 6	79	Silvax	Silcaz	Carbortam	Borosil	Ferro-boron	Manganese Boron
Boron	0.18	0.31	0.52	0.50	0.52	1.60	3.76	18.20	18.00
Silicon	1.34	1.99	4.70	39.1	37.6	3.27	42.0		
Aluminum	9.78	12.2	13.1	5.80	6.93				
Titanium	14.6	22.7	19.2	10.50	8.06	18.3			
Zirconium			3.29	6.50	4.22				
Calcium					8.76				
Vanadium	25.5	13.2		10.0					
Manganese			6.90						74.0
Copper	0.05	0.04	0.22						
Carbon	0.12	0.09	0.19			6.28			

(to avoid loss of boron) or by fusing with sodium carbonate in a platinum crucible. The basic nature of this salt prevents loss of boron effectively. A 100 mg sample was used for ferroboron and manganese boron and a 1 g sample for alloys lower in boron content. If solution was done with acid, 25 ml aqua regia were added to the sample through the condensor and 100 ml water added when reaction ceased. The solution was completed by heating for 40 min at low heat. If the sample was to be fused, a platinum crucible was lined with a melt of 5 g sodium carbonate and the sample, mixed with 5 times its weight of sodium carbonate, was put in. When a good fusion was accomplished the melt was cooled, 50 to 500 mg of sodium nitrate introduced and the fusion finished at full blast of the burner. The melt was decomposed by pouring it into 50 ml 1-1 hydrochloric acid to break up and isolate the silica, which was filtered off after complete decomposition. Ten ml of 3 pct hydrogen peroxide were added to enhance decomposition, and 15 ml more if the alloy contained titanium.

Precipitation of Metals

Experiments were carried out in which the metals were then precipitated with barium hydroxide, sodium hydroxide, calcium carbonate, and barium carbonate. Neither of these precipitants was satisfactory with all the investigated alloys. It was found that the precipitate made with sodium hydroxide and barium hydroxide contained a considerable amount of boron, while aluminum stayed in solution and was titrated as boron. Calcium carbonate and barium carbonate did not precipitate manganese completely. Furthermore, it was feared calcium carbonate might cause the formation of a borate of low solubility in the case of high boron alloys. Barium carbonate effected complete precipitation of the metals of the following alloys: Ferroboron, Grainal #1 and #6, Silvax, Silcaz, and Carbortam. Manganese boron was also precipitated with barium carbonate but a small addition of barium hydroxide to bring the pH to 8.5 and a little bromine water or hydrogen peroxide was necessary to precipitate the manganese completely. A difficulty was presented by alloys that contained manganese as well as aluminum. In this case, a first precipitation was made with barium carbonate to eliminate all metals but manganese, and the manganese precipitated in the filtrate with barium hydroxide and an oxidant. This double precipitation was necessary for Grainal #79 and Borosil. (Although Borosil does not contain manganese or aluminum nominally, the sample investigated contained small amounts of both.)

For economy the acid solution was partly neutralized with sodium hydroxide before barium carbonate (in powder form) was added. The precipitated metals were filtered off, and the filtrate slightly acidified with hydrochloric acid and heated to boiling to expel carbon dioxide, which, if present, would titrate as boric acid. The boiling must be done gently and in a well covered beaker. Boiling for 1 to 3 min was sufficient, but experiments showed that boiling for 10 min under the above conditions caused no loss of boron.

Titration

The filtrate may be titrated with 0.1 or 0.05 N sodium hydroxide in the presence of mannitol visually or potentiometrically. If done visually, a mixed indicator solution of 0.05 g of methyl red, 0.1 g of bromocresol green, 0.30 g of phenolphthalein, and 0.30 g of thymolphthalein in 100 ml of methyl alcohol was used, which gave more distinct end points than the common p-nitrophenol and phenolphthalein, especially at a temperature of about 50°C. This indicator mixture gives a distinct color change from pink to green when the hydrochloric acid is neutralized, the starting point of the boric acid titration, and changes to purple at the end point of the boric acid titration. Eight g of mannitol were added after neutralization of the hydrochloric acid. Titration at elevated temperature shortens the time for cooling the boiling solution and there is, therefore, less

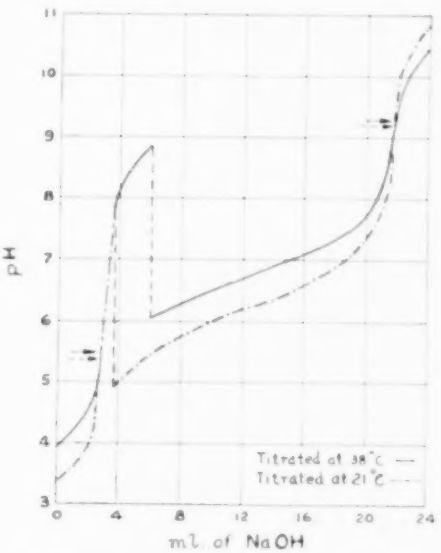

Fig. 1—Determination of boron in ferroboron. Broken line indicates change of pH caused by addition of mannitol.

danger of carbon dioxide pickup from the air. Potentiometric titrations were done at about 40° C, as this was the highest temperature at which the available pH meter could be operated. A blank was deducted in all titrations for the reagents used.

Results

Fig. 1 gives an actual boric acid titration curve for a ferroboron sample. Neutralization of hydrochloric acid occurs at pH 6.3 and of the boric acid complex at 9.0, while the indicator end points, indicated by arrows, are at pH 5.3 and 9.2 respectively. Any pH between 5 and 7 may be chosen as a starting point and between 8.6 and 9.4 as an end point for the potentiometric titration, as the parts of the titration curve between these points are practically parallel. The sodium hydroxide solution used for the titrations must be standardized against a known amount of boric acid at the same pH at which the titration is to be performed.

Table II gives the results of duplicate determinations as well as the analyses of the manufacturers of the different alloys. It shows satisfactory reproducibility but not good agreement with the manufacturers' analyses for manganese boron, Silvaz, and Carbortam.

To prove the accuracy of the described method for these three alloys, a known amount of boron in the form of 25 ml of a boric acid solution containing

Table II. Reproducibility of Boron Determinations

Alloy	Boron, Pct 1st Determination	Boron, Pct 2nd Determination	Manufacturers' Analysis
Ferroboron No. 1	0.18	0.18	0.18
Ferroboron No. 6	0.30	0.32	0.31
Ferroboron No. 79	0.52	0.56	0.52
Silvaz	0.82	0.81	0.50
Silvaz	0.54	0.50	0.52
Carbortam	1.29	1.15	1.60
Borosil	3.65	3.59	3.76
Ferroboron	17.8	18.1	18.2
Manganese Boron	20.3	20.6	18.8

Table III. Recovery of Boron after Boric Acid Additions

Alloy	Boron Added Mg	Boron Recovered Mg	Deviation Mg
Silvaz	4.42	4.68	+0.26
Carbortam	4.42	4.42	0
Manganese Boron	4.14	4.24	+0.10

about 1 g of H_3BO_3 per liter was added to solutions of the three alloys, and the boron content then determined. Table III shows the amount of boron added and recovered, as well as the deviations from the expected values. The results can be called satisfactory and prove the correctness of the analyses. The explanation for the discrepancy with the manufacturers' analyses is probably that the small sample available was not representative for the lot that the manufacturer analyzed.

Acknowledgment

The author wishes to acknowledge the assistance of William Fall, who carried out most of the experimental work. This publication contains parts of a paper presented before the XIIth International Congress of Pure and Applied Chemistry, New York, Sept. 10, 1951. Other parts of this paper were published in *Analytical Chemistry* 23,992 (1951) and *Powder Metallurgy Bulletin* 6, 80 (1951).

References

1. R. S. Dean and B. Silkes: Review of Methods for Determination of Boron in Iron and Steels. U.S. Bureau of Mines, *Inform. Circ.* 7363 (September 1946).
2. Ibid. p. 24.
3. W. H. Chapin: *Journal* Amer. Chem. Soc. 30,1691 (1908).
4. N. Tschischewski: *Industrial Engineering Chemistry* 18,607 (1926).
5. J. M. Lindgren: *Journal* Amer. Chem. Soc. 37,1137 (1915).
6. L. Y. Sabunina and T. V. Styunkel: *Zavodskaya Lab.*, 13,752 (1947), translated by Henry Brutcher.
7. W. H. Hazel and G. H. Ogilvie: *Analytical Chemistry* 22,697 (1950).

Progress Report:

Low Shaft Blast Furnace

THE International Research Project on Low Shaft Blast Furnaces, one of the first large-scale international ventures in industrial research, has progressed rapidly in recent months from the standpoint of design, purchase, and construction of equipment. At the time of the memorandum describing the project, prepared by the Office of Naval Research,* the firm of Klockner-Humboldt-Deutz was the only company that had submitted drawings. Since then, others have placed bids, and it is with one of these firms that the order for the construction of the furnace at Liege has been placed.

To the list of contracting firms, an American participant probably will be added. The Austrian participating firm represents not only itself, but the entire Austrian steel industry, and the British participant is the British Iron and Steel Research Assn. Total funds contributed to date amount to $900,000.

In its earlier stages, the project was sponsored by the Office of European Economic Cooperation. Now, however, it is independent. Since the beginning, the project has been organized by H. Malcor, president of the French Institut de Recherches de la Siderurgie and director of several French companies, and Dr. L. Henry, president of the Belgian Institut pour l'Encouragement de la Recherche Scientifique dans l'Industrie et l'Agriculture. Mr. Malcor is president of the directing committee of the project, and the operating group is Dr. Henry's organization in Belgium.

* *This memorandum was the basis of the article: "International Research Project Studies Low Shaft Blast Furnace," JOURNAL OF METALS, September 1951, p. 720.*

AIME Annual Meeting Program, February 18 to 21, 1952

Statler Hotel, New York

Names of Divisions and Subdivisions are coded as follows: MIED—Mineral Industry Education Div. MED—Mineral Economics Div. M—Mining Subdiv. G—Geology Subdiv. Geophys—Geophysics Subdiv. NM—Nonmetallics; Industrial Minerals Div. Coal—Coal Div. MBD—Minerals Beneficiation Div. IMD—Institute of Metals Div. ISD—Iron and Steel Div. Petroleum Branch—Named as such. SEG—Society of Economic Geologists.

SATURDAY, FEBRUARY 18

10 am to 5 pm
Council of Section Delegates

SUNDAY, FEBRUARY 17

1 pm
Student Relations Committee

2 pm
Board of Directors

2:30 pm
MIED—*Mineral Economics Instruction*

5:30 pm
MIED—*Cocktails and Buffet Supper*

7:30 pm
MIED—*Mineral Education*

8 pm
IMD—Program Committee

MONDAY, FEBRUARY 18

8:30 am
Registration

9:45 am to 12 m
MIED—*General Session*
M—*Drilling Symposium*
MBD—Business Meeting
NM—*Sulphur and Sulphuric Acid*
Coal—*Mining*
IMD—*Properties*
IMD—*Solidification and Physical Metallurgy*
EMD—*Copper and Lead*

10 am
Metals Branch Council

10:30 am
Petroleum Branch—*Technical Session*

12 m
Welcoming Luncheon.
Judge Harold Medina, Speaker

2 pm
IMD—Executive Committee

2:30 pm
MED—*Foreign Development*
M—*Drilling Symposium*
G, Geophys—*General Session*
NM—*Ceramic Raw Materials*
Coal—*Mining*
MBD—*Milling Equipment*
Petroleum Branch—*Technical Session*
IMD—*Research in Progress*
IMD—*Orientation and Plasticity*
EMD—*Zinc*
EMD—*Training Extractive Metallurgists*

4:30 pm
IMD—Membership Committee

5:30 to 7 pm
Pre-Smoker Cocktail Party

7 pm
Dinner-Smoker

TUESDAY, FEBRUARY 19

7:30 am
IMD—Publications Committee Breakfast

8:45 am
Petroleum Branch—*Economics*

9 am to 12 m
MED—*New Production, Uses, and Trends*
M—*Open Pit Mining*
G, SEG—*Lead and Zinc Deposits*
Geophys—*Aerogeophysics*
NM—*Lime Production*
Coal—*Preparation*
MBD—*Materials Handling*
MBD, EMD—*Manganese Conservation*
IMD—*Theory of Metals, Seminar*
ISD—*General Session*
EMD—*Physical Chemistry of Extractive Metallurgy*

9:30 am
Women's Auxiliary Annual Meeting

10 am
Mining Branch Council

11 am
Howe Memorial Lecture,
by Augustus B. Kinzel

12:15 pm
MIED—Luncheon
Indus. Min. Div.—Luncheon
ISD—Executive Committee Luncheon
EMD—Physical Chemistry Committee Luncheon
Mining and Metallurgical Society of America—Luncheon

2 pm
MED—*General Session*
M—*Canadian Mining Practices*
Geophys—*Aerogeophysics*
NM—*Portland Cement*
Coal—*Preparation, Heavy Density Symposium*
MBD—*Pyrolysis and Agglomeration*
MBD—*Flotation Theory*
Petroleum Branch—*Production Review*
EMD—*Physical Chemistry of Extractive Metallurgy*
ISD, EMD—*Manganese Conservation, Symposium*
IMD—*Theory of Metals, Seminar*

4 pm
Annual Institute Business Meeting
Coal—Executive Committee

5 pm
Directors Meeting, Executive
Indus. Min. Div.—Executive Committee

6 pm
Metals Branch—Cocktail Party

Evening
Metals Branch—Dinner
Petroleum Branch—Dinner
Informal Dance, AIME

WEDNESDAY, FEBRUARY 20

8 to 9:15 am
MBD—"Scotch Breakfast"

9 am to 12 m
M—*General Session*
G, SEG—*General Session*
Coal—*Utilization*
Coal—*Gasification and Liquefaction*
MBD, NM—*Beneficiation of Industrial Minerals*
MBD—*Operating*
Petroleum Branch—Executive Committee
IMD—*Crystal Structure*
EMD—*Addition Agents in Electrometallurgy*
EMD—*Physical Chemistry and Uncommon Metals*

9:30 am
Women's Auxiliary—*Round Table*

10:45 am
IMD—Annual Business Meeting

11 am
IMD Annual Lecture,
by William Shockley

12:15 pm
M,G,Geophys—Luncheon
Coal—Luncheon
EMD—Executive Committee Luncheon
ISD—Physical Chemistry of Steelmaking Committee Luncheon

2 pm
M,G—*Exploration Drilling*
NM—*Geology of Industrial Minerals*
Geophys—*Engineering Geophysics*
Coal—*Gasification and Liquefaction*
Coal—*Geology*
MBD—*Crushing and Grinding, Operating*
MBD—*Flotation Theory*
IMD—*High Temperature Alloys, Panel Discussion*
ISD—*Oxygen in Steelmaking, Symposium*
EMD—*Addition Agents in Electrometallurgy*

4:45 pm
EMD—Annual Business Meeting

Evening
Annual Banquet
President's Reception

THURSDAY, FEBRUARY 21

9 am to 12 m
M, NM—*Mechanical Mining*
NM—*General Session*
Coal—*Gasification and Liquefaction*
MBD—*Crushing and Grinding, Theory*
IMD—*Transformation and Hardening*
IMD—*Constitutional Diagrams*
ISD—*Oxygen in Steelmaking, Symposium*
EMD—*Uncommon Metals*
EMD—*Addition Agents in Electrometallurgy*

12:15 pm
MBD—Luncheon
IMD—Powder Metallurgy Committee—Luncheon

2 pm
NM, SEG—*Economic Geology*
Coal—*General Session*
MBD—*Cleanup Session*
IMD—*Powder Metallurgy of Metal Ceramic Materials, Symposium*
IMD—*Physical Properties*
ISD—*Oxygen in Steelmaking, Symposium*
EMD—*Uncommon Metals*
EMD—*Addition Agents in Electrometallurgy*

Research In Progress

There is a vast amount of research work for both Government and private industry now underway in the industrial, Government, and university laboratories. JOURNAL OF METALS brings you a summary of some of the outstanding projects, with abstracts or summarizations of the progress thus far on such work prepared by scientists in charge of the activities. Descriptions of the progress of these research projects will be given in greater detail at the Annual Meeting of the American Institute of Mining & Metallurgical Engineers in New York, at 1:30 pm Monday, Feb. 18, 1952, and continued on Wednesday morning, Feb. 20, 1952.

Vanadium-Base Alloys

by William Wilson, Jr.

HIGH purity vanadium only recently has become available in pound lots. A program to explore the physical properties of vanadium-base alloys is in progress at the Armour Research Foundation under the sponsorship of the Wright Air Development Center.

Vanadium-base alloys with titanium, chromium, iron, cobalt, nickel, molybdenum, tantalum, nitrogen, oxygen, etc. are under investigation. The alloys with titanium, nickel, and tantalum appear most promising.

A second phase has been observed in massive vanadium, but it cannot be identified positively at this time.

When heated in air at 700°C and above, vanadium metal forms a molten scale at a rate invariant with time, but at 600°C and below, short time tests indicate that a protective scale is formed. The true dividing point of these processes is undoubtedly the melting point of vanadium pentoxide, 658°C. The effect of alloying elements on scale formation also is being studied.

Arc melted vanadium metal has been successfully hot rolled below 900°C by sheathing it in stainless steel. However, most of the alloys require higher rolling temperatures and exhibit great hardness increases after rolling. Some alloys were brittle at the rolling temperature, but probably the brittleness is a result of contamination.

Experiments indicate that arc melted vanadium can be held at 1050°C for several hours without a material increase of hardness if calcium is put into the sheath as a *getter*. It is expected that the use of calcium in the sheaths will permit the rolling of alloys which formerly appeared brittle because of contamination.

WILLIAM WILSON, JR. is Research Metallurgist, Metals Research Dept., Armour Research Foundation of Illinois Institute of Technology, Chicago.

Vanadium-Oxygen Solid Solutions

by A. U. Seybolt and H. T. Sumsion

AN investigation of the vanadium-rich portion of the vanadium-oxygen phase diagram has been undertaken as part of a study of the effects of gaseous impurities on the properties of pure vanadium. Initial results surprisingly indicate the occurrence of an order-disorder transition similar to that for Cu-Au and Co-Pt alloys. This kind of transformation ordinarily is characteristic of substitutional type alloys, but in this case the solid solution is probably an interstitial one.

Preliminary results indicate a transformation from a digordered body-centered cubic lattice into an ordered body-centered tetragonal lattice on cooling below some critical temperature. Transformation temperatures and the c/a ratio of the tetragonal unit cell appear to vary with oxygen content up to near the limit of solid solubility of oxygen in vanadium which has been previously established by others to be in the neighborhood of 11 pct oxygen by weight. The order-disorder boundaries are being determined by X-ray diffraction, metallographic and electrical resistivity methods.

A. U. SEYBOLT and H. T. SUMSION are with Knolls Atomic Power Laboratory, General Electric Co., Schenectady.

Studies on the Kinetics of Transformation in Titanium Base Alloys

by W. Rostoker

PREVIOUS work has established that the high temperature beta phase in the titanium-molybdenum system can decompose by normal rejection of alpha or by a diffusionless transformation to a metastable phase termed α', which structurally appears to be a supersaturated α. The time-temperature dependence of these reactions may be represented conveniently on conventional TTT charts. Work on the titanium-chromium system has yielded analogous results with the addition of a eutectoid transformation.

Observations made during the early work pointed to the considerable influence of the interstitial elements oxygen, nitrogen and carbon on reaction rates. The addition of 0.5 pct carbon to a titanium-molybdenum alloy appreciably increased the rate of precipitation of alpha. Similarly, it was shown that there was a pronounced difference in the rate of eutectoid decomposition in a titanium-chromium alloy depending on whether iodide titanium or a less pure titanium was used as melting stock. A program is in progress to study the influence of interstitial additions of up to 0.55 pct on reaction rates. To provide a basis of composition, iodide titanium-base alloys are also under study. Particular attention is being paid to grain growth inhibition and minimum-maximum hardnesses. It was found that free carbide dispersions are particularly active in restraining grain growth while not significantly increasing hardnesses.

The results of limited experiment have shown that alloys made from iodide titanium and containing up to 11 pct molybdenum may either crack almost immediately or tolerate as much as 90 pct cold reduction on rolling, depending on the prior heat treatment.

W. ROSTOKER is Research Metallurgist, Metals Research Dept., Armour Research Foundation of Illinois Institute of Technology, Chicago.

Mechanism of Plastic Flow in Titanium

by F. D. Rosi, C. A. Dube, and B. H. Alexander

THIS study of the glide elements in titanium was undertaken to better understand its mechanical behavior, which has been found to be different from that generally associated with metals of hexagonal close-packed structure. This study is also of considerable theoretical interest, since titanium belongs to that group of elements in this structural class that have a c/a ratio less than the ideal for closest packing (1.633). The lattice of these elements is compressed along the c-axis which, in effect, tends to make the basal plane less favorable for slip inasmuch as it reduces the interplanar spacing and the atomic density of this plane. Thus, for titanium, there is a certain indefiniteness about the glide plane, in that planes other than the basal plane may be expected to operate. This work was sponsored by the Office of Air Research, U.S.A.F. Contract AF-33-038-16031.

The plastic behavior of titanium has been investigated at room temperature in deformed, coarse-grained sheet specimens (grains 2 to 6 mm diam), which were produced by a modification of the strain anneal technique. Determination of slip and twinning planes was based on the use of a stereographic plot of a back reflection Laue photograph describing the region where slip and twinning were observed. Identification resulted from the location in these plots of the poles responsible for the slip and twinning traces on the specimen surface.

A number of these stereographic analyses of

F. D. ROSI, C. A. DUBE, and B. H. ALEXANDER are with Sylvania Electric Products Inc., Bayside, N. Y.

coarse crystals deformed by tension, compression and bending showed that at least two slip planes and three twinning planes are operative in the plastic deformation of these crystals. The slip planes are of the type {1010} and {1011} while the twinning planes are of the type {1012}, {1122} and {1121}. In the case of slip, the prismatic type {1010} is by far the more predominant. It is singularly significant that, no matter how complex the deformation, in no case was slip on the basal plane (0001) established. This observation, in addition to the appearance of more than one twinning plane, is a contradiction to the general rule of plastic behavior in hexagonal close-packed metal crystals (Cd, Zn, Mg).

Unfortunately, this method of stereographic analysis does not permit the determination of the slip direction in the planes of slip. Nevertheless, it is noteworthy that both the prismatic {1010} and the first-order pyramidal {1011} planes contain the $\langle 11\bar{2}0 \rangle$ direction, which is both the direction of closest packing and the slip direction in the hexagonal close-packed lattice. It is reasonable to suspect that the slip direction would be preserved, since it has been established that this is a more fundamental property of a metal than the slip plane.

At present, attempts are being made to determine the slip direction by plotting stereographically the rotation of the specimen axis with increasing deformation. At the same time, this study is being extended to include the mechanism of plastic flow in crystals deformed at elevated temperatures and at the temperature of liquid nitrogen.

Dimensional Changes Normal to the Diffusion Direction

by R. W. Balluffi and B. H. Alexander

BY diffusing silver from the vapor phase into thin gold wires at 940° C linear expansions normal to the direction of diffusion and ranging up to 30 pct were obtained. Expansion normal to the diffusion direction is measured by the increase of length of the wire, and expansion parallel to the diffusion direction is obtained from the movement of fiducial markers originally located on the wire surface. The effect occurred in single and polycrystalline wires but was more marked in polycrystalline specimens. Experiments proved that normal expansion is not caused by grain boundary diffusion.

Normal percentage expansion was found to be over half of the parallel percentage expansion in polycrystalline wires. The overall normal expansion began as soon as silver was diffused into the wire surface. Plastic flow, therefore, occurred in the non-diffused core of the wire as a result of the normal expansion produced by diffusion in the volume next to the wire surface. Evidently such plastic flow is possible in thin wires at elevated temperatures. Corresponding flow is much less in massive sandwich type couples, and most volume expansion produced by diffusion is restricted to the diffusion direction.

R. W. BALLUFFI and B. H. ALEXANDER are associated with Sylvania Electric Products, Inc., Bayside, N. Y.

Embrittlement of High Chromium Ferritic Stainless Steels at 475°C

by A. J. Lena and M. F. Hawkes

THE high chromium ferritic stainless steels when heated in or slowly cooled through the temperature range of 425° to 525° C show a complete loss of ductility. This embrittlement is being investigated by single crystal X-ray methods, metallographically, and by changes in physical and mechanical properties.

Single crystals of a 31.4 pct Cr alloy have been prepared by the strain anneal method. Vickers hardness measurements on single crystals of this alloy aged at 475° C show an initial slight decrease followed by a continuous large increase for times from 0.5 to 400 hr. The hardness increase is equivalent to approximately 15 R$_c$ numbers. These results indicate that the embrittlement is not simply caused by a grain boundary precipitate. A high purity vacuum melted 30 pct Cr alloy has shown a similar increase in hardness; therefore, it is to be expected that the embrittlement is inherently related to the Fe-Cr system.

In addition to the large increase in hardness, the electrical resistance decreases appreciably, and the coercive force increases slightly. The only previously published evidence of any metallographic effect has been that of grain boundary widening with increased aging time using conventional etching reagents. However, a Widmanstätten pattern has been observed in the aged 31.4 pct Cr alloy when etched microscopically in a 50 pct boiling HCl solution. This Widmanstätten type pattern was not found in specimens quenched from 1100° C or in specimens aged at higher temperatures where sigma is known to form. It was not possible to resolve a precipitate, and it is believed that this might be a selective etching effect along planes of alloy depletion.

Single crystal analysis by the Laue back reflection technique shows a small amount of asterism in the early stages of aging. This asterism builds up to a maximum after 50 min at 475° C and then decreases without the formation of any new spots. Further work is now in progress using single crystal-monochromatic radiation methods. It is believed that this work might lead to a prediction as to the nature of this embrittlement; that is, whether the embrittlement is caused by precipitation of a second phase, clustering prior to precipitation of a second phase, or to an ordering reaction.

A. J. LENA is a Graduate Student, and M. F. HAWKES is Associate Professor, Dept. of Metallurgical Engineering, Carnegie Institute of Technology, Pittsburgh.

Diffusion in Iron Oxides

by L. Himmel, R. F. Mehl, and C. E. Birchenall

MEASUREMENTS have been made on the rates of self-diffusion of iron in each of the three oxides of iron, using the decrease in surface activity method with Fe^{59} as tracer. In bulk, homogeneous wüstites, which are prepared by oxidizing pure iron to completion in controlled hydrogen-water vapor atmospheres, the self-diffusion coefficient is a linear function of the composition of the oxide, increasing with increasing deviation from stoichiometric composition, as is to be expected if a vacancy mechanism of diffusion is operative. The temperature dependence of the diffusion coefficient of iron in FeO yields an activation energy, Q, of very nearly 30,000 cal per mol, which is in good agreement with the value obtained from rate constant data for the scaling of iron in air or oxygen.[1] Evidence is thus provided that the rate-determining factor in the oxidation of iron at high temperatures is the rate of transport of iron ions through the innermost wüstite layer.

Suitable magnetite specimens were obtained by complete oxidation of iron in water vapor. At corresponding temperatures, the rates of self-diffusion of iron in Fe_3O_4 are 2 to 3 orders of magnitude lower than in wüstite. Inasmuch as the measured diffusion rates do not appear to be sufficient to account for the observed rate of growth of Fe_3O_4 on wüstite (in the absence of any free iron), it may be inferred that the growth of the Fe_3O_4 layer occurs largely by oxide ion migration, with an appreciable contribution from iron ion diffusion, the relative contributions being dependent upon the temperature.

Diffusion data for hematite have been obtained on natural single crystals of α-Fe_2O_3 (rhombohedral) in directions both parallel and perpendicular to the c-axis. Here the measurements indicate a negligible diffusion rate for iron ions, even at temperatures up to 1200°C; transport by oxide ions rather than by interstitial iron ions is therefore favored in Fe_2O_3. No evidence of any marked anisotropy in diffusion rates has been observed.

These conclusions are in accord with the recent marker movement studies of Davis, Simnad, and Birchenall.[2] A number of interesting microscopical observations have also been made on the growth and structures of oxides formed on pure iron, particularly wüstite. It has been found, for example, that the product (αFe + Fe_3O_4) of the isothermal decomposition of wüstite below 560°C is lamellar or pearlitic in nature.

[1] O. Tesche: Trans ASM 42, p. 641 (1950).
[2] M. H. Davis, M. T. Simnad and C. E. Birchenall: JOURNAL OF METALS, p. 889 (October 1951).

L. HIMMEL is Research Engineer, Westinghouse Research Laboratories, East Pittsburgh; R. F. MEHL is Head, Dept. of Metallurgical Engineering, and Director of Metals Research Laboratory, and C. E. BIRCHENALL is Member of Staff, Metals Research Laboratory, Carnegie Institute of Technology, Pittsburgh.

Deformation of Ferrite Single Crystals

by F. L. Vogel, Jr. and R. M. Brick

THE mechanism and critical resolved shear stresses for deformation of ingot iron single crystals have been studied in the temperature range from −70°C to +200°C.

At room temperature and below, strong double yield behavior is evident and the initial glide markings are observed only macroscopically. These glide markings do not appear necessarily on a specific crystallographic plane but always contain the close packed [111] direction of slip.

As the test temperature is increased above room temperature the double yield behavior becomes weaker, finally disappearing at 200°C where homogeneous yielding is observed. The macroscopic surface markings likewise become less evident and the glide markings are the familiar microscopically visible slip lines. At these slightly elevated temperatures, a definite preference is established for (110) as the plane of slip.

This work is supported by the office of Air Research, Air Material Command, Contract No. AF 33(038)-15889.

F. L. VOGEL, JR. and R. M. BRICK are in the Dept. of Metallurgy, University of Pennsylvania, Philadelphia.

Slip & Twinning in Single Crystals of Beryllium

by H. T. Lee and R. M. Brick

THE critical resolved shear stress for basal slip in beryllium single crystals under compression has been measured at different temperatures in the range from room temperature to 500°C. In these studies, the basal plane has been from 20° to 70° from the stress axis. When the compression axis was normal to basal planes, deformation was practically solely elastic up to rupture at about 300,000 psi. Compression parallel to the basal plane caused the predicted $10\bar{1}2$ twinning and also prismatic slip.

To predict the deformation and operative crystal planes for twinning, it was necessary to know the shear direction. A theory of shear for (1012) twinning has been developed which shows that the irrational atomic shears shown by Barrett[1] for atoms

H. T. LEE and R. M. BRICK are in the Dept. of Metallurgical Engineering, University of Pennsylvania, Philadelphia.

near the composition plane become rational movements, i.e., homogeneous shear, at distances of 50 to 100 atoms from the twin interface. It is postulated that this is the minimum thickness of twin crystal which could form and remain in existence. Lattice bending and the resultant asterism found on twinning tend to support the proposed shear hypothesis.

The atomic movements and individual shears which determine the probability of slip or twinning on various planes of close packed hexagonal, body-centered cubic and face-centered cubic lattices have been included in a generalized analysis.

This report is based in large part on work performed on project N6 onr 24908, sponsored by the Office of Naval Research.

[1] Barrett, Cold Working of Metals. ASM 1949, p. 81.

Solid Solubility of Boron in Iron

by M. E. Nicholson

IN recent years there has been a strong belief that the solid solubilities of boron in iron are much lower than as determined by Wever and Müller.[1] Therefore, the solubility of boron in alpha and gamma iron has been redetermined.

Since the solubilities in question were less than 0.1 pct B, a technique of chemically analyzing saturated solid solution was chosen in preference to X-ray diffraction or metallographic techniques. Boron was introduced into high purity iron obtained from the National Research Corp. in the solid state from boron hydride at temperatures of 800° to 900° C. This produced a two phase sample 0.25 in. diam by 4 in. long with a core of unsaturated ferrite and a case of Fe_2B. To produce a saturated ferrite or austenite the samples were annealed about 150 hr. This treatment was sufficient to produce uniformity in that variation in boron content approximated the experimental error of the analytical technique. The specimens were analyzed chemically by a modified Youngstown Sheet and Tube Co. (quinalizarin) colorimetric technique and spectrographic analysis. The solid solubility of boron in iron at 850° C is 0.0028 ± 0.0003 pct B.

To introduce boron into a sample of iron it was surrounded with crystalline boron powder (99 + pct B, 325 mesh) and heated in a dry hydrogen atmosphere 2 hr at 900° C. Under these conditions a case of Fe_2B approximately 0.003 in. thick was produced. At 600° C, 72 hr were required to produce a case of approximately 0.0005 in. Comparatively intimate contact between boron powder and iron is necessary to effect the boron transfer at the maximum rate. In fact the boron uptake by iron is negligible several centimeters from the powdered boron. Boron transfer to iron is negligible even when the powder is packed about the sample and heated either in vacuum or in "wet" argon. Thus it appears that the mechanism of boron transfer is by means of a boron hydride. Thermodynamic calculations indicate the partial pressure of diborane (B_2H_6) at 1200° K is 10^{-9} atm which is too small to account for the experimental behavior. It seems likely that BH_3 may be the transfer compound.

[1] F. Wever and A. Müller: Mitt. Kaiser Wilhelm Institute, Eisenforsch., Düsseldorf. Vol 11 (1929) pp. 193-218.

M. E. NICHOLSON is Assistant Professor at Institute for the Study of Metals, University of Chicago, Chicago.

The System Molybdenum-Boron

by R. Steinitz

THE system Molybdenum-Boron is being investigated in order to understand the behavior at high temperatures. Three room temperature phases have been reported previously, Mo_2B, MoB, MoB_2. It was found that Mo_2B does not melt undecomposed, but transforms in a peritectic reaction to a liquid and a new phase, which possibly is Mo_3B_2. This phase is not stable below about 1800° C. MoB and MoB_2 have definite melting points of 2180° C and 2100° C respectively. Both show allotropic transformations at very high temperatures. The high temperature form of MoB (beta MoB) is isomorphous with CrB (orthorhombic), while that of MoB_2 is the typical hexagonal diboride structure (MoB_2). Therefore, six different structures are established in this system of which three have not been reported previously.

The high temperature structures of the system Mo-B seem to have great similarity with those of Cr-B. The tendency of the boron atoms to form bonds is very strong, so that a loosening of the lattice by heating brings about a reshuffling of the boron atoms.

All high temperature modifications can be retained at room temperature by quenching. All structures have a metallic nature, but the conductivities and other properties are different for the high and low temperature form. Beta MoB and MoB_2 can be stabilized easily at room temperature by the addition of borides of other metals, the room temperature structures of which are isomorphous with the high temperature forms of the molybdenum borides.

R. STEINITZ is with American Electro Metal Corp., Yonkers, N. Y.

Anelastic Studies of the Effects of Nitrogen in Molybdenum

by R. Maringer and G. T. Muehlenkamp

A STUDY of the anelasticity of molybdenum, as affected by nitrogen, was made by means of internal friction tests. Molybdenum wire, impregnated with nitrogen, is inserted as the suspension of a torsion pendulum and oscillated at low frequencies. A stable peak was observed in the internal friction versus temperature curve at 1300 F and a frequency of 1 cycle per sec.

This peak is believed caused by the stress induced diffusion of nitrogen atom in solid solution. The constants for the diffusion of nitrogen in molybdenum are calculated for this temperature assuming the nitrogen is present interstitially. The effects of nitrogen, in solid solution and as a precipitate, on the mechanical properties as a function of temperature of testing and strain rate are given.

R. MARINGER and G. T. MUEHLENKAMP are with Battelle Memorial Institute, Columbus, Ohio.

Orientation Relationships in Cast Germanium

by W. C. Ellis and Jacqueline Fageant

A CYLINDRICAL germanium ingot, $\frac{3}{4}$x1$\frac{1}{2}$ in. formed by progressive freezing from the base was cut into 21 circular slices which were examined microscopically and by X-ray diffraction. The etched surfaces of the slices are shown in Fig. 1.

This examination revealed the following: 1—All

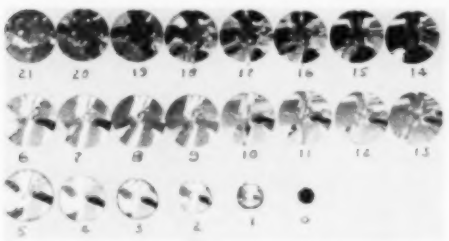

Fig. 1—Etched sections cut from germanium ingot. Freezing began with slice 21 and was complete with slice 0.

regions in the ingot are related through successive orders of octahedral twinning; 2—in the growth of the ingot, twin planes (low energy interfaces) are preserved; 3—regions, when they become large, on further freezing either twin or develop lineage; 4—the growth of regions containing lineage is retarded, and lineage is replaced with a new orientation sweeping in from the side; 5—examination of successive slices shows that crystals sometimes grow sideways with respect to the maximum thermal gradient; 6—there is evidence for the development of first generation twins through sideways growth as a result of accidents in stacking on favorable octahedral planes. These twin planes are those nearly parallel to the maximum thermal gradient of growth.

Explanations are offered for the observations; these are being generalized into the theory of the cast structure of cubic metals.

W. C. ELLIS and JACQUELINE FAGEANT are connected with Bell Telephone Laboratories, Inc., New York.

Distribution of Solute Elements Between Liquid and Solid Germanium

by J. D. Struthers, H. C. Theuerer, E. Buehler, and J. A. Burton

THE distribution of solute elements between liquid and solid germanium has been studied for concentrations in the range from 0.01 to 100 ppm. A known amount of the element is added to a germanium melt from which either a single crystal or a polycrystalline ingot is prepared. The concentration of the element in the resulting solid germanium is determined as a function of the fraction solidified using radioactive tracer techniques and electrical conductivity measurements. These data give the effective distribution coefficient, k, defined as the ratio of the concentration in the solid to that in the liquid from which it solidified. Approximate values of k have been determined for Al, Ga, In, P, As, Sb, Ag, and Au. If appreciable rates of solidification are used equilibrium between the solid and liquid phases may not be maintained, so that nonequilibrium values of k are measured which depend on the exact solidification conditions, and may be several times larger than the true equilibrium distribution coefficients.

J. D. STRUTHERS, H. C. THEUERER, E. BUEHLER, and J. A. BURTON are with Bell Telephone Laboratories, Inc., Murray Hill, N. J.

Orientations in Annealed, Very Large-Grained Aluminum

by R. G. Treuting and W. C. Ellis

IN a run of 2S aluminum (supplied by Scoville Manufacturing Co. through the courtesy of W. D. France) annealed after rolling to 0.027 in., a very large and widely varying grain size was developed, with grains from less than $\frac{1}{8}$ in. to over 2 in. across and an average area of 1 sq in.

Fig. 1—Cube pole orientations in very large grained annealed aluminum strip.

X-ray determination of the mean orientations of 56 grains showed a texture describable in terms of two orientations (Fig. 1): (001) [110] distributed over an oscillation of ± 30° about the rolling direction as axis, along which the [110] is rather eccentrically disposed; and a more closely grouped (within a circle of 15° radius) (011) [$\bar{1}$11] pattern consisting of a twin-related component pair. (The former texture is reported by Hu, Sperry, and Beck[1] as the surface texture of 2S aluminum rolled to a 95 pct reduction while reversing the strip end for end between passes.)

The strip had been annealed as coiled and subsequently flattened prior to this examination. This was evidenced by a progressive and continuous change in orientation across each grain in the rolling direction and little or no change in the transverse direction, corresponding to cylindrical curvature of the lattice on straightening to, closely, the radius of the coiled strip on annealing. A focal effect on the Laue spots was noted, a circular beam being rendered elliptical as by reflection from a cylindrical mirror. No asterism was observed; nor, in this preliminary examination, any evidence of polygonization on a gross scale.

[1] Hu, Sperry, and Beck: (to be published in JOURNAL OF METALS).

R. G. TREUTING and W. C. ELLIS are with Bell Telephone Laboratories, Inc., Murray Hill, N. J.

One and Two Dimensional Sections of Three Dimensional Structures

by C. S. Smith and L. Guttman

BY a simple linear intercept counting method involving no assumptions as to actual shape or distribution of grain boundaries, it is possible to determine accurately the amount of grain boundary surface in any specimen. Consider a three-dimensional array of surfaces having a total area S within an isolated volume V which is to be studied. Now traverse this array with random planes and with random lines in all possible directions. Let L be the length of a given intersecting line and N the number of intersections it makes with the surfaces; let A be the area of an intersecting plane, l the total length of its intercepts with the surfaces, denote by a bar the average value of any of these quantities. The following relations then hold:

$$\frac{S}{V} = 4\frac{\bar{l}}{\bar{A}} = \frac{2\bar{N}}{\bar{L}}$$

These relations are exactly true as long as all possible random sections are averaged. In a similar manner the ratio of number of grain corners to length of boundary trace in a two-dimensional section can be used to give perimeter-to-surface ratio of the faces of the average grains. In a multi-phase alloy each phase can be separately analyzed and the differences between sections in various directions can give information on anisotropy of both shape and size.

C. S. SMITH and L. GUTTMAN are associated with Institute for the Study of Metals, University of Chicago, Chicago.

Principles of Zone-Melting

by W. G. Pfann

A SOLIDIFICATION method known as zone-melting is discussed, a basic feature of which is the traversal of a relatively long charge of solid alloy by a short molten zone, and a basic consequence of which is a high degree of control of the distribution of solute in the ingot. In one class of zone-melting procedures, solute can be spread uniformly over all but a small portion of an ingot. In another, solute can be strongly concentrated at one end of an ingot, thereby purifying the solvent metal in the remainder. Still other variations are possible.

A detailed study has been made of the principles governing the application of zone-melting to the problems of uniformity and purification. The results are expressed mathematically in terms of the number, size, and direction of travel of the zones, and the solute distribution in the starting charge, for idealized freezing conditions, i.e., no diffusion in solid, complete diffusion in liquid, constant value for the distribution coefficient.

W. G. PFANN is with Bell Telephone Laboratories, Inc.

Intercrystalline Failure of Metals at Elevated Temperatures

by O. C. Shepard

THIS investigation is aided by financial support from the Office of Naval Research and has been in progress for five years. It has the objective of finding whether the intercrystalline failure of metals at low strain rates and elevated temperatures is an inherent property of metals or whether it results from environmental damage such as intergranular oxidation in oxidizing atmospheres or reduction of intergranular oxides in reducing atmospheres.

Stress-rupture tests have been made with commercial metals in inert gases and air. Stress-rupture tests of extremely pure gold have been made in air and in a vacuum. Internal friction studies of pure gold are in progress.

Tests to date indicate: 1—In the absence of oxidation, commercial metals are vulnerable to damage from minute amounts of impurities in the environment; and 2—some of the intercrystalline rupture of commercial alloys is caused by damage from the environment but even in the absence of environmental damage metals exhibit a fundamental crystal boundary weakness at high temperatures.

O. C. SHEPARD is associated with Stanford University, Stanford, Calif.

General Aspects of Metallic Binary Phase Diagrams

by R. A. Oriani

IT would be of interest to ascertain how successfully the general features of binary phase diagrams can be correlated with invariant atomic properties of the pure constituents. A group of categories is established and 170 binary systems that fit unambiguously into these classes are culled from the literature. From general considerations, three atomic properties are chosen and defined, and difference parameters calculated for each of the binary systems. These are plotted along three orthogonal axes; the spatial distribution of the points is a measure of the success of the correlation. The fact that this success is only very moderate, demonstrates the inadequacies of the assumptions.

R. A. ORIANI is with the General Electric Co., Schenectady, N. Y.

Effect of Cold Deformation and Annealing on Young's Modulus of Metals

by M. E. Fine and N. T. Kennedy

ACCORDING to simple theory cold deformation, in the absence of a phase change, affects the modulus of metals by 1—introducing residual strains (lowering the modulus), 2—producing or changing a preferred orientation, and 3—in ferromagnetic alloys reducing the stress-produced magnetostriction (increasing the modulus). Furthermore, 4—cold working introduces dislocations and although the applied stresses are probably not high enough to move dislocations past a barrier, the dislocations may move elastically and lower the modulus. Annealing of work-hardened metals decreases residual strains and dislocations, increasing the modulus; may alter the modulus through texture

changes, and in ferromagnetic alloys decreases the modulus by increasing stress-produced magnetostriction.

Effects of cold deformation and annealing on the modulus of aluminum (2S), copper (OFHC), and iron (Armco and electrolytic) are being studied. A dynamic method of measurement is being used; the maximum strains are in the range of 1×10^{-7} to 1×10^{-6}. Although the investigation is not completed, the following observations have been made. In aluminum, elastically isotropic, cold working 20 pct decreases Young's modulus approximately 1 pct presumably by introducing residual strains and dislocations. Cold working copper 20 pct decreases the modulus 3 pct. Some of this may be caused by removal of an annealed texture. Cold working iron 20 pct increases the modulus approximately 2 pct probably because effect 3 predominates.

In iron and copper annealing at a low temperature (100° and 200°C) increases the modulus slightly from removal of residual strains and dislocations. In copper, annealing above 100° to 200°C for a limited temperature range decreases the modulus. For the present this has been attributed to texture development. Annealing above 400° to 600°C decreases the modulus of Armco iron by removal of effect 3.

It is planned to couple these measurements with studies of texture, internal strain, and other properties.

M. E. FINE and N. T. KENNEY are with Bell Telephone Laboratories, Inc., Murray Hill, N. J.

The Influence of Solute Atoms on Crystallographic Texture And Creep Properties

by C. L. Corey

X-RAY integrated intensity measurements were made to determine mosaic block sizes of a base alloy of nominally 20 pct Cr, 20 pct Ni, 20 pct Co, 40 pct Fe and various modifications made by adding individually molybdenum, tungsten, and columbium. The addition of increasing amounts of the large solute atoms generally decreased the mosaic block size, but the effect reached a minimum, after which the size increased with the addition of the solute atoms.

Creep tests were conducted at 1200° and 1500°F. For low stresses at 1200°F, the first additions of the large solute atoms increased the creep rate, but as the concentration of solute atoms was increased, the rate of increase of creep rate was reduced. The creep rate was always reduced by the addition of the incongruous solute atoms for high stresses at 1200°F and for all stresses at 1500°F.

It is postulated that the behavior at 1200°F under low stresses was caused by two interrelated factors: 1—dislocations are initiated predominantly at mosaic boundaries, thus, the smaller the mosaics the larger will be the source area and the greater the rate of generation of dislocations, and 2—the rate of generation of dislocations controls the creep strength at low stresses and low temperatures. At higher stresses and temperatures, the rate of flow of dislocations was assumed to control the creep rate; the rate of flow being restricted by the large solute atoms which 1—acted directly as barriers to the flow of dislocations, and 2—promoted an increasing interaction between moving dislocations which reduced their flow rate.

C. L. COREY is in the Research & Development Dept., Babcock & Wilcox Co., Alliance, Ohio.

Generation of Porosity During Diffusion

by R. W. Balluffi and B. H. Alexander

A METALLOGRAPHIC investigation of copper-alpha brass, nickel-copper, and gold-silver couples revealed that significant porosity is produced in the side of the couple which loses mass by unequal diffusion (e.g. the brass, copper, and silver sides respectively). Careful metallographic preparation was required to reveal this porosity, and a series of critical experiments demonstrated that the porosity was caused directly by diffusion and was not a result of other possible causes. Results indicate that such couples may be considered as the sum of two parts separated by the moving Kirkendall interface. One side loses mass by unequal diffusion and partially contracts causing the Kirkendall effect. The effect is essentially the same as would result from replacing each atom lost by unequal diffusion with a vacancy which is then free to be destroyed by a sintering mechanism or else by hole precipitation. The other side of the couple gains mass and expands but develops no porosity.

It may be shown that the presence of such porosity will strongly influence the measurement of relative diffusivities by the standard Kirkendall method since maximum contraction does not occur. Consequently, copper-alpha brass and silver-gold vapor-solid couples (which do not develop porosity) containing fiducial markers initially on the solid surfaces were used to measure relative diffusivities. The results show that $D_{Cu}/D_{Zn} = 6.5$ and $D_{Ag}/D_{Au} = 3.2$ for both single crystal and polycrystalline specimens at 870° and 940°C respectively.

R. W. BALLUFFI and B. H. ALEXANDER are associated with Sylvania Electric Products, Inc., Bayside, N. Y.

Low Melting Gallium Alloys

by R. M. Evans and R. I. Jaffee

IN recent years, the interest in liquid metals as heat-transfer media for power plants has been very great. The possibility of the development of nuclear power plants has increased this interest and served as the impetus behind much research on low melting metals and alloys for such purposes. The principal reasons for consideration of liquid metals as heat-transfer media lie in their high thermal conductivity and consequent high heat-transfer coefficients, stability at high temperatures, and the high ranges of temperature possible.

The element gallium possesses some of the requisite properties for a heat-transfer liquid. It is a unique material, having a low melting point and a high boiling point. Pure gallium melts at 29.78°C, and suitable alloying will produce a metal which melts below room temperature. The boiling point is about 2000°C. As it is a liquid metal, the heat-transfer characteristics would be good. Gallium is not now readily available, due in part to a lack of uses for the metal. Nevertheless, it is not a rare element, and a sufficient supply of gallium exists to permit its consideration for this use.

Since gallium has some promise as a heat-transfer liquid, owing to its unique properties, research on the subject was carried on at Battelle Memorial Institute at the request of the Bureau of Ships, U.S.N. The research had as its objectives the determination of the effect of alloying on the melting point of gallium, and the study of the corrosion of possible container materials.

In this research, alloys were found which had significantly lower melting points than pure gallium, but none which simultaneously fulfilled other additional requirements, chiefly the corrosion problem. Neither was it found possible to reduce the melting point of certain otherwise suitable alloys appreciably by small additions of gallium or gallium alloys.

The results gave little hope that gallium alloys can be developed which enhance the good properties and minimize the undesirable characteristics of elemental gallium. Thus, gallium now appears less promising than other metallic heat-transfer media.

The experimental thermal-analysis techniques used in this work have been described.[1]

Experimental Results

As a first approximation, the development of low melting gallium alloys was based on alloying elements suitable for use in a nuclear power plant, which also lowered the melting point of gallium.

Information from the literature, summarized in Table I, indicates that tin, aluminum, and zinc are the only suitable elements which cause a lowering of the melting point of gallium. Indium and silver also lower the melting point of gallium, but are of little interest for use in nuclear power plants. Of the elements reported not to lower the melting point of gallium, there is some ambiguity on the behavior of copper. Weibke[2] obtained solidus arrest temperatures of 29°C for Cu-Ga alloys from 60 to 90 pct Ga, 0.8°C lower than the generally accepted melting point. This may be the effect of a eutectic close to gallium, or, more likely, the result of impurities, or experimental error.

The seven elements listed in Table I whose effects were not known were of potential interest if they lowered the melting point of gallium. Their effects were determined experimentally for this reason. Binary alloys containing nominally 2 pct of each of these elements were prepared in the form of 2-g melts by placing the components in a graphite crucible and holding them in an argon atmosphere at 370°C for 5 hr. These melts were then subjected to thermal analysis. In all cases, the solidus temperature was the melting point of gallium. Since these elements (As, Ca, Ce, Mg, Sb, Si, and Tl) did not lower the melting point of gallium, they were not considered further as components of a eutectic-type alloy.

Ga-Sn-Zn Alloys

Preliminary considerations of this system for low-melting alloys were encouraging. All three binary systems were of the simple eutectic type. The composition and melting points of the eutectics were as follows: Sn-9 pct Zn (199°C), Ga-8 pct Sn (20°C), and Ga-5 pct Zn (25°C). Therefore, the probability of a ternary eutectic was high. For reasons to be discussed later, aluminum could not be used as an alloying constituent, leaving the Ga-Sn-Zn system as the only one of interest for low-melting gallium-

Table I. Available Information on the Effect of Binary Additions on the Melting Point of Gallium

Metal	Type of Effect	Ga-Rich Eutectic: Pct Addition	Ga-Rich Eutectic: Temperature, °C	Reference
Sn	Melting point lowering	8	20	2
Al	Melting-point lowering	Near Ga	26	4
Zn	Melting-point lowering	5	25	2
In	Melting-point lowering	25	16	5
Ag	Melting-point lowering	5	25	6
Bi	No effect on melting point	0	30	2
Pb	No effect on melting point	0	30	2
K	No effect on melting point	0	30	7
Na	No effect on melting point	0	30	7
Cd	No effect on melting point	0	30	2
Hg	No effect on melting point	0	30	2
Cu	No effect on melting point	0	30	3
As	Effect not known			
Ca	Effect not known			
Ce	Effect not known			
Mg	Effect not known			
Sb	Effect not known			
Si	Effect not known			
Tl	Effect not known			

R. M. EVANS and R. I. JAFFEE, Members AIME, are associated with Battelle Memorial Institute, Columbus, Ohio.

Discussion on this paper, TP 3239E, may be sent, 2 copies, to AIME by April 1, 1952. Manuscript, Sept. 14, 1951. New York Meeting, February 1952.

rich alloys of three or more components. Consequently, considerable effort was expended in working out the liquidus surface.

By thermal-analysis methods, it was quickly found that the ternary-eutectic temperature was 17°C, 3° lower than that of the Ga-Sn eutectic. The ternary-eutectic composition was found by following the eutectic-valley lines issuing from the three binary eutectics, as determined by thermal analysis of selected ternary alloys. The composition found was 62 pct Ga-12 pct Sn-6 pct Zn. This ternary alloy contained less gallium than either binary eutectic and had a lower melting point.

Compositions and thermal arrests of Ga-Sn-Zn alloys are given in Table II. Data on the binary Ga-Sn and Ga-Zn systems were taken from Puschin and coworkers,[1] and data on the Sn-Zn system from Hansen.[2] The liquidus surface obtained for the Ga-Sn-Zn system is shown in Fig. 1, with an enlarged view of the gallium-rich corner in Fig. 2. The field where primary gallium is crystallized is not known with precision, because not enough alloys were tested to determine it completely. The surface shown is accurate to ±2.5°C, however. The eutectic line arrests obtained experimentally were checked against those expected from the liquidus surface. In all cases, a good check was obtained.

Several attempts were made to determine the ternary-eutectic composition by filtering a partially molten alloy at the ternary-eutectic temperature. An alloy of 85 pct Ga-13 pct Sn-2 pct Zn weighing 16 g was made up for these tests. It was cooled until eutectic supercooling had taken place and solidification started. The partially solidified alloy at 17°C, the eutectic temperature, was then filtered through a sintered-quartz filter. The filtrate weighed 11 g and analyzed 86.4 pct Ga-11.8 pct Sn-2.0 pct Zn. This obviously does not agree with the eutectic composition obtained by thermal analysis. The ternary freezing diagram in Fig. 1 permits an explanation of the discrepancy: the eutectic-line arrest was supercooled, and, when the filtration was made, the liquid of the eutectic-line composition was filtered. The eutectic-line composition, when all primary tin had crystallized, would be 87.5 pct Ga-10.5 pct Sn-2.0 pct Zn. Since the actual filtrate is halfway between this composition and the original melt, it appears that about half the primary tin also got through the filter. From this, and similar experiences, it was concluded that filtration to isolate eutectic liquids is unreliable for gallium-rich alloys.

In considering the Ga-Sn-Zn alloys for liquid-metal use, it would appear better practice to choose compositions on the Ga-Sn side of the eutectic valley because of the steep slope of the liquidus surface of the primary zinc field. In this way, much better control of the liquidus temperature would be possible, since small variations in composition would have little effect on the melting point.

Alloys Containing Aluminum

Aluminum added to Ga-Sn-Zn alloys at first appeared to be advantageous. The invariant point of gallium-rich Ga-Sn-Zn-Al alloys on a virgin run was found to be 15.5°C. However, on rerunning the same alloys, the invariant point obtained was 17°C, identical with that of the Ga-Sn-Zn eutectic.

The Ga-Sn-Zn-Al alloys were found to oxidize very rapidly in air at room temperature. Held at 50°C for 3 to 4 hr, they tended to turn to powder. To see which of the elements was promoting the oxidation, the alloys listed below were held in air at 100°C for 24 hr and the following observations were made:

Alloys	Observations
80 pct Ga-20 pct Sn	Some skin, not serious
97.5 pct Ga-2.5 pct Zn	Heavy skin, not serious
97.5 pct Ga-2.5 pct Al	Heavy skin, re-forms on removal
78 pct Ga-20 pct Sn-2 pct Zn	Some skin, not serious
78 pct Ga-20 pct Sn-2 pct Al	Very bad oxidation, little liquid left

It is apparent that aluminum is responsible for the bad drossing of Ga-Sn-Zn-Al alloys. Drossing caused

Table II. Thermal-Analysis Data on Ga-Sn-Zn Alloys

Alloy No.	Composition, Wt Pct			Thermal Arrests			Type of Curve Used
	Ga	Sn	Zn	Liquidus, °C	Eutectic Line, °C	Solidus, °C	
						17	Inverse Rate
1	20	74.0	6.0	140		17	Inverse Rate
2	20	72.0	8.0	147	146	17	Inverse Rate
3	20	70.0	10.0	165		17	Inverse Rate
4	20	78.0	1.0	163		17	Inverse Rate
21	20	77.0	3.0	157		17	Inverse Rate
22	20	77.0	3.0	225	141	17	Inverse Rate
23	20	60.0	20.0	199	144	Not checked	Inverse Rate
52	20	65.0	15.0	190		Not checked	Inverse Rate
4	40	55.0	5.0	115		19	Inverse Rate
5	40	53.0	7.0	113	111	17	Inverse Rate
6	40	50.0	10.0	120–125*		Not checked	Inverse Rate
24	40	59.0	1.0	122		Not checked	Inverse Rate
25	40	57.0	3.0	117		Not checked	Inverse Rate
29	40	45.0	15.0	163	106	Not checked	Inverse Rate
31	40	47.5	12.5	148	107	17	Inverse Rate
32	40	54.0	6.0	157	85	Not checked	Inverse Rate
18	50	28.0	22.0	182	76	Not checked	Inverse Rate
19	50	28.0	22.0	203	65	Not checked	Inverse Rate
20	50	22.0	28.0	180		17	Inverse Rate
7	60	36.0	4.0	77		Not checked	Inverse Rate
8	60	33.0	7.0		72	Not checked	Inverse Rate
9	60	30.0	10.0			Not checked	Inverse Rate
26	60	39.5	0.5	87		16	Inverse Rate
27	60	38.0	2.0	84	62	Not checked	Inverse Rate
28	60	25.0	15.0	141	64	18	Inverse Rate
30	60	27.5	12.5	125		17	Inverse Rate
10	80	17.0	3.0	72	21	Not checked	Inverse Rate
11	80	14.0	6.0	26		16	I R and time temp.
12	80	11.0	9.0	84	19	16	I R and time temp.
13	80	7.5	12.5	110	21	17	Time temp.
14	80	4.0	16.0	123	18	17	Time temp.
17	85	13.0	2.0	54*	22	17	Time temp.
33	85	8.0	10.0	193		17	Time temp.
34	85	3.0	6.0	15		17	Time temp.
35	90	8.0	2.0	23		17	Time temp.
15	90	5.0	5.0	22		16.5	Time temp.
16	90	4.0	6.0	25		17	Time temp.
36	92	2.0	6.0	27		17	Time temp.
37	94	4.0	2.0	24		17	Time temp.
38	95	2.0	3.0				

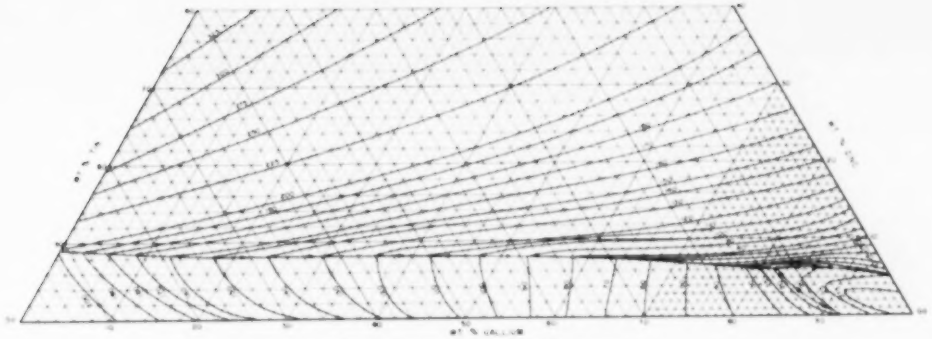

Fig. 1—Liquidus surface of Ga-Sn-Zn system.

by the aluminum appears to be worse when tin is present. The quaternary arrest reverts to the Ga-Sn-Zn arrest as a result of loss of aluminum by oxidation.

Dilution of Ga-Sn-Zn Eutectic

When a material as costly as gallium is intended for heat-transfer purposes, it is of interest to dilute it as much as possible, while still retaining its low melting characteristics. With this view in mind, a study was made of methods of diluting the Ga-Sn-Zn eutectic so as to maintain its 17 °C solidus temperature and minimize the increase in liquidus temperature.

Zinc: The Ga-Sn-Zn eutectic alloy may be diluted to lower gallium contents with minimum increase in temperature by following the eutectic valley to the Sn-Zn eutectic, see Fig. 1. The diluted alloys are sandy or gritty at room temperature, and do not tend to form large lumps.

Lead-Tin: Only limited data were gathered on this dilution. Data obtained on dilution of the Ga-Sn-Zn eutectic with 82 pct Sn-18 pct Pb are given in Table III. The mixed alloys at room temperature were sandy or gritty, similar to the eutectic diluted with zinc.

Lead-Tin-Bismuth: Dilution of the Ga-Sn-Zn eutectic with the Pb-Sn-Bi eutectic was made at several gallium contents. The results are shown in Fig. 3. The liquidus of the Ga-Sn-Zn eutectic is raised sharply to the Pb-Sn-Bi eutectic temperature by the

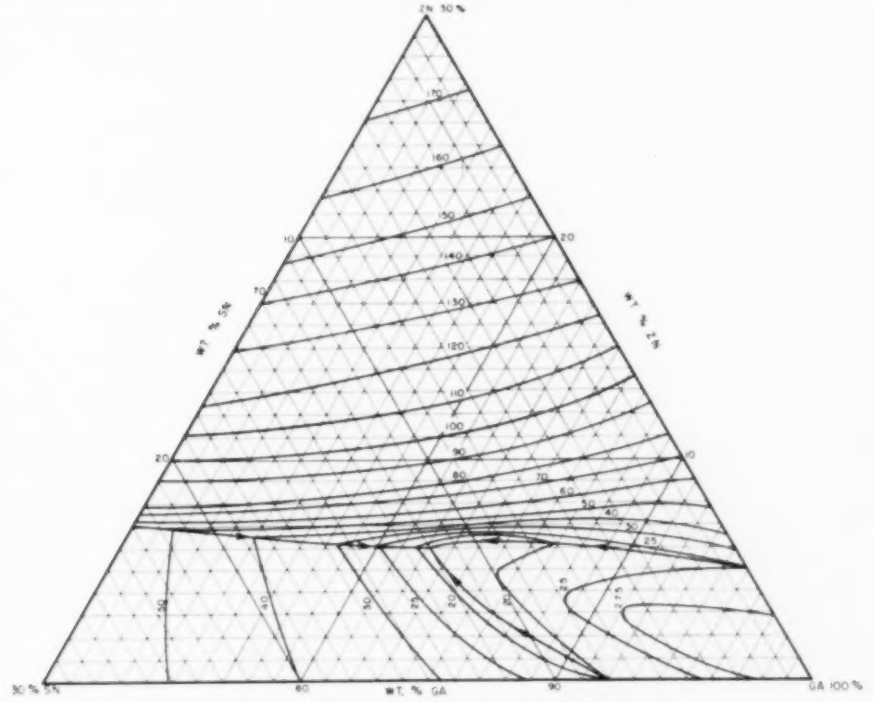

Fig. 2—Liquidus surface of gallium corner of the Ga-Sn-Zn system.

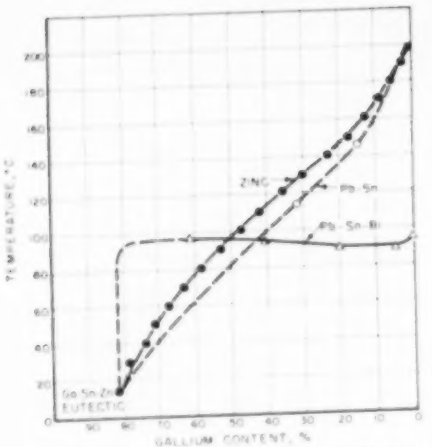

Fig. 3—Dilution of Ga-Sn-Zn eutectic with zinc, Pb-Sn (18 pct Pb), and the Pb-Sn-Bi eutectic, curves show liquidus temperature only. All solidus temperatures in range 17° to 22°C.

addition of Pb-Sn-Bi eutectic. The solidus of the gallium alloy is raised slightly at the same time. These are practically the conditions for two immiscible liquids, each of which freezes at its own melting point. Or, if the liquids are miscible above the Pb-Sn-Bi eutectic melting point, it is clear that the Pb-Sn-Bi alloy practically all freezes out at its freezing point. There appears to be a slight miscibility between the two alloys, because the solidus temperature of the gallium alloy is raised.

Further evidence of selective freezing of the two eutectic components comes from the appearance of these alloys at room temperature. The Pb-Sn-Bi component solidifies into a single hard lump located at the bottom of the liquid-gallium component of the alloy. This is a bad characteristic for liquid metals, which may have to be pumped through zones of variable temperature.

Comparison of Diluents. Fig. 3 shows the liquidus curves obtained with the three diluents. The Zn and Pb-Sn mixtures have normal increases in liquidus temperature as the gallium content decreases. Also, they form true, pasty solid-liquid mixtures on cooling to room temperature. The Pb-Sn-Bi diluent results in a freezing curve characteristic of immiscible liquids and crystallizes as a solid lump in the liquid-gallium alloy. The best alloys, therefore, for reducing the gallium content of a complex system are Pb-Sn and Zn. Pb-Sn is preferred, because its liquidus curve is 10° to 15°C lower than that of zinc. Additional work on variation of the Pb-Sn ratio of this diluent might bring further lowering of the liquidus temperature. The optimum would be reached when the bottom of the eutectic valley to the Pb-Sn binary eutectic was located.

Corrosion of Metals by Ga and Ga Alloys

Gallium has been found to be very corrosive to most solid metals. The present work included an investigation of the corrosion of Ta, W, Be, Ti, Mo, siliconized Mo, and siliconized Fe. The results of this work, together with the results of other work on the problem, were adequately summarized by Kelman, Wilkinson, and Yaggee.[7] It should be pointed out here, however, that the Ga-Sn-Zn eutectic alloy was found to be somewhat less corrosive than gallium itself. Nevertheless, it may be classed as an extremely corrosive material at elevated temperatures.

Table III. Data for Dilution of Ga-Sn-Zn Eutectic with the Pb-Sn Alloy

Ga-Sn-Zn Eutectic, Pct	Pb-Sn, Pct	Overall Percentage Ga	Sn	Zn	Pb	Liquidus, °C	Solidus, °C
0	100	0	82.0	0	18.0	205	183
18	82	14.8	69.1	1.1	15.0	146	17
39	61	32.0	54.7	2.3	11.0	117	17
100	0	82.0	12.0	6.0	0	17	17

Summary

The low melting point and high boiling point of gallium make it of interest as a liquid-metal heat-transfer medium. The only alloying elements which are suitable for use in nuclear power plants, and, at the same time, further lower the melting point of gallium, are tin, aluminum, and zinc. The low melting gallium alloys with these elements were investigated. Aluminum was found to be unsuitable, because it made the gallium alloys susceptible to excessive drossing. Tin and zinc were found to form a ternary eutectic with gallium, located at 82 pct Ga-12 pct Sn-6 pct Zn, melting at 17°C. The liquidus surface of this system was determined. These data show how to dilute the ternary eutectic with zinc with minimum increase in melting point. Pb-Sn was also investigated as a diluent, and appeared to be slightly better than zinc. In the course of this work, it was found that As, Ca, Ce, Mg, Sb, Si, and Tl do not lower the melting point of gallium.

The corrosivity of gallium is so great that the only metals capable of containing it at elevated temperatures are tungsten and tantalum. The Ga-Sn-Zn eutectic is somewhat less corrosive, but still appears to be too corrosive to permit its use as a liquid-metal heat-transfer medium.

Acknowledgment

The authors wish to acknowledge the assistance of E. O. Fromm for much of the experimental work and the Department of the Navy, Bureau of Ships, under whose sponsorship the work was done. Much helpful guidance was received from R. W. Dayton, H. W. Russell, and B. W. Gonser of the Battelle staff.

References

[1] R. M. Evans, E. O. Fromm, and R. I. Jaffee: A Sensitive Method for Thermal Analysis of Very Low Melting Alloys. JOURNAL OF METALS (January 1952), *Trans.* AIME, p. 74.

[2] N. A. Puschin, S. Stepanovik, and V. Stajic: The Alloys of Gallium with Zinc, Cadmium, Mercury, Tin, Lead, Bismuth, and Aluminum. *Ztsch. anorg. allgem. Chem.* (1932) **209**, pp. 320-334.

[3] F. Weibke: *Ztsch. anorg. allgem. Chem.* (1934) **220**, pp. 293-311.

[4] E. Jenckel: Alloys of Aluminum with Gallium. *Ztsch. Metallkunde* (1934) **26**, pp. 249-250.

[5] S. J. French, D. J. Sanders, and G. W. Ingle: The System Gallium-Indium. *Journal Physical Chemistry* (1938) **42**, p. 265.

[6] F. Weibke, K. Meisel, and L. Weigels: *Ztsch. anorg. allgem. Chem.* (1936) **226**, p. 201.

[7] E. Einecke: *Das Gallium*. p. 65. (1937) Leipzig. L. Voss.

[8] M. Hansen: *Aufbau der Zweistoffliegerungen*. (1936) Berlin. J. Springer.

[9] L. R. Kelman, W. D. Wilkinson, and F. L. Yaggee: Resistance of Materials to Attack by Liquid Metals. *Liquid Metals Handbook* (June 1950) pp. 77-126. U. S. Govt. Printing Office.

Cast Molybdenum of High Purity

by G. W. P. Rengstorff and R. B. Fischer

A study was made of the effect of impurities on the bend ductility of cast molybdenum. High purity molybdenum was prepared by remelting under high vacuum. The ductility of "transverse-grain" specimens indicated that intergranular brittleness decreased with an increase in purity of the metal.

THE production of as-cast molybdenum with high ductility at room temperature would make working of the metal easier and increase the usefulness of the as-cast metal. Furthermore, a knowledge of the factors that influence the ductility of as-cast molybdenum might be applied to the problem of making fusion weldments having satisfactory room-temperature ductility.

Individual grains of commercial as-cast molybdenum are slightly ductile at room temperature. However, the presence of carbides at the grain boundaries may cause the metal to fracture in a brittle manner. This behavior has been discussed.[1]

The amount and distribution of the impurities in as-cast molybdenum would be expected, from previous research on the metal, to have considerable influence on its ductility. Some effects of oxygen and carbon on the mechanical behavior of the metal were discussed by Parke and Ham,[2] Woodside,[3] and Zappfe, Landgraf, and Worden.[4] Parke and Ham[2] found that, if a sufficient number of molybdenum oxide particles were present at the grain boundaries, the intergranular cohesion was reduced to the extent that arc-melted molybdenum would rupture intergranularly during hot forging. They also found that if the oxygen content was less than 0.003 pct, the cast molybdenum was hot forgeable. It is suspected, however, that forgeable molybdenum may contain a small amount of oxide that could reduce the ductility of the as-cast metal at room temperature. Also, there is the possibility of the unfavorable distribution of other impurities having a detrimental effect on the ductility of cast molybdenum.

The results of a study of the influence of purity on the room-temperature ductility of cast molybdenum are presented here.

Vacuum Arc-Melting to Produce High Purity Mo

One way of determining the effect of impurities on the ductility of molybdenum is to prepare and test metal as free of all impurities as possible. Accordingly, the present investigation was undertaken with this in view.

Arc melting in high vacuum (less than 0.1 micron of mercury) was chosen as the method for reducing the impurities below the concentrations occurring in commercial molybdenum. Commercial arc melting of molybdenum is carried out at about 50 microns pressure. During the arc melting, carbon and oxygen in the metal react to form carbon monoxide. By virtue of the vacuum process, the partial pressure of carbon monoxide is maintained at such a low value that the reaction greatly lowers oxygen and carbon contents. An excess of at least 0.03 pct C is used in commercial arc melting to insure that the oxygen content will be below 0.003 pct.

The excess carbon remaining after the deoxidation step forms carbides on freezing. Some of the carbides precipitate at the grain boundaries and, as will be shown, have an unfavorable effect on the room-temperature ductility. In the present work, only the small amount of carbon (0.003 pct) contained in the commercial powder-metallurgy molybdenum used for melting stock was present. Partial removal of oxygen from the melt probably occurred as the result of the volatilization of molybdenum oxides, or by distillation of oxygen at the high melting tem-

G. W. P. RENGSTORFF, Junior Member AIME, is Principal Metallurgical Engineer, and R. B. FISCHER is Assistant Supervisor, Battelle Memorial Institute, Columbus, Ohio.

Discussion on this paper, TP 3212E, may be sent, 2 copies, to AIME by April 1, 1952. Manuscript, Sept. 4, 1951. New York Meeting, February 1952.

This research was supported by ONR (Contract No. N9onr 82100, Task Order No. N9onr 82101, Project NR031-339).

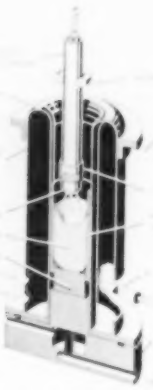

Fig. 1—Vacuum arc furnace used to prepare high purity molybdenum ingots. Arrows show schematically the direction of flow of cooling water.

peratures employed. Some metallic impurities may also have been volatilized. Hydrogen and nitrogen were partially removed during melting. A description of the arc-melting equipment and procedure follows.

Equipment and Procedure: The arc-melting unit used to purify molybdenum consists of a water-cooled, molybdenum-tipped electrode, a water-cooled copper mold, and a feeder mechanism, all contained in a metal bell jar. Part of the furnace is shown in Fig. 1. The bell jar is evacuated by oil-diffusion pumps with a mechanical back-up pump. The water-cooled mold is 1⅝ in. ID and is lined with two layers of 0.010 in. thick molybdenum sheet. The water-cooled copper electrode is coupled to a molybdenum tip about ⅜ in. in diam and 2 in. in length. The electrode is moved upward or downward by electrically driven rolls under control of the furnace operator. Alternating current (60 cycle at an open-circuit voltage of 90) is supplied to the electrode by a 160 kva transformer. A variable resistance in the circuit permits adjustment of the current as desired throughout the melting operation.

Prior to each melt, the equipment was thoroughly cleaned with carbon tetrachloride, the electrode installed and centered, the molybdenum sheet liners

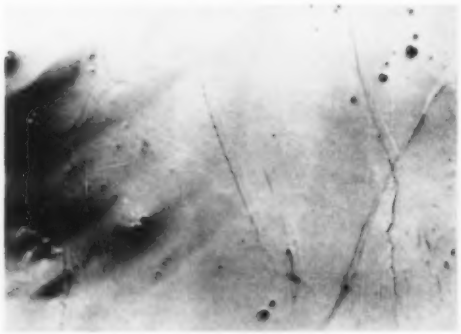

Fig. 2—Micrograph of a grain interface in a fractured molybdenum specimen from high purity ingot No. 1.
This is the surface of a grain revealed when the metal was fractured. Round, dark areas are gas holes. X75. Area reduced approximately 50 pct for reproduction.

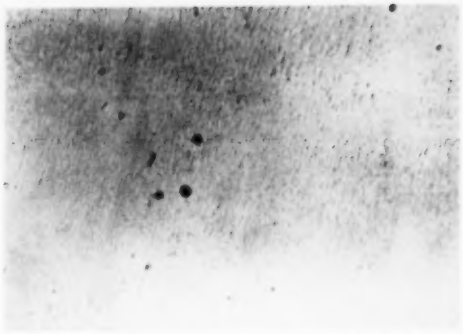

Fig. 3—Reflective area from the interface, shown in Fig. 2, at higher magnification. X400.
Area reduced approximately 50 pct for reproduction.

positioned in the mold, and the mold plug introduced. The molybdenum melting stock was crushed to −8 mesh and placed in a vibrating trough feeder. A molybdenum block was placed on the copper mold plug to prevent adherence of the ingot to the mold plug, as shown in Fig. 1. On top of this plug was placed 50 to 75 g of crushed molybdenum melting stock. Finally, a small ball of molybdenum wool was placed on the crushed melting stock as an aid in starting the arc.

The bell was dropped over the melting chamber, and the chamber evacuated to a pressure of less than 0.1 micron of mercury. The pumping speed was about

Table I. Comparison of Impurity Levels of High Purity Molybdenum and Two Samples of Commercial Molybdenum

Description of Sample	Chemical Composition, Wt Pct			
	Carbon[a]	Oxygen[b]	Hydrogen[c]	Nitrogen[d]
Ingot No. 1, Molybdenum purified by special vacuum arc-melting techniques	0.004[e]	0.0006[f]	0.00004[g]	0.0005[h]
Commercial arc-cast molybdenum	0.032[e]	0.0018[f]	0.00011[g]	0.0006[h]
Commercially sintered molybdenum[i]	0.003[e]	0.007[f]	0.00031[g]	0.001[h]

[a] Analyzed by vacuum fusion.
[b] ± 0.001 pct C.
[c] ± 0.001 pct O.
[d] ± 0.0001 pct O.
[e] ± 0.00005 pct H.
[f] ± 0.00001 pct H.
[g] ± 0.001 pct N.
[h] ± 0.0002 pct N.
[i] Carbon was determined by an improved combustion method.
[j] Melting stock for high purity ingots.

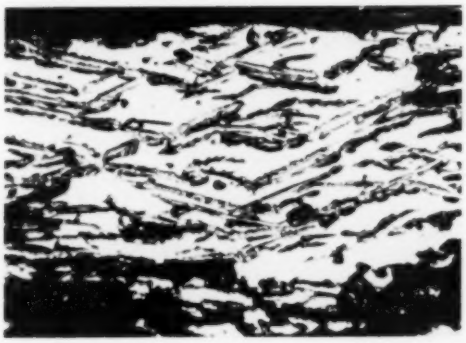

Fig. 4—Carbides at the grain interface in a fractured sample of commercial arc-melted molybdenum containing 0.03 pct carbon.
This is the surface of a grain revealed when the metal was fractured. X75. Area reduced approximately 50 pct for reproduction.

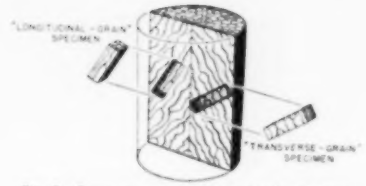

Fig. 5—Orientation of specimens machined from molybdenum ingots.

2800 cu ft per min at 0.1 micron pressure and the volume of the equipment was about 10 cu ft. The leak rate of the equipment was sufficiently low that the pressure rise was less than 1/3 micron of mercury per min when the valves in the lines to the vacuum pumps were closed.

The arc was started by slowly lowering the electrode until it touched the ball of molybdenum wool. Immediately after the arc was struck, the voltage was reduced to about 20 v. At this voltage, and with a $\frac{5}{8}$ in. diam molybdenum electrode tip, the current was about 600 amp. Crushed molybdenum was then fed slowly into the mold and melted to form an ingot. The electrode was gradually retracted as the ingot built up in the mold. Some of the molybdenum tip of the electrode melted during the course of each run and entered the ingot. As the electrode tip shortened, it was necessary to increase the voltage in order to maintain the arc. Near the end of the melting period, the arc voltage had increased to 30 v and the arc current had decreased to 500 amp. The time required for melting a 300 to 450 g ingot was 7 to 10 min. The pressure during the run was less than 0.1 micron. The ingots were cooled to room temperature under the high vacuum.

Ingot No. 1 had a low oxygen content and was produced by arc melting for the purpose of comparing its ductility with that of less pure molybdenum. It was prepared by melting commercially pure molybdenum three successive times according to the melting practice already described. The final ingot weighed about 400 g. The melting stock for the original ingot was a bar sintered from powdered molybdenum and then crushed to −6 +20 mesh. The product of the first melting was crushed to the −6 +20 mesh size and remelted. The product of the second melting was crushed in the same manner to provide the melting stock for the final ingot. Approximately 20 pct of the weight of the ingot produced by each melting came from the electrode tip. The electrode tips were cut from rods made from molybdenum powder, sintered, and swaged. The carbon, oxygen, nitrogen, and hydrogen contents of Ingot No. 1, as well as those of two commercially produced molybdenum samples, are given in Table I.

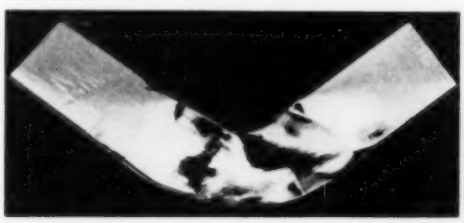

Fig. 6—Side view of transverse-grain specimen "A" of high purity as-cast molybdenum after bend test at room temperature. Compare with Fig. 7. X5. Area reduced approximately 25 pct for reproduction.

Fig. 7—Transverse-grain specimen of commercial as-cast molybdenum containing 0.03 pct carbon after bend test. X5. Area reduced slightly for reproduction.

Table II. Bend-Test Data for Cast Molybdenum Specimens

Specimen	Maximum Angle of Bend, Deg
Transverse-grain specimen A, ingot No. 1 (high purity)	75
Transverse-grain specimen B, ingot No. 1	60
Transverse-grain specimen D, commercial molybdenum, 0.032 pct C	0
Transverse-grain specimen E, commercial molybdenum, 0.032 pct C	0
Longitudinal-grain specimen C, ingot No. 1	53
Longitudinal-grain specimen F, commercial molybdenum, 0.032 pct C	37
Longitudinal-grain specimen G, commercial molybdenum, 0.032 pct C	28

Specimen did not fracture.
Note: The grain sizes of the high purity specimens and the commercial specimens were of the same order.

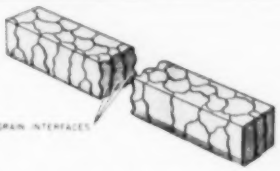

Fig. 8 — Transverse-grain specimen of commercial as-cast molybdenum containing 0.03 pct carbon.

Examination and Testing of Mo

The interfaces of several grains in Ingot No. 1 were examined at high magnification. Fig. 2 is a typical micrograph of these grain interfaces at a magnification of 75 diam. The interfaces were highly reflective. The round, dark areas are gas holes. The parallel lines appear to be traces of crystallographic planes. Fig. 3 is a micrograph of an interface at a magnification of 400 diam. The interface of the high-purity molybdenum shown in Fig. 2 can be compared with the grain interface of a commercial arc-melted molybdenum ingot containing 0.03 pct C shown in Fig. 4. Numerous large carbide particles are present in the latter specimen.

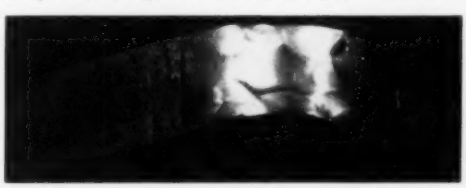

Fig. 9—Relief patterns of grain boundaries on the tension side of high purity bend-test specimen "A."

A transverse bend test was used to determine the ductility of commercial molybdenum and of the high purity molybdenum. The specimens were loaded at the center by means of a cylindrical load applicator $\frac{1}{8}$ in. in diam. The specimens were supported on two cylindrical rolls $\frac{1}{4}$ in. in diam spaced $\frac{5}{8}$ in. between center lines. The size of the transverse bend specimens was 0.15 in. depth x 0.25 in. width x 1 in. length. The bend tests were made at a temperature of about 75°F with a Baldwin-Southwark testing

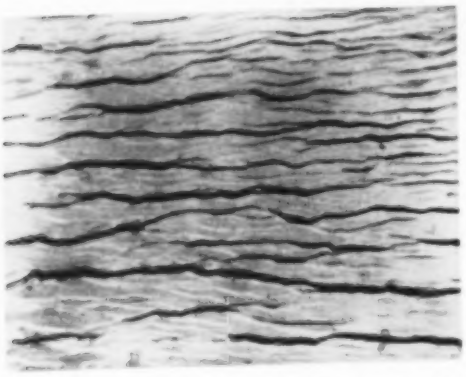

Fig. 10—Micrograph of slip bands in high purity specimen "A" after bend test. X300.
Area reduced approximately 50 pct for reproduction.

machine. A platen speed of 0.005 in. per min was used in applying the load.

The bend-test specimens were machined from small slabs cut from the molybdenum ingots. This was done in such a manner that each specimen was obtained with the major axes of the grains either approximately parallel to or approximately perpendicular to the longitudinal axis of the specimen, as shown in Fig. 5. The specimens were ground to the proper cross-section and given a metallographic polish prior to testing.

The specimens were stressed until fracture occurred, or until very large bend angles were obtained. The bend angle was taken as the measure of ductility. The data obtained from these tests are summarized in Table II. Test results on commercial-cast molybdenum containing 0.03 pct C are included for comparison.

Fig. 6 is a photograph of a "transverse-grain" specimen of high purity molybdenum after bending. Fig. 7 is a photograph and Fig. 8 is a sketch of a transverse-grain specimen of commercial molybdenum containing 0.03 pct C. The brittleness of the latter specimen is evident. The carbides at the grain interface, as shown in Fig. 4, undoubtedly contributed to the brittleness of this specimen. Fig. 9 shows the relief patterns on the bottom of a high purity specimen. The grain size of the specimen is apparent in this macrograph. Fig. 10 is an interesting micrograph of patterns of slip bands found on the high purity specimens.

Inasmuch as the "longitudinal-grain" specimens failed along crystallographic cleavage planes,* as shown in Fig. 11, intercrystalline cohesion did not determine the amounts of bending required for fracture of these specimens. Of the longitudinal-grain specimens, high purity specimen C failed transgranularly at a larger angle of bend than did the less pure specimens F and G. All fractures in the longitudinal-grain specimens, regardless of the degree of bend, were of the cleavage type. Possibly this was because some impurity still remained in the high purity molybdenum and promoted cleavage rather than the shear type of fracture. This is the subject of another investigation now in progress.

* Cleavage planes were the (100) planes; see ref. 1.

† It appeared that the fractures initiated at the grain boundaries and then propagated both intergranularly and transgranularly.

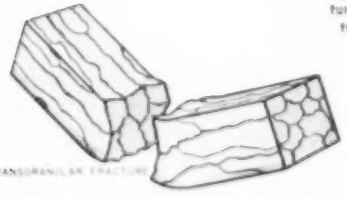

Fig. 11—Fracture of longitudinal-grain specimen

Several ingots of high purity molybdenum were prepared from different lots of commercial molybdenum and studied as described above. The results were found to be reproducible: transverse-grain specimens from these ingots could be bent through cycles of 60 degrees or greater without fracture. Other commercial-cast molybdenum ingots containing 0.03 pct C were found to have mechanical properties similar to those for the commercial ingot mentioned in this work.

Summary

Commercial molybdenum was purified by melting it several times in a high vacuum. Oxygen, hydrogen, and nitrogen (and possibly other elements) were removed from the molybdenum by this treatment. The carbon content, originally at a low level (0.003 pct) in the melting stock, was unchanged by vacuum melting.

The as-cast molybdenum of high purity had considerably greater ductility than did the less pure commercial as-cast metal. Although transverse-grain specimens of the commercial as-cast molybdenum fractured intergranularly† in a brittle manner at room temperature, similar specimens of the high purity molybdenum were ductile under the same test conditions. Therefore, a reduction in the amounts of the impurities at the grain boundaries of cast molybdenum eliminated intergranular brittleness and thereby had a marked influence on the bend ductility of the metal.

Bend tests on longitudinal-grain specimens, in which case the normal stress on the grain boundaries was comparatively low, indicated that the ductility of the individual grains of molybdenum was improved with an increase in purity.

While the influence of reducing the amounts of impurities in molybdenum has been shown, it should be mentioned that data showing the effect of the individual impurities would be most valuable. Also, the possibility should be considered that minor additions of other elements might reduce the effect of the harmful impurities in molybdenum.

Acknowledgment

The support of this work by the Office of Naval Research is gratefully acknowledged. The generous assistance given by R. M. Parke, E. F. Ferrell, C. T. Greenidge, J. H. Jackson, C. B. Griffith, and other staff members of Battelle Memorial Institute is appreciated by the authors.

References

[1] R. B. Fischer and J. H. Jackson: The Ductility of Cast Molybdenum. *Trans.* AIME (1950) **188**, pp. 1149-1153; JOURNAL OF METALS (September 1950).

[2] Robert M. Parke and John L. Ham: The Melting of Molybdenum in the Vacuum Arc. *Trans.* AIME (1947) **171**, pp. 416-427; METALS TECHNOLOGY (September 1946).

[3] G. C. Woodside: Deoxidation Control by Fractography. *Iron Age* (1947) **160**, No. 23, pp. 78-79.

[4] C. A. Zapffe, F. K. Landgraf, and C. O. Worden: Fractographic Study of Cast Molybdenum. *Trans.* AIME (1949) **180**, pp. 616-636; METALS TECHNOLOGY (August 1948).

Internal Friction Measurements On Iron Wires of Commercial Purity

by Åke Josefsson and Eric Kula

DURING the last few years several papers[1-4] have been published in which internal friction measurements have been used to determine the quantity of carbon or nitrogen dissolved in α iron. This method is based on the fact that, in pure Fe-N and Fe-C alloys, nitrogen and carbon cause peaks in the internal friction vs. temperature curve; at a frequency of 1 cycle per sec (cps) these peaks appear at $+20°$ and $+36°$C, respectively, and if internal friction is expressed as Q^{-1}, which is equal to $1/\pi$ times the logarithmic decrement, this figure will, by coincidence, give the weight percentage of nitrogen or carbon in solid solution.[1]

In most of the studies published, very pure iron (Puron) was used. In one case the influence of manganese on the behavior of nitrogen in α iron was mentioned.[4]

It would be of great value, especially for the study of aging and related phenomena, if this method could be applied to commercial mild steel with normal percentages of manganese, phosphorus, sulphur, etc. As a rule, in such steels carbon and nitrogen are present together, and the amounts of these elements in solid solution should preferably be determined separately. The fact that their internal friction peaks appear at different temperatures ($+36°$ and $+20°$C in pure iron) seems promising for such a selective determination. It is necessary, however, that the peaks are narrow enough not to interfere with one another, and further, that there is no effect from carbon on the behavior of nitrogen in stress induced diffusion, and vice versa. According to Fast,[4] however, in the presence of manganese the nitrogen peak gets wider and appears at a higher temperature nearer the carbon peak, and thus the prospects for selective determination are reduced. (The carbon peak was not affected by the presence of manganese.) But even if fully quantitative determinations of the two elements are not attained, some relative figures on the sum of them and an indication of which one is the predominant one, would be of value. Some results from experiments along these lines will be reported here.

Å. JOSEFSSON is Assistant Director of Research, Stora Kopparbergs Bergslags Aktiebolag, Domnarvet, Sweden, and E. KULA, Student Associate AIME, formerly associated with the Research Dept., Stora Kopparbergs Bergslags Aktiebolag, is now Research Assistant, Dept. of Metallurgy, Massachusetts Institute of Technology, Cambridge, Mass.

Discussion on this paper, TP 3180E, may be sent, 2 copies, to AIME by April 1, 1952. Manuscript, May 7, 1951. New York Meeting, February 1952.

Table I. Chemical Composition of Materials

Steel	Analysis, Pct C	Si	Mn	P	S	N	Sol. Al
A	0.02	—	0.27	0.095	0.026	0.015	0.02
B	0.02	—	0.31	0.018	0.013	0.015	
C	0.02	—	0.09	0.012	0.015	0.002	
D	0.04	—	0.34	0.058	0.035	0.013	

An internal friction measuring device was assembled mainly following a description by Ké.[5] The measurements were also carried out as reported in that paper. Table I gives the chemical compositions of the four different materials used in this investigation. All materials were drawn to wires with diameter about 0.8 mm, and the analyses refer to these final shapes.

Determination of Nitrogen Peak

Wires from steels A, B, and C were decarburized in wet hydrogen (about 30 pct H_2O) at 700°C until no carbon or nitrogen could be found by chemical analysis. No peak was then found in the internal friction. The wires were further annealed at 580°C for 16 hr in hydrogen bubbled through a solution of 6.8 pct NH_3 in distilled water. Chemical analyses gave 0.04 pct N in A and C, and 0.06 pct in B. After annealing at 580°C for 15 min in a lead bath and water quenching, the internal friction was immediately measured. The resulting curves are shown in Fig. 1. At these high values of the internal friction the accuracy is comparatively poor; at $Q^{-1} = 0.030$ it is estimated to be ± 0.002. In order to make possible a calculation of the activation energy for diffusion of nitrogen, measurements were made at two different frequencies. Steel A shows rather broad peaks, and their temperatures can hardly be expected to be very accurate. Steels B and especially C are better in this respect. The finding of Fast[4] that manganese broadens the nitrogen peak is con-

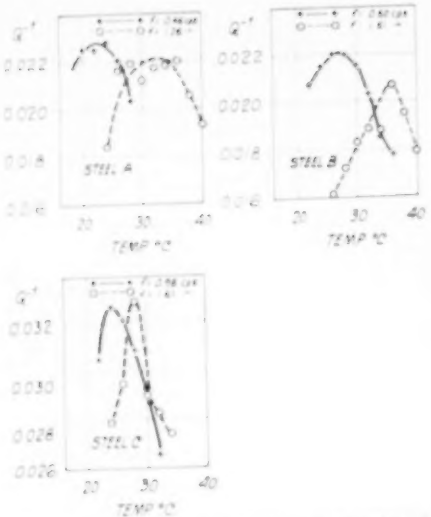

Fig. 1—Internal friction vs. temperature curves for steels A, B and C decarburized and nitrided at two different frequencies.

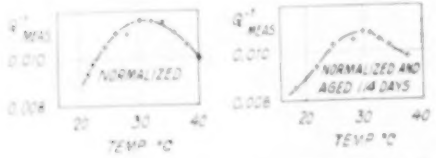

Fig. 2—Internal friction vs. temperature curves for steel D normalized, and normalized and aged.

firmed. The wider peak of steel A as compared to steel B may in some way be due to the higher phosphorus content (and perhaps a more nonuniform distribution of the manganese).

Table II shows the Q^{-1}_{max} values, corrected for the background damping. A rather good agreement between the values obtained at the two different frequencies is obtained. Although the analyzed nitrogen percentages are 0.04 and more, there is much less in solid solution, namely about 0.022 pct in A and B, and 0.033 pct in C. Considering the manganese contents of the steels, it seems possible to assume that manganese lowers the solid solubility of nitrogen (cf. ref. 4).

Table II also shows the values of ΔH (activation energy for diffusion of nitrogen) obtained by applying the equation

$$\Delta H = 2.3\,R\,\frac{\log_{10}(f_1/f_2)}{1/T_1 - 1/T_2}$$

The calculated activation energies can be compared to the figure 20,000 cal per mol obtained by Ke[5] for Puron.

Using the same formula the temperatures for the nitrogen peaks at a frequency $f = 1$ cps have been interpolated for the three steels. Assuming that $t_{1\,cps} = 20°C$ for pure iron with nitrogen in solid solution,[1] this temperature has been raised 4°C in steel C with 0.09 pct Mn and about 10°C in steels A and B with 0.31 and 0.37 pct Mn, respectively. According to Fast, 0.5 pct Mn raises the nitrogen peak from about 25° to 32°C (no frequency specified).

As to the mechanism of the manganese effect, Fast[1] has suggested the existence of "Mn interstitial positions," where at least one of the neighbors of the N atom is an Mn atom. The N atom fits better in an "Mn interstitial position" than in an ordinary "Fe interstitial position." If the two kinds of interstitial nitrogen atoms are named N_{Mn} and N_{Fe}, the N_{Mn} atoms will need a higher amount of energy before they are able to make a jump than the N_{Fe}. The internal friction peak temperature corresponding to the N_{Mn} atoms will therefore be higher than that of the ordinary N_{Fe} atoms; and the resulting peak will be located at a higher temperature, the greater the $N_{Mn}/N_{Mn} + N_{Fe}$ ratio, which is in accordance with the findings. In this connection it might be of interest to note that the temperature of the peak is not changed when the nitrogen content changes; in another experiment, after nitriding steel C to only 0.006 pct N and water quenching from 580°C, the peak temperature was found to be +23°C. Also, when tested in the original composition with 0.002 pct N, after furnace cooling, there was a faint but definite peak at +24°C, as reported in the following.

If the theory is correct, and two peaks, corresponding to N_{Fe} and N_{Mn}, really exist, then the sum of the heights of these peaks will be greater than the height of the resulting peak; consequently, if the factor k in the relation

$$(\text{Pct N}) = k\,Q^{-1}_{max}$$

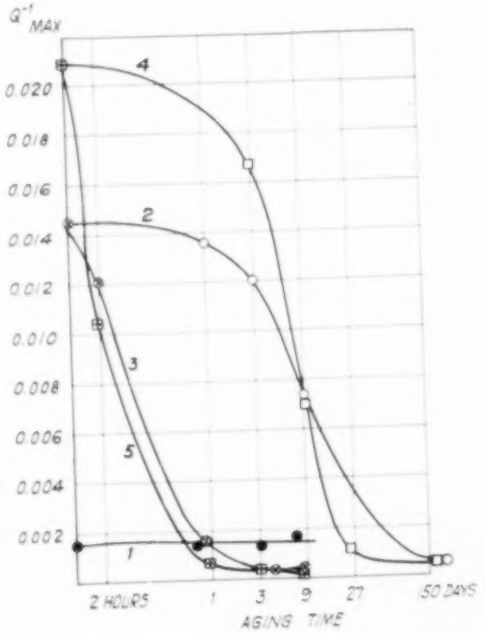

Fig. 3—Internal friction peak values vs. aging time for steel C, nitrided.

Heat treatment:
1—Furnace cooled from 930°C, aged at room temperature.
2—Normalized from 930°C, aged at room temperature.
3—Normalized from 930°C, aged at +23°C.
4—Water quenched from 580°C, aged at room temperature.
5—Water quenched from 580°C, aged at +23°C.

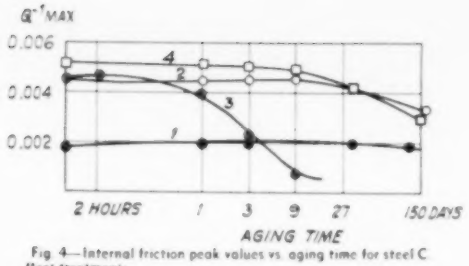

Fig. 4—Internal friction peak values vs. aging time for steel C.
Heat treatment:
1—Furnace cooled from 950°C, aged at room temperature. Peak temperature + 24°C.
2—Normalized from 950°C, aged at room temperature. Peak temperature + 32° to + 40°C.
3—Normalized from 950°C, aged at + 75°C. Peak temperature + 58°C.
4—Water quenched from 680°C, aged at room temperature. Peak temperature + 58° to + 58°C.

is equal to 1 for the two peaks individually, it will be slightly higher than 1 for the resulting peak in relation to the total amount of dissolved nitrogen.

Internal Friction During Aging

The measurements of internal friction in steels of commercial purity during aging were carried out on steels B, C, and D (see Table I), and also on steel C after decarburizing and nitriding (in the way described above) to a nitrogen content of 0.022 pct, as reported by chemical analysis.

Three different heat treatments were applied: 1—furnace cooling from 950°C (10 min at temperature), 2—normalizing from 950°C (10 min at temperature), and 3—water quenching from 680°C (15 min at temperature). For the nitrided specimen, water quenching was carried out from 580°C instead of from 680°C.

For furnace cooling and normalizing, the wires were placed inside four quartz tubes. The outside diameters of these tubes were 3.5, 6, 9, and 13.5 mm. One end of each tube was sealed and one tube placed inside the next larger one with its open end in the sealed end of the latter. This was done partly in order to get a proper cooling rate on normalizing and partly to diminish oxidation. In spite of this some oxidation did appear on furnace cooling. Furnace cooling took about 45 hr from 950° to 100°C. On normalizing, the time for cooling in air from 950° to room temperature was about 10 min. In treatment 3 a lead pot was used.

Internal friction was measured after aging for 0, 1, 3, 9, and 27 days at room temperature, and in some cases after additional aging for 2 hr, 1, 3, and 9 days at +75°C. Examples of curves obtained are shown in Fig. 2. In Figs. 3 to 6 the internal friction peak values are plotted against aging time. All diagrams are corrected for background damping (0.002).

Fig. 3 for steel C, nitrided, shows the usual appearance of an aging process with Q^{-1}_{max} decreasing within 27 days to very low values. If the aging

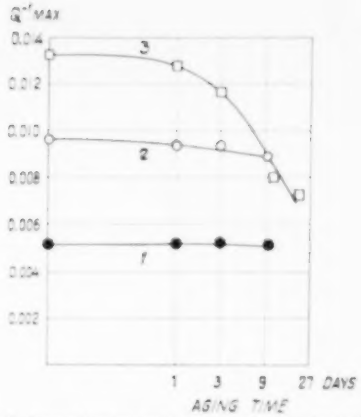

Fig. 5—Internal friction peak values vs. aging time for steel D.
Heat treatment:
1—Furnace cooled from 950°C, aged at room temperature. Peak temperature + 30°C.
2—Normalized from 950°C, aged at room temperature. Peak temperature + 33°C.
3—Water quenched from 680°C, aged at room temperature. Peak temperature + 58°C to + 58°C.

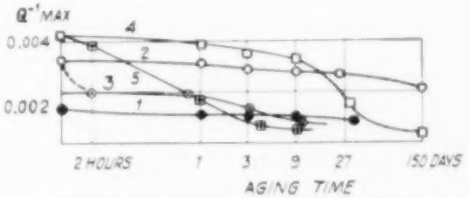

Fig. 6—Internal friction peak values vs. aging time for steel B, aluminum killed.
Heat treatment:
1—Furnace cooled from 950°C, aged at room temperature. Peak temperature ?
2—Normalized from 950°C, aged at room temperature. Peak temperature + 39°C.
3—Normalized from 950°C, aged at + 75°C. Peak temperature + 39°C.
4—Water quenched from 680°C, aged at room temperature. Peak temperature + 58°C.
5—Water quenched from 680°C, aged at + 75°C. Peak temperature + 39°C.

temperature is raised to +75°C, these are reached within 3 days. Normalizing in the manner described above results in a lower degree of supersaturation than water quenching. In spite of this, the time for the aging process to become half complete is almost the same as for the water-quenched specimen. This may readily be explained by the possibility of nucleation at temperatures somewhat higher than room temperature during air cooling. Furnace cooling definitely gives a higher Q^{-1} than normalizing or water quenching after complete aging. Consequently, even this treatment results in supersaturation to some extent. All peaks were located at +24°C.

Aging in the same steel, steel C, of the original chemical composition is shown in Fig. 4. Water quenching and normalizing give almost the same

Table II. Q^{-1}_{max} Values

Steel	Analysis, Pct Mn	P	S	Sol. Al	Internal Friction Q^{-1}_{max} Pct N Low Frequency	High Frequency	Peak Temperature, °C Low Frequency	High Frequency	Corrected to 1 Cps	Activation Energy, Cal per Mol
A	0.37	0.095	0.04		0.0228	0.0221	23	32	29	20,000
B	0.31	0.018	0.06	0.02	0.0221	0.0207	27	36	32	20,400
C	0.09	0.012	0.04		0.0127	0.0329	24	28	24	22,000

Fig. 7—Steel C nitrided and normalized from 950°C. Etched with Nital. X1250

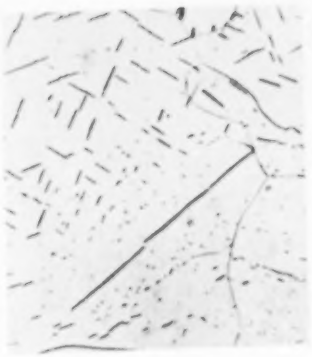

Fig. 8—Steel C nitrided and furnace cooled from 950°C. Etched with Nital. X1250

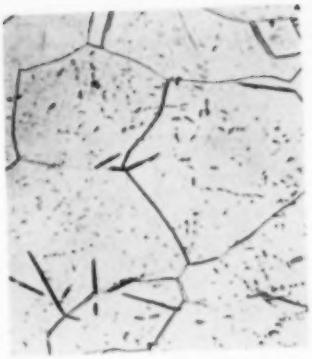

Fig. 9—Steel D furnace cooled from 950°C. Etched with Nital. X750

result with peaks located at +36° to +40°C, obviously mainly associated with carbon, while furnace cooling causes very faint peaks at +24°C, the same temperature that was obtained in nitrided specimens of this steel. It is surprising that even the water-quenched specimen did not show a higher Q^{-1}_{max}, as the chemical analysis reports 0.02 pct C, and the solubility at 680°C should be between 0.010 and 0.015 pct.[7] Whether this discrepancy is to be explained as an error in chemical analysis, or by a lower solid solubility in this steel as compared to pure iron, is not known. It might also be that the relation between Q^{-1}_{max} and the percentage of dissolved carbon referred to above is not valid in iron of commercial purity. Still another possibility is that the critical cooling rate for carbon supersaturation in this material is rather high, and was not attained.

For steel D the aging curves are shown in Fig. 5. After furnace cooling the peak appears at +30°C, after normalizing at +34°C, and after water quenching at +36° to +40°C. From the composition of this steel, especially its manganese content, it would be expected that its nitrogen peak would be around +30°C. Furnace cooling thus gives mainly nitrogen in solid solution, while on normalizing and still more on water quenching from 680°C, carbon is also found. It is interesting to note that the normalized state, though highly supersaturated, has little tendency toward decreasing its Q^{-1}, nor does the furnace-cooled specimen change its rather high Q^{-1}.

Steel B (Fig. 6) is aluminum killed, and consequently the internal friction peaks, both in the normalized and in the water-quenched state, lie at +38° to +39°C, indicating carbon in solid solution. The nitrogen peak in this material after decarburizing and nitriding has previously been found at +32°C, Fig. 1. The aluminum has obviously taken care of the 0.015 pct N that is found by chemical analysis. Again the Q^{-1} value after water quenching seems to be lower than expected.

Microscopic Studies

The decarburized and nitrided specimens of steel C had structures consisting of pure ferrite. In water-quenched specimens the ferrite appeared dotted with a precipitate, too fine to be observed in detail. It was present immediately (2 hr) after quenching and seemed to grow during aging. In the normalized state a very fine precipitate, similar to veining, could be distinguished, Fig. 7. Furnace cooling resulted in "needle shaped" precipitates (sections of disks) of two kinds, see Fig. 8. The shorter needles have three distinct directions within one grain and are sometimes a little "wavy;" the longer ones are more sparsely found, often starting from a grain boundary, without any discernible habit relationship. In the neighborhood of the latter kind, the needles of the former seem to have disappeared. The shorter needles probably are the Fe-N "intermediate phase" of Dijkstra,[1] the longer ones may be Fe_4N.

The same material (steel C) with original composition showed pure ferrite in the water-quenched condition, without any precipitate such as carbides. Normalizing gave a finely dispersed precipitate within the grains, somewhat resembling Fig. 7, but fainter. Very few carbide particles could be detected. The furnace-cooled wire occasionally showed small cementite particles in grain boundary corners. Small round particles, rather sparsely distributed in the ferrite grains, may also be cementite; they are blackened by alkaline sodium picrate etch.

Steel B, water-quenched, showed only pure, smooth ferrite. Normalizing gave some cementite in grain boundary corners; furnace cooling caused the cementite particles to get coarser and decrease in number, but no changes in the ferrite could be detected.

In steel D, after water quenching, some fine cementite particles in grain boundary corners could be distinguished. In the normalized specimen pearlite and cementite were visible; the ferrite seemed to be dotted by a very fine precipitate, sometimes with a resemblance of veining. Furnace cooling gave a few comparatively big cementite particles in some grain boundary corners, and also the precipitate shown in Fig. 9, which is similar to that of Fig. 8. The smaller needles however, were smaller and fewer than those of Fig. 8, while the bigger ones were thicker than the corresponding ones in Fig. 8.

Summary

The internal friction method of determining carbon and nitrogen in solid solution in α iron is applied to some steels of commercial purity. The presence of impurities, such as manganese and perhaps phosphorus, changed the position of the internal friction curve for nitrogen and broadened it.

For carbon, the position was not changed, although the curve may be broadened somewhat. Aging curves after water quenching, normalizing, and furnace cooling are given. The fixation of nitrogen by means of aluminum is illustrated, and further the inclination of nitrogen to stay in supersaturated solid solution, even at rather slow rates of cooling, in some steels is shown.

Acknowledgment

The authors wish to thank the Stora Kopparbergs Bergslags Aktiebolag for permission to publish these results. The encouraging interest of Bo Kalling, Director of Research, is appreciated. Finally thanks are due to Axel Hultgren of the Royal Institute of Technology, Stockholm, where much of the experimental work was carried out, for allowing the use of his facilities. To this end the help of Gunnar Cyraeus is appreciated.

References

[1] L. J. Dijkstra: *Trans.* AIME (1949) **185**, p. 252; JOURNAL OF METALS (March 1949).

[2] C. A. Wert: *Journal of Applied Physics* (1949) **20**, p. 943.

[3] C. A. Wert: *Trans.* AIME (1950) **188**, p. 1242; JOURNAL OF METALS (October 1950).

[4] J. D. Fast: *Iron and Coal Trades Review* (April 14, 1950) p. 837.

[5] T. S. Ké: *Trans.* AIME (1948) **176**, p. 448; METALS TECHNOLOGY (June 1948).

[6] J. K. Stanley: *Trans.* AIME (1949) **185**, p. 752; JOURNAL OF METALS (October 1949).

Technical Note

Twinning in Silicon

by E. I. Salkovitz and F. W. von Batchelder

As Slawson[1] and others have already shown, from a geometrical view twinning in the diamond structure may be considered as a reflection across a (111) plane or as a reflection across a (112) plane. An analysis by Ellis and Treuting[2] showed that the twinning plane must be the (111) plane, but that a twin might have lateral boundaries along (112) planes. Earlier Slawson[1] and Ellis[3] had shown that only (111) twinning was present in diamond and germanium respectively.

Since an ingot of silicon, 1 in. in diam and 1½ in. long, prepared from Dupont silicon to which 0.2 pct Be had been added was available, it was examined for twinning. The ingot had been cooled slowly from the bottom. A section 1/16 in. thick was ground off from the bottom and then the ingot was sliced vertically through the center. Spectrographic analysis indicated only faint traces of iron and silver, in addition to the beryllium.

The sample was first etched with a hot solution of 10 pct NaOH in water and photographed. Back-reflection Laue patterns were made of the vertical and horizontal sections in the regions designated in Fig. 1. Orientations were obtained for each twin using the Greninger technique. Several regions of the same orientation were found; thus regions *A* and *K* were identical, similarly *N* and *P*, and *C*, *G*, *J*, and *L*. Knowing the angles between the traces of the twinning plane on the surface and the specimen axis, the indices of the twinning plane were deduced. In all cases the twinning plane was found to be (111); lateral boundaries, however, were found which were (112) such as the one indicated in Fig. 1. Therefore, as in the case of diamond[1] and germanium[3] only (111) twinning occurs in silicon.

We wish to thank Mr. Hino for the use of the ingot as well as for its metallographic preparation.

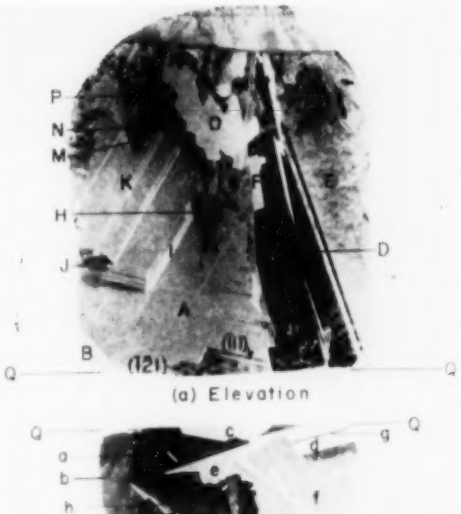

Fig. 1—Plan and elevation of etched silicon ingot

References

[1] C. B. Slawson: *American Mineralogist* (1950) **35**, p. 193.

[2] W. C. Ellis and R. C. Treuting: *Trans.* AIME (1951) **191**, p. 53; JOURNAL OF METALS (January 1951).

[3] W. C. Ellis: *Trans.* AIME (1950) **188**, p. 886; JOURNAL OF METALS (June 1950).

E. I. SALKOVITZ and F. W. VON BATCHELDER are associated with the Metallurgy Div., Naval Research Laboratory, Washington.

TN 96E. Manuscript, Sept. 25, 1951

Tensile Properties of Wrought Austenitic Manganese Steel

In the Temperature Range from + 100° to — 196°C

by H. C. Doepken

Wrought Hadfield steel was tested in axial tension at from 100° to —196°C, to determine flow and fracture stresses as well as conventional properties. Ductility and related properties, such as fracture stress, decreased continuously with temperature. Peculiarities during straining indicated possible martensite formation or mechanical twinning.

THE mechanical properties of austenitic manganese steel have been summarized by Avery and Day,[1] including the low temperature tensile properties reported by Hadfield and coworkers.[2,3] These data show the material to be brittle at both liquid oxygen and liquid hydrogen temperatures. Avery and Day[1] report considerable ductility measured by Charpy V-notch tests at —100°F (—73°C). Since the review of low temperature properties by Seigle and Rinck[4] show face-centered cubic structures, other than Hadfield steel, to be ductile at low temperatures, it was felt that a study of tensile properties, between the reported intervals, should show whether the decrease in ductility was a gradual decline or an abrupt drop beginning at some intermediate point.

X-ray examinations were made in an attempt to shed further light on the mechanism of work hardening of austenitic manganese steel. The presence of a magnetic constituent has been found by Hall[5] and by Avery, Homerberg, and Cook.[6] Krivobok[7] demonstrated the growth of magnetic constituents on reheating cold-worked specimens. Hadfield[2] and Goss[8] found no α iron.

The steel from which the specimens were taken was commercial hot rolled ½ in. diam rod of electric furnace steel. The ladle analysis was as follows: C, 1.40 pct; Mn, 12.11; P, 0.060; S, 0.012; Si, 0.120; Ni, 0.080; and Cr, 0.090.

Fifteen specimens, 6 in. long, were cut from a

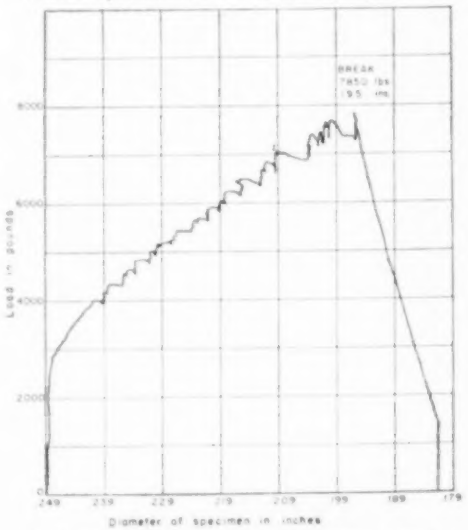

Fig. 1—Microformer recorder chart (load-diameter) of tensile test conducted at 91°C.

H. C. DOEPKEN is General Superintendent, Manganese Steel Forge Co., Philadelphia, Pa.

Discussion on this paper, TP 3238E, may be sent, 2 copies, to AIME by April 1, 1952. Manuscript, Sept. 13, 1951; revision, Dec. 13, 1951. New York Meeting, February 1952.

This paper represents part of a thesis by H. C. Doepken submitted in partial fulfillment of the requirements for the degree of Master of Science in Metallurgical Engineering to the University of Pennsylvania.

single rod. This material was commercially free of inclusions. The samples were given an austenitizing treatment of 1850 F for 30 min followed by a water quench. The resultant grain size was 4 to 5 ASTM. The heat-treated bars were carefully ground to tensile bars of 1 in. gage length and 0.250 in. diam. All grinding was wet and the cuts were light.

Tensile tests were run at the following temperatures using the heating mediums indicated:

100 °C	boiling water
23 °C	room temperature
−29 °C	freon in Dewar flask cooled by passing liquid air through coils—flow regulated automatically to hold desired temperature within 3 °C
−100 °C	same as above
−150 °C	same as above
−196 °C	liquid nitrogen in Dewar flask

All tensile tests were conducted with a crosshead movement of 0.05 in. per min. The method of regulating crosshead movement, maintenance of testing temperature, axial loading with chain supports, and continuously recording the diameter photographically have been previously described.[1] Two methods of measuring the diameter of the specimen continuously during testing were employed. The first was based on photographic procedures.[2] The second means was mechanical. A pair of knife edges were suitably mounted to actuate a microformer which was electrically connected to record diameter in place of crosshead motion on the recorder chart of the tensile machine. The unit was calibrated in the cooling medium against accurate test bars to record room temperature diameters. The knife edges were traversed along the gage section to record minimum diameter for the applied load and could be maintained in this position during testing.[3] The latter method greatly simplified calculations and eliminated the tedious measurement of pictures. The accuracies of the two methods were comparable to the nearest 0.001 in., when compared with micrometer diameters measured before and after testing the bars.

One tensile break of each test temperature was examined microscopically. The specimens were mounted longitudinally in Bakelite to obtain both the fracture edge and relatively unworked shoulder in a single mount. No special treatment was given in mounting these specimens, except that all grinding was wet and care was taken to keep the samples cool. Etching of the specimens followed the procedure of Avery and Day.[4]

Microscopic specimens were utilized for X-ray diffraction examination. A Norelco direct reading spectrometer was used with a molybdenum target X-ray tube operated at 6 ma. A 0.0005 in. zirconium filter was placed before the Geiger tube and maximum amplification was used on the recorder to obtain greatest possible contrast between background and intensity peaks. Diffraction curves were recorded for 2θ angles of 5° to 80° for each specimen. Vicker's diamond pyramid hardness tests were made on the same specimens at room temperature. A load of 2 kg was used throughout and all points were measured with the 10.25 mm objective.

Test Results

The most noticeable observation during tensile testing was that straining was not uniform in the plastic range. Oscillations or jumps in the strain chart became more pronounced as the breaking point was approached. The extent of these jumps in strain are observed in the actual tensile recorder chart, Fig. 1. An audible click accompanied these strain jumps. As has been previously reported,[1] there was no necking of the tensile specimen at fracture and the reduction of diameter was uniform throughout the gage length to within 0.001 to 0.002 in.

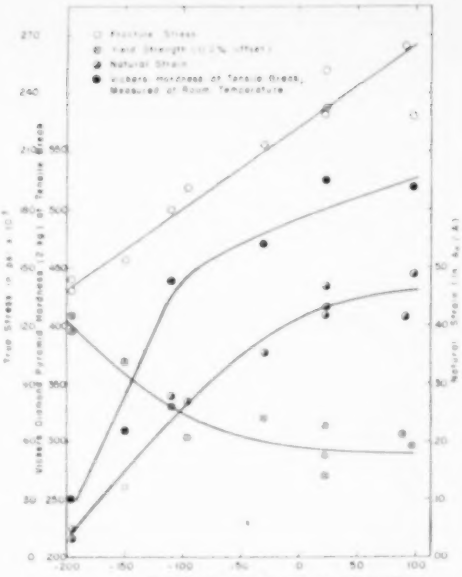
Fracture Stress
Yield Strength (0.2% offset)
Natural Strain
Vickers Hardness at Tensile Stress, Measured at Room Temperature
Test Temperature in Degrees Centigrade

Fig. 2—Variation of true strength properties and hardness of wrought austenitic manganese steel with temperature

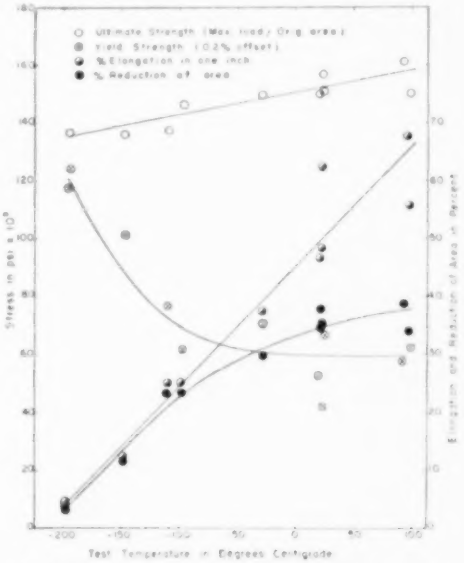
Ultimate Strength (Max. load / Orig. area)
Yield Strength (0.2% offset)
% Elongation in one inch
% Reduction of area
Test Temperature in Degrees Centigrade

Fig. 3—Variation of engineering tensile properties of wrought austenitic manganese steel with temperature

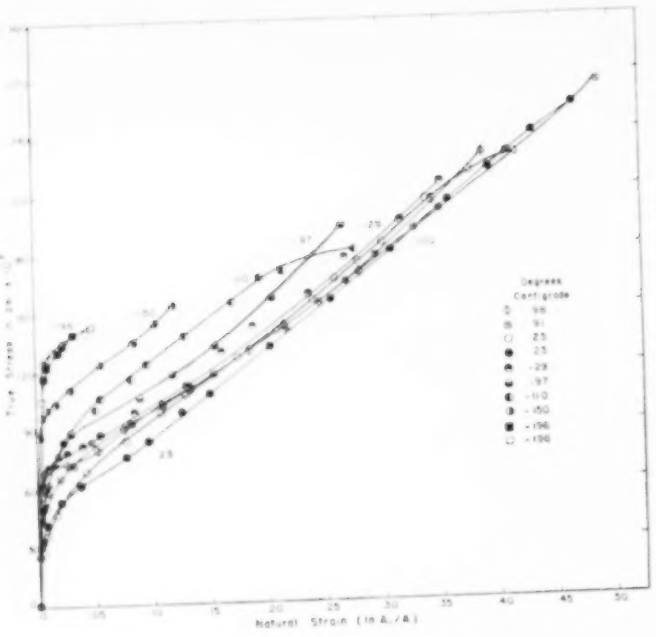

Fig. 4 — True stress-strain tensile curves of wrought austenitic manganese steel at various temperatures.

With decreasing temperature, there was an increase in yield strength (0.2 pct set) from 50,000 psi at room temperature to 120,000 psi at —196°C, Fig. 2. This increase was not uniform as there was little change until —100°C, and then the yield stress increased rapidly to a value almost equal the fracture stress at —196°C. The difference between room temperature and —100°C yield strength is slight with the possibility of a slight increase at the higher temperature, Table I.

Contrary to the increase in yield strength with decreasing temperature the worked fracture stress decreases linearly with decreasing temperature, Fig. 2, corresponding to the decrease in deformation preceding fracture. The extent of this decrease is at variance with general low temperature behavior of steels and particularly austenitic stainless, where fracture stress increases tremendously. A plot of engineering ultimate strength, maximum load divided by the original cross-sectional area, (Fig. 3) shows the same decrease with decreasing temperature dropping from 150,000 psi at room temperature to 136,000 psi at —196°C. Hadfield and his colleagues[2,4] previously found the ultimate strength at both liquid oxygen and hydrogen to be from 1 to 3 tons per sq in. less than the room temperature strength.

Three measures of ductility—natural strain, reduction of area, and percent elongation in 1 in.—all show a decrease with decreasing temperature, Figs. 2 and 3. The drop in elongation follows a straight line decreasing from 50 pct at 23°C to 4 pct at —196°C. The curves for reduction of area and natural strain increase in slope with decreasing temperature.

Table I Results of Tests on Wrought Austenitic Manganese Steel at Various Temperatures

Test Identification	Temperature, °C Tensile Test	Yield Strength, psi at 0.2 Pct Offset	Fracture Stress, psi	Natural Strain, $\ln A_0/A$	Ultimate Strength, psi	Pct Elongation in 1 In.	Pct Reduction in Area	Vickers DPH 2 kg Load at Tensile Break, Room Temperature
								518
S	95	62,500	228,500	0.414	151,111	56.0	34.0	
J	91	57,900	265,000	0.489	182,320	68.0	38.7	524
K	23.5	66,900	232,410	0.431	150,900	48.5	35.1	
A	23.5	52,630	228,900	0.436	150,900	46.8	34.2	
O	22.5	52,630	228,900	0.436	138,110	62.5	37.7	470
P	23.5	42,910	252,500	0.402	150,100	37.5	29.6	
I	23.5	70,400	211,000	0.351	150,100	25.0	23.5	
H	29	70,400	191,800	0.267	146,800	25.0	23.3	438
D	97	61,600	160,040	0.277	138,800	25.0	11.3	317
C	110	76,300	153,800	0.120	136,500	12.2	4.9	251
G	150	100,600	143,700	0.050	136,840	4.0	3.2	
E	196	124,200	138,000	0.033	135,450	4.0		
F	196	117,100						

A uniform strain rate of 0.005 in. per min was used for all tests.
Fracture stress is taken as load at fracture divided by area at fracture. (With no necking fracture load is maximum load.)
Ultimate strength is taken as maximum load divided by original cross-sectional area.

It is noted that hardness increases of 310 points DPH due to cold working were found on the room temperature specimen. A decrease in hardness near the fracture was observed with falling temperature corresponding with a decrease in total strain and the sharp increase in yield strength. At −196°C the hardness increase due to cold working was only 40 points DPH.

Two plots were made of the true stress-natural strain data. Smooth curves were the result of selecting mid points of the sharp load drops shown in Fig. 1. The first plot, Fig. 4, uses arithmetic coordinates. These curves show similar slopes in the plastic region or an apparently uniform strain hardening for variations in temperature. The variations in slope at fracture may be attributed to measuring technique, since the stress-strain values fluctuated appreciably in this region. The graph shows the uniform decrease in fracture stress, decrease in natural strain, and increase in yield strength previously mentioned. A logarithmic plot, Fig. 5, of true stress-natural strain was made in an attempt to establish a strain hardening exponent. These curves do not follow a straight line for the region of strain plotted. There is a general tendency for the slopes to decrease with drop in temperature.

Fig. 6 is a series of traces of X-ray diffractions, as copied from the recorder of a Geiger tube spectrometer. The vertical coordinate is intensity increasing upward, and all curves should have the same base line, but they have been spread out for clarity. The tests covered 2θ angles of 5° to 80°, but the section shown contains all recorded intensity peaks. Using a lattice parameter of 3.564 for γ iron,[7] the four peaks correspond to (111), (200), (311), and (220) planes for a face-centered cubic structure. There are no peaks for similar locations for α iron, with the possible exception of the (110) plane which falls very close to the (111) γ peak and could be included in it. Two factors worthy of notice can be seen from the curves. The first is the decrease in intensity of the (111) and (311) peaks as the temperature and the degree of work hardening increase. The (200) and (220) peaks do not change in as noticeable a manner. The second factor is the broadening of the peaks with increasing temperature.

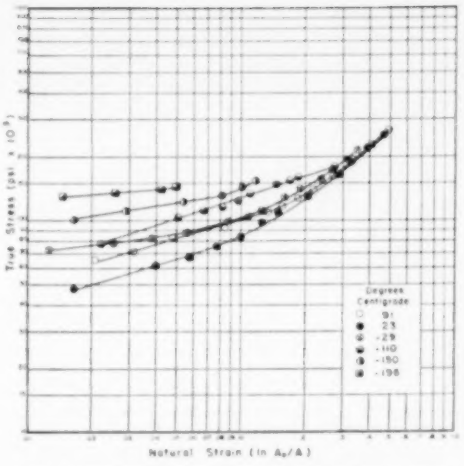

Fig. 5—Logarithmic flow-stress curves of tensile tests at various temperatures.

Fig. 7 is a micrograph of a section near the tensile break of a bar tested at room temperature and Fig. 8 was taken near the break of a tensile bar pulled at −196°C. The decrease in grain elongation with decreasing temperature is noticeable. The presence of deformation markings at three and four different angles in a single grain is fairly common in the 23°C tensile break, but no more than four traces were ever observed. Therefore there is some possibility of

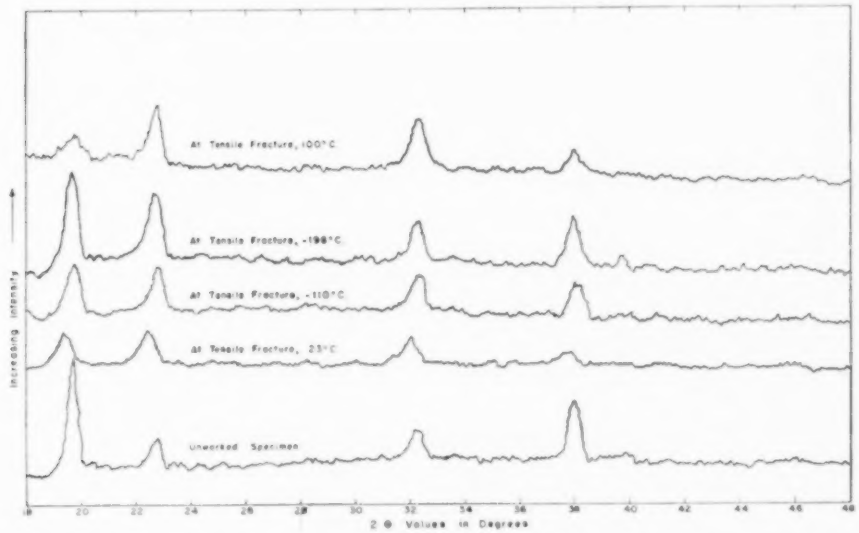

Fig. 6—X-ray diffraction curves of fractures of tensile tests taken at various temperatures traced from spectrometer charts.

Fig. 7—Tensile break of specimen of wrought austenitic manganese steel pulled at 23° C. X250.
Etch was 1 pct nital-alcohol rinse 10 pct HCl in alcohol-alcohol rinse 2 pct NH_4OH in alcohol.

Fig. 8—Tensile break of specimen of wrought austenitic manganese steel pulled at −196° C. X250.
The etch was the same as Fig. 7.

mechanical twinning on (111) plane during cold work. As mechanical twinning in face-centered irons is unknown, much more work would be needed to establish these markings as twins.

Discussion of Results

The results reported by Avery and Day[1] and Hadfield[2] indicating ductility at −73° C and brittleness at −192° C seem to be borne out by the knee in the curves for reduction of area and natural strain between −50° to −100° C. The abrupt increase in yield strength and drop in hardness at −100° C lend support to the ductility curves and possibly place the region of ductility decrease closer to the lower temperature. The decrease in fracture stress and more particularly ultimate strength with temperature is, as far as the writer has found, a characteristic peculiar to the material under study.

The absence of an α phase in the diffraction curves of the tensile breaks does not give positive evidence that no body-centered cubic phase exists. It is questionable whether quantities under 5 pct would be recorded. However, the decrease in intensity of the (111) peak with increased work hardening tends to indicate that any (110) α peak must be of very low intensity. Two factors commonly associated with cold working are present in the curves, i.e., decreasing intensity of peaks with increased cold work and line broadening. This is confirmed by Goss[20] on the same material and by Barrett[21] for cold working in general.

There are three factors which point to possible mechanical twinning. The first is the accelerated strain jumps in the tensile bar as the specimen approaches fracture. The second is the accompanying sound. The third is the micrographs (Figs. 7 and 8) taken in the region of increase in hardness of the tensile bars. However, these same factors could be present in the formation of martensite. The slight increase in hardness of the bar pulled at −196° C together with numerous strain markings (Fig. 8) suggests mechanical twinning.

Conclusions

1—Wrought austenitic manganese steel decreases slightly in ductility with temperature, to a temperature between −50° to −100° C, then the ductility drops rapidly to almost no ductility at −196° C.

2—With decreasing temperature there is a gradual decrease in ultimate strength from 150,000 psi at room temperature to 136,000 psi at −196° C.

3—Jumps in the stress-strain curve and audible clicking during deformation suggest mechanical twinning or martensite formation.

4—The formation of α iron on tensile testing was not apparent from X-ray examination with a recording spectrometer.

Acknowledgment

The author acknowledges his indebtedness to L. W. Jones, Jr. for his encouragement and to R. M. Brick and the members of the Graduate Group of the Department of Metallurgy for their assistance, particularly H. T. Green, R. L. Smith, and F. L. Vogel, Jr.

References

[1] H. S. Avery and M. J. Day: Austenitic Manganese Steel. *Metals Handbook*, pp. 526-534 (1948) Cleveland. A.S.M.

[2] J. Dewar and R. A. Hadfield: The Effects of Liquid Air Temperatures on the Mechanical and Other Properties of Iron and Its Alloys. *Proc.* Royal Soc. (1904) **74**, p. 326.

[3] W. J. DeHaas and R. A. Hadfield: Effect of Temperature Liquid Hydrogen (−252.8°C) on Tensile Properties—41 Alloys. *Phil. Trans.* Royal Soc. (1934) **232A**.

[4] L. Seigle and R. M. Brick: Mechanical Properties of Metals at Low Temperatures; A Survey. *Trans.* A.S.M. (1948) **40**, p. 813.

[5] J. H. Hall: Studies of Hadfield's Manganese Steel With the High Power Microscope. *Trans.* AIME (1929) **84**, pp. 382-427.

[6] H. S. Avery, V. O. Homerberg, and E. Cook: Metallographic Identification of Ferro-Magnetic Phases. *Metals and Alloys* (November 1939).

[7] V. N. Krivobok: A Study of the Constitution of High Manganese Steels. *Trans.* A.S.S.T. (1929) **15**, pp. 893-956.

[20] N. P. Goss: The Effect of Cold Rolling on the Structure of Hadfield Manganese Steel. *Trans.* A.S.M. (1945) **31**, p. 630.

[21] G. A. Moore and H. T. Green: Mechanical Properties of Binary Alloyed Ferrites at Low Temperatures. Progress report to the American Iron and Steel Inst. Published as Contributions to the Metallurgy of Steel, No. 34 (June 1949).

[8] R. L. Smith: The Mechanical Properties of Pure Iron-Carbon Alloys At Low Temperatures. M. S. Thesis, University of Pennsylvania (February 1951).

[9] A. Taylor: *An Introduction to X-ray Metallography*. (1949) New York. John Wiley and Sons.

[10] C. S. Barrett: *Structure of Metals*. (1943) New York. McGraw-Hill Book Co.

[11] D. Niconoff: Some Aspects of Strain Hardenability of Austenitic Manganese Steel. *Trans.* A.S.M. (1943) **31**, p. 519.

Silicon-Oxygen Equilibrium in Liquid Iron

by Nevzat A. Gokcen and John Chipman

SILICON is the most commonly used deoxidizer and an important alloying element in steelmaking; hence a detailed study of this element in liquid iron containing oxygen is of considerable interest. The equilibrium between silicon and oxygen in liquid iron has been studied by a number of investigators but generally with inconclusive or incomplete results. The variation of the activity coefficients of silicon and oxygen with composition is entirely unknown.

Published investigations deal with the reaction of dissolved oxygen with silicon in liquid iron and the results are expressed in terms of a deoxidation product. For consistency and convenience in comparison of the published information, the deoxidation product as referred to the following reaction is expressed in terms of the percentage by weight of silicon and oxygen in the melt in equilibrium with solid silica:

$$SiO_2\,(s) = \underline{Si} + 2\underline{O};\ K'_1 = [\%\ Si]\,[\%\ O]^2 \qquad [1]$$

Theoretical attempts to calculate the deoxidation constant for silicon in liquid iron from the free energies of various reactions yielded results which were invariably lower than the experimental values. Thus, the deoxidation "constants" calculated by McCance,[1] Feild,[2] Schenck,[3] and Chipman[4] were of the order of 10^{-6}, which is below the experimental values by a factor of more than 10.

Experiments of Herty and coworkers[5] in the laboratory and steel plant resulted in an average deoxidation constant of 0.82×10^{-3} at about 1600°C. The technique employed in their investigation was crude and the reported temperature was quite uncertain. The concentration of silicon was obtained by subtracting silicon in the inclusions from the total. Since at least some of the inclusions resulting from chilling must represent a fraction of the silicon in solution at high temperatures, such a subtraction is not justifiable.

Results of Schenck[3] for K'_1 from acid open-hearth plant data yielded a value of 2.8×10^{-3}, which was later revised as 1.24×10^{-3} at 1600°C. Similarly Schenck and Brüggemann[6] obtained 1.76×10^{-3} at 1600°C. The discrepancies and errors involved in the acid open-hearth plant data as compared with the results of more reliable laboratory techniques were attributed by these authors to the lack of equilibrium and the impurities in liquid metal and slag, and are sufficiently discussed elsewhere.[7]

Korber and Oelsen[8] investigated the relation between dissolved oxygen and silicon in liquid iron covered with silica-saturated slags containing varying concentrations of MnO and FeO. The deoxidation products obtained by their method scatter considerably, and their chosen average values of 1.34×10^{-3}, 3.6×10^{-3}, and 10.6×10^{-3} at 1550°, 1600°, and 1650°C, respectively, represent the best experimental results which were available until quite recently. Darken's[9] plant data from a steel bath agree approximately with their data at 1575° to 1625°C.

Zapffe and Sims[10] investigated the reaction of H_2O and H_2 with liquid iron containing less than 1 pct Si and obtained deoxidation products varying by a factor of more than 20. Inadequate gas-metal contact and lack of stirring in the metal bath should require a longer period of time than the 1 to 5.5 hr which they allowed for the attainment of equilibrium. Furthermore, their oxygen analyses were incomplete and irregular and confined to a few unsatisfactory preliminary samples. Their results did indeed indicate that the activity coefficient of oxygen is decreased by the presence of silicon, although they made no such simple statement. They chose to attempt to account for their anomalous data by the unlikely hypothesis that SiO is dissolved in the melt.

Hilty and Crafts[11] investigated the reaction of liquid iron with acid slags under an atmosphere of argon, making careful determinations of silicon and oxygen contents at several temperatures. Despite erroneous interpretation of the data at very low silicon concentrations, their data represent the most dependable information on this equilibrium that has been published. In the range 0.1 to 1.0 pct Si, their data yield the following values for the deoxidation product: 1.6×10^{-3}, 3.0×10^{-3}, and 5.3×10^{-3} at 1550°, 1600°, and 1650°C, respectively.

The purpose of the work described herein was to study the equilibrium represented by eq 1 as well as the following reactions, all in the presence of solid silica:

$$SiO_2\,(s) + 2H_2\,(g) = \underline{Si} + 2H_2O\,(g);$$

$$K'_2 = [\%\ Si]\left(\frac{H_2O}{H_2}\right)^2 \qquad [2]$$

$$H_2\,(g) + \underline{O} = H_2O\,(g);\ K'_3 = \frac{(H_2O)}{(H_2)[\%\ O]} \qquad [3]$$

N. A. GOKCEN, formerly Research Associate, Dept. of Metallurgy, Massachusetts Institute of Technology, is now Associate Professor of Metallurgy, Michigan College of Mining and Technology, Houghton, Mich., and J. CHIPMAN, Member AIME, is Professor, Dept. of Metallurgy, Massachusetts Institute of Technology, Cambridge, Mass.

Discussion on this paper, TP 3243C, may be sent, 2 copies, to AIME by April 1, 1952. Manuscript, Sept. 26, 1951. New York Meeting, February 1952.

This paper represents part of a thesis by Nevzat A. Gokcen submitted in partial fulfillment of the requirements for the degree of Doctor of Science to Massachusetts Institute of Technology.

Fig. 1—Diagram of apparatus

The method of attack was to melt pure iron, usually with an initial charge of silicon, in silica crucibles under a controlled atmosphere of H_2O and H_2 and hold it at temperature until the equilibrium was established between the various phases present. The experimental melts of very small weight thus obtained were quenched to avoid any loss of oxygen and silicon and subsequently were analyzed for these elements.

Apparatus

Gas System: Fig. 1 is a schematic diagram of the apparatus originally used by Dastur and Chipman[7] and later considerably improved and modified for this investigation. Commercially pure hydrogen was led to the safety trap, *T*, containing mercury, through the flowmeter, *F*, and two platinized-asbestos furnaces in series held at 380°C to convert any free oxygen into water vapor. The gas was then passed through one of the two saturator systems. The first of these contained distilled water and was composed of a presaturator, *P*, and three towers, *S*, immersed in a thermostat. The first and second saturator towers were packed with beads and contained distilled water. The third tower, containing only a very small amount of water, acted as an entrainment chamber. Water-vapor pressures ranging from 18 to 500 mm mercury were obtained with this saturator system. Adequate purcaution was taken to avoid condensation of water vapor in the glass tubing by proper resistance heating and insulation.

The second saturator system consisted of four towers containing saturated lithium chloride solution. Vapor pressure of the saturated solution was determined experimentally in the temperature range 19° to 50°C using the same apparatus. Connections to the lithium chloride saturators were made as shown with the dotted lines. All connections were of pyrex glass and the entire apparatus was of glass construction except at *R*. The lithium chloride saturator was used for water-vapor pressures ranging from 1.86 to about 18.0 mm mercury with readily obtainable thermostatic temperatures. Two saturator systems thus yielded a pressure range of 1.86 to 500 mm mercury with a high degree of accuracy. Both saturators were immersed in a water thermostat, the temperature of which was automatically controlled within ±0.03°C.

Dried argon was led through magnesium chips loosely packed in a stainless steel tube and heated to 620°C in order to remove any oxygen that might be present in the commercial argon of welding or lamp grade. The performance of the magnesium furnace was measured qualitatively as follows: Argon was passed through a set of pure water saturators at 20°C with various flow rates and then through the magnesium furnace held at various temperatures. Outgoing gas was passed through a U-tube containing P.O. Up to 475°C, the water vapor in the argon passed through the furnace and was absorbed by P.O. But at 500°C moisture in the argon was completely dissociated by the magnesium at flow rates up to 2 liters per min.

Furnace: The furnace and its accessories are shown in Fig. 2. A silica tube glazed outside as well as inside, 24.5 in. long, 2 in. ID, and 2.5 in. OD was found to be satisfactory as a furnace tube. The furnace was equipped with an all-glass head, comprising an inlet tube and two tungsten leads, which was attached tightly to the silica tube with clamps and a silicone rubber gasket. The preheater tube, *H*, which led the gas mixture to the liquid metal surface, was suspended from the central tube with chromel wires.

The silica crucible, *R*, was placed in a small silica dish resting on an alundum disk, which was in turn supported on an alundum tube 0.5 in. ID and a stainless steel tube passing through the brass bottom. The distance between the liquid metal and the preheater was adjusted by means of a silicone gasket and a compression fitting in the brass bottom. The power for inductive heating was obtained from an oscillating spark-gap type high frequency converter of 35 kva and a variable frequency of about 200 to 250 kilocycles. Efficient and continuous temperature control was obtained by varying the inductance in the high frequency circuit. With constant line voltage the temperature was observed to be constant for periods of 6 hr or more without any adjustments. Usually a variation of ±7 v in the line voltage during the day necessitated frequent temperature readings and adjustment of power throughout the experimental heats.

The brass bottom, *V*, was equipped with two copper tubes, *K*, with special jet holes through which hydrogen or helium was injected to quench the melt when lowered into the proper position.

Preheater: The preheater tube was made of very pure alumina, 0.63 in. ID, 1 in. OD, and 14 in. long. The tube was received in the so-called prefired state (fired at 1250°C) and tapped to 11 threads to the inch for a length of 12 in., after which it was shaped to support the radiation shields and to fit on the glass head. Subsequently it was fired at 1780°C and a hard somewhat shrunk tube of improved mechanical and thermal properties was obtained. A coil of platinum-20 pct rhodium wire of 0.033 in. diam, *S*, 11 threads to the inch and 10.5 in. long, was screwed into position in the threads. The coil was heated with a variable transformer to the desired temperature as observed by sighting the pyrometer on the preheater. The leads were taken out through two small holes in the preheater tube and were connected to the tungsten leads, *D*, as shown in Fig. 2. The preheater was equipped with an alundum sleeve, *G*, and an alumina radiation shield, *I*, in order to avoid excessive heat losses.

Contamination and subsequent failure of the preheater wire under very low ratios of water vapor to hydrogen were a major source of trouble. It was believed that at various spots the localized impurities in the alumina were reduced with hydrogen and absorbed by the preheater coil, resulting in brittle sections in the wire after some 20 to 100 hr at

1600° C. Fractured sections of the wire were brittle and coarsely granular, strongly adhering to the alumina. At higher water-vapor concentrations, the coil was soft and had a considerably longer life.

Control of Gas Mixture: In a mixture of gases containing molecules of different weight, a temperature gradient tends to produce a corresponding composition gradient. This thermal diffusion can produce large errors in the sharp gradient near the hot metal surface unless adequate preventive measures are adopted. Dastur and Chipman[7] have shown that the error can be minimized by admixture of a heavy inert gas and eliminated by preheating the gases to the temperature of the metal. Accordingly purified argon was added to the gas mixture in the approximate ratio 4:1, the rates of flow of argon and hydrogen being respectively 1100 and 260 ml per min. The temperature of the preheater wire was adjusted to the same brightness as the metal, except in certain runs where a "medium preheat" about 60° lower was employed to prolong the life of the wire. A further advantage in diluting the hydrogen with argon lies in the production of sound ingots free from the porosity often found when melting under hydrogen.

Temperature Measurements: Temperature measurements were made with a disappearing filament type optical pyrometer sighted on the clean surface of liquid iron. Optical readings were calibrated against the true temperatures measured with thermocouples by a technique described elsewhere in detail.[8] The optical calibration scale was found to be unaffected by the addition of silicon up to 13.6 pct, provided no oxide scum formed on the bath. Optical readings were duplicated within ±2° C, and the overall accuracy is estimated as ±4° C. The calibration was checked frequently against the melting point of electrolytic iron and against platinum-rhodium thermocouples.

Analytical Methods: Silicon analyses were made by the standard gravimetric method in the range above 0.08 pct with an accuracy of about ±1 pct of the amount present. Below 0.10 pct Si a colorimetric method was used with a reproducibility of ±0.002 to ±0.003 pct in the reported silicon contents. A higher degree of precision would have been desirable, especially in melts containing less than 0.010 pct, but efforts to improve the precision of the method were unsuccessful.

Insoluble silicon was also determined by either method and found to be of the order of 0.004 pct or less in the satisfactorily quenched equilibrium heats.

Oxygen analyses were made by the vacuum-fusion method with an apparatus used in this laboratory for over 12 years. It has been carefully calibrated and checked by exchange of samples with various laboratories. Results reported herein are the mean of two concordant determinations. A large number of samples, including those of lowest oxygen content, were analyzed by Gokcen using all possible precautions to assure precision. Results were reproducible to within about 0.0005 pct.

Experimental Procedure

Electrolytic iron of very high purity was weighed and charged, usually with an initial percentage of silicon in the form of 99.83 pct pure silicon or its alloys made under hydrogen in silica crucibles. The total weight of the charge was 35 g, held in thin-walled crucibles made from fused silica tubing. The charge was placed at a fixed distance of 5 mm from

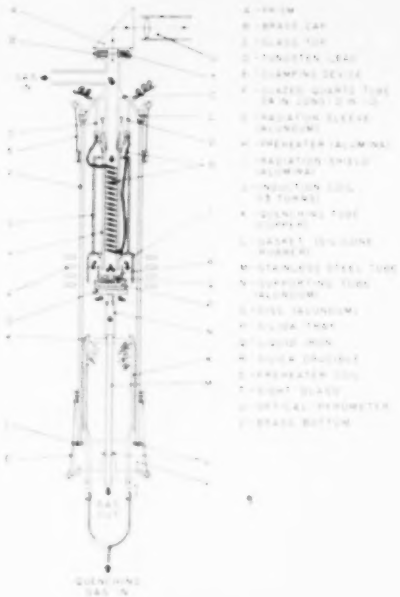

Fig. 2—Furnace arrangement

the preheater. The flow rates of hydrogen and argon were adjusted to 260 and 1100 ml per min, respectively, and the furnace was flushed for a minimum period of 2 hr, while the purification trains were being heated and the temperature of the thermostat adjusted. Simultaneously the preheater was brought to the desired temperature at a very slow rate to avoid excessive thermal shocks. Then the gas outlets from the furnace were closed to test the presence of any possible leakage. Observation of the manometer and flowmeters quickly indicated whether or not any leaks were present in the system. Occasionally the apparatus was sealed after admitting hydrogen at a pressure of 120 mm mercury, after which any drop in pressure within 6 to 8 hr indicated the presence of a slow leak.

After the apparatus was ready, the induction unit was turned on and the metal was brought to the desired temperature, usually within 1 min to avoid any loss of silicon. Repeated tests showed that the silicon recovery in the melt was 99 pct or better from 0.1 pct up to 20 pct Si. The temperature of the melt was observed and controlled frequently by changing the inductance of the circuit, and in the successful heats it did not fluctuate more than ±4° C. Temperature control was of utmost importance due to the strong temperature dependence of the Si-O equilibrium.

The attainment of equilibrium between a gas of known composition, silica, and liquid metal requires a period of 8 to 15 hr or more depending upon the initial metallic charge. Frequently equilibrium was reached from both the high and low silicon sides or the heats were held considerably longer than necessary as judged from the reaction rate study.

Experimental procedure differed in the ranges of silicon between 0.004 to 0.10; 0.1 to 1.6; and above 4.4 pct as follows:

In the silicon range of 0.004 to 0.1 pct it was neces-

sary to attain the desired temperature with the least degree of fluctuation in order to avoid the formation of a scum. This scum usually disappeared in 15 to 20 min, but such heats were always rejected. The pyrometer focused on the surface of the liquid metal permitted a clear observation of any such scum or floating nonmetallic particles due to their higher emissivity than the liquid iron. The surfaces of experimentally successful heats were observed to be clean and uniform. With the H_2O/H_2 ratio of 0.35 at 1600° C, liquid slag appeared on the surface of the liquid iron. Above this ratio the phase rule requires disappearance of SiO_2 or Fe. The interaction between slag and silica occurred in the limited region of contact, causing complete erosion and failure of silica crucibles when excessive slag formation was allowed. In the experimental heats above the ratio 0.35, the successful melts were quenched as soon as a small patch of liquid slag was observed.

In the range of 0.1 to 1.6 pct Si, no difficulty was encountered. The general procedure outlined above was used in making these heats with initial silicon charges as close to the equilibrium value as possible, in order to decrease the time necessary for the attainment of equilibrium.

The range of silicon between 4.4 to 15.0 pct involved the following difficulties in the experimental procedures: 1—The preheater failure was frequent, especially at the H_2O/H_2 ratio corresponding to 15.0 pct Si. Several heats of this and 10 pct Si contents were rejected for this reason. 2—The rate of change in the composition of these melts was very slow. Determination of a single equilibrium silicon content required several long heats under the same atmosphere.

The latter difficulty can be illustrated by certain actual heats. In order to determine the equilibrium silicon content under an atmosphere of H_2O/H_2 = 0.0021, heat 137 was charged with 18.40 pct Si metal. After 13.5 hr at 1600° C, its composition in silicon was 17.60 pct. Accordingly heat 140 was charged with 15.16 pct Si. With 99 pct recovery of silicon, this heat initially contained 15.01 pct of this element. After 13.6 hr at the same temperature, the silicon content remained the same, indicating that the equilibrium concentration was obtained. Determination of the equilibrium concentration at 10.42 pct Si required four successive heats of similar types.

At the end of an experimental heat, the melt was lowered quickly and gas-quenched (a few were furnace cooled). The ingots were sound and somewhat adherent to the crucibles. After removing a thin skin of metal by grinding, the ingots were cut vertically into radial segments for the chemical and vacuum-fusion analyses.

Quenching Technique: Heats 4 to 6 were furnace cooled from 1600 C and freezing required 16 to 20 sec. This was considered to be too long to be certain of retaining the equilibrium concentrations of silicon and oxygen in liquid iron and a quenching technique was therefore developed. The first attempt to quench the liquid iron was to duplicate the water-quenching method described by Zapffe and Sims.[7] These authors dropped their melts directly in a tank of water with a towel on its surface acting as a "parachute." With this technique it was extremely difficult to obtain ingots of regular shape and free of porosity. The oxygen content of the few water-quenched heats that were sound enough to analyze are shown in the first four lines of Table I. It is evident that there is no correlation between the percentage of oxygen and the ratio H_2O/H_2. Moreover, all but one of these specimens are higher in oxygen than corresponding properly quenched melts, and it

Table I. Examples Showing Effect of Quenching Method, 1600° C

Heat No.	$H_2O/H_2 \times 10^3$	O, Pct	$\frac{(H_2O)}{(H_2)(\%\ O)}$	Quench
5	4.73	0.072	1.2	Water
6	4.73	0.035	2.5	Water
12	4.33	0.025	3.0	Water
14	5.64	0.019	2.1	Water
15	4.31	0.021		
8	5.75	0.015	2.9	Furnace
9	5.75	0.015	3.24	Furnace
16	4.86	0.015	4.1	Furnace
20	15.90	0.009		
61	10.52	0.033	3.2	Dry H_2
62	10.47	0.034	3.1	Wet H_2
63	17.20	0.052	3.3	Wet H_2
64	17.06	0.052	3.3	Dry H_2
69	17.30	0.053	3.4	Dry H_2

Table II. Preliminary Heats at 1600° C, H_2O/H_2 = 0.0233

Heat No.	Time, Hr	Si, Pct Charged	Si, Pct Analyzed
37	3.0	0.25	0.237
38	2.0	0.281	0.326
39	2.1	0.30	0.315
40	3.2	0.33	0.344
41	3.0	0.35	0.355
44	3.0	0.41	0.408
45	1.2	0.41	0.433
46	3.0	0.45	0.474
47	3.2	0.50	

Table III. Heats Approaching Equilibrium from both Sides at 1600° C, H_2O/H_2 = 0.0233

Heat No.	Time, Hr	Si, Pct Charged	Si, Pct Analyzed
62	12.2	0.26	0.357
63	16.0	0.26	0.339
43	12.0	0.50	0.414
48	3.2	0.48	0.376
49	16.5	0.42	0.378
50	17.2	0.35	0.378

Table IV. Reaction Rate Heats at 1600° C, H_2O/H_2 = 0.0182

Heat No.	Time, Hr	Si, Pct	O, Pct	$-\frac{d(\%\ Si)}{d(\%\ O)} \times 10^3$
Series I — Initial Charge: Pure Iron				
71	0.25	0.072	0.0180	2.3
70	1.00	0.165	0.0128	2.7
72	2.01	0.241	0.0106	2.7
73	4.08	0.321	0.0095	2.9
88	1.00	0.178	0.0126	2.6
89	3.57	0.35	0.0088	2.8
78	3.57	0.49	0.0073	2.8
79	9.57	0.49	0.0094	2.3
80	16.52	0.603		
Series II — Initial Charge: 1 Pct Si				
84	0.33	0.90	0.0080	4.3
85	1.50	0.840	0.0093	3.4
83	3.74	0.929	0.0084	3.6
81	8.00	0.80	0.0093	2.9
82	9.00	0.80		

Table V. Rate of Transfer and Oxygen Capacity of Gas

Time, Hr	O Transferred, Millimols	Activity of O, a_O	H_2O/H_2 (Equilibrium)	Capacity, Millimols per Hr	Total Capacity, Millimols
Series I					
0.25	0	0.0148	0.059	27.0	0
1.00	2.5	0.0095	0.038	13.2	12.5
2.01	4.4	0.0073	0.029	7.5	22.5
4.08	6.4	0.0062	0.025	4.7	35.5
1.00	2.8	0.0091	0.037	12.6	12.2
3.57	8.6	0.0058	0.024	4.1	41.0
9.57	10.6	0.0046	0.019	0.6	49.0
16.52	13.7	0.0039	0.016	1.4	
Series II					
0.33	0	0.0036		2.6	0
8.00	4.5	0.0034	0.014	2.6	20

is evident that oxygen has been absorbed from the water. This conclusion was substantiated by an experiment in which the quenching medium was a chlorinated hydrocarbon oil; in this case the sample was very porous and contained 1.0 pct C.

The next group of three heats in Table I were furnace cooled by lowering them out of the induction coil. In these samples the oxygen content is at least roughly proportional to the H_2O/H_2 ratio and is comparable to that found later in gas-quenched samples.

The most satisfactory and convenient method of quenching was by the use of hydrogen or helium. Hydrogen was used in most of this work directly from the cylinders or with a controlled amount of water vapor. The experimental procedure consisted of passing hydrogen through the quenching tubes, *K*, shown in Fig. 2, at a pressure of 15 to 20 psi as soon as the melt was pulled down to the position just below the upper jet holes. This operation required about 1 sec with the assistance of another person at this moment. It was an important precaution to flush all the connections between the hydrogen cylinder and the quenching tubes before proceeding with this operation. Helium used in two heats did not chill the sample quite as rapidly as hydrogen, and was considerably more expensive.

Results shown in Tabie I indicate that dry and wet hydrogen produced similar and reproducible results. This technique was used for all heats beginning with No. 28. The time required for freezing from 1600° was 4 to 6 sec compared to 20 sec for furnace cooling.

Reaction Rate Study

Preliminary runs in Table II indicated that a period of 1 to 3 hr was not sufficient for the establishment of equilibrium. These heats were all made under a gas with a constant H_2O/H_2 ratio of 0.0233±0.0002. The rate of change in silicon concentration was smallest in heats 34 and 35, bracketing the equilibrium silicon concentration, and showing that a longer period of time than 3 hr was required to reach equilibrium. Accordingly, heats in Table III were made with longer periods of time and under the same H_2O/H_2 ratio. Further, very closely agreeing silicon values were obtained when the equilibrium was approached from both directions, as shown by heats 49 and 50.

These heats were made in crucibles of 0.875 in. ID and 2.0 in. high, containing 45 g of liquid metal. The surface exposed by the metal was considered to be too small, requiring excessively long periods of time for the attainment of equilibrium even in the case of initial silicon content not far from the equilibrium value. Another series of rate studies was made with crucibles of 1.063 in. ID and 1.13 in. high, permitting 50 pct larger surface area exposed to gases and containing 35 g of liquid iron. These heats were made under a H_2O/H_2 ratio of 1.82×10^{-2} and consisted of: 1—the first series starting with pure iron, and 2—the second series containing an initial charge of 1 pct Si. Table IV gives the experimental results obtained under constant conditions of temperature and gas composition. The charge was brought to 1600°C within 40 sec, in order to eliminate large relative error in time. In the first four heats the preheater was maintained at about 1600°C; in all others this was reduced to about 1400°C, in order to prolong the life of the preheater wire.

The rate data are shown graphically in Fig. 3. It is evident that the approach to equilibrium from either the low or the high silicon side requires many

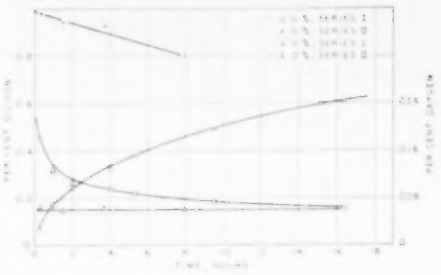

Fig. 3 (above)—Reaction rate at 1600°C. $(H_2O)/(H_2)$ = 0.0182.

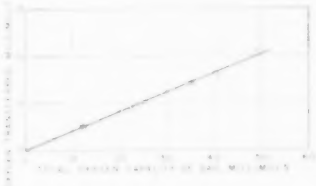

Fig. 4 (right)—Transfer of oxygen from metal to gas.

hours, if the change in composition is even moderately large. This is in sharp contrast to the results obtained in inert crucibles[4] where 15 to 30 min was adequate. The difference lies in the fact that here the oxygen transferred across the metal-gas interface is not simply that associated with the change in oxygen concentration but includes also that resulting from reduction of silica or oxidation of silicon.

Rate of Oxygen Transfer—Series I. In approaching equilibrium from the low silicon side it was found that the product [% Si] [% O]² was essentially independent of time. This indicates that equilibrium is maintained between solid silica and liquid metal and hence that the overall rate is determined by other reactions, presumably those at the liquid-gas surface. The total amount of oxygen transferred from metal to gas is readily obtained from the changes in composition and the total mass of metal, 35 g. The number of millimols of oxygen transferred from metal to gas, beginning with the first sample, is shown in col. 2 of Table V.

The capacity of the gas for removal of oxygen is determined by its hydrogen content and by the difference in H_2O/H_2 ratio for the incoming gas and that which would be in equilibrium with the metal bath. The latter depends upon the activity of oxygen in the metal, which is not the same as its concentration on account of the effect of silicon. It will be shown later that silicon decreases the activity coefficient of oxygen in the manner summarized by Fig. 6. This curve is used to compute the activity of oxygen in each sample, and the results are listed in col. 3 of Table V. The corresponding equilibrium ratio H_2O/H_2 calculated from the equilibrium constant of eq 3 ($K_3 = 3.95$) is listed in col. 4.

The rate of flow of the gas was 260 ml of hydrogen per min, corrected to standard conditions. This equals 696 millimols per hr, and its water-vapor content was 12.7 millimols. Each atom of oxygen removed from the bath consumes one molecule of H_2 and adds one of H_2O. In the limiting case, this process can continue until the equilibrium ratio is reached, and the total number of mols which the gas can absorb is called its oxygen capacity.[7] The oxygen capacity of the gas expressed in millimols per hr is given in col. 5 of Table V. It was assumed that all heats were

Fig. 5—Variation of oxygen content with H_2O/H_2 ratio.

alike at a time of 0.28 hr (the shortest run), and the total capacity of the gas between this time and the end of the run was obtained graphically from a plot of capacity vs. time. The result is in col. 6.

In Fig. 4 the amount of oxygen transferred is plotted against the total oxygen capacity of the gas. The slope of the straight line, 0.2, indicates that the process of oxygen transfer is about 20 pct efficient under the conditions of the experiments.

Rate of Oxygen Transfer—Series II. In oxidizing silicon from the bath, the oxygen activity of the metal remained substantially constant at 0.0035. The oxygen capacity of the gas is, therefore, constant and equal to —2.6 millimols per hr. The rate of silicon removal was also roughly constant at about 0.023 pct or 0.58 millimols of oxygen per hr. The transfer efficiency is thus 22 pct, but this figure is inaccurate on account of the close proximity to equilibrium.

These kinetic studies were not expected to elucidate the mechanism of oxygen transfer. Such a study would require wide variations in concentration and flow rate of the gas, as well as in stirring rate of the bath, the latter conceivably achieved by changes in frequency. About all that can be concluded regarding reaction rates is: 1—that under the experimental conditions oxygen transfer is 20 pct efficient, and 2—that the reactions at the metal-silica interface are fast enough to keep pace with those at the metal-gas surface.

Equilibrium Study, 1600°C

A large number of experimental runs were carried out at 1600°C in order to establish the equilibrium conditions at several levels of silicon concentration. Some of these runs, like the early heats of Table III, showed only the direction in which the reaction was proceeding, and actual equilibrium was not reached. These nonequilibrium heats are summarized in Table VI. The data are useful as approximate confirmation of the more accurate results of heats in which equilibrium was more closely approached.

The data on those heats which attained or very closely approached equilibrium are summarized in Table VII. Two series of results are presented in order of increasing silicon concentration. In the first series, the preheater was held as nearly as possible

Table VI. Nonequilibrium Heats at 1600°C

Heat No.	Si, Pct Charged	Si, Pct Analyzed	H_2O/H_2 x10³	O, Pct	(% Si)²(% O) x10³	Hr at Temperature
27	1.00	0.938	8.77	0.0058	3.2	3.1*
28	1.00	0.830	8.71	0.0065	3.5	4.0*
30	0.50	0.432	8.71	0.0076†	2.5	3.0
98	12.86	12.11	0.486	0.0028†	9.4	14.5
101	12.86	12.11	0.276	0.0012†	3.5	8.4
108	25.0	24.00	0.707	0.0049	7.4	12.0
133	3.41	3.03	0.707	0.0018	2.0	16.0
135	6.52	6.24	0.432	0.0016	3.3	13.0
136	14.00	12.87	0.280			13.5
137	18.40	17.60	0.214			6.5
138	11.52	10.97	0.272			2.2
141	10.47	10.40	0.258			

* Surface partially covered by a scum growing gradually towards the center of metal.
† Single analysis.

Table VII. Equilibrium Data at 1600°C

Heat No.	Si, Pct Charged	Si, Pct Analyzed	H_2O/H_2 x10³	O, Pct	Time, Hr	K' x10³	K_1 x10³	K_2	f_{Si}
Series I									
104	0.00	0.0013†	32.6	0.0780	3.8	1.83*	3.18	4.18	1.05
65	0.009	0.012†	17.36	0.0415	12.0	2.07	3.63	4.18	1.05
69	0.02	0.013†	17.30	0.0502	12.2†	3.27	3.82	3.46	0.87
101	0.02	0.020†	17.00	0.0413	9.0	3.41		4.12	1.03
83	0.00	0.016	13.19	0.0378	6.5	2.30	2.78	3.49	0.88
61	0.06	0.026	10.52	0.0332	8.4	2.86	2.87	3.18	0.80
62	0.00	0.025	10.47	0.0323	10.0	2.64	2.74	3.22	0.81
66	0.046	0.036	8.90	0.0300	11.0	3.24	2.84	2.97	0.75
50	0.08	0.069	5.87	0.0183	12.0	3.02	3.05	3.23	0.81
57	0.18	0.132	4.52	0.0149	12.0	2.93	2.50	2.93	0.74
56	0.12	0.139	4.31	0.0142	9.5	2.80	2.57	3.03	0.76
52	0.20	0.227	3.23	0.0117	18.0	3.10	3.07	2.76	0.70
48	0.42	0.378	2.334	0.0080	16.5	3.07	2.07	2.59	0.64
49	0.55	0.478	2.305	0.0080	17.2	3.10	2.02	2.56	0.65
89	0.73	0.633	1.703	0.0065	12.4	2.43	1.78	2.70	0.68
Series II									
127	0.00	0.004†	20.00	0.0935	3.7	1.85	2.90	4.10	1.03
130	0.005	0.006	21.00	0.0571	4.1	1.05	2.87	4.02	1.01
120	0.011	0.013	16.13	0.0401	7.5	1.72	2.86	2.61	0.78
131	0.056	0.061	6.34		14.5		2.50	3.07	0.60
121	0.425	0.410	3.00	0.0127	13.3	2.74	2.09	2.36	0.66
122	0.177	0.170	2.20	0.00961	11.0	3.78	1.73	2.62	0.53
123	0.425	0.410	2.20	0.0050	12.5	2.52	1.50	2.11	0.51
132	1.10	1.01	1.31	0.0049	11.0	3.40	0.912	2.04	
134	3.77	3.61	0.969	0.0046	10.5	2.24	0.707		
149	4.66	4.39	0.456	0.00231	9.3	3.02	0.660	1.24	0.31
139	10.64	10.42	0.280	0.0017	13.0	4.3			
140	10.53	15.00	0.210	0.0017					

* In Series I, gases were highly preheated. In Series II, preheating was about 60°C lower.
† Six analyses averaged.
‡ Single analysis.

at bath temperature, in the second, about 60° lower. No consistent differences were observed and the two series are considered equivalent. Certain thermodynamic quantities derived from the data are also tabulated. Results at other temperatures will be shown subsequently.

Several heats were made under a gas sufficiently oxidizing to produce a slag on the metal surface. Such runs could not be carried to equilibrium, since this would entail destruction of the crucible. Each run was discontinued shortly after the visual appearance of slag. The data which are assembled in Table VIII show conditions under which slag forms. The average oxygen content of these heats, 0.088 ±0.002 pct, is taken as the limiting concentration corresponding to saturation with slag and solid silica. The corresponding silicon content is of the order of 0.003 pct, but this is not considered an accurate figure.

The data of Tables VII and VIII are plotted in Fig. 5. The slope of the equilibrium line agrees with the value of $K_s' = 3.95$ reported by Dastur and Chipman. Deviations below about 0.04 pct O are real and will be discussed in the following section. The limiting H_2O/H_2 ratio is 0.35 corresponding to the oxygen limit 0.088 pct.

Thermodynamic Calculations, 1600°C

Activity of Oxygen: It is known from the early work of Fontana and Chipman[7] and of Chipman and Samarin[8] that in the binary solution of oxygen in iron the activity of oxygen is proportional to its concentration. This is the basis for setting the activity coefficient f_o in the binary solution equal to unity, in the equation:

$$H_2 (g) + O = H_2O (g); K_s = \frac{p_{H_2O}}{p_{H_2} \cdot f_o \cdot [\% O]} \quad [4]$$

Values of f_o in the presence of silicon are considerably less than unity as shown in the last column of Table VII. Here values of f_o were obtained by dividing the tabulated values of K_s' by 3.95, the observed[7,8] value of K_s at 1600°. Fig. 6 is a plot of the logarithm of f_o against silicon concentration. The shape of the curve is quite different from the straight line that was expected. Up to 0.5 pct Si it is fitted by the empirical equation:

$$\log f_o^{(Si)} = -0.12 [\% Si] - 0.38 [\% Si]^2 \quad [5]$$

where the symbol $f_o^{(Si)}$ designates the contribution of silicon to the activity coefficient of oxygen.

Activity of FeO in Slag: The metal under a ferrous silicate slag contains a negligible amount of silicon,

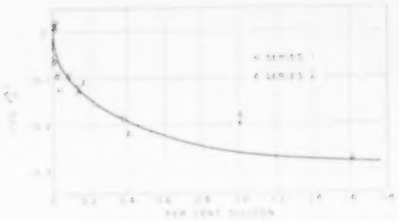

Fig. 6—Effect of silicon on f_o = a_o/[% O] at 1600°C

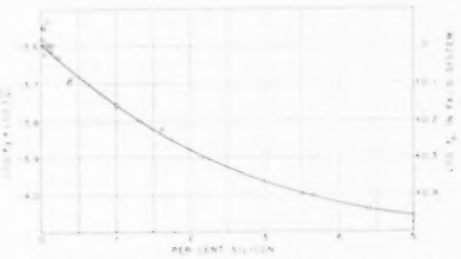

Fig. 7—Plot used in determining value of f_{FeO} at 1600°C. Scale on right shows activity coefficient of silicon (f'_{Si}).

and its oxygen activity is equal to its concentration, 0.088 pct (Fig. 5). Under a pure iron oxide slag the oxygen solubility is 0.225 pct.[9] Hence, the activity of FeO in the silica-saturated slag is 0.088/0.225 = 0.39.

Activity of Silicon: The effect of oxygen upon the activity coefficient of silicon is related to the effect of silicon upon that of oxygen through an equation derived by Wagner.[10] He has shown that in a very dilute solution of components 2 and 3 in component 1, as the concentrations of 2 and 3 approach zero:

$$\partial \ln \gamma_2 / \partial x_2 = \partial \ln \gamma_3 / \partial x_3 \quad [6]$$

where γ is the activity coefficient and x, the mol fraction. It can be shown also that the equation is approximately valid when $x_2 = 1$ and $x_3 = 1$. Applied to oxygen and silicon with concentration in weight percent and designating by f_o the ratio a_o/[% Si], this becomes:

$$\partial \log f_o / \partial [\% Si] = \frac{16}{28} \partial \log f_o / \partial [\% O] \quad [7]$$

and from eq 5 by differentiation:

$$\partial \log f_o / \partial [\% Si] = -0.12 - 0.19 [\% Si] \quad [8]$$

Table VIII. Heats in Which a Slag Was Formed at 1600°C

Heat No.	Si, Pct Charged	Si, Pct Analyzed*	H_2O/H_2	O, Pct	Hr at 1600°C	Remarks
With Full Preheat						
100			0.735			Crucible failed due to slagging after 0.34 hr.
101	0.009	0.007	0.735	0.0864	0.75	Slag appeared after 0.38 hr.
102	0.012	0.004	0.590	0.0867	1.2	Slag appeared after 0.42 hr, heat furnace cooled.
103	0.011		0.430	0.0857	2.2	Slag appeared after 0.67 hr.
With Lower Preheat						
126	0.00	0.003	0.716	0.0932	0.40	Slag appeared after 0.38 hr. Ingot unsound.
129	0.00	0.005	0.542	0.0920	0.42	Slag appeared after 0.30 hr.
128	0.00		0.454	0.0873	0.54	Slag appeared after 0.38 hr.

* Si analyses unreliable.

Fig. 8—Logarithm of activity coefficient of silicon, f_{Si}, vs [% Si] in binary system, Fe-Si, at 1600°C.

Combination of eqs 7 and 8 gives:

$$\delta \log f_{Si}/\delta [\%\ O] = 0.21 - 0.33\,[\%\ Si] \qquad [9]$$

At any given silicon concentration eq 9 may be integrated between oxygen limits of zero and [% O] keeping [% Si] constant. Letting f_{Si} represent the activity coefficient of silicon in the binary (oxygen-free) solution, and defining f''_{Si} as the contribution of oxygen to the activity in the ternary solution, the integration gives:

$$\log f''_{Si} = \log f_{Si} - \log f_{Si} = (0.21 - 0.33\,[\%\ Si])\,[\%\ O] \qquad [10]$$

Both eqs 5 and 10 are empirical and are used only for convenience in calculation. They are restricted to a range of silicon concentrations from about 0.01 to 0.50 pct.

The next step includes the evaluation of both f_{Si} and K_1, the latter defined by the equation:

Table IX. Computation of f''_{Si}, f'_{Si}, and K'_1 at 1600°C

Heat No.	Si, Pct	O, Pct	$-\log f''_{Si}$	$K'_1 = f''_{Si}$	log f'_{Si}
55	0.012	0.0435	0.110	2.558	0.042
49	0.013	0.0502	0.136	2.546	0.054
50	0.014	0.0550	0.092	2.652	0.052
83	0.026	0.0332	0.062	2.604	0.004
81	0.026	0.0332	0.062	2.604	0.004
82	0.035	0.0225	0.061	2.624	0.024
80	0.036	0.0209	0.046	2.582	0.008
48	0.059	0.0183	0.017	2.534	0.066
57	0.132	0.0149	0.013	2.613	0.013
56	0.139	0.0162	0.010	2.600	0.00
52	0.227	0.0117	0.006	2.629	0.029
53	0.379	0.0080	0.003	2.667	0.067
54	0.528	0.0060	0.003	2.695	0.088
127	0.004	0.0583	0.350	3.807	0.207
130	0.006	0.017	0.233	3.775	0.175
131	0.013	0.0401	0.119	3.692	0.092
121	0.063		0.04	3.62	0.02
122	0.170	0.0127	0.008	3.586	0.004
123	0.410	0.0086	0.00	3.620	0.000
132	1.01		0.00	3.782	0.162
134	1.61	0.0046	0.00	3.624	0.224
149	4.59	0.0023	0.00	4.039	0.439
138	10.42		0.00	4.73	0.55
140	13.90	0.0017	0.00	4.18	0.58

Fig. 9—Si-O equilibrium at 1600°C.

$$SiO_2 + 2H_2 = Si + 2H_2O,\ K_1 = \left(\frac{H_2O}{H_2}\right)^2 \cdot f_{Si} \cdot f''_{Si} \cdot [\%\ Si] \qquad [11]$$

The equilibrium constant K_1 is related to K'_1 of eq 2 and Table VII as follows:

$$K_1 = K'_1 \cdot f_{Si} \cdot f''_{Si} \qquad [12]$$

The data are shown in Table IX in which col. 4 shows $\log f''_{Si}$ computed from eq 10. Fig. 7 is a plot of $\log K'_1 + \log f''_{Si}$ against [% Si] using values of K'_1 from Table VII. The extrapolated value at zero silicon concentration gives the value $\log K_1 = -3.60$. Values of $\log f_{Si}$ are found from eq 12 and may be read from the curve of Fig. 7 by the auxiliary scale on the right. By the same method values of f_{Si} for the binary system Fe-Si are obtained also for the higher concentrations of silicon and the data are summarized in Fig. 8.

Deoxidation Equilibrium

The silicon and oxygen concentrations in metal which is in equilibrium with SiO_2 at 1600° are plotted in Fig. 9. The straight line corresponds to a product [% Si] [% O]^2 = 2.8×10^{-4} which represents the data approximately over a very wide range of composition. The greatest deviations are found at very low silicon contents, where the silicon analysis is inaccurate, or at very high silicon, where the oxygen concentration is low and rather uncertain. Hence, for all practical purposes the value of this product may be taken as 2.8×10^{-4} at 1600°C in the range 0.02 to 15.0 pct Si.

This, however, is not the true equilibrium constant for the reaction. The values for K_1 and K'_1 at 1600° of 2.5×10^{-4} and 3.95, respectively, have been accepted. From eqs 1, 2, and 3, it is evident that $K_1 = K_w/K'_1$, hence at 1600° $K_w = 1.6 \times 10^{-3}$. The disagreement between K'_1 and K_1 is due entirely to the ac-

Table X. Equilibrium Data at 1545° and 1650°C

Heat No.	Si, Pct Charged	Si, Pct Analyzed	$H_2O/H_2 \times 10^3$	O, Pct	Time, Hr	$K'_1 \times 10^4$	$K_1 \times 10^4$	K_w	f_{Si}
Temperature 1545°C									
90	0.10	0.040	5.21	0.0125*	12.3	0.63	1.09	4.16	0.82
91	0.04	0.018	6.78	0.0242	13.0	1.03	1.39	3.63	0.71
93	0.08	0.073	3.87	0.0112	12.0	0.92	1.10	3.46	0.68
94	0.60	0.073	3.87	0.0112	13.1	0.98	1.13	3.44	0.68
107	0.090	0.129	3.02	0.0088	13.5	0.95	1.20	3.56	0.70
108	0.063	0.080	3.88	0.0109	12.5	0.97	1.27	3.54	0.70
109	0.042	0.044	5.27	0.0156	12.4	1.07	1.36	3.45	0.68
144	0.074	0.053	4.27	0.0124	8.0	1.13			
Temperature 1650°C									
97	0.50	0.400	2.73	0.0198	11.0	5.94	3.82	2.67	0.84
145	0.063	0.068	7.96	0.0250*	9.5	4.95	4.20	2.90	0.91
146	0.078	0.045	6.01	0.0263	9.5	5.46	4.02	2.71	0.85
147	0.062	0.035	8.37		6.5		4.04		
148	0.086	0.081	7.16	0.0252	6.5	5.77	4.59	2.82	0.89

* Single analysis.

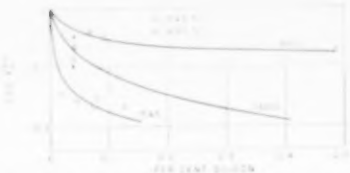

Fig. 10—Effect of silicon on the activity coefficient of oxygen at three temperatures.

tivity coefficients of oxygen and silicon discussed in the foregoing section. Within the experimental range of composition the product of the activity coefficients is, fortuitously, nearly constant, which results in a nearly constant value of K'_2. Actually, this product varies slightly with composition but the experimental data, especially those at low silicon content, are not sufficiently accurate to permit a detailed examination of this question.

The same uncertainty applies to the following estimate of the silicon content of the metal in equilibrium with solid silica and liquid slag. In an earlier section the oxygen content was found to be 0.088 pct. If the product K'_2 remains constant at 2.8×10^{-3}, this corresponds to 0.0036 pct Si. The lower trend noticeable in Fig. 9 would indicate about 0.0024 pct, while the empirical equations for activity coefficient point to a slightly higher value. Our best estimate is, therefore, 0.003 ± 0.001 pct Si at 1600°.

Effect of Temperature on the Equilibrium

Experimental data at 1545° and 1650°C are given in Table X. The detailed study of the approach to equilibrium at 1600° was not repeated at these temperatures. Nevertheless, equilibrium was approached from both sides and, in most cases, there can be little doubt but that equilibrium was substantially reached.

The values of K_2 at these temperatures, according to Dastur and Chipman, are 5.10 and 3.15, respectively. These and tabulated values of K'_2 yield the activity coefficients of oxygen in the last column. These are plotted in Fig. 10 along with the curve for 1600° from Fig. 6. The curves are drawn by analogy with the 1600° results, and it is obvious that the data yield only crude values for $f_{O}^{(Si)}$.

The effect of oxygen on the activity coefficient of silicon was computed as described for the data at 1600°, using empirical expressions which need not be recorded here. The activity coefficient, f'_{Si}, of silicon in the binary system Fe-Si was assumed to follow the curve established at 1600° (Fig. 8). Errors in these coefficients cannot seriously affect the resultant values of K_2, since all values of f involved

Table XI. Computation of K_2 at 1545° and 1650°C

Heat No.	log K'_2	log $f_{O}^{(Si)}$	log f'_{Si}	− log K_2
Temperature 1545°				
90	3.964	0.027	0.007	3.984
91	3.859	0.098	0.003	3.954
94	3.959	0.010	0.012	3.957
107	3.940	0.003	0.021	3.922
108	3.921	0.010	0.013	3.918
109	3.897	0.030	0.007	3.920
144	3.867	0.016	0.012	3.871
			Weighted average	3.920 ± 0.03
Temperature 1650°				
97	3.441	0.000	0.080	3.361
145	3.377	0.013	0.011	3.379
146	3.395	0.025	0.008	3.412
147	3.394	0.019	0.009	3.404
148	3.338	0.009	0.015	3.334
			Weighted average	3.375 ± 0.025

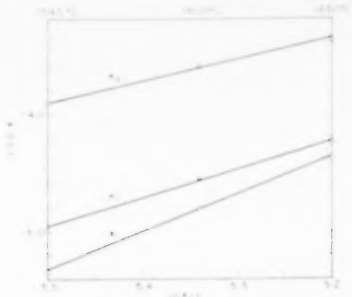

Fig. 11—Effect of temperature on equilibrium

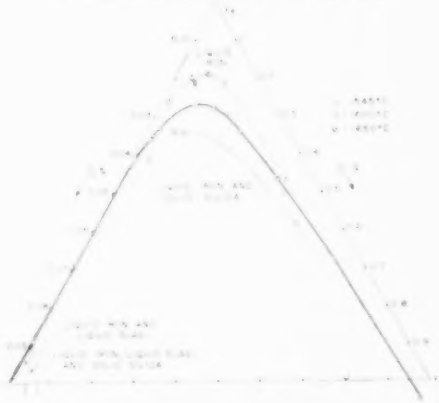

Fig. 12—Isothermal section of ternary system Fe-Si-O at 1600°C. Dotted lines show solubility lines at 1545° and 1650°C.

are near unity. The calculation is summarized in Table XI from which the values of K_2 at 1545° and 1650°, respectively, are $(1.20 \pm 0.08) \times 10^{-3}$ and $(4.2 \pm 0.3) \times 10^{-4}$.

From K_2 and K_3 the values of K_1 at these temperatures are 4.6×10^{-4} and 4.2×10^{-5}. These figures represent the equilibrium constants for silica saturation, namely $a_{Si} \cdot a^2_O$. The concentration products, [% Si] [% O]^2 are best obtained as the average values of K'_2, which for the two temperatures are respectively 1.02×10^{-3} and 5.5×10^{-4}.

The effect of temperature on K_1, K'_2, and K_3 is shown graphically in Fig. 11 where log K is plotted against reciprocal temperature. The straight lines correspond to the following equations for log K and for the free energy change in the reactions; the corresponding values for K_2 are quoted from Dastur and Chipman:

$$SiO_2\ (s) = \underline{Si} + 2\underline{O};\ \Delta F^\circ = + 146{,}500 - 56.3T$$

$$K_1 = a_{Si} \cdot a^2_O;\ \log K_1 = -32{,}000/T + 12.29 \quad [13]$$

$$SiO_2\ (s) + 2H_2\ (g) = \underline{Si} + 2H_2O\ (g);$$

$$\Delta F^\circ = + 82{,}000 - 27.3T$$

$$K_3 = a_{Si}\ (p_{H_2O}/p_{H_2})^2;\ \log K_3 = -18{,}000/T + 5.98 \quad [14]$$

$$H_2\ (g) + \underline{O} = H_2O;\ \Delta F^\circ = -32{,}250 + 14.50T$$

$$K_3 = p_{H_2O}/(p_{H_2} \cdot a_O);\ \log K_3 = + 7050/T - 3.17 \quad [15]$$

Fig. 13—Comparison of data on equilibrium between H_2, H_2O, and Si in liquid iron at 1600° C.

The solid form of silica to which eqs 13 and 14 apply is cristobalite, the stable form at the experimental temperatures. The crucibles which were originally vitreous silica were always thoroughly devitrified. It should be remarked that K_1 and K_2 are less certain than K_3 because of uncertainties in the activity coefficients. The heat terms in the equations of ΔF_1 and ΔF_2 are subject to uncertainties of at least ± 5000 cal.

The isothermal section of the iron-rich corner of the ternary system Fe-Si-O at 1600° is shown in Fig. 12. The solid curve passes through experimental points up to 0.088 pct O, beyond which solid silica disappears. The three-phase area in the lower left corner contains solid silica, a liquid slag whose composition varies only with temperature, and liquid metal containing 0.088 pct O and about 0.003 pct Si. The experimental data at the lower and higher temperatures are shown by broken lines which indicate the solubility of SiO_2 at these temperatures.

Comparison With Previous Work: The experimental work of Körber and Oelsen led to average values of the product $K'_3 = [\%\ Si]\ [\%\ O]^2$ which do not differ greatly from those reported here. The comparison is shown in Table XII. The good agreement at lower temperatures is somewhat fortuitous, since the earlier results showed very wide scatter and only the average is recorded here.

In the experiments of Zapffe and Sims this product was not determined, but a basis of comparison can be found in the gas-metal equilibrium represented by eq 2. The data for 1600° are shown in Fig. 13 where values of $(H_2/H_2O)^2$ are plotted against silicon content. Wide deviations in the earlier data are attributed to failure to reach equilibrium in the reaction.

In the more recent work of Hilty and Crafts, an apparent break was reported in the Si-O relationship at about 0.04 pct Si. The results reported here

Fig. 14—Si-O equilibrium in liquid iron at 1600° C. Comparison of results in silica crucibles.

Table XII. Comparison of Results for Product $[\%\ Si]\cdot[\%\ O]^2 \times 10^3$

Temperature, °C	1550	1600	1650
Körber and Oelsen	1.3	3.6	10.6
Hilty and Crafts	1.6	3.0	5.3
Gokcen and Chipman	1.2	2.8	5.5

do not confirm this break though they do agree rather well with the actual data. Fig. 14 shows their experimental points obtained in silica crucibles at 1600° and our line for the same temperature. On the average the agreement is excellent. Their average values of K'_3 at three temperatures are included in Table XII.

Summary

Molten Fe-Si-O alloys in silica crucibles were brought into equilibrium with atmospheres of controlled H_2O/H_2 ratio, quenched in hydrogen, and analyzed.

The rates of oxidation and reduction were studied in experiments lasting up to 16 hr at 1600°. The rate determining part of the process is the transfer of oxygen from gas to metal or the reverse, which, under the experimental conditions, was about 20 pct efficient. Reactions at the metal-silica interface are fast enough to keep pace with those at the metal-gas surface.

A detailed study was carried out at 1600° and up to 15 pct Si of equilibrium in the reactions:

$$SiO_2\ (s) = Si + 2O \qquad [1]$$

$$SiO_2\ (s) + 2H_2\ (g) = Si + 2H_2O\ (g) \qquad [2]$$

$$H_2\ (g) + O = H_2O\ (g) \qquad [3]$$

From the previously known equilibrium constant of eq 3 the activity coefficient of oxygen was determined and found to be strongly diminished by even small amounts of silicon. A reciprocal relation permits calculation of the effect of oxygen on the activity coefficient of silicon.

From the equilibrium data at 1545°, 1600°, and 1650°, the activity of silicon and the constants of eqs 1 and 2 were obtained, as well as the free energies and heat effects in these reactions.

At 1600° the metal in equilibrium with solid silica (cristobalite) and liquid slag contains 0.088 pct O and about 0.003 pct Si. The activity of FeO in the slag is 0.39.

The concentration product $[\%\ Si]\cdot[\%\ O]^2$ is not the true equilibrium constant of reaction 1 because the activity coefficients are far from unity. Approximately compensating changes in the coefficients result in a nearly constant product and for practical purposes it may be considered constant in the range 0.02 to 15.0 pct Si. Values of the product agree fairly well with previous studies as shown in Table XII.

Acknowledgments

The authors wish to thank Donald L. Guernsey and William T. Martin for their careful chemical analyses and Henry A. Wriedt for assistance in many of the experiments. This work is part of a study of the physical chemistry of steelmaking sponsored by the Office of Naval Research under Contract No. N5ori-78/XVI.

References

[1] A. McCance: *Trans.* Faraday Soc. (1925-1926) **21**, pp. 176-201.

[2] A. McCance: Iron and Steel Inst. (London) Special Report No. 22, pp. 331-371 (1938).

[9] A. L. Feild: *Trans.* Faraday Soc. (1925-1926) **21**, pp. 255-267.
[10] H. Schenck: *Physical Chemistry of Steelmaking*. (English Translation). British Iron and Steel Research Assn., pp. 186 and 200 (1945).
[11] J. Chipman: *Trans.* A.S.M. (1934) **22**, pp. 384-446.
[12] C. H. Herty and G. R. Fitterer: *Physical Chemistry of Steelmaking*. Carnegie Inst. of Tech. and U. S. Bur. Mines, Coop Bull. 36 (1928). C. H. Herty, G. R. Fitterer, C. F. Christopher: Ibid. *Tech. Paper* 492 (1931).
[13] H. Schenck and O. Bruggemann: *Archiv. Eisenhüttenwesen* (1935-1936) **9**, pp. 543-553.
[14] F. Körber: *Stahl und Eisen* (1934) **15**, pp. 535-543.
[15] F. Körber and W. Oelsen: *Mitt. K.-W. Inst. Eisenforschung* (1933) **15**, pp. 271-309.
[16] L. S. Darken: *Trans.* AIME (1940) **140**, pp. 204-221.
[17] C. A. Zapffe and C. E. Sims: *Trans.* AIME (1943) **154**, pp. 192-227.
[18] D. C. Hilty and W. Crafts: *Trans.* AIME (1950) **188**, p. 425; JOURNAL OF METALS (February 1950).
[19] M. N. Dastur and J. Chipman: *Trans.* AIME (1949) **185**, pp. 441-445; JOURNAL OF METALS (August 1949).
[20] N. A. Gokcen: *Journal* Amer. Chem. Soc. (1951) **73**, p. 3789.
[21] M. N. Dastur and J. Chipman: *Discussions*, Faraday Soc. (1948) No. 4, p. 100.
[22] M. N. Dastur and N. A. Gokcen: *Trans.* AIME (1949) **185**, p. 665; JOURNAL OF METALS (October 1949).
[23] C. F. Goodeve: *Discussions*, Faraday Soc. (1948) No. 4, p. 9.
[24] M. G. Fontana and J. Chipman: *Trans.* A.S.M. (1936) **24**, p. 313.
[25] J. Chipman and A. M. Samarin: *Trans.* AIME (1937) **125**, p. 331.
[26] C. R. Taylor and J. Chipman: *Trans.* AIME (1943) **154**, p. 228.
[27] C. Wagner: *Journal of Chemical Physics* (1951) **19**, p. 626.

Technical Note

Growth of Austenite in Cold-Rolled Tempered Martensite

by A. E. Nehrenberg

IN an earlier publication[1] it was shown that the shape assumed by a volume of growing austenite is inherited from the prior structure. The matrix grains of pearlitic microstructures are equiaxed, and austenite grows in an equiaxed manner in these prior structures. Martensite and bainite, on the other hand, have an acicular grain structure, and the austenite produced in such structures grows in an acicular manner.

In the discussion of this paper[2] it was pointed out that in cold-rolled tempered martensite, austenite grows in an equiaxed, rather than an acicular manner. The results of an experiment carried out to arrive at an understanding of this behavior are illustrated by the micrographs.

Fig. 1 shows the acicular microstructure produced by heating tempered martensite to a temperature within the Ac1-Ac3 range, 1350°F. When tempered martensite is cold rolled, then heated to the same temperature, the equiaxed structure shown in Fig. 2 is produced. A sample of cold-rolled tempered martensite heated at 1350°F just long enough for the formation of a small amount of austenite is shown by Fig. 3 to have an equiaxed (recrystallized) ferrite grain structure. The small particles of austenite which formed at 1350°F in the equiaxed ferrite matrix are likewise equiaxed.

Thus, the equiaxed growth of austenite in cold-worked tempered martensite is not a contradiction of the principles described in the previous paper, for the growth pattern reflects the matrix grain structure existing at the time of austenite formation.

Figs. 1 to 3—Effect of cold rolling on growth pattern of austenite in tempered martensite. X2000.

Fig. 1—Tempered martensite heated ½ hr at 1350°F, quenched, and tempered ½ hr at 600°F. Dark etching structure (tempered martensite) was austenite at time of quench. 2 pct Zephiran chloride-picral etch.

Fig. 2—Tempered martensite cold rolled 50 pct, then heat treated in the same manner as Fig. 1. Etch same as Fig. 1.

Fig. 3—Tempered martensite cold rolled 50 pct and heated 2 min total time in lead at 1350°F, quenched, and tempered ½ hr at 600°F. Nominal composition of steel used was: 0.25 pct C, 1.3 pct Mn, 1.5 pct Si, 1.8 pct Ni, and 0.30 pct Mo. Etched in Allen's reagent.

References

[1] A. E. Nehrenberg: The Growth of Austenite as Related to Prior Structure. *Trans.* AIME (1950) **188**, pp. 162-174; JOURNAL OF METALS (January 1950).
[2] J. R. Vilella and R. A. Grange: Discussion of ref. 1. *Trans.* AIME (1950) **188**, pp. 1378-1381; JOURNAL OF METALS (November 1950).

A. E. NEHRENBERG, Member AIME, is associated with the Metallurgical Dept., Crucible Steel Co. of America, Harrison, N. J.
TN 101E. Manuscript, Nov. 15, 1951.

Dislocation Collision and the Yield Point of Iron

By A. N. Holden

A DISLOCATION mechanism has been described by Cottrell[1] by which metals can yield locally, i.e., form Lüders bands, giving rise to a characteristic stress-strain curve with a sharp yield point and appreciable strain at constant or decreasing stress. It is undoubtedly the best mechanism that has been suggested to date.*

In its present development, however, the dislocation mechanism provides a more satisfying explanation for the sharp yield point than for the extensive localized flow occurring at the lower yield stress.

The primary objective in this paper is to extend the dislocation mechanism to account for localized cataclysmic flow by a dislocation collision process and to give experimental evidence to support such a process. Only the yielding of iron containing carbon will be discussed, although other metal-solute systems are known to behave similarly.

Cottrell Mechanism

In brief, Cottrell explains the yield point in the following way. The dislocations in iron which must propagate to produce slip usually lie at the center of local concentrations of carbon atoms, since segregation about these dislocations relieves some of the local stress resulting from them. A dislocation surrounded by a "cloud" of carbon atoms is thus anchored, and a higher stress is required to set it in motion than to move a free dislocation. Considering all available dislocations to be anchored in this fashion, the iron exhibits a yield point when the first dislocations break free and move through the lattice causing slip. This first breaking away of a dislocation enables other dislocations to break loose by "interaction" and the process becomes a cataclysm producing local deformation or Lüders bands.

The yield point in the stress-strain diagram for iron is absent in freshly deformed material, but returns gradually with time; the phenomenon is one aspect of what is called strain aging. The rate at which the yield point returns following straining depends on the temperature of aging. According to Cottrell the rate of return of the yield point in strained iron is limited by the rate of diffusion of carbon at the aging temperature; the mechanism is one of reforming the solute atmospheres around carbon-free dislocations that had stopped moving coincident with the removal of stress. If the specimen is retested immediately after straining and unloading, carbon will not have had time to diffuse to, and re-anchor, dislocations and the yield point will not occur.

The carbon diffusion limitation for the rate of strain aging apparently applies if the criterion for strain aging is either the change in hardness[2] or the change in electrical resistance[3] of the strained specimen with aging time. The possibility exists, however, that the yield point actually returns to strained iron at some rate other than that deduced from hardness or electrical resistance data. Therefore, as a preliminary experiment, the rate of yield point return in a rimmed sheet steel strained 6 pct in tension was measured at 27°, 77°, and 100° C. A plot of yield-point elongation for each of these temperatures against aging time appears in Fig. 1. The aging process is described by curves which rise to a plateau value of elongation that seems independent of temperature, but at a rate that depends on temperature. Very long times lead to a further rise in the yield-point elongation above the plateau value. However, if the later increase in yield-point elongation is ignored and the log of the time to reach half the plateau value of elongation is plotted against 1/T, a straight line results for which an activation energy of about 25 kcal per mol may be assigned. Within the accuracy of this sort of experiment this is approximately the activation energy for the diffusion of carbon in iron (20 kcal per mol), and the carbon diffusion limitation suggested for the yield-point return on strain aging is valid.

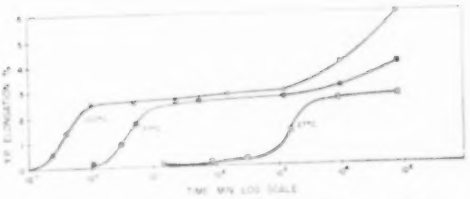

Fig. 1—Rate of return of yield point upon strain aging.

The Cottrell mechanism thus explains in a qualitative manner the occurrence of a yield point in iron and its return with strain aging. It fails, however, to explain some of the other experimental observations that have been made of the yielding behavior of iron.

For example, it is known that the yield point in iron becomes less pronounced with increasing grain size. Annealed single crystals of iron have very small yield-point elongations,[4] if indeed they have any, compared to a polycrystalline steel. If the only requirement for a yield point is that the dislocations in the lattice of the annealed material be anchored by carbon atoms, the difference in the behavior of single crystals and polycrystals is not explained. That a dislocation mechanism may be entirely consistent with little or no yield point in an annealed single crystal will become apparent later when dislocation interaction is discussed.

Strain aging produces a definite yield point even in single crystals. This accentuation of the yield-point phenomenon in single crystals after strain

A. N. HOLDEN, Junior Member AIME, is associated with Knolls Atomic Power Laboratory, General Electric Co., Schenectady.

Discussion on this paper, TP 3234E, may be sent, 2 copies, to AIME by April 1, 1952. Manuscript, June 29, 1951. New York Meeting, February 1952.

* For a review of other mechanisms that have been employed to explain the yield point, the reader is referred to Low and Gensamer.[3]

aging also is not explained by the behavior of anchored dislocations unless some change in the number of dislocations, their arrangement, or both, occurs during the strain-aging process.

Cottrell has recently extended his theory[7] to show that a polygonized structure, one containing dislocations arranged in subboundaries, could explain dislocation interaction and account for a yield point in single crystals. These boundaries of dislocations merely act as added barriers to dislocation migration, according to Cottrell, and the breaking of one of these barriers under stress releases an avalanche of dislocations. Presumably, if such boundaries of dislocations are present, and if they become better defined during strain aging, the more pronounced yield point in the strain-aged crystal also could be explained. Unless polygonization does occur at strain-aging temperatures, however, (i.e., room temperature to 100°C) some other mechanism for dislocation interaction and resultant cataclysmic flow must apply.

Dislocation Interaction by Collision

An alternative mechanism for dislocation interaction based on chance collision between moving and anchored dislocations will now be described. This mechanism does not require the presence of polygonization boundaries, and the enhancement of the yield point by strain aging can be explained as a strain dependent increase in dislocation population. Furthermore, this mechanism predicts that an annealed single crystal will not have a yield point.

A qualitative picture of a yielding process in which an avalanche of dislocations is released by collision would be as follows: All dislocations are distributed randomly through the iron crystal and are anchored by local concentrations of carbon atoms as Cottrell has suggested. When the crystal is stressed in tension, a dislocation breaks loose from its carbon cloud because of some stress concentration and accelerates rapidly to a high velocity. After moving freely for several thousand unit slip distances (approximately 10^{-4} cm), it passes close to another dislocation (within a few atom distances) that is anchored by carbon atoms. Since the local stress fields around each of these dislocations interact rather strongly as they come near each other, the second dislocation will be knocked free of its carbon cloud at the expense of part of the kinetic energy of the moving dislocation. This gives two dislocations in motion without any increase in applied stress, and the opportunity exists for each of these to "collide" and free others. Thus is envisioned the genesis of a cataclysm and consequent formation of a Lüders band.

For such a process to occur it is apparent that the mean free path between collisions must be less than the crystal dimensions. In addition, the interaction between an anchored and moving dislocation must be of a magnitude that will cause the anchored dislocation to be torn free. Finally, the necessary energy to tear a dislocation free must be obtained at the expense of the momentum of the moving dislocation, hence the kinetic energy of the moving dislocation must be sufficient to carry it beyond the position of maximum interaction with the anchored dislocation.

Fortunately, calculations have already been made for the interaction between dislocations,[8] for the stress required to free a dislocation from its solute

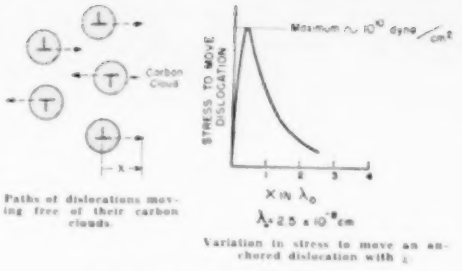

Fig. 2—Stress to move anchored dislocations.

cloud,[9] and for the kinetic energy of a moving dislocation,[10] and these results will be used to make more quantitative our proposed interaction mechanism.

Stress to Release an Anchored Dislocation

The shear stress required to pull a dislocation free of its cloud of solute atoms at absolute zero has been estimated by Cottrell and Bilby[8] and is given by:

$$\tau_0 = \frac{3\sqrt{3A}}{8\lambda^3\mu} \qquad [1]$$

where τ_0 is the shear stress; λ, the interatomic spacing in slip direction; μ, the average distance from dislocation center to first row of carbon atoms in its atmosphere (2×10^{-8} cm); and $A = 4/3\,G\epsilon r_s{}^3\lambda\left(\frac{1+\mu}{1-\mu}\right)$ $= 3\times10^{-4}$ dyne per sq cm, a constant in which G is the rigidity modulus, μ is Poisson's ratio, λ is as above, r_s and $r_s(1+\epsilon)$ are the atomic radii of solvent and solute atoms respectively, and ϵ is the volume strain in the iron lattice due to the interstitial solute.

Using the known lattice constants of iron and the average elastic constants of polycrystalline iron, this gives:

$$\tau_0 = 7.8\times10^{10} \text{ dyne per sq cm} \qquad [2]$$

Applying a temperature correction suggested by Cottrell and Bilby, the shear stress to free a dislocation at room temperature would be:

$$\tau_{300°K} = 9\times10^{9} \text{ dyne per sq cm} \qquad [3]$$

This is, of course, a very large stress and much higher than is customarily measured for a yield stress. In order to make the stress agree with measured values, Cottrell and Bilby have altered the value of the constant A in eq 1 by an order of magnitude. They have overlooked an important feature of their calculated shear stress, however; namely, that it is a theoretical value for the upper yield stress and as such is rarely approached in actual measurements. Stress concentrations due to surface defects, sharp fillet radii, nonaxiality of loading, precipitated impurities, and grain boundaries may each contribute to breaking a dislocation free of its solute cloud at some apparent stress less than the theoretical value.

In the subsequent calculation of a mean free path between collisions, only a situation where interaction between moving and anchored dislocations actually attains a stress equivalent to the theoretical value of $\tau_{300°K}$ in eq 3 will be considered as a collision.

The values of τ given by eqs 2 and 3 are maximum

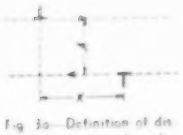

Fig. 3a—Definition of distances x and h when dislocations shear past each other.

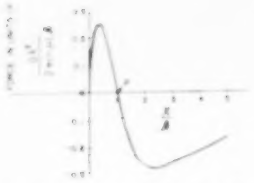

Fig. 3b—Variation of force in x direction due to interaction between dislocations with distance apart in the x direction.

values of stress. The actual stress to move a dislocation varies with the distance from its equilibrium position in the carbon atmosphere as shown in Fig. 2, from Cottrell and Bilby.

Interaction Between Two Dislocations

According to Cottrell[7] as a dislocation moves through the lattice in the x direction under the influence of a shear stress, and passes another dislocation of opposite sign at a distance of closest approach h, as defined by the geometry of Fig. 3a, the interaction force Fx in the shear direction per unit dislocation length varies with the distance x according to the equation:

$$F_x = \frac{Gb^2}{2\pi(1-\mu)} \cdot \frac{h(x^2-h^2)}{(x^2+h^2)^2} \qquad [4]$$

where G, b, and μ have their former significance. Cottrell's plot of this interaction force against distance x/h is shown in Fig. 3b.

The equivalent maximum value of shear stress to move two such dislocations past each other is:

$$\tau = \frac{Gb}{8\pi(1-\mu)h} \qquad [5]$$

From this relation the values of interaction shear stress vs. distance between dislocations h given in Table I were obtained.

The interaction of interest in the dislocation collision process is not between two dislocations with equal stress fields, but between a highly stressed moving dislocation[8] and an anchored dislocation about which considerable stress has been relieved by interstitial atoms. It does not seem reasonable to expect the stress about the anchored dislocation to be entirely relieved, however, since the perturbation in the lattice still exists. It will be assumed, therefore, that the interaction between moving and anchored dislocations differs little from that given in Table I.

Mean Free Path Between Collisions

An effective collision may now be described. It results when a moving dislocation passes within 10^{-7} cm, or 3 or 4 interatomic distances, of the anchored dislocation, at which distance the interaction stress from Table I is equivalent to the stress, computed from eq 3, that will free the anchored dislocation from its solute cloud. The number of effective collisions or the extent of the cataclysmic flow will depend on the mean free path between collisions and in turn on the density of dislocations in the specimen.

Consider a crystal having N anchored line dislocations per sq cm arranged in random fashion on any plane in the crystal. The mean free path D between dislocation collisions for dislocations moving in that plane is given by:

$$D = \frac{1}{2hs\,N} \text{ atoms} \qquad [6]$$

or

$$D = \frac{1}{2hsN} \text{ cm} \qquad [7]$$

where h is in units of interatomic spacing.

It has been estimated that an annealed metal contains 10^{7} cm^{-2} dislocations. The first such estimate was made by Seitz and Read.[9] More recently Cottrell[7] has made a similar estimate based on the ease with which annealed metals yield plastically, which in turn indicates a low value for the overall interaction between dislocations and hence a low dislocation density. A severely cold-worked metal saturates with a concentration of 10^{11} cm^{-2} dislocations according to several estimates.[10,11]

Substituting three interatomic distances for h in eq 7, the mean free path between collisions will vary from 10^{-3} to 10^{-5} cm as N varies from 10^{7} to 10^{11} dislocations per sq cm. It is assumed, of course, that time was allotted in each instance for all available dislocations to be anchored by solute atoms. Actually the mean free path between collisions in the annealed crystal is probably considerably greater than that given by eq 7, since it seems reasonable that only a fraction of the dislocations in the collision path of the moving dislocation will be so oriented that slip will occur under the applied stress. Furthermore, the annihilation of a positive dislocation by a negative dislocation in the same plane of atoms may also occur.

It seems reasonable to expect that the cataclysm released in a normal size annealed crystal would be of undetectable magnitude, because the mean free path between dislocation collisions is approaching specimen size.

As dislocations are added by strain however, the mean free path is decreased for two reasons. First, there are more dislocations present, and second, the added dislocations are, by the crystallographic nature of the strain, all properly oriented for slip. A strained and aged crystal would then be expected to show an increased yield-point effect with increasing strain up to the saturation density of dislocations, and the most pronounced increase in the strain-aged yield point should occur after the first small amounts of deformation.

Kinetic Energy of a Moving Dislocation

So far in this discussion only the static energy situation has been considered, and it has been shown that should a moving dislocation pass within three atom planes of an anchored dislocation, the interaction would be sufficient to break the latter free. This interaction, however, retards the movement of the free dislocation, and the kinetic energy of the moving dislocation must be sufficient to overcome the interaction barrier.

The kinetic energy of a moving dislocation arises from the shear displacement of actual material on

Table I. Values of Interaction Shear Stress vs. Distance between Dislocations

Distance between dislocations h (cm)	10^{-5}	10^{-6}	10^{-7}	10^{-8}
Shear stress, dyne per sq cm	6×10^{7}	8×10^{8}	6×10^{9}	6×10^{10}

[8] The character of the stress field also depends on the velocity of the moving dislocation, as was pointed out to the author by F. C. Frank. In view of the many other assumptions in this discussion, this effect of velocity has not been included.

either side of the dislocation, since the dislocation defect itself has no mass. Frank[10] has shown that the kinetic energy of a dislocation moving at the velocity of sound is given by:

$$E = \frac{Gla^2}{8\pi} \log \frac{R}{R_0} \qquad [8]$$

where G is the shear modulus, l the dislocation length; a, the interatomic distance;[‡] and R and R_0 are respectively an outer and inner radius around the dislocation defining the limits over which the kinetic energy is calculated.

Under conditions where $\log R/R_0 = 1$, the solution to eq 8 is approximately 1.7×10^{-5} ergs per unit length of line dislocation. It has been shown by Frank[10] that the velocity of sound could be reached in G/τ atom distances,[‡] where τ is the yield stress; or for iron deforming at the lower yield stress in the neighborhood of 100 to 1000 atom distances. Since this distance is less than the mean free path calculated in this study, most dislocations in iron must reach this velocity before collision occurs.

The potential energy barrier which a fast moving dislocation must overcome to collide can only be estimated readily for forces in the x direction, and is given by:

$$E_x = \frac{Gal}{2\pi(1-\mu)} \left[-\ln\left(1 + \frac{x^2}{h^2}\right)^{1/2} + \frac{1}{1 + \frac{h^2}{x^2}} \right] \qquad [9]$$

which reduces at the conditions of the minimum potential energy, namely when $x = h$, to:

$$E_x = \frac{Gal}{2\pi(1-\mu)} (0.156) \qquad [10]$$

or:

$E_x = -1.62 \times 10^{-6}$ erg per unit length of dislocation [11]

Such a calculation is of little importance, however, for other than a rough indication, for, while it agrees with the result of eq 8, the actual kinetic energy of the moving dislocation depends entirely on the quantity chosen for $\log R/R_0$ in eq 8 and can readily be made to exceed the potential energy barrier by any amount. Furthermore, the variation of the total potential energy barrier with h is not known.

It can be stated approximately that if a dislocation moves with the velocity of sound or an appreciable fraction of it, the dislocation will have enough kinetic energy to collide with anchored dislocations.

Discussion

The feasibility of a dislocation collision interaction mechanism for cataclysmic yielding has now been quantitatively established. On the basis of this mechanism annealed single crystals should not have a yield point because the mean free path between dislocation collisions would approach the specimen size. Strain-aged single crystals should have yield points, with the magnitude of the effect depending on the

‡ Leibfried[10] has calculated that dislocations cannot move as rapidly as the velocity of sound because of thermal scattering effects, rather they move only about one tenth the velocity of sound. Apparently, if this limitation applies, the kinetic energy of moving dislocations will be less. It was pointed out to the author by F. C. Frank that it may be possible to get around this limitation with a Doppler effect.

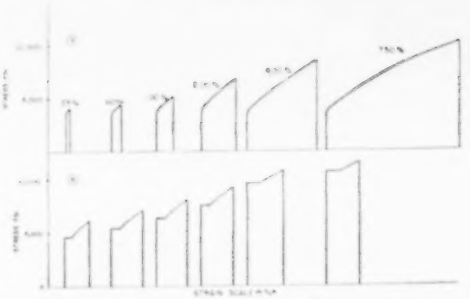

Fig. 4—Yield point in strain-aged crystals of iron as a function of prestrain for six identical crystals.

A—Initial deformation of crystals. B—Deformation after aging crystals from Fig. 4A.

number of dislocations added by strain. As the strain is increased, the dislocation density increases and the mean free path between dislocation collisions decreases, accounting for the behavior of a strain-aged crystal.

The behavior of annealed iron polycrystals is a special case. In these the mean free path between collisions is, for most grain sizes, the grain diameter itself. The boundaries between grains in accordance with recent concepts are made up of dislocations.[12] These dislocations are anchored both by boundary interaction forces and by carbon atoms, and they may be knocked free by other moving dislocations in a manner analogous to the dislocation collisions within the lattice. Annealed iron polycrystals then will always be expected to have yield points when carbon is present.

Critical Experiments

The idea of the importance of dislocation density and the mean free path between dislocations to the yielding behavior of iron suggests several important experiments.

If, for example, the manner in which strain changes the population of dislocations were known, the yielding behavior of iron after strain aging might be predicted. Harper[13] has recently made an attempt to measure the number of dislocations in iron by observing the rate of decrease in the internal friction peak due to dissolved carbon as a function of strain. The assumption in his work was that the carbon was precipitating in the strained region around dislocations, and the rate of precipitation is controlled by the dislocation density. Harper found the number of dislocations by this method to be about 2×10^{11} cm^{-2}

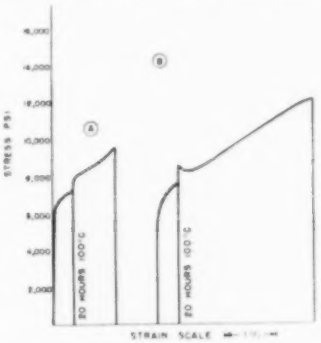

Fig. 5—Effect of crystal size on strain-aged yield point for identical crystals of iron with B about eight times A.

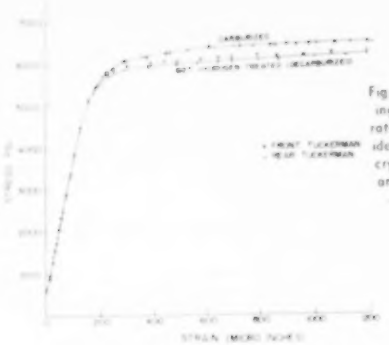

Fig. 6—Yielding of accurately aligned identical iron crystals with and without carbon

after 5 pct strain and 4×10^{-4} cm after 15 pct strain, merely a twofold change.

These experiments should be repeated employing single crystals to eliminate grain boundary precipitation, and employing deformations smaller than used by Harper. The dislocation population must change much more rapidly in the region from 0 to 5 pct strain than it does beyond 5 pct.

Extremely small strains evidently add enough dislocations to cause a yield point in a single crystal after subsequent aging. In Fig. 4 are shown the initial stress-strain diagrams for six identically oriented carburized and annealed iron crystals, together with the diagrams obtained from these same crystals after suitable aging and retesting. Strains in Fig. 4 vary from 0.0025 to 0.075. None of these crystals had an initial yield point, but all had a yield point after strain aging. The strain-aged yield point elongation varied from 0.4 to 0.75 pct for the strain variation mentioned above.

The mean free path concept leads to the prediction of an effect of specimen size on the yield point of single crystals. At any dislocation density, the number of dislocations set free by a migrating dislocation should depend on the length of the dislocation path through the crystal. To test this prediction the following experiment was performed.

Two crystals of identical orientation were machined from a larger crystal so that one was about eight times the cross-sectional area of the other. The limit in size difference used was merely one of convenience, since too small a crystal would not support the strain gage and an extremely large crystal was not available. These crystals were annealed, carburized, strained 0.4 pct, and aged 20 hr at 100 C. It was felt that the crystals were now in nearly identical condition in regard to concentration of dislocations. As shown in Fig. 5, the smaller crystal showed little indication of a yield point, while the larger crystal had a drop in load and nearly 0.25 pct yield-point elongation. The actual cross-section of the small crystal was 0.060 in., while the large crystal was 0.060x0.5 in.

Since the prediction frequently has been made in this paper that annealed single crystals ought not to have a yield point, it was imperative to recheck this point. In a previous paper the author had been unable to obtain yield points in single crystals, and this has since been attributed to misalignment.[7]

Several iron crystals, made of decarburized aluminum-killed sheet as described in the previous paper,[7] were carburized in a mixture of hydrogen and N-heptane and then annealed. Extreme precautions were taken to assure that these crystals were accurately aligned. Special grips were constructed that operated in a gimbal ring principle not unlike the grips used by Jillson[8] in tests on zinc crystals. The grips were modified to allow some adjustment of the centerline of the crystal with respect to the axis of the grip after the crystal had been clamped. A Tuckerman optical strain gage was mounted on each face of the crystal and very small loads applied (stresses were less than 1500 psi). The position of the crystal was then shifted until the elastic strain on both faces of the crystal was the same over any increment in stress. The process was repeated on the edges of the crystal. After alignment had been achieved, the crystals were tested at very slow rates with simultaneous readings of both load and strain. A typical curve is shown in Fig. 6 for a carburized and a decarburized crystal of identical orientation. The crystals behave as reported previously, having no indication of a yield point when in the annealed condition, although the carbon does strengthen the material.

The conclusion is reached that the single crystals grown from this aluminum-killed material do not have a yield point even when carburized. Furthermore, since other investigators have probably used as great care in alignment, the difference in results must be due to differences in crystal perfection as-grown, or to small amounts of strain aging in crystals that had yield points.

It is known that the yield point of iron is more pronounced at rapid rates of loading, so an additional experiment was performed in which a crystal was first aligned with the Tuckerman gages and then tested at a strain rate of approximately 0.002 sec^{-1} with a recording strain gage attached. The result of the test is shown in Fig. 7. A slightly lower slope is apparent in the early part of the stress-strain curve which could be interpreted as a yield-point tendency if so desired, but the sharp yield point is definitely absent even at these more rapid rates of straining.

The dislocations added to a crystal by straining to produce a yield point must be added in a very selective fashion, that is, they must be added largely to planes along which slip occurs under the stress applied. This is demonstrated by an experiment in

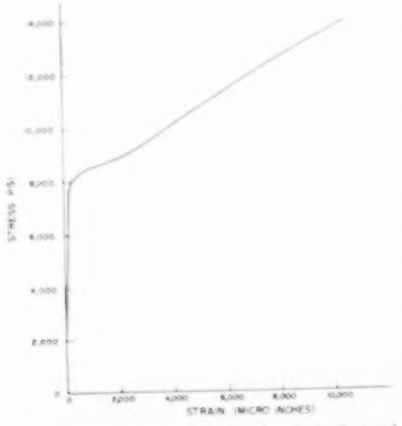

Fig. 7—Yielding of accurately aligned carburized crystal of iron at rate of 0.002 sec^{-1}

which several flat thin single crystals were strained 1 to 3 pct by rolling and were then aged up to 20 hr at 100°C. These flat crystals, when retested in tension, did not have yield points. If, after the tensile test, the specimens were again aged for much shorter times and retested in tension, the crystals had a marked yield point. A typical test is shown in Fig. 8. While the overall density of dislocations undoubtedly was increased by rolling, the majority of these dislocations were added with their slip vectors parallel to the slip planes operative during rolling. Since other slip planes may operate in tension, the aging of a rolled crystal, i.e., anchoring its additional dislocations, does not affect the number of collisions possible on the tensile deformation planes.

Interaction Between Dislocations in Boundaries

It is well established that a crystal which has been strained and subsequently annealed will have a block structure of crystallites at small angles with respect to each other. The boundaries of this block structure are best explained as being rows or walls of dislocations of like sign. This phenomenon of subgrains appearing in strained and annealed crystals has been generally referred to as polygonization.

It has been argued by Cottrell[1] that these boundaries provide an interaction mechanism for the yield point, particularly in annealed single crystals. If a dislocation is anchored by carbon atoms and also is part of a boundary of dislocations of the same sign, it will be more difficult to move the dislocation than if it were not part of that boundary. Cottrell has calculated the contribution of the boundary condition to the stress required to move such a dislocation, and he finds that appreciable stress increase can be realized if the dislocations in the boundary are not too far apart. For example, an increase of 3×10^7 dyne per sq cm has been estimated by Cottrell for a spacing of 10^{-4} cm between dislocations in the boundary. While this is a reasonable increase in yield point for a strain-aged crystal, as Cottrell points out, the requirement of spacings of 10^{-4} cm will not permit a random boundary network or the density would be 10^{12} cm^{-2} dislocations, equivalent to highly cold-worked metal. In view of the nature of polygonization it is reasonable to assume that the boundaries line up in preferred directions perpendicular to the direction of slip, and a fairly high density of dislocations could then exist on a polygonization boundary.

The model Cottrell has assumed to represent the yielding crystal is one containing anchored dislocations, both on dislocation boundaries and within the polygonized blocks. The dislocations in the blocks move first but are unable to get through the boundaries until they have piled up to considerable extent, whereupon they break through and move in a cataclysmic fashion through subsequent boundaries. This viewpoint predicts a considerable amount of homogeneous plastic flow before the Lüders band forms, and, as Cottrell points out, it is inconsistent with experiment. Cottrell chooses to get around all but a small amount of this prior homogeneous flow by allowing only dislocations associated with high stress concentrations within the crystal to move and produce flow.

If dislocation boundaries are present it does not seem essential to the argument to have the process set off by the piling up of dislocations at a boundary. For example, if a dislocation is once set free from a boundary, the dislocations adjacent to the vacant position in the dislocation boundary should be moved readily by the stress obtaining, and large portions of a boundary of dislocations would move at once.

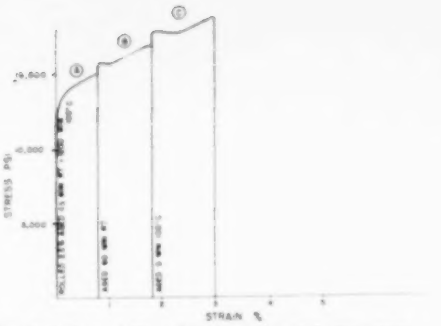

Fig. 8—A shows yielding of strain-aged crystal where strain was initially by rolling. Subsequent yield points in B and C are the result of tensile strain aging.

Polygonization Experiments

In order to determine whether an arrangement of dislocations in boundaries would cause the yield point, an attempt was made to correlate the perfection of carburized single crystals as revealed by X-ray diffraction with their yielding behavior. Several crystals 100 mils x 40 mils x 4 in. in length were machined from larger crystals and were annealed 64 hr at 850°C in wet hydrogen and then carburized 1 hr at 700°C in hydrogen saturated with N-heptane at room temperature. The crystals were then further annealed 1 hr at 850°C.

Each of these crystals had been deformed during machining and each showed a different degree of perfection of Laue spots. The spots from some crystals had a substructure not unlike that obtained by coarse polygonization, while the spots from other crystals were single and sharp at the resolution available. Upon tensile testing, no correlation between Laue spot perfection and the occurrence of an initial yield point could be detected. Some of the imperfect crystals had a slight initial yield point, while others did not.

A second experiment was performed to determine whether any observable change in the Laue spots from a strained crystal occurred during aging in the length of time usually required for the yield point to return. Crystals were strained 5 pct and aged either at room temperature or at 100°C. A small yield point was detected in the stress-strain curve for crystals strained 5 pct and aged at room temperature in 200 min and for those aged at 100°C in 1 min. However, a crystal aged at 100°C for three days showed no change in the asterism in an X-ray Laue pattern over that immediately after deforming.

It was found in a subsequent experiment with a bent iron crystal (the most favorable deformation for polygonization observations) that 1 hr at 850°C was required to produce an observable breaking up of the asterism in the Laue spot.

The conclusion must be, therefore, that the imperfections of the magnitude detectable by ordinary Laue methods contribute little to the yielding behavior of iron crystals. Furthermore, at usual strain-aging temperatures (room temperature to 100°C) a strained crystal will acquire a yield point in a subsequent tensile test many times faster than any change in its coarse substructure can be detected.

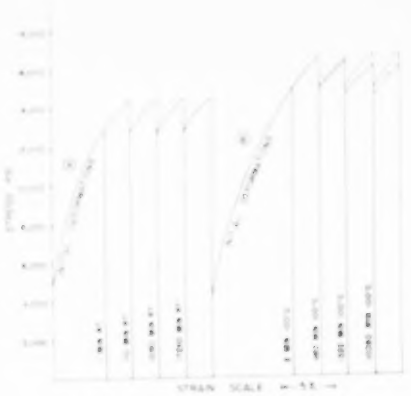

Fig. 9—Recovery in decarburized iron. A—Strained 5 pct and recovered various times at room temperature. B—Strained 7.5 pct and recovered various times at 100°C.

It is well known that the ordinary Laue technique is quite insensitive to the early stages of polygonization, and therefore the absence of changes in the Laue spot during strain aging is not conclusive evidence that fine scale polygonization does not occur. It is possible that more elaborate techniques such as Guinier's[27] focusing transmission method would indicate polygonization at strain-aging temperatures, but as yet Guinier and others using these sensitive methods have required higher temperatures to bring about polygonization.

If the early stages of polygonization, while probably not resolvable even by Guinier's technique, do occur rapidly even at the low temperature required for strain aging, this should affect the mechanical properties of strained iron. If polygonization does occur, some significant recovery ought to be observed in strained iron in the length of time the yield point would return at the appropriate aging temperature.

Tests on decarburized polycrystalline iron after straining 5 pct and aging at room temperature showed no mechanical recovery in 17,000 min. After straining 7.5 pct and aging at 100°C the iron began to show some mechanical recovery in 1000 min. These data are plotted in Fig. 9.

If polygonization is the cause of the mechanical recovery noted, it occurs far more slowly than does the yield-point return after strain aging.

Conclusions

1—The yield point in iron is due to the cataclysmic release of dislocations anchored by carbon atoms, as has been suggested by Cottrell.

2—The interaction between dislocations by which a yield point is produced does not require the dislocations to be situated on polygonization boundaries, since random arrays of dislocations can interact by collision. There is no experimental evidence, furthermore, that polygonization does exist in strain-aged crystals of iron possessing a yield point.

3—The Cottrell mechanism is not inconsistent with the absence of a yield point in annealed single crystals of iron containing carbon.

4—Some small strain is required to introduce sufficient dislocations into an annealed iron crystal to cause a yield point, and the yield point produced is a result of strain aging during which carbon diffuses to and anchors the added dislocations.

5—No plastic strain is required in the case of polycrystals since these already contain dislocations at grain boundaries in sufficient concentration to propagate under the influence of stress concentrations caused by slip in neighboring grains.

Acknowledgment

The author wishes to thank J. R. Low, Jr., J. E. Burke, and W. W. Tyler for their many helpful discussions and their interest in the yield-point problem. The material from which most of the single crystals were grown was kindly supplied by M. W. Lightner of the Carnegie-Illinois Steel Co. Many of the computations were made with the assistance of F. W. Kunz and J. A. Krumhansl.

References

1. A. H. Cottrell: Effect of Solute Atoms on the Behavior of Dislocations. Report of Conference on Strength of Solids, Bristol. Physical Soc. London. (1948) p. 30.
2. J. R. Low and M. Gensamer: Aging and the Yield Point in Steel. *Trans.* AIME (1943) **158**, p. 207.
3. F. R. N. Nabarro: Mechanical Effects of Carbon in Iron. Report of Conference on Strength of Solids, Bristol. Physical Soc. London (1948) p. 38.
4. A. H. Cottrell and A. T. Churchman: Change of Electrical Resistance During the Strain Aging of Iron. *Journal* Iron and Steel Inst. (1949) **162**, p. 271.
5. A. H. Cottrell and A. T. Churchman: Discussion. *Trans.* AIME (1949) **185**, p. 377; JOURNAL OF METALS (November 1949).
6. H. Schwartzbart and J. R. Low: The Yielding and Strain-Aging of Carburized and Nitrided Single Crystals of Iron. *Trans.* AIME (1949) **185**, p. 637; JOURNAL OF METALS (September 1949).
7. A. N. Holden and J. H. Hollomon: Homogeneous Yielding of Carburized and Nitrided Iron Single Crystals. *Trans.* AIME (1949) **185**, p. 179; JOURNAL OF METALS (February 1949).
8. A. H. Cottrell: The Yield Point in Single Crystal and Polycrystalline Metals. Symposium on Plastic Deformation of Crystalline Solids. Mellon Institute, Pittsburgh (1950) p. 60.
9. A. H. Cottrell and B. A. Bilby: Dislocation Theory of Yielding and Strain Aging of Iron. *Proc.* Physical Soc. London (1949) **62A**, p. 49.
10. A. H. Cottrell: Theory of Dislocations. *Progress in Metal Physics* (1949) **1**, p. 77.
11. F. C. Frank: On Slip Bands as a Consequence of the Dynamic Behavior of Dislocations. Report of Conference on Strength of Solids, Bristol. Physical Soc. London (1948) p. 46.
12. F. Seitz and T. A. Read: Theory of the Plastic Properties of Solids II. *Journal of Applied Physics* (1941) **12**, p. 170.
13. J. S. Koehler: On the Dislocation Theory of Plastic Deformation. *Physical Review* (1941) **60**, p. 397.
14. W. F. Brown, Jr.: Theory of the Approach to Magnetic Saturation. *Physical Review* (1940) **58**, p. 736.
15. F. C. Frank: The Origin of Dislocations. Symposium on Plastic Deformation of Solids. Mellon Institute, Pittsburgh (1950) p. 89.
16. G. Leibfried: Uber den Einfluss Thermisch Angeregter Schallwellen auf die Plastische Deformation. *Ztsch. Physik* (1950) **127**, p. 344.
17. W. T. Read and W. Shockley: Dislocation Models of Crystal Grain Boundaries. *Physical Review* (1950) **78**, p. 275.
18. S. Harper: Precipitation of Carbon and Nitrogen in Cold Worked Alpha-Iron. *Physical Review* (1951) **83**, p. 709.
19. D. C. Jillson: Quantitative Stress Strain Studies on Zinc Single Crystals in Tension. *Trans.* AIME (1950) **188**, p. 1129; JOURNAL OF METALS (September 1950).
20. A. Guinier and J. Tennevin: Sur Deux Variantes de la Methode de Laue et leurs Applications. *Journal Acta Cryst.* (1949) **2**, p. 133.

Kinetics and Orientation Relationships Of Secondary Recrystallization in Silver

by F. D. Rosi, B. H. Alexander, and C. A. Dube

WHEN a deformed polycrystalline metal is heated to a sufficiently high temperature, a recrystallized structure develops which consists of small, essentially stress-free grains. This transformation is referred to as primary recrystallization. Under certain conditions, on prolonged annealing of the specimens, a type of grain coarsening occurs in which a small number of grains commence to grow at various points by devouring the neighboring fine-grained primary structure, which, in itself, exhibits a marked stability toward normal grain growth. This grain coarsening process has been referred to by Burgers[1] as "secondary recrystallization" or "exaggerated grain growth."

Although much work has been done on recrystallization and growth processes, present knowledge of the factors which determine the occurrence and growth of secondary grains is inadequate for the advancement of a theory which accounts for the observed characteristics of this recrystallization phenomenon. In this respect, it would be important to make measurements of the velocity of growth of these large secondary grains. The early work of Feitnecht[2] on aluminum showed that the size of secondary grains increased with temperature and time, suggesting that such measurements would be possible. More recently, Burgers[1] found that the growth velocity of these grains in aluminum was constant over a large time interval, as is generally found for the growth velocity of primary grains in a uniformly deformed test piece.[3] It is reasonable to expect that the determination of the activation energy of the secondary growth process might lead to a better understanding of the underlying atomic mechanism.

This investigation, therefore, is one of a series primarily designed to measure the growth velocity of secondary grains at various temperatures for silver, copper, and aluminum. It is hoped that these studies along with those of orientation relationships, will establish a sound basis for theorizing as to the origin and nature of the secondary transformation.

Experimental Procedure

The metal used in the present investigation was high-purity silver (999.9 fine), which was supplied in the form of cold-rolled plates 0.250 in. thick. These plates were annealed at 500 C for 1 hr and then straight-rolled to a thickness of 0.04 in. in three reductions of approximately 45 pct, followed in each case by an anneal at 450 C for ½ hr. The 0.04 in. sheets were given a final reduction of approximately 50 pct, which resulted in a thickness of 0.02 in., thereby insuring two-dimensional crystal growth. Individual specimens of this material about 1x3 cm were used for all heat treatments, unless otherwise noted. The annealing was carried out under an atmosphere of argon in an Inconel tube furnace whose temperature was controlled to within ±2°C.

Metallographic examination of the secondary transformation was accomplished by mechanically polishing the specimens on one side to approximately one half their thickness through 2/0 metallographic emery paper, and then electrolytically polishing in a solution of potassium ferrocyanide and sodium cyanide. With a current density of approximately 20 amp per sq dm, the time required to obtain a satisfactory surface varied from 3 to 5 min. Standard potassium bichromate was used to etch the electrolytically polished surfaces. A heavy etch with this solution produced a sharp contrast between the secondary grains and the fine-grained primary structure, darkening the latter while leaving the large secondary grains bright. All area measurements of the secondary crystals were made with a planimeter on enlarged tracings of the grains.

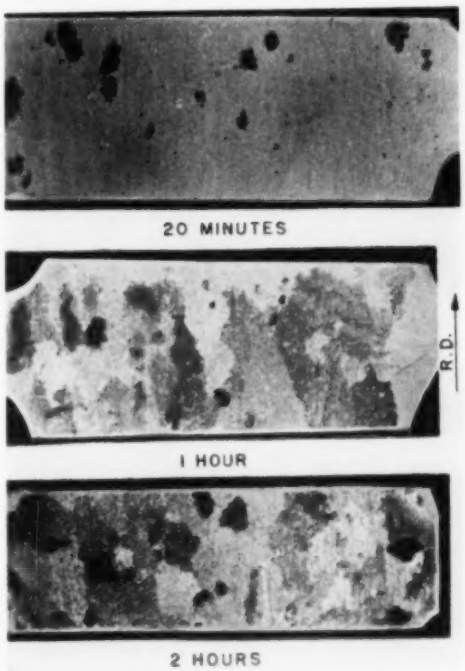

Fig. 1—Appearance of secondary recrystallization in silver specimens annealed at 533 C. X7.5.
Area reduced approximately 50 pct for reproduction.

F. D. ROSI, B. H. ALEXANDER, Junior Members AIME, and C. A. DUBE are associated with the Metallurgical Laboratories, Sylvania Electric Products Inc., Bayside, N. Y.

Discussion on this paper, TP 3235E, may be sent, 2 copies, to AIME by April 1, 1952. Manuscript, Aug. 22, 1951. New York Meeting, February 1952.

This work was supported in part by A.E.C. Contract AT-30-1 GEN 367.

The crystallographic orientation of the secondary crystals was determined from back-reflection Laue X-ray photograms according to the method described by Greninger.[7]

Results

Rolling Texture: A pole figure representing the complete distribution of the dodecahedral planes of the crystal lattice was determined for the rolled strips. This figure shows the existence of a twinned double-texture such that the {110} plane is parallel to the rolling plane with either the [112] or [$\bar{1}$12] axis parallel to the rolling direction. There was an angular spread in the position of the {110} plane of 10° to 15° in the direction of rolling. This texture is in agreement with that obtained by Glocker[8] in rolled silver.

Although no pole figure was determined for the primary recrystallized structure, several X-ray photograms indicated a {113}<$\bar{1}$12> texture. This same texture was reported by Glocker[8] upon annealing rolled silver below 800°C. In view of the annealing temperature range of the present experiments, 400° to 550°C, such a texture would be expected.

Development of Secondary Recrystallization: Annealing the rolled specimens in the temperature range of 433° to 533°C produced a primary recrystallized structure with a grain size of the order of 0.02 mm. On prolonged heating in this temperature range, secondary crystals appeared ranging in size up to several millimeters in diameter, and eventually covering the entire specimen. This characteristic behavior of the secondary transformation is shown in Fig. 1.

In many of the large grains, it was not unusual to find a number of small crystals of the primary structure which offered considerable resistance to dissolution. This behavior, which is frequently associated with the secondary reaction, implies that these embedded grains have an orientation similar to that of the growing grains; i.e. they possess low grain boundary energy. It was found that on annealing at high temperatures (900°C) these small grains can be absorbed.

Shape of Secondary Crystals: The secondary crystals generally exhibited a preferential growth in the direction of rolling and showed corrugated boundaries, which are simply a manifestation of the growth of the secondary grains toward the center of curvature of the small primary grains. This characteristic boundary of the growing grains is similar to that reported by Bowles and Boas[9] in aluminum and silver and by Kronberg and Wilson[10] in OFHC copper. It is, moreover, similar in appearance to the advancing boundary of growing primary grains in a lightly deformed matrix.[11,12]

Typical examples of the shape of the secondary grains are shown in Fig. 2, from which it is apparent that the maximum rate of growth in these crystals is in the direction of rolling; i.e. <112>. It will also be noticed that these large crystals have three sets of twin islands. Two of these appear as short segments whose length is about equal or a small multiple of the mean diameter of the small grains in the primary structure. Furthermore, it was observed that these twinned segments appear to originate at certain points along the advancing interface of the growing grain, which suggests that their origin and the extent of their growth is intimately connected with the growth of the secondary crystals.

The third set of twins is much more predominant, as may be seen from Fig. 2b (see also Fig. 4). In fact, in some crystals these twinned regions are so abundant that it is difficult to decide which of the two orientations is the parent one. As in the secondary crystals of OFHC copper,[10] these twins are long and broad. The approximate angles which the three sets of twins make with the direction of rolling are 55°, 0°, and 70°. This, of course, defines the orientation of the secondary crystals as {110}<112>, which is simply that of the parent deformation texture. Consequently, these angles are the positions of the traces of the four sets of octahedral planes in the surface of the specimen; two of which yield parallel traces. Similar sets of twins have been reported by Cook and Richards[13] in secondary crystals of copper which had been produced in specimens cold-rolled 85 pct and annealed at 400°C.

It is interesting to note that in both silver and copper[10] the shape of the secondary grains can best

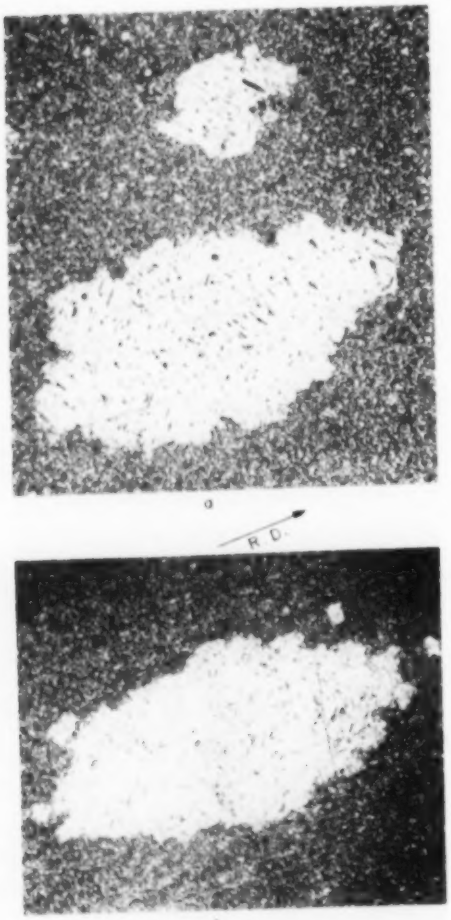

Fig. 2—Typical grain shapes during growth of secondary grains, and the characteristic positioning of twins in these grains. Nat. Area reduced approximately 50 pct for reproduction.

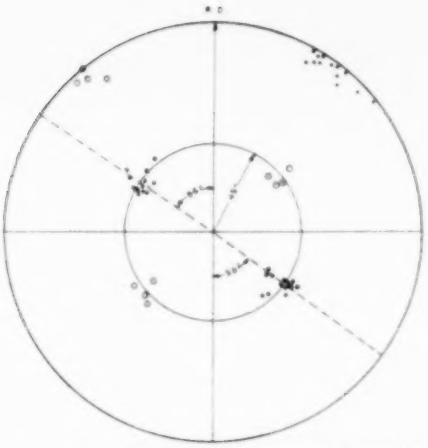

Fig. 3—Stereographic projection of orientations of secondary crystals in silver specimens. Open circles are twins of the main group of crystals.

be described as an ellipse. Even more significant, in both metals the direction of maximum growth is along {111} planes corresponding to the trace of long twin boundaries with the surface of the specimen, while the direction of minimum growth is along the normal to the {111} composition plane of these twinned regions. This similarity in the positioning of the long, massive twins with respect to the anisotropic character in the growth of the secondary grains suggests that the very formation of annealing twins is directly connected with this shape anisotropy. Thus, in aluminum, which unlike other face-centered cubic metals shows no annealing twins, the shape of the secondary grains are roughly spherical.[7]

Orientations of Secondary Crystals: The crystallographic orientations of 13 of the secondary crystals were determined from a number of specimens and are shown in the stereographic plot of Fig. 3. In this figure, the cube poles of the secondary crystals are plotted, and it may be seen that all but four of the crystals have a common orientation. These four are twins of the main group of crystals, and were determined from faint Laue spots appearing in the X-ray photograms of the parent grain. This background of spots was to be expected in view of the large number of twinned regions appearing in most of the secondary crystals.

It is also apparent from this pole figure that the rolling plane in these crystals can best be described by the indices (110), since the degree of radial scattering of the poles about the circle at 45° from the center of the projection is not large. Moreover, the extent of circumferential scatter is such that the rolling direction in these crystals can reasonably be identified as <112>, as indicated by the angles (56° and 54.5°) which the arbitrarily drawn dotted lines make with the rolling direction. Thus, the observed secondary grains have an orientation similar to their parent deformation structure, (110) <112>, as already indicated by the characteristic positioning of the three sets of twins in these grains. These results are in agreement with the orientation relationships reported by Bowles and Boas,[5] who used the same method of analysis. These investigators, however, found it difficult to describe the indices of the rolling direction because of the considerable degree of scattering of the orientations.

If the assumption is made that there is a strong (113) <112> primary recrystallized texture in the present material, then it can be shown that components of the coarsening texture, as well as those of the deformation texture, are related to components of the (113) <112> recrystallization texture by a simple rotation about a <111> pole. Such a rotational analysis was demonstrated by Cook and Richards,[8] who related the (110) <112> deformation texture of 70:30 brass to the (113) <112> low temperature recrystallization texture by a rotation of 30° about a <111> pole near the rolling direction. More recently, it was pointed out by Kronberg and Wilson[9] that this orientation relationship can be similarly described as a 22° rotation in one direction and a 38° rotation in the other around the same <111> pole. The similarity in the orientations of the secondary grains and their unique rotational re-

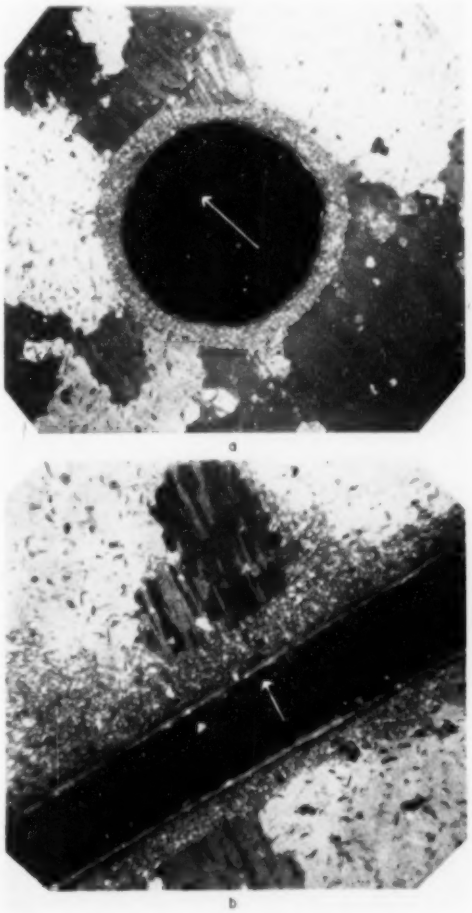

Fig. 4—Resistance to growth encountered by secondary grains: a—at drilled hole, b—at sheared edges. Arrow indicates rolling direction. X78. Area reduced approximately 66 pct for reproduction.

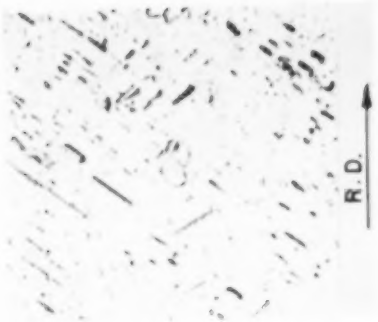

Fig. 5—Unconsumed crystal in large secondary grains. X200

lationships with the orientation of the primary recrystallization structure suggest that their relative orientation with the surrounding fine-grained matrix is largely responsible for their occurrence and selective growth.

The micrographs of Fig. 4 show striking examples of the resistance to growth encountered by large secondary grains on approaching a ring of fine-grained material contiguous to a drilled hole, Fig. 4a, and at sheared edges, Fig. 4b, of the test specimen. In both cases the specimen was annealed at 533°C long enough for complete secondary recrystallization to occur. In view of the inhomogeneous stress pattern resulting from these modes of deformation, certainly no orientation dependence can account for this resistance to growth. The observation that this phenomenon invariably occurs adjacent to exposed surfaces of the specimen indicates that in these cases the resistance to growth is a result of an increase in impurity concentration (oxygen) at the surface.

The polarized micrographs of Fig. 4 also demonstrate clearly the three sets of twins invariably appearing in the secondary crystals, and their angular relation to the rolling direction, shown by the arrow. In this connection, it is interesting to note that in the smaller secondary grains the direction of rolling does not correspond to a <112>, as in the case of the much larger grains, even though a (110) plane is parallel to the sheet surface. This directional deviation might well explain the lower capacity for growth of these grains and, hence, their smaller size. In fact, it may be observed from Fig. 4a that two of the smaller secondary grains, whose twinned regions show the same directionality, are very similar in size. Also, of some significance is the occasional appearance of two or three sets of twins in some of the unabsorbed grains which had grown somewhat prior to being engulfed by the large secondary crystals, as shown in Fig. 5. The positioning of these twins implies that in these unabsorbed grains a (110) plane corresponds closely to the plane of the sheet. Hence, it is probable that these small grains are similar in orientation to the secondary grains.

Measurements on Growth Rate of Secondary Crystals: Samples (1x3 cm) of the cold-rolled strip were annealed in groups of four, or more, at 433°, 478°, 502°, and 533°C for various times. Following the annealing treatment, the specimens were polished and etched as described above, and measurements were made of the area of the largest secondary crystal in each group, which had not impinged on another growing grain. The diameter of a circle of equivalent area was used as a measure of crystal size and determined as a function of the annealing time. The micrographs of Fig. 6 show the progress of growth of secondary crystals at 502°C.

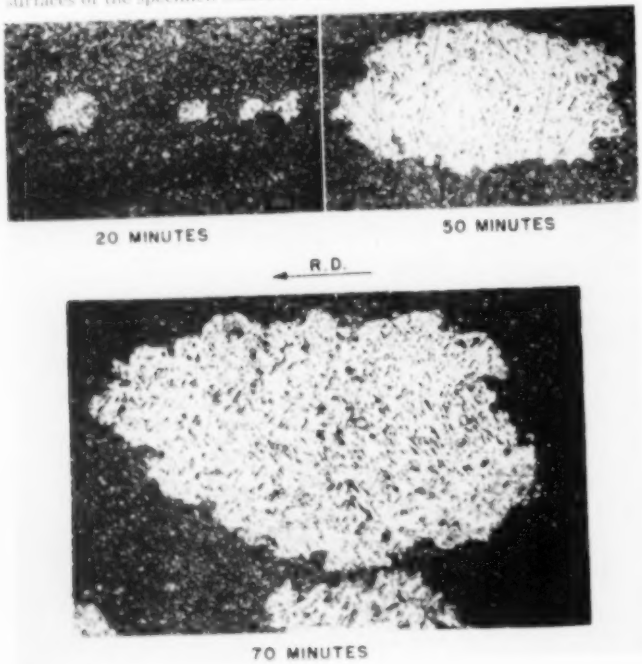

Fig. 6—Progress of secondary recrystallization at 502°C. X60.

Area reduced approximately 50 pct for reproduction.

An attempt was made to follow the velocity of growth in a single specimen, which had been electrolytically polished prior to successive anneals to remove the possible inhibiting effect of the etchant.[7] In a few cases, the growth of existing grains occurred which agreed quite well with the results from statistical analysis. However, in the majority of cases, the growth rate of individual grains was erratic; and this may be attributed to the incomplete removal of the etchant. The results of the growth velocity measurement at the four temperatures are shown in Figs. 7 and 8, where the "diameter" of the largest grain is plotted against time. It may be seen that the rate of growth is invariant with time, and increases with rising temperature in a manner suggestive of the growth rate of primary grains in a uniformly deformed test-piece. Furthermore, the curves intersect the positive time axis, thereby associating an "induction period" with the growth phenomenon. This induction period decreases with increasing temperature.

The temperature dependency of the rate of grain growth is shown by the curve of Fig. 9, where the logarithm of the growth velocity, G, in cm per min is plotted against the reciprocal of absolute temperature, T. It is observed that the curve shows a linear relationship, from which may be calculated an activation energy, Q, describing the temperature dependence of the growth process. Thus, the velocity of grain growth in secondary recrystallization increases rapidly with a rise in temperature according to the expression:

$$G = G_0 e^{-Q/RT} \qquad [1]$$

where for silver G varies from 8×10^{-7} to 7×10^{-5} cm per sec, $G_0 = 3 \times 10^{7}$ cm per sec, and $Q = 28{,}000$ cal per mol. Since a similar relation is obtained in the work on primary crystal growth,[8] it is natural to suspect that the atomic mechanism governing these growth processes is the same.

In view of the characteristic appearance of an induction period during the growth process and its variation with temperature, it was anticipated that the reciprocal of this induction period would vary with the temperature in a manner similar to the velocity of growth. Fig. 10 shows a plot of the logarithm of the reciprocal of the induction period against the reciprocal of the absolute temperature, and it may be seen that a straight line is obtained which permits the temperature dependence of the induction period or "invisible grain growth" ($1/t$) to be expressed by the formula:

$$1/t = A \exp(-Q'/RT) \qquad [2]$$

which has the same form as eq 1. Here, the activation energy, Q', was calculated to be 30,000 cal per mol, which is within experimental error the same as that obtained for the velocity of visible grain growth. It would appear from this that grain growth is taking place during the so-called induction period by the same processes governing the growth of visible grains. A similar plot of log $1/t$ vs. $1/T$ was made for aluminum using the data of Anderson and Mehl,[9] and it was found that the value of activation energy agrees closely with the value they obtained from growth rate measurements. Also, the work of Müller[10] on the rate of growth in rock salt gives similar results over a wide range of temperature. These observations favor the conception that nuclei of the secondary crystals are small grains

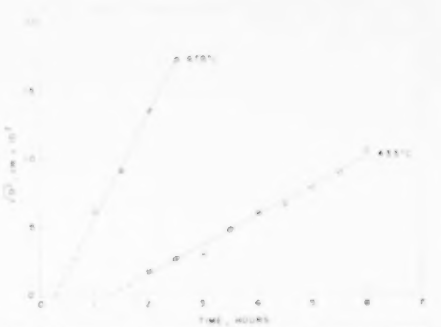

Fig. 7—Diameter of largest grain vs. time of heating at 433 and 478°C.

which in their earlier stages of growth are impeded either by insoluble impurities accumulating in the advancing boundary, or by the small number of contact areas between the growing grain and its surrounding fine-grained structure.

Discussion of Results

Origin of Secondary Grains: Experimental observations on a number of face-centered cubic metals,[11-13] including those of the present investigation, have established with certainty that the secondary grains in annealed cold-rolled sheets show a preferred orientation which differs from the orientation of the primary recrystallization structure and can be related to it by a rotation around a <111> axis. Beck[14] has pointed out that such a rotation leads to a high energy grain boundary between the primary and secondary grains, and he has further shown that the mobility of the grain boundary is greater, the higher the grain boundary energy. Thus, Beck suggests that the secondary grains develop from a small fraction of the primary grains which are misoriented with respect to the general primary texture, and that their growth capacity is due to this misorientation. This has been termed the "oriented growth" theory as opposed to the "oriented nucleation" theory[15] which supposes that, upon annealing the primary structure, nuclei are formed of the required orientation for growth.

Unfortunately, the present data cannot differentiate between nucleation in the classical sense, or nucleation arising from remnants of the deformation

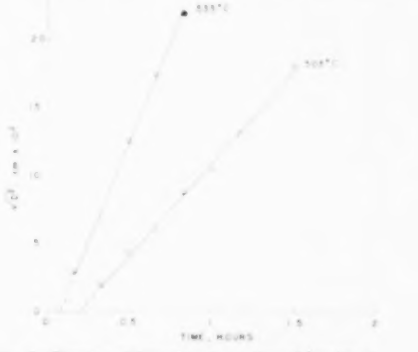

Fig. 8—Diameter of largest grain vs. time of heating at 502° and 533°C. Solid circle indicates grain contact.

Fig. 9—Logarithm of growth rate vs. reciprocal of absolute temperature.

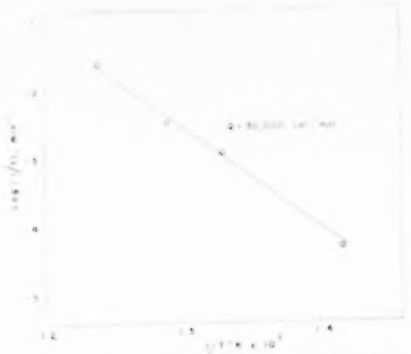

Fig. 10—Logarithm of reciprocal of "induction period" vs. reciprocal of absolute temperature.

structure, and, hence, cannot distinguish between these two apparently conflicting viewpoints. However, it is believed, in conformity with Beck's ideas, that scattered throughout the primary recrystallization structure are some small grains whose orientation relative to the primary structure is such that they possess a maximum grain boundary energy, and consequently, maximum capacity for crystal growth. Furthermore, a simple consideration will show that these grains must, from their beginning, be several times larger than the surrounding primary grains. Because of their common orientation, the boundaries of the primary grains have relatively low energies. If a grain of the same size, but of different orientation (and consequently higher boundary energy), were situated in the midst of these primary grains, it should promptly disappear because the direction of migration of a grain boundary in an annealed metal is toward its center of curvature and the centers of curvature of the boundaries of this "odd" grain are within the grain itself. Only when the secondary grain is several times larger than its neighbors are the curvatures of its boundaries suitable for its continued enlargement, as shown in Fig. 11. That several grains of favorable orientation out of thousands should possess such a critical size is certainly statistically feasible.

This simple picture offers an explanation of the "induction period," for the rate of growth of the secondary grains (depending upon the curvature of the boundaries) would vary with the size of the secondary grain in the manner shown schematically in Fig. 12. Only those secondary grains which are larger than D_c can grow at all, and their rate of growth increases as their size increases until they reach D_s, after which their growth rate is constant. The time associated with growth at an increasing rate from D_c to D_s leads to the "induction period." The points shown in Fig. 12, in the range D_c to D_s, were actual measurements at 433° C.

Mechanism of Grain Growth: Using the observations that the grain boundary mobility is dependent on the boundary energy and curvature, the rate of grain growth can be calculated according to the following simple model. It will be assumed that the curved grain boundary separates two surfaces of opposite curvature and that the rate of transfer of atoms across the boundary is controlled by grain boundary self-diffusion. Further it will be assumed that diffusion occurs because of a vacancy gradient across the curved boundary; this vacancy gradient can be obtained from the Kelvin equation:

$$\Delta C = \frac{2\sigma\delta^3}{kT}\left(\frac{1}{a} - \frac{1}{-a}\right)C_o \qquad [3]$$

where ΔC is the difference in concentration of vacancies on two sides of a curved boundary; σ, the grain boundary energy; δ, the interatomic distance; k, Boltzmann's constant; T, the absolute temperature; a, the radius of curvature of the grain boundary; and C_o, the equilibrium concentration of vacancies in a plane grain boundary.

In our experiments the radius of curvature, a, is approximately equal to the diameter, d, of the primary grains (see Fig. 11b). If this is substituted and the assumption is made that $C_o = e^{-Q/RT}$, where Q is the energy required to form vacancies at the grain boundary, the following is obtained:

$$\Delta C = \frac{4\sigma\delta^3}{kTd}\, e^{-Q/RT} \qquad [3a]$$

This difference in concentration applies across the thickness of the grain boundary which may be assumed to be equal to 2δ. Then from Fick's law it follows that:

$$A \cdot \frac{\Delta C}{2\delta} \cdot D' = \frac{dV}{dt} = A\frac{dR}{dt} \qquad [4]$$

where A is the area of contact between the primary and secondary grain; R, the radius of the secondary grain; V, its volume; and D', the diffusion coefficient for vacancies.

Combining eqs 3a and 4 gives:

$$2\frac{dR}{dt} = \frac{4\sigma\delta^3}{kTd} D' e^{-Q/RT} \qquad [5]$$

Now $D' e^{-Q/RT}$ is the grain boundary self-diffusion coefficient, D_{sb}, and since the rate of growth:

$$G = 2\frac{dR}{dt}$$

the following is obtained:

$$G = \frac{4\sigma\delta}{kTd} D_{sb} \qquad [6]$$

Upon substituting the appropriate values for the constants and taking Greenough's value[5] of 300 ergs

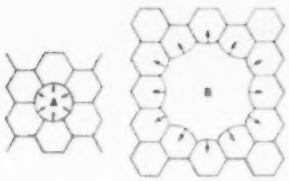

Fig. 11—Schematic drawing of grains.

a—Grain A is the same size as the surrounding primary grains, but is oriented differently and thus has higher grain boundary energy. As a result of the higher energy the boundaries will be curved and will move toward their centers of curvature (as indicated by the arrows) causing the disappearance of grain A. b—Grain B is oriented differently but is larger than the surrounding primary grains. In this case the curvatures of the boundaries are such as to cause the continued enlargement of grain B.

per sq cm for σ and the value of 2×10^{-7} cm for d, for 475° C, the result is:

$$G = 2.5 \times 10^{7} D_{v} \qquad [5]$$

Turnbull[7] reports that for silver $D_{v} = 0.025\, e^{-}$, so that the calculated rate of growth:

$$G_{calc.} = 62\, e^{-} \qquad [6]$$

whereas the measured rate of growth was:

$$G_{meas.} = 3000 \times e^{-} \qquad [7]$$

The discrepancy between the calculated and measured values is not as great as it appears from the last two equations. Table I lists the calculated and measured values for the four temperatures used in this study. It can be seen that these are in fairly good agreement over the temperature range involved. If it is taken into account that both the grain growth measurements and the diffusion measurements[7] were made over a temperature range of only about 100° C, it is likely that the Q values in both could be in error. It was concluded from this that our model of grain boundary movement during secondary recrystallization is basically correct.

Conclusions

The phenomenon of secondary recrystallization in 999.9 fine silver has been investigated in cold-rolled specimens, which were given prolonged anneals in the temperature range of 433° to 533° C. The shapes

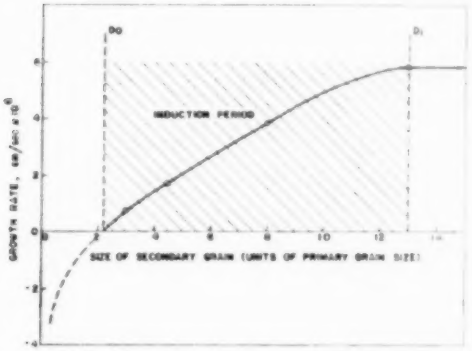

Fig. 12—Variation of growth rate of secondary grain with size of secondary grain during "induction period." Points are from data taken at 433° C.

Table I. Calculated and Measured Values for Four Temperatures

Temperature, °C	$G_{calc.}$ (Cm per Sec)	$G_{meas.}$ (Cm per Sec)
706	2.8×10^{-3}	0.7×10^{-3}
751	9.1×10^{-3}	2.5×10^{-3}
776	14.0×10^{-3}	4.6×10^{-3}
806	22.8×10^{-3}	8.8×10^{-3}

of the secondary grains can best be described as ellipses, with the maximum growth rate in the direction of rolling and minimum growth rate in a direction normal to the composition plane of long, massive twins appearing in these grains. It is believed that the very formation of these twinned regions is directly connected with the observed shape anisotropy.

Orientation studies showed that the secondary grains have a preferred orientation which corresponds closely to that of the original deformation texture. This coarsening structure can be related to components of the primary recrystallization structure by a rotation about a <111> axis.

Measurements on the growth rate of secondary grains showed that, after an induction period, the rate of growth was constant. The temperature dependence of the average rate of invisible grain growth (reciprocal of "induction period") as well as the constant rate of visible grain growth may be given by the expression:

$$G = G_{0}\, e^{-}$$

Activation energies have been calculated describing the temperature dependence of both the visible and invisible growth processes. These values suggest that the atomic process of crystal growth is one of grain boundary self-diffusion. These results further suggest that grain growth is taking place during the so-called induction period by the same process governing the growth of visible grains, and that at this early stage growth is probably impeded by the small number of contact areas between the growing grain and its surrounding fine-grained structure.

Under the assumption that the grain boundary mobility is dependent upon boundary energy and curvature, an expression for the growth velocity has been derived, which predicts growth rates in reasonable agreement with measured values.

References

W. G. Burgers: *Handbuch der Metallphysik*. Vol. 3 (1941) Leipzig. Teil.

W. Feitnecht: Crystal Growth in Recrystallized Cold Worked Metals. *Journal* Inst. Metals (1926) **35**, p. 131.

W. A. Anderson and R. F. Mehl: Recrystallization of Aluminum in Terms of the Rate of Nucleation and the Rate of Growth. *Trans.* AIME (1945) **161**, p. 140.

M. Kornfeld: Nucleus Formation During Recrystallization. *Physikal Z. Sowjetunion* (1935) **7**, p. 432; (1934) **6**, p. 170.

H. G. Müller: Zur Natur der Rekristallisationsvorgange. *Ztsch. Physik* (1935) **96**, p. 279.

A. B. Greninger: Determination of Orientation of Metallic Crystals by Means of Back-Reflection Laue Photographs. *Trans.* AIME (1935) **117**, p. 61.

R. Glocker: Uber Deformations-und Rekristallisations Structuren von Metallen. *Ztsch. Metallkunde* (1924) **16**, p. 377; (1925) **17**, p. 353; (1927) **19**, p. 41; *Ztsch. Physik* (1925) **31**, p. 386.

J. S. Bowles and W. Boas: The Effect of Crystal Arrangement on Secondary Recrystallization in Metals. *Journal* Inst. Metals (1948) **74**, p. 501.

[7] M. L. Kronberg and F. H. Wilson: Secondary Recrystallization in Copper. *Trans.* AIME (1949) **185**, p. 501; JOURNAL OF METALS (August 1949).

[8] J. K. Stanley and R. F. Mehl: Recrystallization of Silicon Ferrite in Terms of Rate of Nucleation and Rate of Growth. *Trans.* AIME (1942) **150**, p. 260.

[9] M. Cook and T. L. Richards: The Structural Changes in Copper Effected by Cold Rolling and Annealing. *Journal* Inst. Metals (1940) **66**, p. 1.

[10] M. Cook and T. L. Richards: The Structural Changes Effected in 70/30 Brass Strip by Cold Rolling and Annealing. *Journal* Inst. Metals (1943) **69**, p. 351.

[11] P. A. Beck and Hsun Hu: Recrystallization Texture and Coarsening Texture in High Purity Aluminum. *Trans.* AIME (1949) **185**, p. 627; JOURNAL OF METALS (September 1949).

[12] P. A. Beck, P. R. Sperry, and H. Hu: The Orientation Dependence of the Rate of Grain Boundary Migration. *Journal of Applied Physics* (1950) **21**, p. 420.

[13] P. A. Beck: Theory of Annealing Textures. *Trans.* AIME (1951) **191**, p. 475; JOURNAL OF METALS (June 1951).

[14] A. P. Greenough: Grain Boundary Energies in Silver. Royal Aircraft Establishment, Farnborough. Report No. Met. 52 (May 1950).

[15] D. Turnbull: Grain Boundary and Surface Diffusion. Seminar, Atom Movements. *Trans.* A.S.M. (1951) **43A**, p. 129.

Technical Note

Effect of Cold Work and Annealing on the Thermoelectric Power Of Molybdenum

by J. Howard Kittel

THE properties of the metal molybdenum have been the subject of recent investigations[1-3] which have included studies of the changes that occur in the metal when it is annealed after having been cold worked. Most of the data which have been reported have pertained to only one aspect of annealing, that is, the conditions under which recrystallization has been observed. The process of recovery which may precede recrystallization does not appear to have been investigated, and it is the purpose of this note to report observations on the recovery process in cold-worked molybdenum as determined by changes in the thermoelectric power which occur as the metal is annealed.

The measurements were made on commercially pure molybdenum wires which, after annealing at 1035°C in dried hydrogen for 1 hr, were swaged to give a series of reductions up to a maximum of 84.5 pct. The variously cold-worked wires were then annealed in dried hydrogen for periods of 16 hr at progressively higher temperatures from 200° to 1000°C, with a final annealing treatment of 70 hr at 1100°C. After each annealing treatment the thermal emf's were determined against a length of original unworked material that had received the initial hydrogen annealing treatment. The difference in temperature between the hot and cold junctions was maintained at about 75°C, and the thermal emf's were measured with a potentiometer that could be read to 0.01 microvolt.

Fig. 1 shows the thermoelectric power (dE/dT) in microvolts per °C between annealed and cold-worked molybdenum as a function of the degree of cold work. The effect of annealing is shown in Fig. 2. The general shape of the curves in both figures is similar to results which have been obtained for copper.[4] It was observed that after annealing at temperatures as low as 200°C recovery was well under way. The rapid changes in thermoelectric power observed near 900°C are probably associated with recrystallization, since such a relation has been observed with copper.[4] Beyond 900°C the thermal emf's changed in polarity, indicating that from this point on the specimens were more highly annealed

Fig. 1—Effect of cold work on the thermoelectric power of molybdenum.

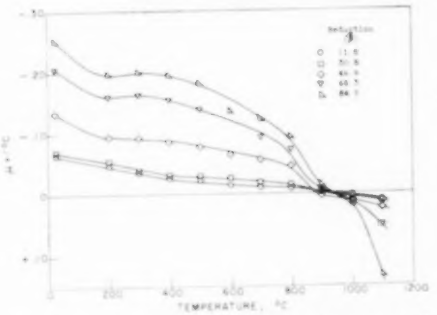

Fig. 2—Effect of annealing on the thermoelectric power of cold worked molybdenum.

than the standard. Annealing treatments could not be given at temperatures higher than 1100°C due to limitations of the furnace, and it is evident that, since equilibrium values of thermoelectric powers were far from having been attained, temperatures considerably higher are required to fully anneal molybdenum.

References

[1] Robert M. Parke: Molybdenum, A New High-Temperature Material. *Metal Progress* (1951) **60**, pp. 81-96.

[2] R. A. Long, K. C. Dike, and H. R. Bear: Some Properties of High-Purity Sintered Wrought Molybdenum Metal at Temperatures up to 2400°F. NACA TN 2319 (March 1951).

[3] G. W. Brindley: A Thermo-Electric Study of the Cold-Rolling and Heat-Treatment of Copper. Report of a Conference on the Strength of Solids. Physical Society, London (1948) pp. 95-106.

J. HOWARD KITTEL, formerly with NACA Lewis Flight Propulsion Laboratory, Cleveland, is now with Argonne National Laboratory, Chicago.

TN 92E. Manuscript, Sept. 13, 1951

Delay Time for the Initiation of Slip in Metal Single Crystals

by I. R. Kramer and R. Maddin

The delay time for the initiation of slip was studied in single crystals of α brass, aluminum, and β brass. A delay time for slip was found in β brass when the specimens were tested below room temperature; however, one was not found for α brass or aluminum. A general theory for the existence of the brittle transition temperature is proposed.

ALTHOUGH a considerable amount of effort has been devoted to the study of the deformation and fracture of single crystals, the vast majority of the work was concerned with static tests or with tests carried out at relatively slow strain rates. The necessity for the study of a possible incubation time for slip becomes apparent when the various theories which have been postulated for the elucidation of the mechanism of slip are considered. The existence of an incubation period would strongly indicate that slip occurs by a process of nucleation and growth; whereas the absence of an incubation would present rather convincing evidence that slip occurs by a cataclysmic process. In addition to shedding light on the process of plastic deformation, an understanding of the early stages of plastic deformation may be helpful in finding an explanation for the brittle behavior of the body-centered metals under certain conditions. It is well known that these metals, such as iron, molybdenum, tungsten, β brass, etc., will become brittle as the test temperature is lowered or the strain rate is increased. In spite of the fact that this subject has received considerable attention since the turn of the century, no adequate theory exists today which explains the phenomenon. In the ductile temperature range the metal breaks with a "fibrous" fracture after considerable slip has taken place. In the brittle temperature range the metal fails essentially by cleavage on the {100} planes; however, some plastic flow is always present even in the most brittle fractures. It is possible, as will be explained later, to ascribe this brittle behavior to the length of the incubation time for slip.

Clark and Wood,[1] using polycrystalline metals, showed that a delay time existed for the yield point in mild steels and that the delay time depended upon the applied stress. These authors stated that the delay time was observed only with those materials for which the stress-strain curve showed a definite yield point. In their work only the mild steel specimens exhibited a delay time at the yield point, while the other materials studied—type 302 stainless steel, SAE 4130 normalized steel, SAE 4130 quenched and tempered steel, 24S-T aluminum—did not show a delay time. These authors[1] in an extension of their work, found that as the temperature was lowered the delay time was increased.

It is, then, the purpose of this investigation to measure or to set an upper limit on the delay time for plastic flow in single crystals of α brass, aluminum, and β brass. The delay time will also be studied as a function of temperature.

The incubation time may be measured by determining the length of time the specimen will support a stress without slip occurring when the stress is greater than the static critical resolved shear stress. In order to accomplish these measurements use was made of a pendulum which was so designed that a single crystal specimen could be placed at various positions along its length. When a pendulum is struck by another pendulum of the same length, an elastic wave is transmitted down the bar with the velocity of sound in the material and is reflected from the far end of the bar. The reflected wave then travels back and unloads the stress until it reaches the impacted end of the bar and the two pendulums separate. The length of time that the specimen is subjected to the stress is equal to the time it takes for the stress wave to travel twice the distance from the specimen to the end of the bar. The stress applied to the specimen is governed by the velocity of impact of the two pendulums. The stress at which the specimen first suffers plastic deformation was determined in these experiments by examining the specimen under the microscope for the first appearance of slip lines and by measuring the residual strain after each impact. In these experiments the critical resolved shear stress was approached from the low stress side and no attempt was made to determine it exactly. To determine it exactly, it would have been necessary to find that stress at which slip would have just started. However, since the stresses were increased in rather small increments the critical stress is believed to be approached rather closely, as will be seen from the experimental results. The critical stress will be taken as the highest stress obtained before the onset of plastic deformation. The stresses

I. R. KRAMER, Member AIME, is Assistant to the President, Horizons Titanium, Inc., Princeton, N. J., and R. Maddin, Junior Member AIME, is Assistant Professor of Metallurgy, Johns Hopkins University, Baltimore.

Discussion on this paper, TP 3237E, may be sent, 2 copies, to AIME by April 1, 1952. Manuscript, Aug. 30, 1951. New York Meeting, February 1952.

This paper represents part of a thesis by I. R. Kramer submitted in partial fulfillment of requirements for the degree of Doctor of Engineering to the Graduate School of Engineering, Johns Hopkins University.

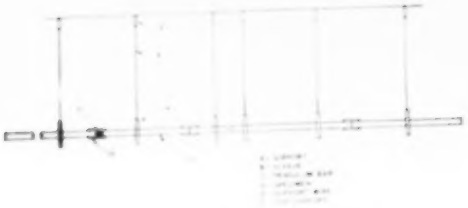

Fig. 1a—Schematic arrangement of pendulum

Fig. 1b—Block diagram of recording unit

in all cases were obtained by multiplying the strains obtained by a suitable elastic modulus.

Experimental Procedure

The pendulum shown schematically in Fig. 1a, consisted of ½ in. diam bars of 1, 2, 4, and 8 ft in length on one side and bars 7 and 8 ft on the other. The ends of these bars were ground flat and lapped in order to insure intimate contact over the entire surface when the bars were butted together. Steel sleeves 8 in. long were machined and reamed to fit very snugly over the ends of the bars. The ends of the sleeves were fitted with three Allen screws spaced 120° apart, which clamped down on the bars to hold them securely in place. Three aluminum supports were used on each pendulum. These supports were suspended by means of two steel wires at an angle of 40° placed in the same vertical plane and which was perpendicular to the axis of the pendulum. The wires which were 0.01 in. in diam and 7 ft long were supported by steel clamps which were attached to the wall of the building by wooden supports.

The method used in recording the strains experienced by the specimens is shown in Fig. 1b. An SR-4 type A-8 resistance strain gage is applied to the vertical plates of a cathode ray tube through a high-gain pre-amplifier and the internal Y axis amplifier of an RCA type 304-H oscilloscope. In order to observe this pattern it is necessary to use a driven sweep which must be initiated at the instant the bars come together. One additional requirement is that on successive impacts of the pendulum the sweep must be disabled so that one and only one sweep will be obtained. This was accomplished simply by firing a miniature thyratron at the instant of bar contact. The oscilloscope screen was photographed on 35 mm panchromatic film. A strain calibration was photographed before each pendulum impact. It was found that this procedure insured accurate strain measurements, since there was little chance for drift in the short interval of time allowed between recordings.

Single crystals of α brass, 70 pct Cu, 30 pct Zn, and single crystals of β brass, 52 pct Cu and 48 pct Zn, were made by the Bridgman technique. The aluminum single crystals, also made by the Bridgman technique, with a purity of 99.996 pct Al were supplied by the Aluminum Co. of America.

The aluminum and brass single crystals were homogenized near their melting points for 16 hr, etched, and examined microscopically.

The β brass specimens were made by essentially the same method as that used in the α brass. However, since the β brass region exists only over a rather small range of composition, care must be taken to prevent too great a loss of zinc. For these crystals the zinc and copper were placed in Vicore tubes which were sealed before the alloy was melted. The resulting crystals were homogenized at 800°C for 16 hr.

The specimens used in this investigation were ⅜ in. long and ½ in. in diam. Extreme care was taken in the preparation of these specimens to prevent straining. They were cut from ½ in. diam bars by cutting very slowly and lightly with a jeweler's saw and were then smoothed down on a surface grinder so that the two opposite faces were parallel to each other and were also perpendicular to the axis of the specimens. The specimens were ground by hand on numbers 2, 1, 0, 00, and 000 emery paper. The specimens were etched after the use of each grinding paper to remove the cold work. An electrolytic polish was used for the final polish.

Experimental Results

In order to determine the order of magnitude of the stress and time necessary to cause plastic deformation, a number of observations were made on α brass, aluminum, and β brass at room temperature. These specimens were placed in the pendulum and subjected to increasing amounts of impact loads. This was done by drawing the pendulum back from its equilibrium position in 1 in. increments. The strain-time curve was observed visually on the oscilloscope and the residual plastic strains were measured by means of a Baldwin strain indicator type K. After each impact, the specimen was removed from the pendulum and examined under the microscope at various magnifications for the appearance of slip lines. Within the limits of observation in these experiments, the appearance of slip lines occurred at the same time that a plastic strain was found. The fact that a measurable plastic strain was found coincident with the first appearance of slip lines is not unexpected. In the stress-strain curve for metal single crystals, the plastic strain region is generally very flat and almost parallel to the strain axis. Thus a small increase in the stress produces a very large increase in the strain. This is a very fortunate condition, for it makes it possible to bracket closely the value of the critical resolved shear stress. This fact was also used to great advantage when the measurements were made at liquid nitrogen and dry ice temperatures. After it was established that at these temperatures slip lines also appeared at the

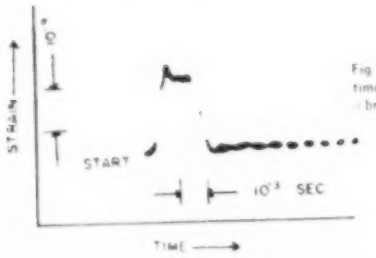

Fig. 2—Strain time curve for α brass at 25°C

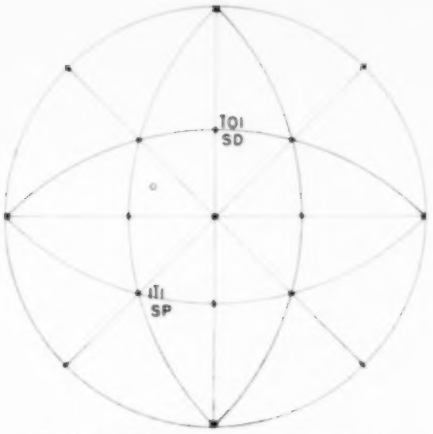

Fig. 3—Orientation of α brass crystal investigated.

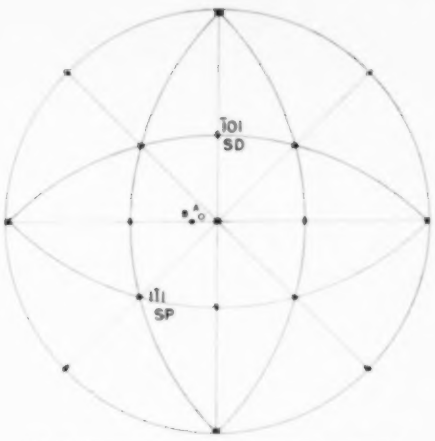

Fig. 4—Orientations of aluminum crystals investigated.

same time as plastic strains, the measurement of a plastic strain was used to indicate the end of the elastic region. At these temperatures, as in the case at room temperature, the onset of plastic flow was characterized by a residual plastic strain of at least 20 to 40 microin.

A typical strain-time curve is shown in Fig. 2. This curve was obtained from β brass tested at 25°C. The diagram of Fig. 2 is typical of the curves obtained for specimens tested at room temperature, except, in many cases, the sharp peak at the initial portion of the curve was not present.

The orientations of the specimens used are shown in Figs. 3, 4, and 5. The moduli of elasticity for β brass were calculated from the data presented by Rinehart,[7] who measured the moduli of elasticity in [100], [110], and [111] for temperatures down to −183°C. The appropriate values of the moduli of elasticity for the α brass crystals were calculated from the elastic coefficients obtained by Fenn, Hibbard, and Lepper,[8] while those of aluminum were obtained from the data of Rosi and Mathewson.[9] Although the latter authors reported values of Young's modulus down to temperatures of −195°C, they did not determine the values as a function of orientation. However, since aluminum single crystals are known to be fairly isotropic, little error may be expected from this source. The values of the orientation and moduli of elasticity of the α brass, β brass, and aluminum single crystals used in this investigation are given in Tables I and II. In Table I the angle λ is the angle between the specimen axis and the slip plane, while ϕ is the angle between the specimen axis and the slip direction.

The measurements of the stress are reported as resolved shear stresses which were calculated from the strain measurements taken from the strain-time oscilloscope recordings. The time for the duration of the stress was measured at the point midway between the base line of the strain-time recording and the maximum strain.

The data obtained for the single crystals of α and β brass and aluminum are presented in Figs. 6 to 10 and Tables III to IX. In these tables the strains measured for each impact are recorded, and the corresponding stress values and the resolved shear stresses have been calculated. In col. 5 is recorded the time of duration of the stress. This value was derived by averaging the values obtained for each test. The abreviation CRSS designates the critical resolved shear stress. Specimens tested at higher stresses were plastically deformed. The data plotted in Figs. 6 to 10 are the critical resolved shear stress vs. the time for the duration of the stress.

The data obtained for α brass when tested at room temperature (Fig. 6 and Table III) indicate that the critical resolved shear stress is not affected by the duration of the stress. Although the strain rates employed during these experiments were extremely high, the critical resolved shear stress value of 1650 psi is in quite good agreement with that obtained under static conditions by Maddin[10] and Fenn.[11] The values obtained by these authors range from 1600 to 1900 psi.

The data obtained for the single crystals of aluminum, presented in Figs. 7, 8, and 9 and in Tables IV, V, and VI also fail to reveal a change in the critical resolved shear stress as the time for the duration of stress was decreased. In fact, here too,

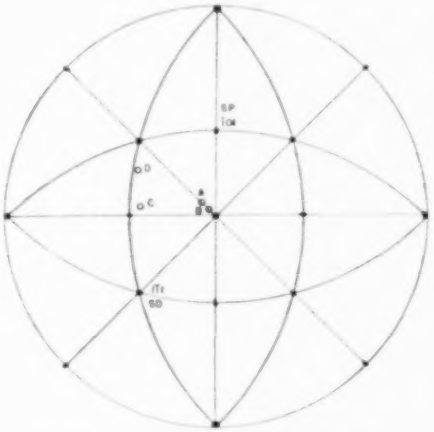

Fig. 5—Orientations of β brass crystals investigated.

Table I. Orientation of Crystals

Specimens	ϕ deg	λ deg	$\cos\chi\cos\phi$	Slip Plane and Direction
[illegible]	65.5	63	0.412	(111) [101]
[illegible]	57.5	45	0.440	(111) [101]
[illegible]	45	45	0.483	(111) [101]
[illegible]	52	54	0.464	(101) [111]
[illegible]	50	50	0.460	(101) [111]
[illegible]	80	87	0.469	(101) [111]
[illegible]	60	58	0.40	(101) [111]

Table II. Young's Modulus for Crystals Investigated

Crystals	Modulus of Elasticity, 10^{-6} psi		
	77°K	90°K	190°K
β brass	9.5	8.1	8.1
A	6.2	6.0	8.8
B	14.9	14.9	14.9
C	29.0	28.0	29.2
D	20.0	12.0	16.7
Aluminum A	9.9	54°C	
Aluminum B	22.1		

Table III. Delay Time of α Brass at 25° C

Specimen No.	Strain $\times 10^{-6}$	Stress psi	Resolved shear stress	Time $\times 10^{-6}$ Sec
6-1	90	2120	1080	12.3
6-2	134	2060	1020	
6-3	109	2050	1590	
6-4	144	3100	1630 CRSS	
6-5				24.0
7-1	77.5	171	975	
7-2	85.0	2160	1040	
7-3	101.5	2230	1140	
7-4	108.5	2300	1230	
7-5	140	3292	1660 CRSS	
8-1	100	2500	1400 CRSS exceeded	2.4
9-1	110	2430	1250	
9-2	145	3200	1650 CRSS	

Table IV. Delay Time for Aluminum at 25° C

Specimen No.	Strain $\times 10^{-6}$	Stress psi	Resolved shear stress	Time $\times 10^{-6}$ Sec
11-1	2.9	255	128	17
11-2	3.1	300	150 CRSS	
12-1				11
12-2	2.05	264	95	
12-3	2.1	260	93	
12-4	2.5	220	102	
12-5	2.5	240	111	
12-6	2.6	250	115	
12-7	2.6	275	124	
12-8	2.9	290	133	
12-9	2.9	300	130 CRSS	
13-1	1.95	151	67.4	2.3
13-2	1.95	151	67.4	
14-2	1.95	173	77.0	
14-3	1.95	195	87.0	
14-4	1.97	235	106	
14-5	2.4	310	139 CRSS	
14-6	3.3	340		

the values observed agree with those measured under static conditions.[7] The data measured at −54° C were obtained by testing the specimens in a mixture of kerosene and dry ice. The temperatures were measured with a thermometer placed as close as possible to the specimen. The data derived at −190° C were obtained by allowing the specimen to come directly in contact with liquid nitrogen. Since the resistance of strain gages of the SR-4 type is very sensitive to temperature, the gages were also used as a means of measuring temperature changes. Following each impact, a reading was taken after which more coolant was added. When the readings reached steady state, further impacts were made. It should be pointed out that an increase in temperature caused positive strain-gage readings, while plastic deformation caused negative readings. Thus it was easy to differentiate plastic deformation from a temperature change.

Using the same methods as those employed for the experiments on aluminum, β brass specimens were tested at 28°, −52°, and −190° C. In these specimens the effect of the duration of the stress was quite marked. At room temperature, (Fig. 10, Table VII) no delay time could be found, but at −52° C (Table VIII) and −190° C (Table IX) it was quite definite. At room temperature the average critical resolved shear stress is 350 psi. At −52° C the critical resolved shear stress is about 350 psi, when the stress is maintained for a period longer than 35×10^{-6} sec; but for a time of 5×10^{-6} sec the critical resolved shear stress rises to 1120 psi. The data obtained at −190° C shows that at this temperature the effect of the duration of impact is quite marked. At a time of 60×10^{-6} sec the critical resolved shear stress is 500 psi and is only 150 psi larger than that obtained at −52° C. However, as the duration of the stress becomes smaller, the specimens are able to withstand very high stresses before plastic deformation occurs. At a time of 27×10^{-6} sec the critical resolved shear stress is 2900 psi, while at 20×10^{-6} sec it is 4400 psi (see Fig. 10).

After each of the specimens was tested, a microscopic examination was made on the surface of the specimens to determine the distance between slip lines and the active slip plane. The examination of the specimens tested at room temperature did not present a problem, but those specimens tested at low temperatures were generally stained and it was difficult to study the slip lines in detail. In general, the slip lines were fairly regular and widely spaced, indicating that very little plastic deformation had taken place. The slip planes of the α brass and aluminum crystals were determined and found to be in agreement with those reported in the literature. The slip was found to occur on (111) planes in the [101] direction. The slip plane of the β brass, however, appeared to be in disagreement with that reported in the literature.[7] The slip planes at low temperatures are reported as the {110} and {112}. A specimen, No. A (Fig. 5), of β brass which had been subjected to impact at liquid nitrogen temperatures to produce substantial deformation was examined to determine the slip plane. For the specimen studied only slip on the {110} planes could be found.

In general, body-centered cubic metals may be deformed by twinning as well as by slip. Accordingly, specimens of β brass which had been deformed at room temperature, −52°, and −190° C were polished and etched to determine the possible existence of twins. As far as could be determined by examination under the optical microscope, the specimens deformed by slip since twins could not be found.

Discussion of Results

It has been the purpose of this work to determine whether or not a delay time existed for slip. The existence of a delay time for slip would indicate that slip occurred by a process of nucleation and growth rather than by a cataclysmic process. This latter is the method proposed by Frankel,[8] who postulated that slip would occur whenever the stress reached a critical value. Others[9, 10] assumed that slip occurs by nucleation and growth. This latter process

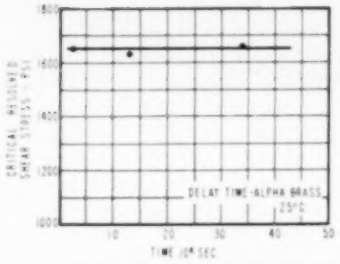

Fig. 6 — Delay-time curve for α brass at 25°C.

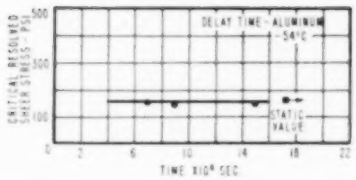

Fig. 8 — Delay-time curve for aluminum at −54°C.

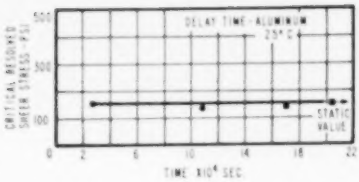

Fig. 7 — Delay-time curve for aluminum at 25°C.

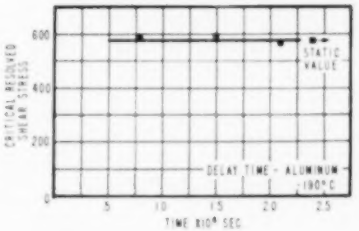

Fig. 9 — Delay-time curve for aluminum at −190°C.

implies that a delay time for plastic flow should occur.

In this investigation, while it was found that the body-centered cubic metal, β brass, had a very pronounced delay time for plastic deformation, no delay time was found for the face-centered cubic metals, aluminum and α brass. The difference in the behavior of the body-centered cubic metals is quite significant. While it cannot be said that the face-centered cubic metals would not have a delay time if lower temperatures and shorter times than used in these experiments were employed, it is quite definite that if there is a delay time for slip in these metals, it is small. The last consideration may well be the case, since there is no reason to suspect that the mechanism for slip in the face-centered cubic metals differs markedly from that of the body-centered cubic metals. This latter statement, however, may be modified if the role of impurities, which may be in solid solution, is considered. According to Cottrell,[5] dislocations can become anchored on impurity atoms and thus inhibit the slip process, since the energy necessary to dislodge the dislocation becomes larger than the energy necessary to propagate the dislocation. Frank[6] postulated that for this to be effective the impurity atoms must strain the lattice structure unequally in different directions. This is a very stringent condition and impurities may be expected to affect the body-centered cubic metals and the face-centered cubic metals in quite different manners. Thus, if the dislocation theory is adopted to explain the existence of a delay time for slip, then there remains the question as to whether the delay time is due to the presence of impurities, or whether it is associated with a particular type of lattice structure. This question is difficult to answer since it is thermodynamically impossible to prepare a metal without any impurities in solution. However, a study of the delay time in alloys of face-centered cubic materials might reveal the role of foreign atoms.

The theories for plastic flow postulated by Zener[7] and Leschen[8] are not detailed enough to predict a difference in the behavior of face-centered cubic and body-centered metals. Both theories allow for the existence of a delay time in slip for the two classes of metals discussed here.

The fact that body-centered cubic metals exhibit a delay time for slip and face-centered cubic metals either have an extremely small delay time or perhaps none at all, may furnish a basis for an explanation of the brittle transition in metals.

It is well known that when body-centered cubic metals are tested over a range of temperatures there will exist a temperature range in which the energy absorbed by the specimen upon fracturing will decrease abruptly. The temperature at which the energy drops rapidly is called the brittle transition temperature. In contrast to this, face-centered cubic metals do not have such a brittle transition temperature and the energy absorbed upon fracturing remains rather constant as the temperature is lowered.

The brittle transition temperature for any given body-centered cubic metal is greatly affected by the conditions of the test. In general, a decrease in strain rate will lower the transition temperature, while an increase in the size of the specimen will cause the transition temperature to be raised. The presence of

Table V. Delay Time for Aluminum at −54°C

Specimen No.	Strain X10⁶	Stress, psi	Resolved Shear Stress	Time X10⁴ Sec
15-2	65.6	785	450 CRSS exceeded	21
16-1	7.0	84	37	15
16-2	27.2	326	145 CRSS	
17-1	26.4	316	142	
18-1	22.6	271	121	9
18-2	28.4	340	151 CRSS	7.0

Table VI. Delay Time for Aluminum at −190°C

Specimen No.	Strain X10⁶	Stress, psi	Resolved Shear Stress	Time X10⁴ Sec
28-2	22.6	378	185	1.5
28-3	17.0	284	135	
28-4	22.6	378	185	
28-5	36.8	615	295	
28-6	51.0	850	410	
28-7	53.8	900	435	
28-8	62.4	1040	500	
28-9	73.5	1230	590 CRSS	
29-2	37.8	630	305	0.6
29-3	63.0	1050	510	
29-4	72.0	1203	585 CRSS	
30-1	34.6	575	280	2.1
30-2	50.4	844	410	
30-3	63.0	1050	510	
30-4	68.4	1150	560 CRSS	

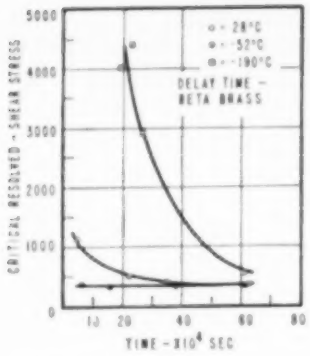

Fig. 10—Delay time curves for β brass at 28°, −52°, and −190°C.

sharp notches or other stress risers generally has a marked effect in raising the transition temperature.

In spite of the fact that the existence of a brittle transition in metals has been known for a considerable period of time, no satisfactory explanation for its cause has been given. Most of the explanations have been based on the theory proposed by Ludwik,[1] who postulated that fracture occurred at the intersection of a flow-stress and a fracture-stress curve. Ludwik's hypothesis, while simple, is subject to at least two important objections. It is seen that the area under the flow curve is a measure of the energy absorbed by the specimen. As the temperature is lowered the flow curve is raised much faster than the fracture curve, causing the fracture stress to intersect the flow curve at a lower strain. This produces a decrease in the absorbed energy, but the existence of a sharp brittle transition temperature is completely fortuitous since it can be easily seen that this effect is purely geometric and depends only on the relative shape of the two curves. The second and perhaps more important objection is that Ludwik's concept does not allow for any change in the mechanism of the fracture. At the upper portion of the brittle transition curve where the energy absorbed by the specimen is high, the fracture is accompanied by large amounts of plastic deformation, whereas below the brittle transition temperature range a brittle fracture occurs, where the fracture is caused by cleavage on the {100} planes. Any theory, which attempts to explain the transition temperature, must be able to account for this change. Further, the fact that a brittle transition temperature is found in body-centered cubic metals and not for face-centered cubic metals must also be explained.

The fact that a delay time for slip was found in body-centered cubic metals and not in face-centered cubic metals can form the basis for an explanation of the brittle transition temperature phenomenon. If the initiation of plastic flow requires a definite time, then at any temperature it is possible to apply a stress to a specimen sufficiently rapidly so that the delay time is nowhere exceeded, and, if the stress is sufficiently high to cause fracture, the specimen must fail by cleavage. Whether or not it is possible to obtain a 100 pct cleavage fracture will depend on the shape of the delay time curve in the region near the fracture stress.

This theory can perhaps be best explained with the aid of Figs. 11 and 12. Since in this investigation it was not possible to attain stresses high enough to cause fracture, the curves obtained must be extrapolated to the fracture stress. This can be done in two ways. In Fig. 11 the curves have been merely extended to the fracture stress (σ_f), while in Fig. 12 the upper portions of the curves have been drawn so that they intersect the fracture stress only at the zero time axis. These latter curves imply that it would be impossible to achieve a completely brittle break, while those of Fig. 11 would admit to such a possibility.

Table VII. Delay Time for β Brass at 28°C

Specimen No.	Strain X10⁴	Stress, psi	Resolved Shear Stress	Time X10⁴ Sec
23-1	29.4	821	328	38
23-2	32.7	915	366 CRSS	
25-1	4.5	126	50	15.7
25-2	12.8	358	140	
25-3	14.8	415	165	
25-4	18.7	575	230	
25-5	29.0	814	325 CRSS	
26-1	23.5	658	265	6.2
26-2	29.4	825	330 CRSS	

Suppose as indicated in Fig. 11 a stress is applied to a specimen such that the stress-time curve may be represented by the curve *OD*. This curve intersects the delay time curves for temperatures T_1, T_2, T_3, and T, at the points *A*, *B*, *C*, and *D*. The temperatures are selected so that T_1 is higher than T_2, etc. Thus it is seen that at temperatures T_1, T_2, and T_3 the delay time for slip is exceeded by an appreciable amount and a corresponding large amount of plastic flow can occur. However, at temperature T, the delay time is not exceeded and the specimen must fracture by cleavage since sufficient time has not been available for the start of slip. If it is assumed that the delay time curves are similar to those presented in Fig. 12, only a slight modification of the above explanation is necessary. Here it is seen that some plastic flow will always occur no matter how high the strain rate or how low the temperature. However, at the temperature T, since only a small time is allowed for plastic deformation, the fracture will be essentially brittle.

In the attempt to present this theory in as simple a manner as possible, it was tacitly assumed that a stress-time curve of the type *OD* in Fig. 11 could be applied directly. Actually, however, this is not the case, for the delay time curves were obtained under conditions where the stress was held at a constant value while the curve *OD* was not. Since the slip process appears to be associated with a nucleation process, nucleation may very well begin to occur as soon as the stress exceeds the critical shear stress found under static conditions.

This effect would have a tendency to move the delay time curves to the left. To this end, it should

Table VIII. Delay Time for β Brass at −58°C

Specimen No.	Strain X10⁴	Stress, psi	Resolved Shear Stress	Time X10⁴ Sec
34-1	27.2	172	80	22
34-2	168	1060	490 CRSS	
35-1	22.8	144	70	62.7
35-2	51.4	324	150	
35-3	57.0	359	165	
35-4	60.0	378	175	
35-5	125.2	790	365 CRSS	
36-1	128	805	374	35
36-2				
36-3	134	843	392 CRSS	
37-1	34.8	219	143	4.5
37-5	27.2	1710	1120 CRSS	

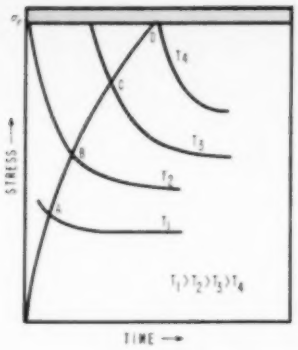

Fig. 11—Schematic diagram of delay time for the initiation of plastic deformation as a function of stress.

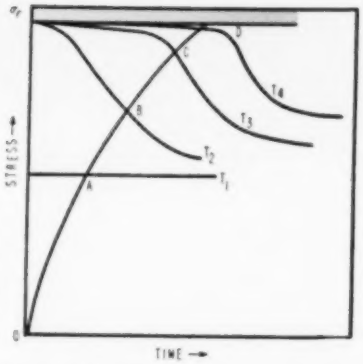

Fig. 12—Schematic diagram of delay time for the initiation of plastic deformation as a function of stress.

be pointed out that the customary use of strain rate as a parameter for describing the plastic flow phenomenon is somewhat misleading since even under conditions where the strain rate is constant, the stress rate varies continuously. The strain rate will only be a measure of the average time that a specimen is at a given stress. It may be more meaningful to conduct the studies of plastic flow under conditions of constant stress.

Summary

1—The delay time for slip was measured in single crystals of α brass, aluminum, and β brass. For the face-centered cubic metals, α brass and aluminum, a delay time could not be found even though the measurements on the aluminum crystals were carried out at −190° C for an impact time of 8×10^{-4} sec. A delay time was found in β brass which was strongly dependent upon the temperature.

2—A general theory for the explanation of the brittle transition temperature was proposed. This theory proposed that the existence of a delay time for the initiation for slip will permit a specimen to be loaded at a rate sufficiently rapid such that the delay time is nowhere exceeded. Under these conditions plastic deformation cannot occur and the specimen must fail by cleavage.

3—An examination of the spacing of the slip lines and the determination of the slip plane confirmed the findings already reported in the literature. However, for the β brass specimens deformed at liquid nitrogen temperature only slip on the {110} planes could be found. This is contrary to the data present in the literature which reports that at low temperatures slip occurs on the {110} and {112} planes.

4—The critical resolved shear stress determined in this investigation for the single crystals of α brass and aluminum agreed very well with those reported in the literature. For α brass at 28° C a value of 1650 psi was obtained as compared to values reported in the literature of 1600 and 1900 psi. A value of 150 psi at 25° C, 155 psi at −54° C, and 580 psi at −190° C was found for the critical resolved shear stress of aluminum.

Table IX. Delay Time for β Brass at −190° C

Specimen No.	Strain X10⁴	Stress, psi	Resolved Shear Stress	Time X10⁴ Sec
31-1	196.5	2920	1370	19.6
31-2	302.0	4500	2110	
31-3	426.0	6350	2980	
31-4	446	6640	3120	
31-5	575	8550	4000 CRSS	
33-1	192	286	1340	27
33-2	237	373	1750	
33-3				
33-4	352	525	2470	
33-5	396	590	2780 CRSS	
39-1				
39-2	420	625	295	61
39-3	465	694	325	
39-4				
39-5	716	1070	500 CRSS	
40-1	72	1070	500	23.4
40-2	288	4300	1870	
40-3	324	4840	2260	
40-4	635	9450	4420	
40-5	660	9850	4600 CRSS	

Acknowledgment

The authors wish to acknowledge with thanks the contributions of N. K. Chen for his helpful discussions and suggestions and B. Averbach for supplying the β brass crystals.

References

[1] D. S. Clark and D. S. Wood: The Time Delay for the Initiation of Plastic Deformation at Rapidly Applied Constant Stress. A.S.T.M. (1949) **29**, p. 717.

[2] D. S. Clark and D. S. Wood: The Influence of Temperature Upon the Time for Yielding in Annealed Mild Carbon Steel. A.S.M. (1951) **43**, p. 571.

[3] J. S. Rinehart: Behavior of Young's Modulus of Beta-Brass Single-Crystals at Low Temperature. *Physical Review* (1941) **59**, p. 308.

[4] R. W. Fenn, W. Hibbard, Jr., and H. H. Lepper, Jr.: The Elastic Coefficients of Single Crystals of Alpha Brass. *Trans.* AIME (1950) **188**, p. 175; JOURNAL OF METALS (January 1950).

[5] F. D. Rosi and C. H. Mathewson: A Study of the Plastic Behavior of High Purity Aluminum Single Crystals at Various Temperatures. *Trans.* AIME (1950) **188**, p. 1159; JOURNAL OF METALS (September 1950).

[6] R. Maddin, C. H. Mathewson, and W. R. Hibbard, Jr.: Unpredicted Cross-Slip in Single Crystals of Alpha Brass. *Trans.* AIME (1948) **175**, p. 86; METALS TECHNOLOGY (February 1948).

[7] G. I. Taylor: The Deformation of Crystals of Beta Brass. *Proc.* Royal Soc. (1928) **A118**, p. 1.

[8] J. I. Frenkel and T. A. Kontorova: Theory of Plastic Deformation and Twinning. *Journal of Physics* U.S.S.R. (1939) **1**, No. 2, p. 137.

[9] C. Zener: A Theoretical Criterion for the Initiation of Slip Bands. *Physical Review* (1946) **69**, p. 128.

[10] J. G. Leschen, R. P. Carreker, and J. H. Holloman: Nucleation of Slip Bands. *Trans.* AIME (1949) **180**, p. 131; METALS TECHNOLOGY (September 1948).

[11] A. H. Cottrell: Report on the Strength of Solids. Physical Society, London. (1948) p. 30.

[12] F. C. Frank: Symposium on Plastic Deformation of Crystalline Solids. Office of Naval Research (May 1950), p. 63.

[13] P. Ludwik: *Elements der Technologischen Mechanik*. (1909) Berlin.

Diffraction Patterns and Crystal Structure of Si_3N_4 and Ge_3N_4

by W. C. Leslie, K. G. Carroll, and R. M. Fisher

A nitride, believed to be Si_3N_4, has been separated from three nitrided silicon steels. Germanium nitride, Ge_3N_4, has been prepared from pure germanium. Comparison of the diffraction patterns indicates that the two nitrides are isomorphous; an orthorhombic structure is suggested in place of the rhombohedral structure previously reported for Ge_3N_4.

THE possibility that a nitride of silicon may, under appropriate conditions, precipitate in silicon steels or in steels killed with silicon makes it desirable to have some positive means of identifying such a compound. One such means is the X-ray or electron diffraction pattern of the nitride.

A review of the meager data in the literature indicates that the nitride most likely to form is Si_3N_4, a conclusion supported by the results of a study of nitrided silicon steels to be published shortly by L. S. Darken and R. P. Smith, of this Laboratory. Unfortunately, there is available no diffraction pattern for this nitride. Data have been reported, however, for Ge_3N_4, which, judging from the similarity between germanium and silicon, might be expected to be isomorphous with Si_3N_4. An effort was made, therefore, to form such a silicon nitride, to determine its composition and diffraction pattern and, if possible, its structure.

To this end a series of three silicon steels was nitrided under controlled conditions with the resultant formation of nitride particles which yielded an electron diffraction pattern in situ. The particles were then extracted from the steel and an attempt was made to determine their chemical composition. X-ray and electron diffraction patterns were also obtained from the extracted particles, which indicate that the nitride is isomorphous with Ge_3N_4, although a complete determination of the structure has not been possible. These results show that a silicon nitride with a well-defined diffraction pattern can form in silicon steels, and they suggest that this nitride is Si_3N_4.

Materials and Procedures

The silicon steels investigated were in the form of thin sheet or strip and had the composition shown in Table I. The 0.58 and 1.21 pct Si steels were nitrided by holding them at 1110°F in an H_2-NH_3 atmosphere containing 3 pct ammonia for 48 hr. The nitride particle size was increased by subsequent heating at 1500°F for 13½ hr in helium. The resulting microstructure is shown in Fig. 1. The steel containing 3.20 pct Si was nitrided at 1200°F for 16½ hr after which it was held in helium at 1500°F for 4 hr. Its structure as seen under the electron microscope is illustrated by Fig. 2. As would be expected from the higher silicon content and the shorter holding time at 1500°F, the nitride particles are smaller and more numerous than those in the 1.21 pct Si steel. The ammonia-hydrogen treatment reduced the carbon content of the steels to a very low level, so no interference was encountered from carbon or carbides. In the case of the 3.2 pct Si steel, the carbon was reduced to 0.003 pct before nitriding by heating in dry hydrogen.

Table I. Composition of Silicon Steels Investigated

Composition					Thickness, In.
Si	C	Mn	P	S	
0.58	0.073	0.28	0.020	0.022	0.062
1.21	0.074	0.28	0.012	0.015	0.062
3.20*	0.013	0.26*	0.003*	0.020*	0.0185

* Ladle analyses.

Attempts to obtain an X-ray diffraction pattern from polished and etched surfaces of the 1.21 and the 3.20 pct Si steels were unsuccessful. However, an electron diffraction pattern was obtained from the surface of the steels. The interplanar spacings obtained from these patterns are shown in Table II, col. 5. The nitride particles were then extracted from all three steels by dissolving the ferrite matrix in bromine-methyl acetate, the solution used in the Beeghly[1] method for the extraction of aluminum nitride from steel. X-ray diffraction patterns of these residues, obtained by means of a spectrometer and by a 57 mm Debye-Scherrer powder camera using filtered cobalt or chromium radiation, are given in Table II along with the pattern obtained by

W. C. LESLIE, Junior Member AIME, K. G. CARROLL and R. M. FISHER are associated with the Research Laboratory, U. S. Steel Co., Kearny, N. J.

Discussion on this paper, TP 3214E, may be sent, 2 copies, to AIME by April 1, 1952. Manuscript, Aug. 16, 1951; revision, Dec. 11, 1951. New York Meeting, February 1952.

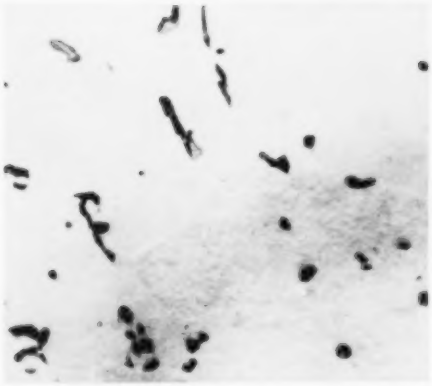

Fig. 1—Silicon nitride in a 1.2 pct Si steel nitrided at 1110°F to 0.74 pct N, then held 13.5 hr at 1500°F and slowly cooled.

1 pct nital etch. Area reproduced approximately 50 pct for reproduction.

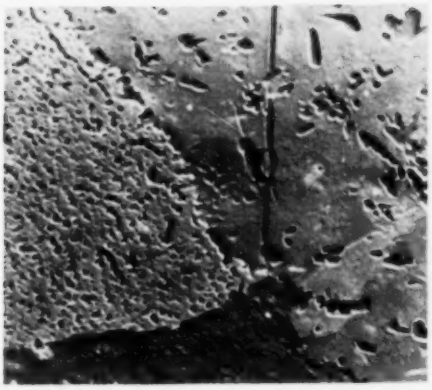

Fig. 2—Electron micrograph of silicon nitride in a 3.2 pct Si steel nitrided at 1200°F, then held 4 hr at 1500°F and slowly cooled.

1 pct nital etch. Uranium shadow-cast. X5630. Area reduced approximately 50 pct for reproduction.

transmission electron diffraction from the powder. Agreement between the X-ray and electron diffraction data is quite good, when the relative inaccuracy of electron diffraction is considered. It was concluded that the nitride was unchanged by removal from the steel.

A sample of the steel containing 3.20 pct Si was given the same thermal treatment as the nitrided specimen, without introduction of ammonia, and was then dissolved in bromine-methyl acetate. No X-ray diffraction pattern could be obtained from the small amount of residue. A few lines were obtained from

Table II. Orthorhombic Indexing of Diffraction Patterns of Si_3N_4 and Ge_3N_4

	Si_3N_4: $a = 13.38 \pm 0.03$A; $b = 8.60 \pm 0.02$A; $c = 7.74 \pm 0.02$A				Ge_3N_4: $a = 13.84 \pm 0.03$A; $b = 9.06 \pm 0.02$A; $c = 8.18 \pm 0.02$A			Ge_3N_4: Juza and Hahn[2]	
1	2	3	4	5	6	7	8	9	10
hkl	Intensity	d Observed	d Calculated	Reflection Electron Diffraction	Intensity	d Observed	d Calculated	Intensity	d Observed
200	VW	6.68 *	6.690		W	6.94	6.920		
020	S	4.28 *	4.300		MS	4.52	4.530	VW	4.50
002	M	3.856*	3.870		M	4.08	4.090	M	3.95
301					M	3.99	4.018		
202					MW	3.533	3.521		
400	M	3.344*	3.345		S	3.458	3.460	M	3.464
410	VW	3.107	3.118		VW	3.230	3.242		
030	S	2.873*	2.867	2.90	MS	3.031	3.020	VW	3.063
130	VW	2.801	2.803		W	2.953	2.951		
222	VW	2.651	2.643		S	2.802	2.780	S	2.817
003	S	2.583*	2.580	2.59	MS	2.727	2.727	W	2.734
103	S	2.529*	2.533		MS	2.675	2.675		
231	W	2.483	2.494		VS	2.621	2.622	VS	2.620
311	W	2.427	2.426						
213	S	2.305*	2.318	2.30	MS	2.439	2.443	W	2.445
320	W	2.267	2.272		VW	2.362	2.362		
600	W	2.232	2.230	2.21	S	2.297	2.307	S	2.303
040	M	2.149*	2.150	2.15	M	2.270	2.265	VW	2.275
041	S	2.074*	2.072		M	2.193	2.183	VW	2.199
004	W	1.933	1.935		VW	2.043	2.045		
602					VW	1.997	2.009	W	1.998
341	W	1.881*	1.879	1.89					
701	W	1.859	1.856	1.85	W	1.926	1.922	W	1.921
242	W	1.806	1.809		VW	1.907	1.905		
024	M	1.764*	1.765		W	1.865	1.864		
333					M	1.847	1.853	S	1.845
				Following lines of both patterns listed in order:					
	VW	1.747		1.74					
	M	1.594*		1.59	W	1.682		VW	1.683
	W	1.507			W	1.632		W	1.620
	MS	1.485*		1.46	W	1.593		M	1.589
	M	1.436			W	1.570		VW	1.574
	M	1.416			W	1.539		W	1.539
	MW	1.405		1.38	MW	1.517		M	1.510
	M	1.353			W	1.499		S	1.498
	W	1.320		1.33	M	1.414		S	1.410
	W	1.309		1.31	VW	1.395		VW	1.385
	MW	1.301			W	1.362		M	1.356
	W	1.295			W	1.327		VW	1.332
	VW	1.260		1.25					
	W	1.223							

* Observed both by transmission electron diffraction and X-ray diffraction. All other data in col. 3 obtained by X-ray diffraction only. VS means very strong; S, strong; MS, medium strong; M, medium; MW, medium weak; W, weak; and VW, very weak.

Table III. Comparison of Juza and Hahn Data with that of Present Authors

Line No.	Juza and Hahn: $\sin^2\theta \times 10^4$ observed	Juza and Hahn: $\sin^2\theta$ Calculated	Revision: hkl (hexagonal)	Revision: hkl (hexagonal)	Revision: $\sin^2\theta$ Calculated
1	0.0293	0.0291, should be 0.0318	012	210	0.0291
6	0.0781	0.0781, should be 0.0812	312	203	0.0787

the powder by transmission electron diffraction, but these did not correspond to any of the lines obtained from the nitride residue, nor to the pattern of any substance listed in the A.S.T.M. card index.

Attempts to establish the chemical constitution of the extracted nitride particles were only partially successful due to the well-known difficulties in working with very small particles extracted from steel. An X-ray fluorescence analysis revealed the presence of a significant content of bromine, manganese, and iron in spite of efforts to purify the residue. A specimen of the 0.58 pct Si steel, equilibrated by Darken and Smith by heating in a 3 pct NH_3-H_2 atmosphere at 1110°F for 352 hr, was digested in the Beeghly solvent, and the residue analyzed for nitrogen. The result, on the basis of the original sample, was 0.38 pct N. Considering all silicon combined as the nitride, this gives a formula for the nitride of $Si_3N_{3.6}$. Attempts to analyze the residue for silicon yielded very erratic results. Two attempts made to nitride silicon in dry, purified nitrogen resulted in a product contaminated by quartz and α tridymite. This agrees with the experience of previous investigators.[2,3]

Finally, in order to compare the diffraction pattern of the extracted nitride with that of Ge_3N_4, the germanium compound was prepared by nitriding high purity germanium obtained through the courtesy of the Bell Telephone Laboratories. The metal, crushed to −325 mesh, was heated in flowing ammonia at 1300°F for 16 hr. This process, which was carried out without difficulty, yielded a product which gave a well-defined diffraction pattern as indicated in Table II.

Results and Discussion

Juza and Hahn[4] give an X-ray diffraction pattern, obtained from powdered Ge_3N_4, with copper radiation, which is in good agreement with that obtained in this investigation. Their pattern is listed in cols. 9 and 10 of Table II. Ten more lines, down to a lattice spacing of 1.327A, were obtained in the present work. Juza and Hahn were able to index all their lines on the basis of a rhombohedral structure, with $a = 8.57 \pm 0.01$A, $\alpha = 107° 48'$, or, alternatively, on the basis of a hexagonal cell, with $a = 13.84 \pm 0.01$A, $c/a = 0.668$. Attempts to index the pattern obtained from Si_3N_4 on the basis of a similar structure led to a recalculation of the indices listed by Juza and Hahn. To calculate $\sin^2\theta$ for various indices these authors used the equation $\sin^2\theta = 0.00412\ (h^2 + k^2 + hk) + 0.00691\ (l)^2$. The coefficients in this equation are correct, but errors were found in calculation of $\sin^2\theta$ for their first and sixth lines. When these errors are corrected the indices used by Juza and Hahn are no longer in good agreement with the observed $\sin^2\theta$ for these two lines. Their observations and calculations, extracted from Table 4 of ref. 4, and our corrections are given in Table III.

Changing (012) to (210) and (312) to (203) does not affect assignment of the structure to the hexagonal system, but it eliminates the possibility that the structure is rhombohedral, since the revised indices cannot be transformed to the rhombohedral system.

Changing the parameters of Ge_3N_4 from those used by Juza and Hahn to $a = 13.88 \pm 0.03$A, $c/a = 0.654$ and using parameters for Si_3N_4 of $a = 13.44 \pm 0.03$A, $c/a = 0.637$, makes it possible to index both patterns in the hexagonal system. One line in the observed Ge_3N_4 pattern ($d = 3.533$A), however, cannot be indexed using these parameters.

The diffraction patterns for both nitrides can be fitted more closely to an orthorhombic structure, with the parameters given in Table IV. Only the first 22 lines of Si_3N_4 and the first 24 lines of Ge_3N_4 are indexed, since with decreasing interplanar spacings the number of possible planes becomes so large that the unique assignment of indices is not practicable. Below the last index (Table II) the d spacings of the Si_3N_4 and Ge_3N_4 patterns are simply listed in order.

On the basis of 12 molecules per unit cell, the density of Si_3N_4 was calculated from the X-ray data to be 3.15, as compared with a value of 3.44 measured by Weiss and Engelhardt[5] in 1910. The density of Ge_3N_4 was calculated from the X-ray data to be 5.31, whereas that measured by Juza and Hahn was 5.25.

Table IV. Lattice Parameters of Si_3N_4 and Ge_3N_4

	a	b	c
Si_3N_4	13.88 ± 0.03A	8.60 ± 0.02A	7.74 ± 0.02A
Ge_3N_4	13.84 ± 0.03A	8.66 ± 0.02A	8.18 ± 0.02A

Summary and Conclusions

X-ray and electron diffraction patterns of nitride particles present in nitrided silicon steels have been determined. The method of preparation and other data offer presumptive, though not conclusive, evidence that this nitride is Si_3N_4. Moreover, a comparison of the X-ray diffraction pattern with that obtained from Ge_3N_4 has led to the conclusion that these two nitrides are isomorphous, the most probable structure being orthorhombic, with the parameters as given in Table IV. In the absence of diffraction patterns from single crystals of either Si_3N_4 or Ge_3N_4, however, it is not possible to determine their structure unequivocally.

Acknowledgment

The germanium used was provided by the Bell Telephone Laboratories, Murray Hill, N. J. The aid of L. S. Darken, R. P. Smith, and E. W. Filer in nitriding the germanium is gratefully acknowledged.

References

1. H. F. Beeghly: Determination of Aluminum Nitride in Steel. *Analytical Chemistry* (1949) **21**, p. 1513.
2. W. B. Hincke and L. R. Brantley: High Temperature Equilibrium Between Silicon Nitride, Silicon and Nitrogen. *Journal* Amer. Chem. Soc. (1930) **52**, p. 48.
3. S. Sato: The Heat of Formation and Specific Heat of Silicon Nitride. Sci. Papers, Inst. Phys. Chem. Res. (Tokyo) (1938) **34**, p. 50.
4. R. Juza and H. Hahn: On the Crystal Structure of Zn_3N_2, Cd_3N_2 and Ge_3N_4. *Ztsch. anorg. allgem. Chem.* (1940) **244**, p. 125.
5. L. Weiss and T. Engelhardt: *Ztsch. anorg. allgem. Chem.* (1910) **65**, p. 38.

Effect of Temperature on the Lattice Parameters Of Magnesium Alloys

by R. S. Busk

A PREVIOUS paper[1] has summarized the effect of all metallic elements on the lattice parameters of magnesium. The present paper deals with the effect of temperature on the lattice parameters and the way in which that effect is modified by alloyed elements.

The experimental techniques for sample preparation, exposure to the X-ray beam, measurement of line diameters, and calculation of the parameters were the same as reported in the previous paper. The temperature of the specimen was raised by surrounding the mounted compact with a conical Glas-Col,* the base of which was sealed with Saran film. In this way the temperature of the specimen could be raised to 200°C, which was the maximum desired in the present study. Control of temperature was effected by maintaining a constant, desired voltage to the resistance coils of the Glas-Col through a Variac. Temperature was measured by an iron constantan thermocouple embedded in the body of the specimen so that the thermocouple bead was within 1/16 in. of the surface exposed to the X-ray beam. Variation of temperature during an exposure was less than ± ¼°F.

A series of eight alloys, consisting of pure Mg, Mg + Ag, Mg + Al, and Mg + Sn were studied. All percentage values are in atomic percent. The results are given in Table I. The density values given in Table I were calculated from the lattice parameters, using an equation due to Foote and Jette:[4]

R. S. BUSK, Member AIME, is associated with Dow Chemical Co., Midland, Mich.

Discussion on this paper, TP 3236E, may be sent, 2 copies, to AIME by April 1, 1952. Manuscript, Aug. 29, 1951. New York Meeting, February 1952.

The work reported here was cooperatively supported by the ONR and the AEC through Contract Number N9onr-85902.

* Glas-Col Apparatus Co., Terre Haute, Ind.

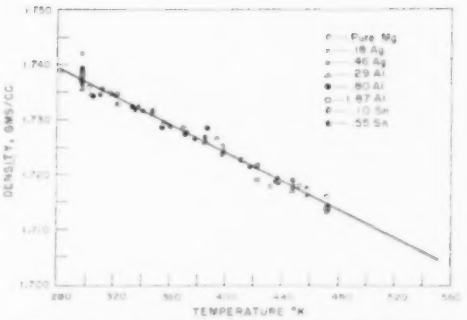

Fig. 1—Effect of temperature on the density of magnesium alloys. The density for each alloy is corrected to that for pure magnesium.

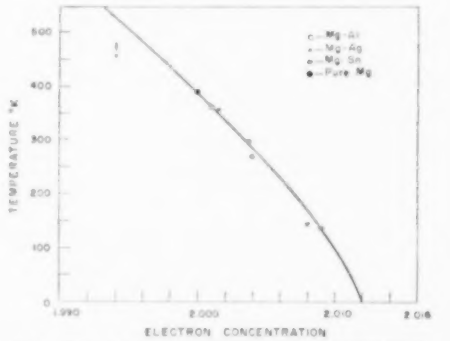

Fig. 2—Effect of electron concentration on the temperature at which the c/a ratio for the magnesium-base alloys begins to increase.

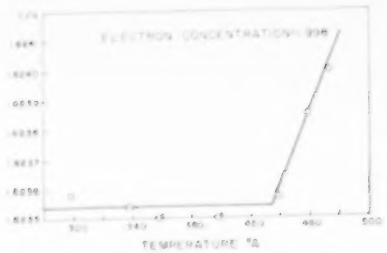

Fig. 3—Effect of temperature on the c/a ratio of Mg + 0.18 pct Ag.

$$P = \frac{KnM}{V^3}$$

where, P is the density in g per cc, K, 1.65023; n, the number of atoms per cell, is 2, M is the molecular weight, and V^3, volume of lattice in $(kX)^3$ units.

Discussion of Results

As is to be expected, the main effect of temperature is an increase in the size of the unit cell. This is most clearly shown by the density which decreases linearly with increasing temperature. The coefficient of expansion in the temperature range investigated is not affected by alloy addition, as shown in Fig. 1. In Fig. 1, the density curve for each alloy has been displaced vertically to coincide with that for pure magnesium in order to emphasize the constant coefficient of expansion with alloy content.

The variation of the c/a ratio with temperature is of particular interest. As was pointed out in the previous paper,[2] the c/a ratio is dependent upon the electron concentration of the alloy. As the electron concentration is raised above the value of 2.000 for pure magnesium, there is at first no effect on the c/a ratio. Then, after a threshold value of electron concentration is reached, further increase results in an increase in the c/a ratio. By assuming that electron concentration is the sole cause of a change in the c/a ratio, it was possible to calculate "relative effective valencies" for each element when alloyed with magnesium.

Raynor[1] and Hume-Rothery and Raynor[3] have advanced an explanation of the dependence of the c/a ratio on electron concentration based upon the energy levels occupied by the conduction electrons. Briefly, as electrons are added to the magnesium lattice, additional energy levels are occupied. This leads to an early occupation of levels in the second Brillouin Zone, the overlap occurring in the c direction. The overlap results in a stress that is relieved by an additional expansion in the c direction and hence an increase in the c/a ratio.

When the temperature of a metal is above absolute zero, some of the conduction electrons are thermally excited into higher energy levels than they would occupy at absolute zero. The higher the temperature, the more electrons there are in higher levels, and the higher the highest level occupied. On the

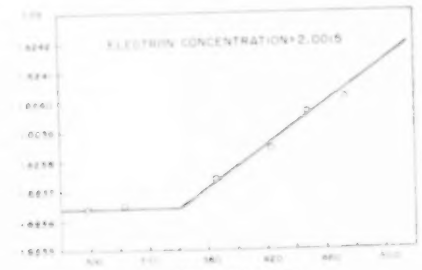

Fig. 4—Effect of temperature on the c/a ratio of Mg + 0.10 pct Sn.

Table I. Effect of Temperature on the Lattice Parameters of Magnesium and Magnesium Alloys

Composition*	Temperature °C	Temperature °K	a_0 (kX)	c_0 (kX)	c/a	Density, g per cc
Pure Mg	10†	283	3.2017	5.1998	1.6237	1.739
Elec. conc. = 2.000	25	298	3.2023	5.1994	1.62364	1.738
	30†	303	3.2035	5.2015	1.6237	1.736
	46	319	3.2041	5.2021	1.62364	1.735
	90	371	3.2087	5.2086	1.62343	1.728
	160†	433	3.2147	5.2203	1.6239	1.718
	180	453	3.2149	5.2205	1.62384	1.718
	200	473	3.2162	5.2222	1.62372	1.716
	310.5†	583.5	3.2278	5.2423	1.6241	1.697
	455†	728	3.2420	5.2663	1.6244	1.674
	506.8†	779.8	3.2485	5.2772	1.6245	1.664
	597†	870	3.2589	5.2960	1.6246	1.647
Mg + 0.18 pct Ag	25	298	3.1979	5.1920	1.62358	1.736
Elec. conc. = 1.998	63	336	3.2042	5.2021	1.62354	1.746
	85	358	3.2058	5.2047	1.62350	1.743
	125	398	3.2094	5.2105	1.62350	1.738
	165	438	3.2123	5.2155	1.62357	1.733
	185	458	3.2139	5.2189	1.62385	1.730
	200	473	3.2147	5.2221	1.62409	1.728
Mg + 0.46 pct Ag	25	298	3.1996	5.1951	1.62354	1.770
Elec. conc. = 1.994	66	339	3.2021	5.1993	1.62375	1.766
	105	378	3.2063	5.2046	1.62323	1.760
	125	398	3.2056	5.2066	1.62376	1.759
	145	418	3.2086	5.2094	1.62357	1.755
	165	438	3.2106	5.2127	1.62357	1.752
	185	458	3.2116	5.2137	1.62341	1.751
Mg + 0.29 pct Al	25	298	3.2018	5.1985	1.62364	1.740
Elec. conc. = 2.001	31.5	304.5	3.2024	5.1984	1.62331	1.739
	38.5	311.5	3.2021	5.1979	1.62329	1.740
	46	319	3.2026	5.1984	1.62338	1.739
	68	341	3.2043	5.2019	1.62339	1.736
	82.5	355.5	3.2054	5.2036	1.62338	1.734
	91	364	3.2061	5.2054	1.62361	1.733
	98	371	3.2055	5.2058	1.62402	1.733
	99	372	3.2082	5.2068	1.62400	1.732
	121	394	3.2088	5.2085	1.62421	1.731
Mg + 0.80 pct Al	25	298	3.1971	5.1914	1.62379	1.748
Elec. conc. = 2.004	32	305	3.2001	5.1962	1.62378	1.743
	59.5	333	3.2016	5.1992	1.62393	1.741
	82	355	3.2037	5.2028	1.62403	1.737
	98	371	3.2042	5.2040	1.62412	1.736
	114	387	3.2038	5.2037	1.62423	1.737
Mg + 1.87 pct Al	25	298	3.1953	5.1896	1.62406	1.753
Elec. conc. = 2.009	50	323	3.1970	5.1924	1.62413	1.750
	75	348	3.1997	5.1968	1.62417	1.746
	150	423	3.2068	5.2084	1.62429	1.734
	175	448	3.2076	5.2107	1.62450	1.732
	200	473	3.2096	5.2140	1.62452	1.729
Mg + 0.10 pct Sn	25	298	3.2028	5.1995	1.62364	1.744
Elec. conc. = 2.0015	50	323	3.2053	5.2043	1.62365	1.740
	113	386	3.2111	5.2140	1.62374	1.731
	150	423	3.2133	5.2179	1.62384	1.727
	175	448	3.2156	5.2220	1.62386	1.723
	200	473	3.2182	5.2263	1.62401	1.719
Mg + 0.55 pct Sn	25	298	3.2025	5.2010	1.62404	1.775
Elec. conc. = 2.008	38	311	3.2036	5.2033	1.62423	1.773
	50	323	3.2044	5.2042	1.62407	1.771
	63	336	3.2047	5.2062	1.62453	1.770
	75	348	3.2054	5.2086	1.62429	1.770
	88	361	3.2067	5.2084	1.62425	1.767
	113	386	3.2080	5.2122	1.62473	1.765
	125	398	3.2096	5.2151	1.62485	1.762
	138	411	3.2105	5.2150	1.62435	1.761
	163	436	3.2134	5.2190	1.62414	1.757
	175	448	3.2132	5.2195	1.62442	1.757

* All percentages are atomic.
† Ref. 2.

basis of the theory proposed by Raynor and Hume-Rothery, it is therefore to be expected that there is a threshold temperature for magnesium beyond which a further increase in temperature will result in an increase in the c/a ratio. The threshold temperature would be dependent upon the electron concentration of the alloy being heated. That this expectation is fulfilled is clearly shown by the data in Table I. For better visualization of the sharpness of the threshold temperature, Figs. 3, 4, and 5 reproduce the data for three of the alloys studied. For the Mg + 0.18 pct Ag and Mg + 0.10 pct Sn, the threshold temperature is higher than room temperature and consequently the initial invariance of c/a with temperature can be seen. When 1.87 pct Al is added to magnesium, the threshold value has been more than reached by alloying. The experimental curve was therefore linearly extrapolated to a c/a value of 1.62364 and the threshold temperature calculated to be 131°K.

Fig. 2 shows the dependence of the threshold temperature on the electron concentration of the metal where the electron concentration is calculated by means of the relative effective valencies.[1] The value in the Mg-Al series at 298°K is also obtained from the previous paper. These values of threshold temperature below 298°K were determined by extrapolation as illustrated in Fig. 5.

The point for Mg + 0.46 pct Ag requires some explanation. This alloy has an electron concentration of 1.994, and from the relationship established by the other alloys would be expected to have a threshold temperature of about 520°K. Since, with the experimental setup used, the maximum temperature obtainable was 473°K, it would be expected that no change in c/a with temperature would be observed. This is the case, as shown by the data in the table. The arrow attached to the point for this alloy in

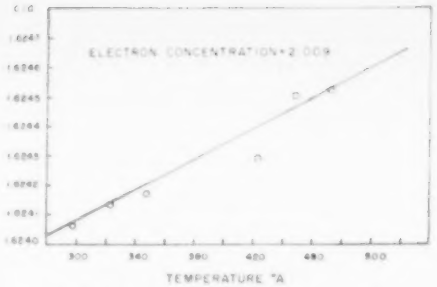

Fig. 5—Effect of temperature on the c/a ratio of Mg + 1.87 pct Al

Fig. 2 therefore means that the threshold temperature is higher than 473°K.

From Fig. 2 it is seen that the threshold value of electron concentration is about 2.012 at absolute zero. Once the threshold value is reached, either by temperature or by electron concentration, a further rise of 125°K is equivalent in effect to a further increase of 0.01 electrons per atom.

References

[1] R. S. Busk: *Trans.* AIME (1950) **188**, p. 1460; JOURNAL OF METALS (December 1950).

[2] G. V. Raynor and W. Hume-Rothery: *Journal* Inst. Metals (1939) **65**, p. 379.

[3] F. Foote and E. R. Jette: *Physical Review* (1940) **58**, p. 81.

[4] G. V. Raynor: *Proc.* Royal Soc. (1940) **174A**, p. 457.

[5] G. V. Raynor: *Proc.* Royal Soc. (1942) **180A**, p. 107.

[6] W. Hume-Rothery and G. V. Raynor: *Proc.* Royal Soc. (1940) **177A**, p. 27.

Technical Note

Observations on the Occurrence of Ti_2X Phases

by W. Rostoker

LAVES and Wallbaum[1] and more recently Duwez and Taylor[2] have reported on the occurrence of a family of intermediate phases having the composition Ti_2X, where X may be Cu, Ni, Co, Fe, or Mn.

W. ROSTOKER is Research Metallurgist, Metals Research Dept., Armour Research Foundation of Illinois Institute of Technology, Chicago.

TN 105E. Manuscript, Dec. 3, 1951.

The structure of these phases is face-centered cubic, and the unit cell is very large, containing 96 to 112 atoms. Some dispute exists as to whether all of these phases really exist at the reported compositions. Karlsson[3] denies the existence of the phase Ti_2Cu. Recent work on the Ti-Fe system[4,5] using iodide titanium failed to confirm the existence of Ti_2Fe.

These points of difference seemed to warrant a re-examination of this whole family. Karlsson[3] reports that the accidental contamination with oxygen of a titanium alloy containing 50 pct (atomic) Cu yielded a new structure which was face-centered cubic and isomorphous with Fe_4W_2C. The close similarity of the structure of this carbide and of the oxide phase in the Ti-Cu-O system with that of the Ti_2X phases suggests that inadvertent oxygen contamination is the source of apparent disagreements.

A preliminary test of this idea was performed by preparing three alloys having the composition Ti_2Fe, Ti_2Fe_2O, and Ti_2Fe_2O. Iodide titanium and a very pure grade of TiO_2 were used as melting stock. An argon arc melting furnace described elsewhere[6] was used. Powder patterns were taken of the homogenized alloys in a 14 cm Debye-Scherrer camera using filtered CuK_α radiation.

The Ti_2Fe alloy gave predominantly the structure of the TiFe phase[7] and extra lines belonging either to α or to β titanium, depending on the heat treatment. Both the Ti_2Fe_2O and the Ti_2Fe_2O alloys yielded single-phase patterns which were almost identical to that reported by Duwez and Taylor[7] for the Ti_2Fe phase. A comparison of the diffraction lines is shown in Table I. It appears, therefore, that a ternary phase exists in the Ti-Fe-O system which permits a broad replacement of iron atoms by titanium atoms.

A more comprehensive survey was made next. The following alloys were prepared: Ti_2Cu, Ti_2Cu_2O, Ti_2Ni, Ti_2Ni_2O, Ti_2Co, Ti_2Co_2O, Ti_2Mn, and Ti_2Mn_2O. A summary of structures and lattice parameters of the phases found is given in Table II.

Table I. Comparison of Interplanar Spacings for Ti_2Fe_2O and Ti_2Fe Reported Elsewhere[7]

hkl	d_{hkl}, Å Ti_2Fe_2O	d_{hkl}, Å Ti_2Fe*	hkl	d_{hkl}, Å Ti_2Fe_2O	d_{hkl}, Å Ti_2Fe*
311	2.500		842	1.230	1.234
422	2.290	2.31	953,771,733	1.132	1.136
440,430	2.250		862	1.106	1.109
431	2.205		666	1.084	1.087
531,511	2.161	2.17	775	1.016	1.019
440	1.966	2.00	955,971	0.9897	0.9898
442,600	1.872	1.88	882	0.9858	0.9847
622	1.785	1.72	886	0.9652	0.9697
444	1.619	1.63	10.6.2	0.9521	0.9563
551,711	1.572	1.58	12.00,884	0.9397	0.9423
553,731	1.478	1.472	11.11,777	0.9300	0.9330
620,642	1.393	1.41	10.6.4, 12.2.2	0.9146	0.9172
731	1.373	1.392	10.82	0.8711	0.8726
821,742	1.293		11.11,11.33	0.8633	0.8648
660,822	1.329	1.334	11.73,12.31	0.8440	0.8456
555,751	1.303	1.309	13.33,993	0.8294	0.8277
840	1.270		14.20,10.86	0.7904	0.7997
911,753	1.250	1.242			

* Errors ref. 7

Table II. Crystal Structure Data for Ti_2X and Ti_2X_2O Compositions

Composition	Structure and Lattice Parameters		
Ti_2Cu	f.c.c.	Fe_4W_2C type	$a = 11.24$Å
Ti_2Cu_2O	f.c.c.	Fe_4W_2C type	$a = 11.47$Å
Ti_2Ni	f.c.c.	Fe_4W_2C type	$a = 11.28$Å
Ti_2Ni_2O	f.c.c.	Fe_4W_2C type	$a = 11.36$Å
Ti_2Co	Predominantly cubic, $MgCu_2$ type cf. Wallbaum and Witte[1]		$a = 6.73$Å $a = 6.691$Å
Ti_2Co_2O	f.c.c.	Fe_4W_2C type	$a = 11.295$Å
Ti_2Fe	Predominantly b.c.c. TiX type cf. Duwez and Taylor[7]		$a = 2.975$Å $a = 2.969$Å
Ti_2Fe_2O	f.c.c.	Fe_4W_2C type	$a = 11.275$Å
Ti_2Fe_2O	f.c.c.	Fe_4W_2C type	$a = 11.15$Å
Ti_2Mn	Predominantly β titanium solid solution		
Ti_2Mn_2O	f.c.c.	Fe_4W_2C type	$a = 11.29$Å

The Ti_2Cu and Ti_2Cu_2O compositions gave almost identical patterns. This is in disagreement with Karlsson[3] but as regards the Ti_2Cu structure, is in agreement with others.[1,2] The Ti_2Ni and Ti_2Ni_2O compositions yielded similar results. It appears, therefore, that under certain conditions the Fe_4W_2C type structure can tolerate a complete evacuation of oxygen atoms. The Ti_2Co_2O composition yielded another member of this family, but the Ti_2Co composition showed neither this structure nor that reported[1] for the TiCo phase. The predominant structure for the composition was found to agree with that reported by Wallbaum and Witte[1] for the alloy containing 35 atomic pct Ti. The Ti_2Mn_2O composition has a structure isomorphous with Fe_4W_2C but the Ti_2Mn composition gave a pattern of β titanium only.

At the time of writing, a further note by Karlsson appeared,[8] which briefly describes studies of the oxide ternary phases chronologically prior to the work reported here. In general, the results presented agree closely, although Karlsson was apparently unconcerned with the Ti_2X problem. This note states that no Ti_2Cr_2O or Ti_2V_2O phases exist.

In summary, the family of structures isomorphous with Fe_4W_2C may be recognized as having the provisional composition Ti_2X_2O to Ti_2X_2O. The occurrence depends on the metal X. When X is Cu or Ni this structure occurs with or without oxygen. When X is Co, Fe, or Mn, the structure occurs with oxygen, but not without. Apparently from Karlsson's work and from other work on the pure binary systems, this structure does not occur under any conditions when X is Cr or V.

References

[1] F. Laves and H. J. Wallbaum: *Naturwissenschaften* (1939) **27**, p. 674.

[2] P. Duwez and J. Taylor: *Trans.* AIME (1950) **188**, p. 1173; JOURNAL OF METALS (September 1950).

[3] N. Karlsson: *Journal* Inst. Metals (1951) **79**, p. 391.

[4] R. J. Van Thyne, H. D. Kessler, and M. Hansen: A.S.M. (To be published).

[5] H. W. Worner: *Journal* Inst. Metals (1951) **79**, p. 173.

[6] M. Hansen, H. D. Kessler, and D. J. McPherson: *Trans.* A.S.M., Preprint No. 4 (1951).

[7] Unpublished work, Massachusetts Institute of Technology.

[8] H. J. Wallbaum and H. Witte: *Ztsch. Metallkunde* (1939) **31**, p. 185.

[9] N. Karlsson: *Nature* (Sept. 29, 1951), p. 558.

Crystal Structure of Ti_3Sn

by Paul Pietrokowsky

THE formation of intermediate phases in the solid state reaction of titanium with silicon, germanium, and tin (of subgroup 4*B* in the periodic table) was the subject of a recent paper.[1] Further investigation of the system Ti-Sn revealed the presence of a new compound on the titanium-rich side of this phase diagram. Metallographic evidence indicated that this new phase was situated very close to 75 atomic pct Ti. The present work is concerned with the crystal structure of the intermediate phase Ti_3Sn.

Iodide-process titanium metal, furnished by the New Jersey Zinc Co., was used in this investigation. The metallic tin was received in powder form from Charles Hardy Inc., New York; its purity was 99.80 pct. The titanium rod was machined into small cups 1 cm in diam and about 1.5 cm in height. The tin powder was compacted, melted, and then placed in the titanium cups and alloyed by electric arc melting in a helium atmosphere. The alloys, weighing approximately 8 g, were sealed in evacuated quartz tubes and homogenized at 1030°C for 5 days. This isothermal heat treatment was terminated by a water quench from the soaking temperature. Filings of the alloyed pellets were sealed in evacuated quartz bulbs and quenched from 1030°C into liquid argon.

A 14.32 cm Debye Scherrer X-ray camera was used for the powder diffraction study. The copper radiation was filtered. X-ray diffraction data for the compound Ti_3Sn are given in Table I. The data were indexed on the basis of a hexagonal lattice. Good agreement between observed and calculated values of the square of the reciprocal interplanar spacings was obtained with the following expression:

$$(1/d)^2 = 0.03810\,(h^2 + hk + k^2) + 0.04410\,(l^2)$$

Unit cell parameters were calculated by the method of least squares from the reflections (20.3), (22.2), (40.1), and (42.1); $a_o = 5.916 \pm 0.004$A, $c_o = 4.764 \pm 0.004$A, and $c_o/a_o = 0.805$.

The relatively small size of the unit cell allowed the unambiguous indexing of most of the reflections from planes of large spacing. An inspection of the assigned indices (Table I) reveals the absence of $(hk.l)$ reflections when $l \neq 2n$. A systematic absence of this type leads to the space group C $6/mmc$ or one of its subgroups. Assuming, for a first approximation, a linear increase in the density of titanium with the addition of tin, it follows that there are two stoichiometric molecules of Ti_3Sn per unit cell. The density calculated from X-ray measurements is 5.194 g cm^{-3}. At this point it became clear that Ti_3Sn might be isomorphous with Mg_3Cd. The 6 Ti and 2 Sn atoms were placed in the following positions of space group D^4_{6h}, C $6/mmc$:

$$6\,\text{Ti in } (h):\ x\,2x\,{}^1\!/_4;\ 2\bar{x}\,\bar{x}\,{}^1\!/_4;\ x\,\bar{x}\,{}^1\!/_4;\ \bar{x}\,2\bar{x}\,{}^3\!/_4;$$
$$2x\,x\,{}^3\!/_4;\ \bar{x}\,x\,{}^3\!/_4;\ \text{with } x = 5/6$$

$$2\,\text{Sn in } (c):\ 1/3\ 2/3\ {}^1\!/_4;\ 2/3\ 1/3\ {}^3\!/_4.$$

Table I. X-Ray Powder Diffraction Data for Ti_3Sn Filtered Copper Radiation

hk.l	$(1/d)^2$ Observed A^{-2}	$(1/d)^2$ Calculated A^{-2}	Relative Intensity Observed	Relative Intensity Calculated
10.0	0.0324	0.0321	w	99
10.1	0.0823	0.0823	m	244
11.0	0.1144	0.1143	m	108
20.0	0.1532	0.1524	s	257
00.2	0.1758	0.1763	s	234
20.1	0.1967	0.1963	vs	1000
10.2	0.2134	0.2144	vw	23
21.0	0.2674	0.2667	vw	16
11.2	0.2910	0.2906	w	54
21.1	0.3109	0.3109	w-m	73
20.2	0.3215	0.3287	m	139
22.0	0.4578	0.4572	m	152
20.3	0.5489	0.5491	s	244
40.0	0.6107	0.6096	w	25
22.2	0.6324	0.6325	s	179
40.1	0.6541	0.6537	m	127
00.4	0.7046	0.7052	w	25
40.2	0.7842	0.7858	w	33
20.4	0.8539	0.8576	w	31
21.4	0.9745	0.9719	vw	5
41.2		0.9764		19
50.1		0.9866		7
40.3	1.0018	1.0007	m	79
42.0	1.0682	1.0667	w	25
42.1	1.1099	1.1107	s	154
22.4	1.1595	1.1623	m-d	102
42.2	1.2487	1.2430	s-d	54
20.5		1.2543		81
21.5	1.3708	1.3686	m-d	17
60.0		1.3645		61

vs = very strong, s = strong, m = medium, w-m = weak medium, w = weak, vw = very weak, d = diffuse line.

P. PIETROKOWSKY, Junior Member AIME, is Research Engineer, Jet Propulsion Laboratory, California Institute of Technology, Pasadena, Calif.

Discussion on this paper, TP 3241E, may be sent, 2 copies, to AIME by April 1, 1952. Manuscript, Sept. 28, 1951. New York Meeting, February 1952.

Intensity calculations were made using the formula:

$$I = \text{Constant } p \left| \Sigma f_i e^{2\pi i(hx_i + ky_i + lz_i)} \right|^2 \left(\frac{1 + \cos^2 2\theta}{\sin^2 \theta \cos \theta} \right)$$

Calculated relative intensities are listed in Table I. This table presents observed reflections; extinctions required by the space group symmetry have been omitted together with 35 calculated very, very weak reflections. Broadening of the X-ray pattern, coupled with high background is responsible for the difficulty in observing the very weak reflections. The diffraction lines at large Bragg angles were quite diffuse.

Ti_3Sn is isomorphous with MgCd, DO_a type; this crystal structure was determined by Dehlinger.[2] The structure consists of layers of atoms in the sequence *ABABAB*, each layer having a ratio of 3 Ti to 1 Sn atom. This crystallographic arrangement can be considered as a super unit cell of the *A*3 type, magnesium structure. The DO_a structure is composed of four *A*3 type unit cells, so arranged that the new unit cell has twice the original axial length a_o, thus halving the original c/a_o. In addition, it is necessary for the titanium and tin atoms to assume definite crystallographic positions.

The nearest neighbors to a tin atom in (*c*) are: 6 Ti atoms at 2.94A, 6 Ti atoms at 2.96A, and 6 Sn atoms at 4.16A. The environment of a titanium atom located in (*h*) is 2 Sn atoms at 2.94A, another pair of Sn atoms at 2.96A, and two pairs of Ti atoms at 2.94 and 2.96A, respectively.

Compounds known to be isomorphous with Ti_3Sn are Mg_3Cd,[3] $MgCd_3$,[4] Ni_3Sn,[5] Co_3Mo,[6] Co_3W,[7,8] Hg_3Li,[9] Mn_3Sn_a,[10] Ti_3Pb,[11] Ti_3Sb,[12] Ni_3In,[13] and Fe_3Sn.[14]

Acknowledgment

This work was done at the Jet Propulsion Laboratory, California Institute of Technology, under contract number DA-04-495-ORD-18 with the Army Ordnance Corps, Washington. The author wishes to thank this agency for the permission to publish the results of this investigation.

References

[1] P. Pietrokowsky and P. Duwez: The Crystal Structure of Ti_5Si_3, Ti_5Ge_3 and Ti_5Sn_3. *Trans.* AIME (1951) **191**, pp. 772-773; JOURNAL OF METALS (September 1951).

[2] U. Dehlinger: X-Ray Investigation of the System Cadmium-Magnesium. *Ztsch. anorg. allgem. Chem.* (1930) **194**, pp. 223-238.

[3] P. Rahlfs: Crystal Structure of Ni_3Sn. *Metallwirtschaft* (1937) **16**, pp. 343-345.

[4] M. Babich, E. Kislyakova, and Y. S. Umanskii: The Intermetallic Compound of the System Molybdenum-Cobalt. *Tech. Physik.* (USSR) (1938) **5**, pp. 193-194.

[5] M. Babich, E. Kislyakova, and Y. S. Umanskii: The Intermetallic Phases of the System Wolfram-Cobalt. *Journal Tech. Physics* (USSR) (1938) **8**, pp. 181-192.

[6] A. Magneli and A. Westgren: X-Ray Investigation of Cobalt-Wolfram Alloys. *Ztsch. anorg. allgem. Chem.* (1938) **238**, pp. 268-272.

[7] E. Zintl and A. Schneider: X-Ray Analysis of Lithium Amalgams. *Ztsch. Elektrochemie* (1935) **41**, pp. 771-774.

[8] H. Nowotny and K. Schubert: The System Manganese-Tin. *Ztsch. Metallforschung* (1946) **1**, pp. 17-23.

[9] H. Nowotny and J. Pesl: Investigations of the System Titanium-Lead. *Monatschefte für Chemie und verwandte Teile anderer Wissenschaften* (1951) **82**, pp. 344-347.

[10] H. Nowotny, R. Funk, and J. Pesl: Crystal Chemical Investigation of the Systems Manganese-Arsenic, Vanadium-Antimony, and Titanium-Antimony. *Monatshefte für Chemie und verwandte Teile anderer Wissenschaften* (1951) **82**, pp. 513-525.

[11] *Structure Reports for 1947-48*. Vol. II, pp. 132, 147. N. V. A. Oosthoeks Uitgevers Mij, Utrecht.

Technical Note

Observations on the Lattice Parameters of the Alpha Solid Solution in the Titanium-Aluminum System

by W. Rostoker

PART of a program of research on the Ti-Al system[1] involved a study of the lattice parameters of the titanium-rich α solid solution, which has a hexagonal close-packed structure. For this work, a 14 cm Debye-Scherrer powder camera and filtered CuK$_\alpha$ radiation was used. For each pattern, the parameters were calculated by a least squares solution of the five strongest high angle lines. This provides an accuracy of ± 0.003A or better.

W. ROSTOKER is Research Metallurgist, Metals Research Dept., Armour Research Foundation of Illinois Institute of Technology, Chicago.

TN 107E. Manuscript, Dec. 3, 1951.

The results are shown graphically in Fig. 1. It will be seen that an unusual change of slope occurs in the curve for the C parameter at high aluminum contents. Such anomalous changes in slope have been recorded by Raynor[2] for several magnesium-rich solid solutions. The effects were interpreted in terms of a special contribution to the lattice distortion due to factors of electronic origin predicted by Jones.[3] Jones' theory, in substance, suggested that an unusually large expansion of the lattice would begin when the electron per atom concentration in the alloy was increased to a value at which an overlap just began from one Brillouin zone to another. Con-

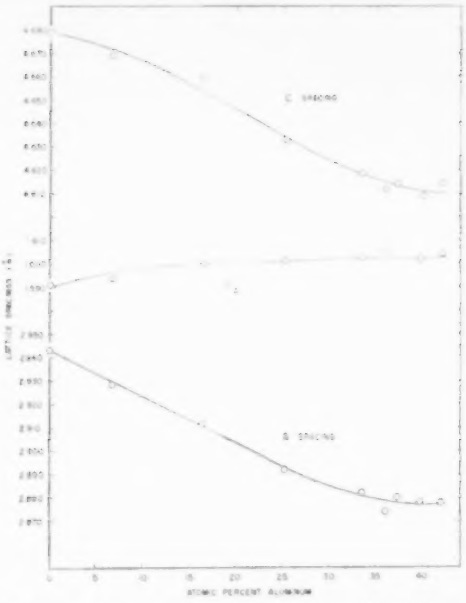

Fig. 1—Effect of aluminum on the lattice parameters of Ti-Al alloys.

zone is formed by the {1012} and {1120} planes. The inscribed sphere of maximum radius touches the {1012} faces and corresponds with 3.59 electrons per atom. Thus, pure titanium exhibits a pronounced overlap on the $\{10\bar{1}2\}$ faces. The addition of trivalent aluminum serves to reduce the electron to atom ratio. At the point of disappearance of this overlap, the interplanar spacing of the $\{10\bar{1}2\}$ planes may be expected to exhibit a discontinuous change in trend. For the case of decreasing aluminum content (direction of increasing overlap) the change should be in the nature of a superimposed expansion.

Fig. 2 shows that the plot of calculated spacings of $\{10\bar{1}2\}$ planes as a function of aluminum content is in qualitative agreement with expected behavior. Certain discrepancies appear, however. The disappearance of the overlap may be expected to occur at 41 atomic pct Al, whereas the experimental data indicate a change in slope at about 35.8 atomic pct Al. This derives from the calculation that the overlap corresponds to 3.59 electrons per atom, which in turn is based on lattice constants for titanium which have since been revised. Using Clark's[5] more accurate data, however, introduces changes only in the fourth significant figure for the electronic concentration. It appears, therefore, that an increase of about 0.5 electrons per atom is necessary to actually force the overlap to occur. This is not unreasonable, since the diffracted intensities from the {1012} planes are among the strongest in the Debye patterns.

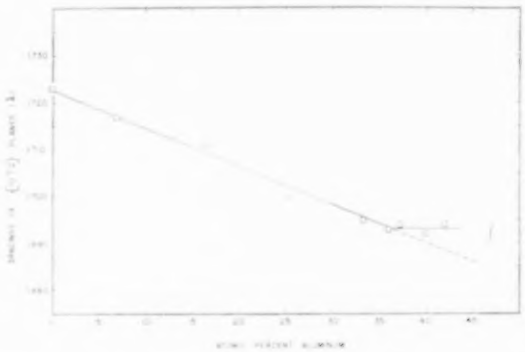

Fig. 2—Effect of aluminum on the interplanar spacing of the {1012} planes.

versely, a lattice contraction would occur if the electronic concentration was decreased by alloying to a point such that an existing overlap was caused to disappear. The expansion or contraction would actually be imposed on the spacings of the planes which demarcate the Brillouin zone in the direction of the overlap. This effect would be reflected in the c and a values for the structure cell.

Examination of the data herein presented indicates that the titanium-rich α phase is an example of this phenomenon, although as yet no other evidence exists which suggests that electronic effects are of significance in the alloying behavior of titanium.

An analysis of first and second Brillouin zones for hexagonal close-packed structure having the lattice parameters of titanium has been published by Berry, Waldron, and Raynor.[4] If titanium, from its chemical behavior, may be assumed to be tetravalent, the second Brillouin zone is of particular interest. This Further, the Fermi "sphere" which makes contact with the {1012} faces has already overlapped the faces of the inner zone and may therefore not be spherically symmetrical any longer. Such distortion of the outer electronic energy surface may itself account for the difference between calculated and observed electron concentrations.

The data presented seem to indicate that electronic factors are significant in the stability of the α phase. It may be noted further that maximum solubility occurs very shortly after the overlap has disappeared.

References

[1] E. Bumps, H. Kessler, M. Hansen: Unpublished.

[2] G. V. Raynor: *Proc.* Royal Soc. (1940) **74**, A1, p. 457; (1942) **80**, A1, p. 107.

[3] H. Jones: *Proc.* Royal Soc. (1934) **47**, A1, p. 400.

[4] R. L. Berry, M. B. Waldron, G. V. Raynor: *Research* (1949) **2**, p. 195.

[5] H. T. Clark: *Trans.* AIME (1949) **185**, p. 588; JOURNAL OF METALS (September 1949).

Mechanism of the Reduction Of Oxides and Sulphides to Metals

by Carl Wagner

AT elevated temperatures, most metals react with oxygen, sulphur, or halogen rather rapidly, although a coherent layer of the reaction product is formed and separates the two reactants from each other. The reaction proceeds, since one of the reactants or both dissolve and diffuse across the reaction product. In many cases the rate is diffusion-controlled as is indicated by the validity of the parabolic rate law of Tammann[1] and Pilling and Bedworth.[2] Mott and Gurney[3] have suggested that diffusion processes also play an important part in the case of reduction reactions. This is confirmed by observations reported below. In general, however, the rate of reduction reactions is determined not exclusively by diffusion processes.

Reduction of Silver Sulphide

Above 179° C silver reacts with liquid sulphur very rapidly. Since the volume of silver sulphide is much greater than that of the equivalent amount of silver, a coherent layer of silver sulphide is formed in accordance with a rule established by Pilling and Bedworth. According to Wagner[4] silver ions and electrons migrate from the Ag-Ag$_2$S interface across the silver sulphide layer to the Ag$_2$S-S interface where the following chemical reaction takes place:

$$2\,Ag^+ + 2\,e^- + S \rightarrow Ag_2S$$

If silver sulphide is reduced by means of hydrogen, the equivalent volume of the reaction product, silver, is less than that of the initial substance. Accordingly, no coherent layer of silver is formed. Instead, fine filaments of silver grow from the silver sulphide surface into the ambient gas. This phenomenon has been investigated by many authors, especially by Kohlschütter,[5] who has also reviewed previous literature. Kohlschütter has interpreted the observed phenomena by migration of "silver" dissolved in silver sulphide. According to Wagner,[4] silver ions and electrons are the migrating particles. The sequence of consecutive steps involved in the reduction of silver sulphide is shown in Fig. 1. Everywhere at the silver sulphide surface, hydrogen reacts with sulphur so that excess silver ions and electrons are formed, which migrate at random until they are captured by a nucleus of metallic silver. If such a nucleus lies on the surface and material is furnished only from the base, the original nucleus is pushed outward and thus a filament grows.

Removal of sulphur and formation of metallic silver may also take place at different points when silver sulphide is reduced by copper. The reaction is usually formulated as:

$$Ag_2S + 2\,Cu \rightarrow Cu_2S + 2\,Ag$$

but the actual reaction products are silver and a solid solution of the two sulphides. Primarily, excess silver and electrons dissolved in silver sulphide are formed. After a certain degree of supersaturation has been reached, nuclei of metallic silver may form. If, however, a silver foil is in contact with the silver-sulphide phase, as is shown in Fig. 2, silver ions and electrons will migrate to the Ag$_2$S-Ag interface where they are captured. To confirm this scheme, a composite sample, with the geometry shown in Fig. 2, was made by pressing silver sulphide tablets 0.6 cm in diam and 0.4 cm high together with a copper cylinder and a silver foil in crucibles of iron, which does not react appreciably with silver sulphide at 400° C. After heating for 3 to 7 hr at 400° C, the specimens were cut normal to the phase boundaries. It was found that the thickness of the silver foil had increased from 0.01 cm as initial value to a maximum value of 0.06 cm. In the interior of the silver sulphide tablets only traces of metallic silver were observed.

These observations show clearly that silver ions and electrons may migrate over distances of several millimeters before they form metallic silver.

Reduction of Cuprous Sulphide by Iron

The behavior of cuprous sulphide is very similar to that of silver sulphide, since the lattices of the high temperature modifications are identical, but in Cu$_2$S there is a variable deficit rather than an excess of metal. To investigate the displacement of copper by iron, cuprous sulphide powder covered by a copper foil was pressed in iron crucibles and heated up to 800° C for 3 to 7 hr. The thickness of the copper foil increased from an initial value of 0.005 cm to a maximum value of 0.029 cm. In the interior of the

C. WAGNER, Member AIME, is Visiting Professor of Metallurgy, Dept. of Metallurgy, Massachusetts Institute of Technology, Cambridge, Mass.

Discussion on this paper, TP 3149D, may be sent, 2 copies, to AIME by April 1, 1952. Manuscript received Aug. 10, 1951. New York Meeting, February 1952.

cuprous-sulphide pellets (about 0.3 cm high), only traces of metallic copper were found. These observations may be interpreted in the same manner as in the case of the reduction of silver sulphide by copper.

Reaction Between Cuprous Sulphide and Cuprous Oxide

There has also been an investigation of the reaction:

$$Cu_2S + 2\,Cu_2O = 6\,Cu + SO_2$$

It might be expected that copper would be formed at the interface between cuprous sulphide and cuprous oxide. In this case, the reaction would come practically to a standstill because of the separation of the reactants, which have a very low solubility in metallic copper. Instead, copper dissolved in cuprous sulphide may be formed as the primary product and may migrate to points remote from the Cu_2S-Cu_2O interface where conditions for nucleation are favorable, see Fig. 3. Copper ions and electrons can also migrate in cuprous oxide,[7,8] but this variant is less likely because the diffusion rates in cuprous oxide are far less than those observed in cuprous sulphide.[9,10]

To confirm the scheme in Fig. 3, cuprous sulphide was pressed around a copper cylinder. The diameter of the copper cylinder was 0.192 cm, and that of the cuprous sulphide pellet 0.62 cm. The composite system was put in a quartz tube and loosely surrounded by finely powdered cuprous oxide, see Fig. 4. After heating in a gentle stream of carbon dioxide for 2 hr at 750°C, the composite cylinder was cut normal to its axis. It was found that the diameter of the inner copper cylinder had increased from 0.192 to 0.241 ±0.010 cm. Thus, migration of copper as assumed in Fig. 3 has been confirmed. In addition, some copper was found near the Cu_2S-Cu_2O interface. This is not contradictory to the foregoing considerations, since formation of new nuclei, especially at points involving high supersaturation with respect to copper, cannot be ruled out.

Reduction of Wustite

Richardson and Dancy[11] and Gellner and Richardson[12] built up a film of wüstite on iron in a controlled H_2O-H_2 atmosphere at 900°C. Upon decreasing the water vapor pressure and thus reducing gradually the wüstite film at 900°C, it was found that the thickness of the inner iron core had increased, rather than that metallic iron was formed at the outer surface. When oxygen is removed by hydrogen from the outer surface, iron ions and electrons migrate backward to the iron-wüstite interface.[13,14] If, however, the wüstite film is reduced at 700°C, spongy iron is formed at the outer surface of the oxide.[15]

Discussion

From the foregoing observations the following conclusions may be drawn with regard to the reduction of oxides in metallurgical processes without the presence of metallic nuclei.

In cuprous oxide, wüstite, cobalt oxide, and nickel oxide, the metal/oxygen ratio is always somewhat less than the ideal stoichiometric ratio because of the presence of cation vacancies and cations in a higher valence state, i.e., Cu^{++}, Fe^{+++}, Co^{+++}, Ni^{+++} (= electron holes).[7,8,16,17] Thus in the first stage of a reduction process, an increase of the metal/oxygen ratio takes place by filling cation vacanies and decreasing the number of cations in higher valence states. According to Dünwald and Wagner[18,19] and Anderson[20] the change in the metal/oxygen ratio may be followed

Fig. 1 (right) — Reduction of silver sulphide by hydrogen: $Ag_2S + H_2 = 2\,Ag + H_2S$

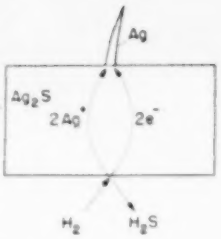

Fig. 2 (below) — Reduction of silver sulphide by copper: $Ag_2S + 2\,Cu = 2\,Ag + Cu_2S$

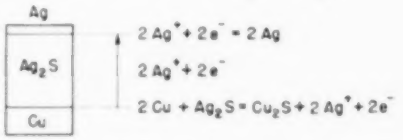

by measuring the electrical conductivity. In contrast, zinc oxide and cadmium oxide contain excess metal even in oxygen of atmospheric pressure, possibly in the form of cations on interstitial sites and quasi-free electrons.[21] In these oxides, the first stage of a reduction process leads to an increase of the concentration of cations and electrons.

After a certain induction period the oxide phase will become supersaturated with respect to metal. Since the reducing agent acts on the surface of the oxide, supersaturation at the surface will be higher than in the bulk of the oxide, and accordingly spotwise formation of metallic nuclei will occur preponderately at the surface after a sufficient supersaturation has been reached. In the vicinity of metallic nuclei, supersaturation will sharply decrease, and diffusion of cations and electrons towards the metal-oxide interface will take place. Eventually, anions may also migrate. Supersaturation along the whole surface will be relatively small after a sufficient number of nuclei has been formed. Subsequently no further nuclei will appear unless special conditions lead to a breakdown of the growth of the primary nuclei. Disregarding the latter possibility and migration of anions, there is quasi-steady state with the following consecutive reactions: 1—Phase-boundary reaction at the surface of the oxide with the reducing agent by which either excess cations and electrons are formed, or cation vacancies and electron holes are filled up. 2—Diffusion of cations and electrons toward the base of metallic nuclei in contact with oxide. 3—Phase-boundary reaction at the interface between oxide and metal, i.e., transfer of cations and electrons into the metallic phase.

The overall reaction rate is determined by the area of the initial surface of the ore, the local composition of the gas phase, the rate constants of the

Fig. 3 — Scheme for the reaction $Cu_2S + 2\,Cu_2O = 6\,Cu + SO_2$

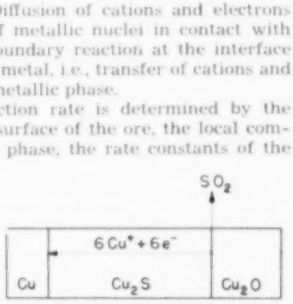

Fig. 4 — Composite sample for the investigation of the reaction $Cu_2S + 2\,Cu_2O = 6\,Cu + SO_2$

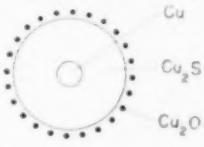

aforementioned elementary reactions, diffusion coefficients, the average distance over which cations and electrons have to migrate before they are captured by a metallic nucleus, and the area of the interface between oxide and metal. Diffusion path and area of the interface between oxide and metal in turn depend on the interplay of the aforementioned elementary reactions and nucleation. Hence it is recognized that a complete interpretation of the overall reaction rate requires a detailed knowledge of all elementary reactions and nucleation as well.

In many cases, the gas composition varies considerably both along and normal to the flow direction. Then the transport and diffusion processes in the gas phase must also be taken into account.

Frequently, only one or two of the aforementioned consecutive reactions will be controlling factors after steady-state conditions have been reached. But even then the degree of dispersion of the metallic phase and other important geometrical factors will depend on the interplay of the various reactions enumerated above. For any further theoretical analysis, more basic information about phase boundary reactions is needed.

In the case of the reaction between carbon monoxide and wüstite, the rate necessarily depends not only on the partial pressures of carbon monoxide and carbon dioxide, but also on the Fe/O ratio of the solid phase. As shown especially by Darken and Gurry,[1] there is a well-defined Fe/O equilibrium ratio for any given CO_2/CO ratio of the gas phase. Thus, if for a given CO_2/CO ratio the actual Fe/O ratio of a sample equals the Fe/O equilibrium ratio, the reaction rate will be zero. If the actual Fe/O ratio is greater than the equilibrium ratio, the sample will take up oxygen. Conversely, if the actual Fe/O ratio is less than the equilibrium ratio, oxygen will be removed. This statement can be made regardless of any details of the reaction mechanism and shows clearly that the net rate of the reaction:

$$CO + O \text{ (in wüstite)} \rightarrow CO_2$$

depends decisively on the Fe/O ratio of the solid phase.

The Fe/O ratio in turn determines the concentration of cation vacancies and trivalent iron ions in wüstite. Consequently, in a detailed analysis, not only the collisions between CO and CO_2 molecules and the wüstite surface as a whole must be considered, but also the role of cation vacancies, trivalent iron ions, and similar lattice defects. An analogous problem has been discussed recently in connection with the decomposition of nitrous oxide on zinc oxide as catalyst.[2]

Likewise, information is needed concerning the rate of the phase boundary reaction at the metal-oxide interface and its dependence on the metal/oxygen ratio of the oxide phase. In certain reactions, surface diffusion may play an important part besides diffusion in the interior of crystals.

Eventually, reduction can occur without diffusion if the reducing agent acts at the three-phase boundary at which gas, ore, and metal are in touch with each other. Reactions at three-phase boundaries have been discussed especially by Schwab and Pietsch.[3] A clear-cut proof, however, is difficult to obtain. Predominant formation of reaction products along such lines may also be due to short diffusion paths. In the reactions indicated in Figs. 1 and 3, a higher local reduction rate in the vicinity of three-phase border lines is to be expected if the diffusion rate and the nucleation rate are low. Thus, the importance of three-phase border lines remains, even if the contribution of reactions involving atoms only along such lines is negligible.

Summary

Reduction of oxides and sulphides to metals can be interpreted by the following consecutive reactions:

1—Removal of nonmetal everywhere at the surface of the oxide or sulphide, so that a solid solution of metal supersaturated with respect to metal is formed.

2—Formation of metallic nuclei, especially at the surface.

3—Diffusion of metal ions and electrons from the surface across oxide or sulphide to metallic nuclei (or diffusion of anions from the metal-compound interface to the outer surface and diffusion of electrons in the opposite direction).

4—Transfer of metal ions and electrons from oxide or sulphide to metal.

Migration of metal over distances of several millimeters has been observed in the following reactions: 1—reduction of silver sulphide by copper, 2—reduction of cuprous sulphide by iron, and 3—$Cu_2S + 2\,Cu_2O \rightarrow 6\,Cu + SO_2$.

References

G. Tammann: *Ztsch. anorg. allgem. Chem.* (1920) **111**, p. 78.

[1] N. B. Pilling and R. E. Bedworth: *Journal* Inst. Metals (1923) **29**, p. 529.

[2] N. F. Mott and R. W. Gurney: *Electronic Processes in Ionic Crystals*, p. 263. (1940) Oxford, Clarendon Press.

[3] C. Wagner: *Ztsch. physik. Chem. B* (1933) **21**, p. 25.

[4] C. Wagner: Diffusion and High Temperature Oxidation. *Atom Movements*, p. 153. (1951) Cleveland, A.S.M.

[5] H. W. Kohlschütter: *Ztsch. Elektrochem.* (1932) **38**, p. 345.

[6] C. Wagner and H. Hammen: *Ztsch. physik. Chem. B* (1938) **40**, p. 197.

[7] C. Wagner and K. Grünewald: *Ztsch. physik. Chem. B* (1938) **40**, p. 455.

[8] H. Braune and O. Kahn: *Ztsch. physik. Chem.* (1924) **112**, p. 270.

[9] H. Braune: *Ztsch. Elektrochem.* (1925) **31**, p. 576.

[10] C. Tubandt, H. Reinhold, and W. Jost: *Ztsch. anorg. allgem. Chem.* (1929) **177**, p. 253.

[11] F. D. Richardson and E. Dancy: Discussions of the Faraday Society (1948) No. 4, p. 230.

[12] H. Gellner and F. D. Richardson: *Nature* (1951) **168**, p. 23.

[13] T. P. Hoar: Discussions of the Faraday Society (1948) No. 4, p. 230.

[14] C. Wagner: *Ztsch. physik. Chem. B* (1933) **22**, p. 181.

[15] H. Dünwald and C. Wagner: *Ztsch. physik. Chem. B* (1933) **22**, p. 212.

[16] E. R. Jette and F. Foote: *Journal of Chemical Physics* (1933) **1**, p. 29.

[17] C. Wagner and E. Koch: *Ztsch. physik. Chem. B* (1936) **32**, p. 439.

[18] L. S. Darken and R. W. Gurry: *Journal* Amer. Chem. Soc. (1945) **67**, p. 1345.

[19] H. H. von Baumbach and C. Wagner: *Ztsch. physik. Chem. B* (1934) **24**, p. 59.

[20] H. H. von Baumbach and C. Wagner: *Ztsch. physik. Chem. B* (1933) **22**, p. 199.

[21] H. Dünwald and C. Wagner: *Ztsch. physik. Chem. B* (1934) **24**, p. 53.

[22] J. S. Anderson: Discussion of the Faraday Society (1948) No. 4, p. 163.

[23] C. Wagner: *Journal of Chemical Physics* (1950) **18**, p. 69.

[24] G. M. Schwab and E. Pietsch: *Ztsch. Elektrochem.* (1929) **35**, p. 573.

AIME OFFICERS

President—
Vice Presidents—

Vice President and Treasurer—

AIME STAFF

Secretary—
Ass't. Secretaries—

Ass't. to Secretary—
Ass't. Treasurer—

aime NEWS

Council of Section Delegates Amend Bylaws

In accordance with instructions from the Feb. 17, 1951 meeting of the Council of Section Delegates at St. Louis, the Executive Committee of AIME drafted amendments of Articles 6 and 10 of the AIME bylaws. In September and October, these amendments were submitted to the delegates who, by mail ballot, voted the adoption of the amendments. The amended Articles are:

Article 6—There shall be one regular annual meeting of the Council at the time of the annual winter meeting of the Institute. This meeting shall precede, by a day or so, the scheduled Board meeting.

Additional special meetings may be authorized by the Executive Committee of the Council.

Article 10—The current Executive Committee of the Council shall constitute the Nominating Committee for officers and members of the Executive Committee for the following year.

In selecting the nominees, the Committee shall consider the principal professional interests as well as the geographic location of the nominees and shall keep in mind the necessity for rotating the nominees for chairman, vice-chairman and secretary through the three branches of the Institute.

The report of the Nominating Committee shall be submitted at the annual meeting of the Council, at which time additional nominations will be received from the Council at large. The election of officers will be by written ballot either at the Council meeting or by letter ballot at some time before November 1. The elected officers and members of the Executive Committee shall assume office on November 15 for a one year term.

Following the approval of these amendments, the Executive Committee acted as the Nominating Committee and submitted a slate of Council officers for 1952 to the delegates. By letter ballot, the delegates elected the following officers of the Council for 1952: Chairman—Jack A. Crichton (North Texas); Vice-chairman—Allan T. Cole (Florida); and Secretary—Merten I. Signer (Colorado). The Executive Committee nominations included W. C. Leonard (North Pacific), W. K. Bock (Cleveland), W. W. Leonard (East Texas), and C. Evans, Jr. (Pa. Anthracite).

Metals Branch Conference To Be Held In Northwest

Plans have been completed with only details to be arranged for the first Metals Branch Conference in the Northwest. The two day meeting will be held jointly with the Industrial Minerals Div. on Friday and Saturday, May 9 and 10, 1952, at the Davenport Hotel in Spokane, Wash. For some time the metals activities in this area have been neglected. Expansion of metal producing and fabricating industries in Washington and neighboring states has brought sufficient interest to insure the success of such a meeting, which could become an annual affair.

A committee has been hard at work for several months. Nonferrous extractive metallurgy men will find an extensive program in the April issue of JOURNAL OF METALS. Sessions for iron and steel producers, physical metallurgists, and educators will make the Metals Branch picture complete. Metals Branch members residing in Washington, British Columbia, Oregon, Idaho, Montana, Wyoming, Nevada, and Utah, or who can be in the Northwest at this time should make plans now to attend.

A Metals Branch luncheon is planned for Friday and a dinner jointly with the Industrial Minerals Div. is planned for Saturday according to F. R. Morral, metallurgist with the metallurgical research div. of Kaiser Aluminum & Chemical Corp., P. O. Box 1451, Spokane, Wash., chairman of the organizing committee.

Organizers of the First Northwest Metals Branch Meeting who met in Spokane. Front Row: L. A. Grant, Day Mines Inc.; R. R. McNaughton, Consolidated Mining & Smelting Co.; W. G. Woolf, Sullivan Mining Co.; and F. C. Fedderson, Bunker Hill & Sullivan Mining & Concentrating Co. Standing: W. W. Staley, Idaho School of Mines, Chairman AIME Columbia Section; F. R. Morral, Kaiser Aluminum & Chemical Corp., Chairman of the Organizing Committee; J. P. Spielman, Washington State College; Kuno Doerr, Helena, Mont.

IMD Professional Consciousness Committee Submits Preliminary Report

Robert M. Brick, Chairman of the Institute of Metals Div., appointed a committee consisting of Clyde Williams, Albert J. Phillips, John H. Hollomon, and Walter A. Dean to study the subject of the professional consciousness of the metallurgist. The many phases of the subject made it necessary to limit the field considered, at least for the present, and the committee therefore devoted its attention to the services which should be offered by a society that fosters the professional consciousness of its members.

Preliminary consideration led to the conclusion that meetings could be improved by the formation within the IMD of groups in fields of current or anticipated future interest, for example, the field of high temperature alloys. Technical sessions composed of papers presented by those active in these fields would form part of annual and fall programs.

Thought was given to the influence the society should exert to persuade young men to enter the field of metallurgy and to encourage the professional development of the young metallurgist during the period following his graduation during which time he is becoming integrated into his business concern or group.

The committee discussed the subject of providing stimulation among the IMD members in the local sections and also that of correlating activity at the national with that at the local level.

The Committee realizes the important part a publication program plays in the activities of a professional society and has considered some of the problems that beset the publication program of any society in these times.

A progress report in which the proposals of the Committee are set forth has been prepared for the consideration of the Executive Committee of the IMD. Undoubtedly the Executive Committee will wish to submit some of the proposals to the AIME Board of Directors for their approval.

This condensation of the preliminary report is being published.

The Committee will welcome suggestions or comments on this subject. These should be sent to Walter A. Dean, chairman of the Professional Consciousness Committee.

Metals Branch Dinner Set

The Metals Branch dinner will be held in the Keystone Room of the Statler Hotel on Tuesday, February 19th at 7 p. m. Ladies are invited and the price of tickets will be $6.00. Business suits will be appropriate. An A La Carte cocktail party preceding the dinner will take place in the foyer of the Keystone Room at 6 p. m. The Toastmaster will be Carleton C. Long, Chairman of the Metals Branch Council and Director of Research, Dept., St. Joseph Lead Co. of Pa., Monaca, Pa. The Speaker of the evening will be John D. Sullivan, Assistant Director, Battelle Memorial Institute, Columbus, Ohio, and his subject is "*Metals' Contribution to the American Standard of Living.*"

C. G. Goetzel Addresses Powder Metallurgy Group

Powder metallurgists in the New York area met at the Brass Rail on Fifth Ave. to hear Dr. C. G. Goetzel, vice president, Sintercast Corp. of America, speak on *Powder Preparation*. R. P. Seelig, vice president, American Electro Metal Corp., was chairman for the dinner meeting, that was attended by 53 men.

Dr. Goetzel divided powder preparation into two phases: 1—Treatment of powder after manufacturing, and 2—powder treatment prior to molding. The first phase could be done best by the powder producers, while the second phase was the parts manufacturers' responsibility in order to meet requirements peculiar to him. The major exception is with cemented carbide and refractory powders, where powder manufacture and parts production is usually carried out by the same company. The speaker elaborated on various powder treatments for specific purposes, and then opened the discussion to the group.

Change of Address

When notifying AIME headquarters of a change of address, or of company position or affiliation, please mention the Branch of the Institute to which you belong—Mining, Metals, or Petroleum and your name and address to which publications and correspondence should be sent. Mark this "Publications address." This will make for a more expeditious handling of the change and will facilitate the preparation of various reports.

Obituaries

Hellmuth R. Brandenburg (Member 1948) died at Reno, Nev. on Nov. 29, 1950. Mr. Brandenburg was born in Stettin, Germany on Apr. 23, 1887 and attended the Royal Polytechnic College at Hannover. He came to the United States and was employed by the Cambria Steel Co., Johnstown, Pa. In 1919 he became chief chemist and plant operations manager for the Cowell Portland Cement Co. Mr. Brandenburg remained with this firm for approximately 23 years. He maintained his private practice and in 1942 was engaged as consultant for the magnesium branch, Idaho Maryland Mines Co.

J. Moore Samuel (Member 1916) died on Nov. 5, 1951. Mr. Samuel was born at Wrexham, North Wales in 1888. He attended the Royal School of Mines, London and graduated with the degree of A.R.S.M. in 1909. For two years he did post graduate work at the Copper Queen smelter in Arizona and was then made testing engineer. In 1916 he was made head of the investigation dept., Phelps Dodge Corp., for the company at the Copper Queen reduction works, Douglas, Ariz. He remained with this firm for several years and in 1935 opened his office as a consulting engineer. At the time of his death he was residing in California.

NECROLOGY

Date Elected	Name	Date of Death
1948	Hellmuth R. Brandenburg	Nov. 29, 1950
1936	Oscar A. Dingman	December, 1951
1947	Donald G. Lauck	May, 1951
1925	C. R. Millar	June 1951
1937	Kenneth Moodie	Unknown
1922	James H. Morley	Apr. 3, 1951
1908	F. B. Nold	Unknown
1928	Norman F. Robertson	August, 1951
1905	Benjamin F. Tillson	Dec. 4, 1951
1915	Albert L. Tourges	Dec. 19, 1951

Training of Extractive Metallurgists

Topics for the round table discussion on Training of Extractive Metallurgists at the EMD session on Monday, Feb. 18, 1952 at the AIME Annual Meeting include:

1—Do we need men trained in extractive metallurgy?
2—What jobs are to be filled by young metallurgy graduates?
3—What part of education is left for industry?
4—Does industry need or want graduate work for some of the graduates?
5—Is industry attempting to encourage young men to go into metallurgy?
6—Does the extractive metallurgy industry—particularly nonferrous—have a realistic hiring program?
7—Can metallurgy courses and textbooks be modernized?
8—Can industry help the professor to keep up with the times?

The discussion will be led by a panel of experts from industry, research, and education including: B. W. Gonser, J. C. Kinnear, Jr., B. M. Larsen, C. C. Long, R. R. McNaughton, W. O. Philbrook, R. Schuhmann, Jr., and A. W. Schlechten. The latter two are associate chairmen for the session.

Personals

FRANCIS R. FRARY

KENT R. VAN HORN

S. E. MADDIGAN

Francis R. Frary has retired as director of research for the Aluminum Co. of America. In 1950 he was awarded the James Douglas Metallurgical Medal by AIME. **Kent R. Van Horn** will succeed Dr. Frary as director of research. Dr. Van Horn has been associate research director. He joined Alcoa in 1929 as a research metallurgist in the aluminum research laboratories at Cleveland.

Alan R. Pels has joined the staff of the research dept. of Bridgeport Brass Co. where he will be employed as a research metallurgist.

J. C. Willey was recently appointed assistant to the president of Harbison-Walker Refractories Co., Pittsburgh. He has worked with the company in a variety of operating and executive positions since 1934.

Thomas N. Peck, director of the aluminum alloy div. of Vanadium Corp. of America, has been appointed deputy director of the aluminum and magnesium div. of the NPA.

Frederick W. Holshuher has been appointed controller of the Cerro de Pasco Corp., New York.

W. J. O'Connor, Sr., former Utah dept. manager, American Smelting & Refining Co., was elected president and general manager of the Independent Coal & Coke Co.

M. Nielsen has been elected an assistant vice-president of the Babcock & Wilcox Co., New York. His headquarters will be at Barberton, Ohio.

James T. Barnard was appointed assistant manager of the Detroit branch, Pittsburgh Crucible Div., Crucible Steel Co. of America. Mr. Barnard was formerly midwestern manager of the agricultural div. in Chicago.

John W. McDermott has been appointed business manager and director of personnel for U. S. Steel's public relations organization.

Chester M. McCreery was appointed manager of the Rome mfg. div. of Revere Copper & Brass, Inc. **Edwin D. Howell** will be Mr. McCreery's assistant. **Harold J. Schindler** succeeds Mr. Howell as works manager, Clinton mfg. div., Clinton, Ill.

Ralph R. Kelley has joined Brooks & Perkins, Inc., Detroit as general superintendent of the new magnesium rolling mill, to be called the Livonia Mill Div.

Leonard W. Bughman was elected a vice-president for the Great Lakes Carbon Corp., New York.

Don Bussey was named plant superintendent at Kaiser Aluminum & Chemical Corp.'s Moss Landing, Calif., refractory brick plant.

Frank F. Cambest, assistant general superintendent, Jones & Laughlin Steel Corp., has been made works manager of the Pittsburgh works div.

John Bidner has been made assistant to the general superintendent, Sharon Steel Corp. He was formerly open hearth superintendent at the company's Roemer Works. **Francis J. Herman** replaces Mr. Bidner as open hearth superintendent.

Roy J. Heinz was elected vice-president of the Pittsburgh Steel Foundry Corp. and is in charge of operations at the Glassport, Pa., foundry.

Richard P. Molt has been named a research engineer in the structural research dept. at the Armour Research Foundation of Illinois Institute of Technology.

Carl F. Floe, professor of metallurgy, has been appointed assistant provost at the Massachusetts Institute of Technology.

S. E. Maddigan has resigned as director of the British Columbia Research Council, University of British Columbia. He has accepted a position with the Kaiser Aluminum & Chemical Corp., Spokane, Wash.

Samuel A. Madrid is now metallurgist for the Utah Construction Co., San Francisco.

John H. Hollomon has been named manager of the metallurgy research dept. of the General Electric Research Laboratory. He will succeed **William E. Ruder,** who has retired. Dr. Hollomon joined General Electric in 1946 and was later named assistant manager of the metallurgy research dept.

J. P. Dick has joined the Aluminum Co. of Canada, Ltd., Montreal. He had been associated with Dominion Magnesium Ltd., Haley, Ont.

Giuseppe Bagna is assistant general manager, iron and steel div., FIAT S. A., Torino, Italy.

Clyde B. Colwell, Jr. has been appointed district manager for the Twin Cities District, U. S. Steel Supply Div., U. S. Steel Co.

Robert E. Peppers is assistant metallurgist with the Key Co., East St. Louis, Ill.

Austin Hiller, General Electric Co., is now with the welding dept. in Chicago. He had been located in Milwaukee.

John E. Didrickson has joined the Blaw-Knox Co., steel plant equipment dept., Chicago.

R. E. Hough has retired as general manager of the Bethlehem Steel Co. Johnstown plant. He joined the company in 1905. **A. J. Fisher** succeeds Mr. Hough as plant general manager.

John W. Schreiber, associated with the Aluminum Co. of America for 42 years, has retired as chief construction engineer. He will serve until July 1 as a special consultant on construction.

Coming Events

Feb. 11-Feb. 15. ASM, technical meeting, Arlington Prin. Hotel, Pittsburgh.

Feb. 8. AIME, Southwestern Section, National Open Hearth Steel Committee, Park Plaza Hotel, St. Louis.

Feb. 14. AIME, Philadelphia, Engineering Bldg., University of Pennsylvania, Philadelphia.

Feb. 18-21. AIME, annual meeting, Hotel Statler, New York.

Feb. 28. AIME, Cleveland Section, Lecture Room, Metallurgy Bldg., Case Institute of Technology, Cleveland.

Mar. 3-7. ASME, spring meeting and committee week, Hotel Statler, Cleveland.

Mar. 10-14. National Electrical Mfrs. Assn., spring meeting, Chicago.

Mar. 10-14. National Assn. of Corrosion Engineers, annual convention, Galveston.

Mar. 17. AIME, Chicago Section, National Open Hearth Steel Committee, Del Prado Hotel, Chicago.

Mar. 18-19. American Institute of Chemical Engineers, Atlanta Biltmore Hotel, Atlanta.

Mar. 17-21. ASTE, annual meeting, Chicago.

Mar. 18-19. Steel Founders' Society of America, annual meeting, Chicago.

Mar. 19. AIME, Western Section, National Open Hearth Steel Committee, Rodger Young Auditorium, Los Angeles.

Mar. 20. AIME, Philadelphia, Engineering Bldg., University of Pennsylvania, Philadelphia.

Mar. 27-Apr. 6. Chicago International Trade Fair, Navy Pier, Chicago.

Mar. 31-Apr. 4. ASME, spring meeting, Seattle.

Mar. 31-Apr. 2. AIME, annual conference, Blast Furnace, Coke Ovens, Raw Materials Committee and Open Hearth Steel Committee, William Penn Hotel, Pittsburgh.

Apr. 17. AIME, Philadelphia, Engineering Bldg., University of Pennsylvania, Philadelphia.

Apr. 21. AIME, Chicago Section, National Open Hearth Steel Committee, Phil Smidt & Sons, Whiting, Ind.

Apr. 21-24. SAE, national aeronautical meeting, New York.

Apr. 22. Assn. of Consulting Chemists & Chemical Engineers, Inc., general symposium, Hotel Belmont Plaza, New York.

Apr. 25-26. AIME, New England Regional Conference, Kenmore Hotel, Boston.

Apr. 26-May 11. Liege International Fair, Liege, Belgium.

Apr. 28-30. Metal Powder Assn., annual meeting and exhibit, Chicago.

May 1-7. American Foundrymen's Society, International Foundry Congress and Show, Convention Hall, Atlantic City, N. J.

May 6-9. Scientific Apparatus Makers' Assn., annual meeting, Edgewater Beach Hotel, Chicago.

May 22-24. American Society for Quality Control, annual convention, Onondaga County War Memorial, Syracuse, N. Y.

June 16-20. Industrial Finishing Exposition, International Amphitheatre, Chicago.

June 23-27. ASTM, 50th anniversary meeting, Hotel Statler, New York.

July 1-Sept. 30. Centennial of Engineering, Chicago.

Sept. 11-13. American Institute of Chemical Engineers, Palmer House, Chicago.

Sept. 22-25. American Mining Congress, Metal and Nonmetallic Mining Convention and Exposition, public auditorium, Denver.

Oct. 3. AIME, Southern Ohio Section, National Open Hearth Steel Committee, Deshler-Wallick Hotel, Columbus, Ohio.

Oct. 10. AIME, Eastern Section, National Open Hearth Steel Committee, Warwick Hotel, Philadelphia.

Proposed for Membership
— Metals Branch AIME —

From *AIME* membership on Nov. 30, 1951 was 15,405, in addition 2079 Student Associate members enrolled.

ADMISSIONS COMMITTEE

Thomas G. Moore, Chairman; Carroll A. Hochwalt, Vice Chairman; George H. Clevenger, F. W. Hooven, Albert J. Phillips, Lloyd C. Tribus, R. D. Mollison, John T. Sherman, Alexander A. C. Hewitt, H. W. Hillyard, Philip Williamson, Dan Gunn, T. D. Jones and R. A. Finch, Jr.

The Institute desires to extend its privileges to every person to whom it can be of service, but does not desire as members persons who are unqualified. Institute members are urged to review this list as soon as possible and immediately to inform the Secretary's office if names of people are found who are known to be unqualified for *AIME* membership.

To the following list *CJS* means change of status, *R* reinstatement, *M* Member, *J* Junior Member, *A* Associate Member, *S* Student Associate.

California
Livermore—Blumer, Saul E. (J) (C S—S-J)

Illinois
Champaign—Craig, William J. (M) (R C S—S-M)
Chicago—Carney, Dennis J. (M) (C S—J-M)
Genzel, Otto (M) Hu, Hsun (J) (C S—S-J)
McLain, William R. (M)—Mohr, Robert C. (J)

Indiana
Gary—Krubsack, Clifton A. (J)
Griffith—Bamberg, William R. (J)
Hammond—Ham, Coy S. (M)

Michigan
Detroit—Roberts, Sidney G. (J)
Grosse Pointe—Skinnin, George J. (M)
St. Joseph—Preston, James King (J) (C S—S-J)

New Jersey
Butler—Hosford, William F. (J) (C S—S-J)
Ramsey—Alessandrini, Hugh V. (M)

New York
Brooklyn—Bauer, Richard J. (J) (R C S—S-J)—Carlson, Robert G. (J) (R C S—S-J)
Schenectady—Brenner, Sidney S. (J) (C S—S-J)

Ohio
Akron—Heath, Russel (J) (C S—S-J)
Alliance—Corey, Clark L. (J) (R C S—S-J)
Cincinnati—Tancous, Ernest (M)
Columbus—Reiswig, Robert D. (J) (C S—S-J)
Lima—Harf, Fredric H. (J) (C S—S-J)

Pennsylvania
Beaver—Simkins, Verne W. (C S—J-M)
Collegeville—Elsworth, Edwin F. (J)
Hellertown—Jenkins, Jerome M. (C S—S-J)
Latrobe—Anderson, Leroy L., Jr. (J) (C S—S-J)
Oakmont—Ennor, William T. (M)
Palmerton—Schulz, Frank Herbert (J)
Pittsburgh—Merdian, Raymond R. (M)—Williams, Don D. (J)—Zillmann, Rudolf W. (M) (R C S—S-M)

Texas
Corpus Christi—Henderson, John J. (J) (C S—S-J)

Utah
Salt Lake City—Bradford, Harold R. (M)—McKewan, William M. (J) (R C S—S-J)

Washington
Seattle—Elmore, Marion E. (M) (C S—J-M)
Spokane—Gaffney, Richard E. (J) (C S—S-J)
West Kelso—Baker, Lynn M. (J) (C S—S-J)

Wisconsin
Sheboygan—Hoag, James G. (J) (C S—S-J)

Brazil
Sao Paulo—Haenel, Joao G. (C S—J-M)

Canada
Montreal—Bridgstock, Guy (A)

England
Co. Durham—Thompson, John S. (J)

France
Chatillon—Bourdariat, Marc (M)
Paris—Dedieu, Jacques M. B. (J) (C S—S-J)

Japan
Fukuoka—Ken-Kamura, Heihachi (M) (R C S—J-M)

Annual Meeting Social Events

This is a tentative list of the social events of the Annual Meeting.

Monday, February 18

Welcoming Luncheon will have Harold R. Medina, famous jurist as guest speaker.

Cocktail Party, Statler Hotel. The mining companies in the New York area extend a cordial invitation to the registrants and their wives to attend this informal get-together session. The **Dinner-Smoker** will follow the Cocktail Party at the Statler. Entertainment will be by Nelba of the Cotillion Room in the Hotel Pierre. Following the dinner, there will be an hour show by entertainers that will lend a night club atmosphere to the event.

Tuesday, February 19

Metals Branch Dinner, Keystone Room, Hotel Statler, preceded by an A La Carte cocktail party.

Informal Dance, Hotel Statler. Music by 12-piece orchestra. Refreshments and entertainment during the intermission.

Wednesday, February 20

The Annual Banquet will be held at the Waldorf-Astoria Hotel. The banquet will be preceded by the President's reception and followed by dancing.

STOKES HIGH VACUUM EQUIPMENT... for every requirement of vacuum processing

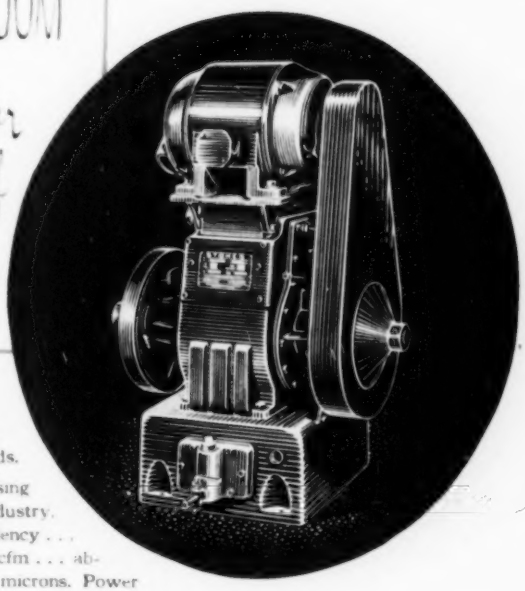

Modern design of Stokes vacuum equipment develops from the continuing contact of Stokes Engineers with processors in many fields.

Stokes Microvac Pumps — basic to vacuum processing — are designed for the broadest requirements of industry. They have high volumetric and mechanical efficiency . . . capacities of 15 to 500 cfm . . . absolute pressures to 10 microns. Power consumption is low. Compact design with top-mounted motor requires minimum floor space.

There are but four moving parts including the high speed, full-opening exhaust valve of corrosion-resistant Teflon. Lubrication is completely automatic, without packing, stuffing-boxes or grease fittings. Wear is kept to a minimum, and long trouble-free service assured. Parts are precision-finished, standard and interchangeable.

Stokes is the only manufacturer of equipment for complete vacuum systems, including Microvac mechanical pumps, oil diffusion pumps, McLeod Gages and Vacuum Valves.

Consult with Stokes on the application of vacuum to vacuum sintering, melting, de-gassing, heat treating, inert gas purging, vacuum metallizing, and to other applications in which vacuum deserves exploration.

Send for FREE Stokes Vacuum Calculator. This slide rule determines needed pump capacity for any job... shows Centigrade to Fahrenheit conversion. Other useful conversion tables and scales on reverse of rule.

STOKES

STOKES MAKES

Plastics Molding Presses,
Industrial Tabletting
and Powder Metal Presses,
Pharmaceutical Equipment,
Vacuum Processing Equipment,
High Vacuum Pumps and Gages,
Special Machinery

F. J. STOKES MACHINE COMPANY, 5916 TABOR ROAD, PHILADELPHIA 20, PA.

PROGRESS REPORT ON NATIONAL CARBON BLAST FURNACE LININGS

TRADE-MARK

33 BLAST FURNACES lined with "NATIONAL" carbon have now produced over 1 million tons. Of these, 12 furnaces have produced more than 1½ million tons and 4 have passed the 2 million ton mark.

These tonnages are for *original linings*. In every case, production has been characterized by remarkably trouble-free operation.

The term "National" is a registered trade mark of Union Carbide and Carbon Corporation.

NATIONAL CARBON COMPANY
A Division of Union Carbide and Carbon Corporation
30 East 42nd Street, New York 17, N. Y.
District Sales Offices: Atlanta, Chicago, Dallas, Kansas City, New York, Pittsburgh, San Francisco
In Canada: National Carbon Limited, Montreal, Toronto, Winnipeg

OTHER **NATIONAL CARBON** *PRODUCTS*

BLAST FURNACE LININGS • BRICK • CINDER NOTCH LINERS • CINDER NOTCH PLUGS • SKIMMER BLOCKS • SPLASH PLATES • RUNOUT TROUGH LINERS • MOLD PLUGS • TANK HEATERS